1-P

NATIONAL AERONAUTICS AND SPACE ADMINISTRATION

Technical Memorandum 33-671

The NASA/JPL 64-Meter-Diameter Antenna at Goldstone, California: Project Report

Technical Staff, Tracking and Data Acquisition Organization

JET PROPULSION LABORATORY

CALIFORNIA INSTITUTE OF TECHNOLOGY

PASADENA, CALIFORNIA

July 15, 1974

200

NATIONAL AERONAUTICS AND SPACE ADMINISTRATION

Technical Memorandum 33-671

The NASA/JPL 64-Meter-Diameter Antenna at Goldstone, California: Project Report

Technical Staff, Tracking and Data Acquisition Organization

JET PROPULSION LABORATORY
CALIFORNIA INSTITUTE OF TECHNOLOGY
PASADENA, CALIFORNIA

July 15, 1974

Prepared Under Contract No. NAS 7-100
National Aeronautics and Space Administration

PREFACE

Since the early days of NASA, two fundamental objectives have evolved with respect to earth-based facilities needed for the return of science and engineering data from spacecraft destined for interplanetary and planetary missions.

The first of these objectives was to advance the state-of-the-art of telecommunications such that it would be feasible from an engineering standpoint to build and operate large steerable antennas to track spacecraft in order to return science and engineering data to earth. These spacecraft were limited in weight and, therefore, power because of the nonavailability of large launch vehicles. In 1960, or just two years after the initiation of the U.S. space program, it appeared that a 64-meter-diameter, steerable, paraboloid antenna could be built with a predictable schedule and cost. Several years of engineering study and analysis were still required, and the studies indicated the feasibility of this project. Concurrently, the Australian scientific community had embarked on building a similar antenna system for radio astronomy. Although the requirements for the latter use are not as severe as those for the space application, important engineering parameters were established.

The addition of the 64-meter station to the Deep Space Network was inaugurated with the tracking of the Mariner 4 spacecraft as it was occulted by the sun in April 1966. Since that time, the antenna has been a primary instrument in the return of imaging data obtained from spacecraft in the vicinity of Mars and Jupiter, considerable other scientific data from interplanetary space and the planet Venus, and many of the special events of the Apollo program in connection with the lunar phases of those missions.

The second objective was to build those earth-based facilities which would make it possible to provide continuous radio contact with the spacecraft. This required a minimum of three space communications stations around the earth, nominally 120 deg in longitude apart. In order to minimize the rates of motion in tracking the spacecraft, the stations were located within ±45 deg latitude since the spacecraft would be nominally in the equatorial plane. This policy had been invoked in building the 26-meter-diameter stations, and after the success of the first 64-meter project at Goldstone, California, two additional 64-meter stations were built in Spain and Australia. These additions provide a 3-station network which maintains continuous contact with spacecraft on missions to the planets.

N. A. Renzetti
Office of Tracking and Data Acquisition

ACKNOWLEDGMENT

The information required to document the Goldstone 64-meter-diameter antenna, like the creation of the antenna itself, is the total result of the efforts contributed by many different organizations and individuals. It is, therefore, impossible to list each individual contributor by name. Those who may not find their names mentioned within this report are assured that their achievements are also acknowledged as an important part of the teamwork that made this project a successful reality.

Assigned NASA Headquarters personnel were responsible for interproject, intra-NASA, and interagency coordination; allocation and reprogramming of major resources; establishment of project objectives and guidelines, and overall technical direction and guidance. Advanced Antenna System Project responsibilities were assigned to C.R. Morrison of the Office of Tracking and Data Acquisition (OTDA) under the direction of E.C. Buckley, Director, OTDA, and G.M. Truszynski, Deputy Director, OTDA.

CONTENTS

CHAPTER III. DESCRIPTION OF THE ANTENNA SYSTEM

CHAPTER IV. DESIGN AND ANALYSIS OF CRITICAL AREAS

CHAPTER V. ANTENNA PERFORMANCE

TABLES

FIGURES

ABSTRACT

This report describes the significant management and technical aspects of the JPL Project to develop and implement a 64-meter-diameter antenna at the Goldstone Deep Space Communications Complex in California, which was the first of the Advanced Antenna Systems of the National Aeronautics and Space Administration/Jet Propulsion Laboratory Deep Space Network.

The original need foreseen for a large-diameter antenna to accomplish communication and tracking support of NASA's solar system exploration program is reviewed, and the translation of those needs into the technical specification of an appropriate ground station antenna is described.

The antenna Project is delineated by phases to show the key technical and managerial skills and the technical facility resources involved. There is a brief engineering description of the antenna and its closely related facilities.

Some difficult and interesting engineering problems, then at the state-of-the-art level, which were met in the accomplishment of the Project, are described. The key performance characteristics of the antenna, in relation to the original specifications and the methods of their determination, are stated.

By virtue of its large aperture size and very-low-noise receiving systems, the 64-m antenna has provided unique communication and tracking support capability to many NASA space exploration missions. Its use in radio science and advanced engineering experiments has provided a number of scientific and technological accomplishments. Such ventures, and the philosophy of the use of the antenna, are described.

Improvements in the use factors of the antenna, both in technical performance and operational effectiveness, have been pursued since the antenna has been in operation.

CHAPTER I. INTRODUCTION

The 64-m (210-ft) diameter antenna at the Goldstone Deep Space Communications Complex in California is a facility of the Deep Space Network, which is operated by the Jet Propulsion Laboratory (JPL) for NASA's Office of Tracking and Data Acquisition. The Deep Space Network provides the communications and tracking support for NASA's unmanned lunar and planetary exploration spacecraft.

A world-wide network of space communications and tracking stations makes up the Deep Space Network (DSN). The network, at Project inception, comprised three communications and tracking stations at the Goldstone Complex and one station each at Woomera and Tidbinbilla, Australia; Johannesburg, South Africa; and Cebreros and Robledo, Spain (near Madrid). Additional support is provided by a spacecraft compatibility test area at the Jet Propulsion Laboratory in Pasadena, California, a launch support station at Cape Kennedy, Florida, and a research and development station at the Goldstone Complex. The stations of the Deep Space Network are located approximately 120 deg apart in longitude in order to provide continuous coverage capability for a spacecraft in or near the plane of the ecliptic on its journey through our solar system (Fig. 1).

The Goldstone Complex, located on a part of the Fort Irwin reservation of the United States Army, is 176 square kilometers (68 square miles) in area and 72 kilometers (45 miles) from Barstow, California, in the Mojave Desert. The Goldstone 64-m-diameter antenna, along with its support buildings and facilities, is designated as the Mars Deep Space Station (DSS 14). The three other Goldstone antenna stations are equipped with 26-m (85-ft) diameter antennas (Fig. 2), as are the other stations in the Deep Space Network. The locations of the antenna stations and other pertinent facilities at the Goldstone Complex are shown in Fig. 3, and the names, locations, and pertinent characteristics of all DSN stations are shown in Table A-1 of the Appendix.

The JPL effort to plan, design, and build the 64-m-diameter antenna was carried out by the Advanced Antenna System (AAS) Project. This report describes the AAS Project organization and the development, design, construction, performance, and use of the antenna from the beginning of the Project until January 1, 1970. A summary of highlights of usage and major engineering changes through January 1974 is included in Chapter VI.

Throughout the work described here, customary English units of measurement were used. These have been converted to International System units for the purpose of this report, and a system of presenting double units has generally been followed.

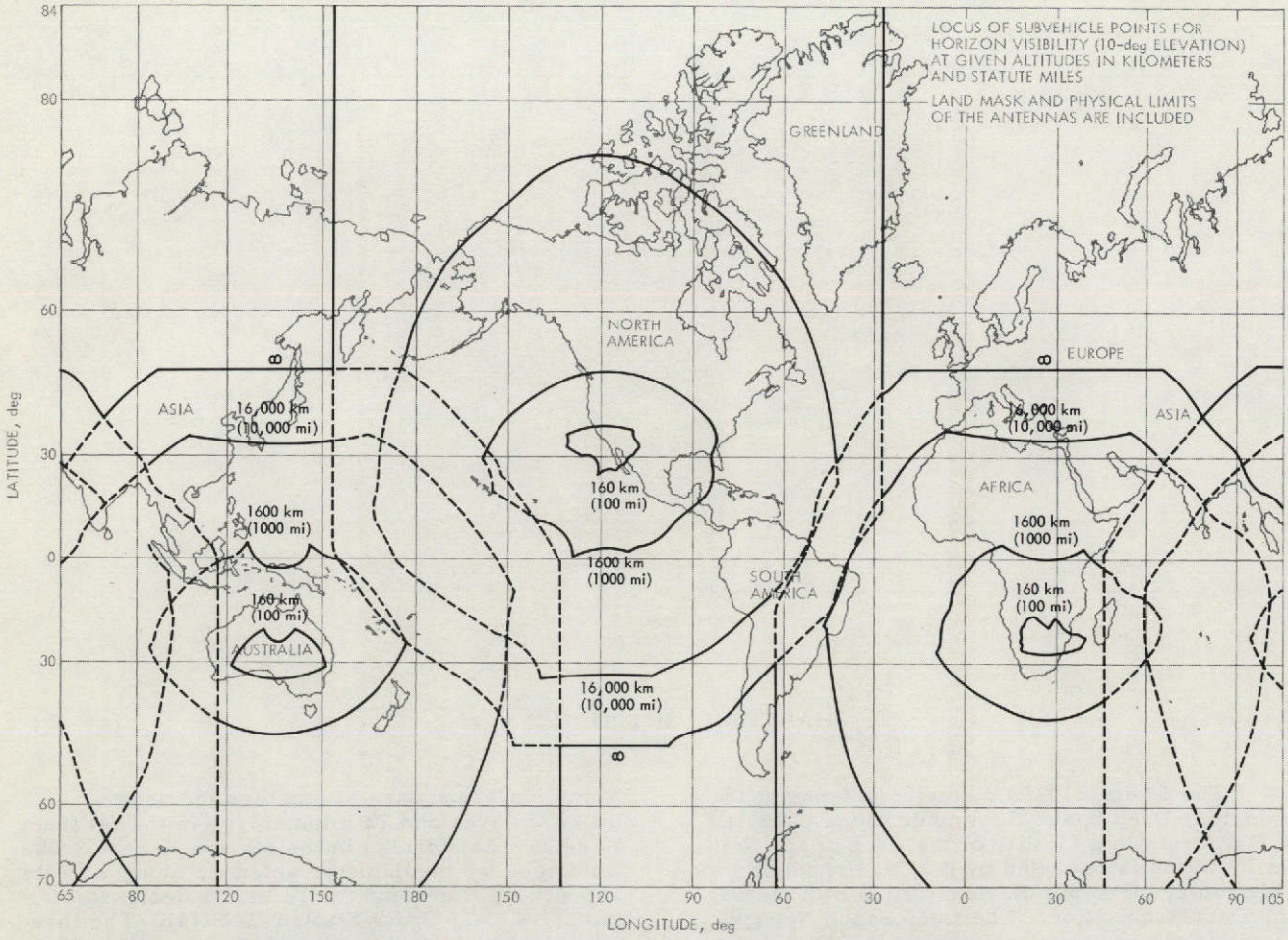

Fig. 1. Deep Space Stations of the Deep Space Network at the inception of the project. Overlapping station coverage ensures continuous monitoring of spacecraft.

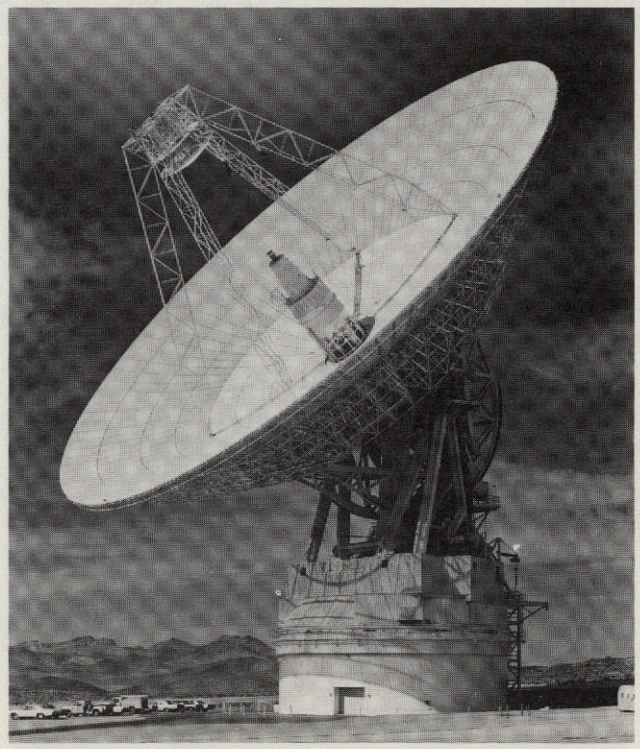

Fig. 2. The 26-m (85-ft) diameter antenna at the Echo Deep Space Station

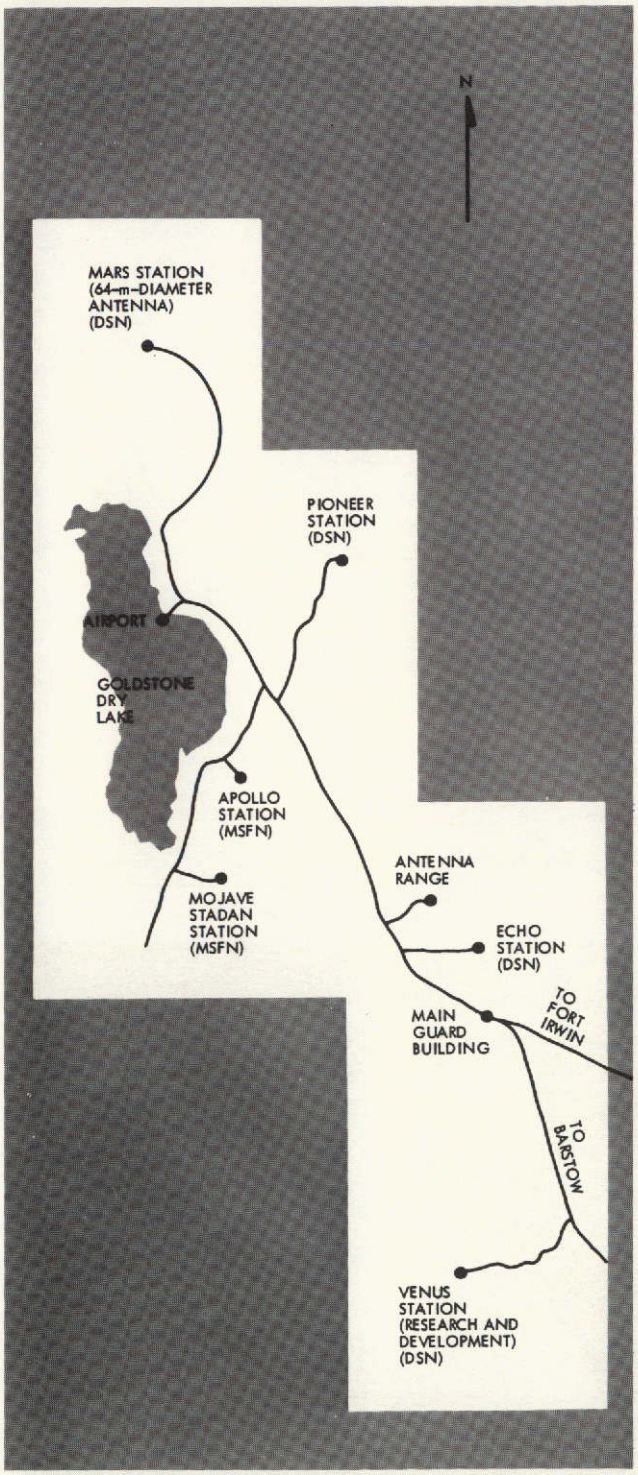

Fig. 3. The Goldstone Deep Space Communications Complex. The Apollo and Mojave stations are part of the Manned Space Flight Network (MSFN)

CHAPTER II. THE ADVANCED ANTENNA SYSTEM PROJECT

The programmatic and management aspects of the Advanced Antenna System Project to design, build, and initially use the 64-m-diameter antenna are described in this chapter. Observations on technical aspects of the antenna are incidental and are included only to illustrate the structure or workings of the project organization.

I. SUMMARY OF KEY FACTORS

The AAS Project was completed on schedule, within its original budget allocation, and the antenna has met or exceeded its original performance specifications. Key factors in this accomplishment are discussed below.

The antenna facility had a basically sound and stable justification in terms of the programmatic need of a bona fide user: the program of solar system exploration using unmanned spacecraft sponsored by the NASA Office of Space Science and Application would require an increased deep space communications capability over that available in 1960. This requirement and the desirability of satisfying a significant portion of it by application of larger ground antennas were recognized early and were continuously supported by the NASA Office of Tracking and Data Acquisition, the office directly cognizant of the JPL Deep Space Network program.

The technical and management personnel involved with the research, engineering development, and operational use of the Deep Space Network antenna facilities were all within a single technical line organization, reporting directly to the responsible JPL programmatic office. This arrangement allowed the prospective users to give realistic advice on the technical and operational specifications and provided rapid access to the wide spectrum of advanced technical skills and laboratory facilities needed at various times in the course of the project.

A hard-core team of experienced antenna system designers was continuously involved from the pre-beginning to the post-ending phase of the project. The team's close daily observation of the project's progress, with continuous personal liaison and immediate attention to problems and potential problems, provided effective project control and positive results.

A lengthy, intensive period of design, analysis, and design review led to the development of the antenna specification. This effort was supported by a large amount of experimental verification of the analysis methods and design concepts, using antennas and mock-ups that were within a comfortable scale factor of the real antenna. Much of the work of the JPL project personnel was accomplished — and 50 percent of the scheduled project time was consumed — before the first piece of steel for the antenna was cut.

Viewed as a total instrument, the antenna represented an advanced design. However, only a few individual state-of-the-art design areas were involved, and none of these required extrapolation of more than a factor of 2 to 4 from previously demonstrated designs.

Prospective users of the antenna facility from the DSIF operations staff were assigned to the project, starting with the on-site erection of

the antenna, in order to become familiar with the facility. However, the development design team retained direct responsibility for performance of the antenna during the early operational application and thus could easily correct any deficiencies in the original design or its implementation.

A close, cooperative, and continuous working relationship was maintained between JPL procurement, quality assurance, administrative, and technical services personnel, the technical team representatives, and the major industrial contractors working on the design and implementation of the antenna and its directly related facilities.

The factors listed above are believed to be generally applicable to the design, implementation, and initial use of any comparably sized advanced technical facility.

II. MILESTONE SCHEDULE OF SIGNIFICANT EVENTS

The major milestones of the AAS Project are tabulated in Fig. 4. Milestones set forth in this figure are referred to by number in the text as they are discussed.

III. JUSTIFICATION FOR THE ADVANCED ANTENNA SYSTEM PROJECT

A. RATIONALE

Development of the justification for adding antennas significantly larger than 26 m in diameter to the stations of the DSN was started in 1960 (Milestone 1). The original justification remained basically stable, although it was reexamined, upgraded, and modified as the project progressed and as plans for future spacecraft missions requiring DSN support became better defined. Extracts from the early justification and rationale — much of which is recognizable as accurate prophesy — are included in the text below.

From the beginning, the intended network design was for three deep space stations equipped with the large antennas, carrying on the basic DSN design philosophy of providing the capability for continuous two-way communications with unmanned solar system spacecraft, when and if it was required by the spacecraft mission operations.

The project described in this report deals with the first 64-m-diameter antenna at the Goldstone Complex, although, as stated, the original justification properly deals with the total network concept.

The future needs for a large-aperture, ground-based antenna with increased capability over the then-existing 26-m-diameter antennas was foreseen and documented in early 1960. The following are extracts from original justifications forwarded to NASA by Dr. Eberhardt Rechtin, who was at that time the JPL DSIF Program Director and who provided programmatic leadership and guidance from the start of the project to its conclusion.

Although an improvement in communications by a factor of ten would be useful to Deep Space exploration at any time, this improvement becomes a virtual requirement with the coming of Saturn-class vehicles.[1] These vehicles are capable of launching spacecraft which can perform missions unachievable before. Typical of such new missions are lunar roving vehicles, high resolution photographic lunar satellites, satellites around the planets, and manned vehicles going around the Moon.

If significant capability improvements were not made in one or more elements of the communications link, the only option of the communicator would be to provide less good data per unit time. For the new types of missions, particularly, this option of low data rate is undesirable. Roving vehicles would be required to explore at reduced speed, slowing motion to a few feet per second. A lunar satellite would take ten times as long to send the same data, greatly increasing the operational cost chargeable to it by the ground data acquisition stations and, of course, tying up and saturating these ground stations in the process. If resolution is sacrificed, the value of a lunar satellite is far less compared to available data taken from Earth observatories. With limited communications capability, satellites around the planets suffer in their effectiveness to observe clouds (or fortuitous breaks in the Venusian clouds) and to observe the planet throughout its full passage around the Sun. Planetary satellites would less well observe seasonal and diurnal changes of the planets. For the manned vehicles, it is sufficient to say that every conceivable technique should be exploited which obtains good communications in the most direct and simple manner possible; system margins should be far greater than allowed for unmanned vehicles in order to permit communications under emergency conditions.

---

[1] The use of this class of vehicle has not yet materialized in planetary exploration; however, the Mariner 1969 Mars flyby high-resolution photographic missions and the Mariner 1971 Mars orbiters were real examples of quite sophisticated second- and third-generation unmanned planetary exploration missions.

In a United Press International news release of March 8, 1962, it was stated that Edmond C. Buckley, then Director of Tracking and Data Acquisition for NASA, informed Congress of NASA's plan to build a 64-m-diameter radio antenna capable of receiving "live television from the Moon." This prediction became a reality in 1969.

B. STUDY OF COST EFFECTIVENESS

Before the development of the larger antenna was permitted to reach the preliminary design phase, a study was made to determine the least expensive ways of improving communications by significant amounts.

An improvement of less than a factor of 4 was felt to be too little, since that factor is the approximate uncertainty in design performance in any event. An improvement by much more than a factor of 10 due to improving a single element in the communications system was recognized to be rather unlikely.

Evident improvements, such as the incorporation of parametric amplifiers and masers in the ground receivers, the use of special-purpose antenna feeds, the coding and storing of information, and the increasing of spacecraft antenna diameters to the practical limit, were all under way and the limits of the improvements possible were considered to be well understood.

Obviously uneconomic ways of increasing the data by a factor of 10 — such as launching ten times as many space probes — were discarded.

The principal option then remaining to compete with the large ground antenna was that of the larger spacecraft transmitter. Spacecraft transmitters radiate 10 to 100 watts of power. Cost estimates were therefore made to determine the cost per spacecraft of increasing the power levels from 100 to 1000 watts. The least expensive method, one that made no effort to conserve spacecraft weight, was then estimated to cost $800,000 per spacecraft. This figure included the cost of solar panels or their radioisotope equivalent, the cost of developing and procuring the higher-power transmitters, the cost of thermal control devices, and the cost of critical component spares. Constructing larger ground antennas also adds expense, but this expense is invested in permanent equipment on the ground. Since the choice of the larger ground antenna followed a generally good rule that if complexity must be added, it should be added to the ground equipment, not the spacecraft, no attempt was made to evaluate the cost trade-offs of this factor.

Cost data for antennas of the size and precision necessary to improve communications by a factor of 10 were then obtained. To this were added the estimated costs of primary power, buildings, electronics, and so forth, to obtain the complete cost of an installation. The cost estimate was $15 million per installation. From this estimate was subtracted the cost of a smaller installation required to provide the relief from overloading of the stations (because of simultaneous tracking of several active spacecraft) which the larger antenna would otherwise provide.

At the rate of spacecraft launchings expected, the cost of the large antennas would be written off in 7 years. Design specifications consequently called for a minimum lifetime of 10 years, a requirement that is easily met for structures of this type.

Operating costs were also studied. To a first approximation, operating costs for the large antenna installation are not significantly different from those for an installation in which almost everything else is the same, but the antenna diameter is smaller. It takes very little more operating cost to maintain the larger mass of inert steel of the bigger antenna. The operating cost of the remaining buildings, electronics, communications, and so forth, is about the same. There is a possible argument that the smaller installation would even cost more to operate for some kinds of mission support, since it would have to be operated ten times as long to obtain the same amount of data.

C. SURVEY OF PROPOSED AND EXISTING LARGE ANTENNA FACILITIES

To ensure that no practical means of providing increased communication capabilities was overlooked, a survey was made of the possible antenna facilities such as the United States Navy's antenna at Sugar Grove, West Virginia, the spherical bowl antenna of the Arecibo Ionospheric Observatory in Puerto Rico, the Jodrell Bank antenna of the University of Manchester in England, and the Australian 64-m (210-ft) diameter radio telescope of the Commonwealth Scientific Information Research Organization (CSIRO).

Briefly stated, the results of the survey were that these installations were not available for the necessary time durations at the required priority level and were not subject to necessary control for fulfillment of the deep space communications commitments of the DSN. These facilities could possibly be used as supplementary (or occasional backup) stations, however, provided their modification and operating costs were acceptable.

It was concluded that the large antenna should be a new device. In the interests of accurate cost estimating and scheduling, the design would be consistent with limited extrapolations of known techniques. Compared with the then-planned 183-m (600-ft) diameter Sugar Grove antenna, the antennas foreseen for the DSN application would be smaller, simpler, and considerably less expensive. Of the estimated $15 million per installation, $10 to $12 million would apply to the antenna's mechanical system itself. Cost estimates by a variety of different techniques and by a number of different companies and consultants confirmed that appropriate antennas could be built within these stated costs.

IV. INITIAL PROJECT ORGANIZATION

After the initial justification was developed and the functional and the basic overall performance specifications were prepared for the antenna (Milestone 2), an engineering group was specifically identified as the Advanced Antenna System Hard-Core Team to support the needed ongoing investigations and establish and define the overall project (Milestone 3). This team later evolved into a formal project organization after the initial studies had been accomplished and the construction of the 64-m-diameter antenna had been authorized and funded. The project organization is described in Section IX of this Chapter.

A senior engineer, William D. Merrick, who had been project engineer for implementation of the 26-m-diameter antennas in the Deep Space Network, was appointed to head the AAS Hard-Core Team. Other members of the initial team were three senior mechanical engineers, a senior civil-structural engineer, a senior field engineer, and a senior contract negotiator.

The initial AAS Hard-Core Team provided a balanced mix of engineering and technical management experience including university-based, research-type operations and conventional up-to-date industry practice. In addition, other JPL personnel from various technical and management disciplines were identified to be available for counsel and services. Consultant assistance was also obtained from the California Institute of Technology as required in the planning and design phases.

V. IDENTIFICATION OF SPECIFIC REQUIREMENTS AND CONSTRAINTS

The first major responsibility of the newly organized team was to outline basic policies and procedures for carrying out the project and to identify specific technical and managerial requirements and constraints applicable to the preparation of requests for proposals. The requests for proposals were used for soliciting bids from industrial firms to participate in the design, development, and implementation of the antenna facility.

In September, 1960, the first issue of the specification for the antenna, Engineering Planning Document 5 (Ref. 1) was completed (Milestone 4). This document was prepared for two basic purposes:

(1) To define the technical and operational requirements to be met by the new antenna system.

(2) To describe the major aspects of the planned program for accomplishing, through the use of major industrial contractors, the design, construction, and testing of the new antenna system.

In general, the new antenna system, as specified in Ref. 1, was to provide a low-noise, large-diameter precision antenna with a communication capability 6 to 12 dB greater than that of the 26-meter antennas. The specific configuration of the antenna was undefined at that time; however, a "representative configuration" of a large, open-environment, azimuth-elevation steerable paraboloid was described as an example.

VI. PROJECT PHASING

The project was defined in three phases as described below.

A. PHASE I – DESIGN STUDIES

The objectives of Phase I were to identify a specific conceptual configuration for the antenna, substantiate its engineering feasibility, develop the detailed specifications and criteria to provide the basis for selecting an industrial contractor, and define the contract to accomplish the next phase. The approach in Phase I was to have industrial contractors do independent studies to determine their preferred solutions to the requirements of Ref. 1. At the same time, the AAS Hard-Core Team did a similar conceptual design study. To complete Phase I, the results of the several design studies would be reviewed and a particular design, possibly using results from all of the studies, would be identified and specified.

B. PHASE II – COMPLETION OF THE FIRST ANTENNA

Phase II was to include the final design, preparation of detailed drawings, fabrication, transportation, erection, and acceptance testing of the first 64-m-diameter antenna at the Goldstone Complex.

C. PHASE III – COMPLETION OF ADDITIONAL ANTENNAS

Phase III was to complete the large antenna network. It was to include fabrication, transportation, erection, and acceptance testing of two additional antennas at overseas locations. As previously noted, and for a variety of reasons, this phase was not undertaken as an integral part of the initial project, but has been the objective of a later project currently underway.

VII. PHASE I – DESIGN STUDIES

A. SOURCE SELECTION AND EVALUATION

At the beginning of Phase I, an industry-wide survey was made, by reviewing trade journals and other documents, to obtain a comprehensive list of industrial firms that were interested in the antenna field and could be considered potential proposers.

A NASA/JPL Source Evaluation Board was established to aid in contractor evaluation for the project. The board reviewed the listing that resulted from the industry-wide survey and reduced the number of companies selected for initial solicitation to 33.

The Source Evaluation Board extended invitations to participate only to those firms that were believed to have the capability to undertake the design and completion of the large antenna facility as a prime contractor. Companies that indicated interest in the project were sent a request for proposal, along with appropriate documents, including a work statement for the activity, and were invited to a 2-day preproposal conference at JPL in Pasadena and at the Goldstone Complex.

In response to the request for proposal for Phase I, 17 formal proposals describing a Phase I design study effort were received by JPL. These

proposals were made by the following firms and groups of firms:

Blaw-Knox

Dalmo Victor Company
Alpha Corporation of Texas

Boeing Antenna Department

Convair San Diego Electronics,
Convair Division,
General Dynamics Corporation

Goodyear Aircraft Corporation

Hughes Aircraft Company, Ground Systems

Hughes Tool Company, Aircraft Division

Arthur D. Little, Incorporated

North American Aviation, Incorporated

Philco Corporation

Radiation, Incorporated

Radio Corporation of America, Moorestown
Missile and Surface Radar Division

Raytheon Company, Equipment Division

The Siegler Corporation

Sperry Gyroscope Company,
Surface Armament Division

Sylvania Electronic Systems,
A Division of Sylvania Electric Products

Telecomputing Corporation

ETS-Hokin and Galvan
Rantech Corporation
McKiernan-Terry Corporation
Reeves Instrument Company

Westinghouse Electric Corporation

The designs represented in the 17 proposals encompassed a wide variety of basic antenna configurations. Four of the more extreme configurations are shown in Fig. 5. These configurations were:

(1) A planar array of many hexagonal small paraboloidal antennas positioned by a track-over-azimuth mount (Fig. 5a).

(2) A parallel-plate metal lens supported by form-maintaining hoops (Fig. 5b).

(3) Several mounts similar to the configuration of the University of Manchester's 76-m (250-ft) radio telescope at Jodrell Bank, England (Fig. 5c).

(4) A fixed spherical bowl with a spherical rotating shell as a continuation of the bowl contour (Fig. 5d).

Other proposed basic antenna configurations were:

(1) Ten separate 26-m-diameter antennas arranged in a circle and working as a synchronized array.

(2) An offset paraboloid mounted on an azimuth-elevation mount.

(3) A segment aperture with individually controlled segments.

(4) An array of four large paraboloidal reflectors mounted on a single pedestal.

(5) A scaled-down version of the 183-m (600-ft) Manchester-type mounted Sugar Grove antenna design.

(6) A spherical structure supported by trunions, in which one-half of the sphere serves as a radome.

(7) A track-over-azimuth mount supporting a paraboloidal reflector.

(8) Several conventional paraboloidal reflectors supported on azimuth-elevation pedestal mounts.

The engineering evaluation of the 17 proposals received for the Phase I effort produced some significant conclusions for the project.

First, for the specified application, the illustrative system design, which was given in Ref. 1, was a proper basic instrument. None of the 17 alternative configuration proposals offered the az-el mounted Cassegrain-fed steerable paraboloid any serious competition in cost, delivery schedule, or minimization of risk. No good reasons could be given why drastically different designs might result in lesser cost. On the other hand, the more unusual solutions all appeared to afford a higher risk, in that they might not be completed on time, on cost, or with performance acceptable for use in the DSIF.

Second, because of the complex antenna system that was required, no proposal gave a total specified solution of all of the problem areas such as pointing accuracy, data readouts, and detailed operational refinements.

Third, it was concluded that complicated, servo-corrected structures or reflector surfaces were not necessary for the reflector diameters appropriate to the project requirements.

From the 17 proposals received for the Phase I effort, the Source Evaluation Board, considering the analysis and recommendations by the AAS Hard-Core Team, selected the four proposers that showed the most promising basic design concepts and showed an understanding of the basic problems of the project. The proposers selected to do the Phase I studies were Hughes Aircraft Company, Westinghouse Electric Corporation, Blaw-Knox Company, and North American Aviation, Inc.

Designs submitted by these companies are depicted in Fig. 6. The significant characteristics of these designs were as follows:

(1) Hughes Aircraft Company — a king post, alidade[2] configuration with a stressed-skin, truncated-cone reflector.

(2) Westinghouse Electric Corporation — a "Manchester" type of mount, with electric drives, and an "egg crate" reflector.

(3) Blaw-Knox Company — a king post, alidade configuration with a reflector utilizing a center hub, box girder, and radial ribs.

(4) North American Aviation, Inc. — a king post, alidade configuration with a torsion-bar, radial-ring reflector similar to that being applied to the 37-m (120-ft) diameter Haystack antenna of the Massachusetts Institute of Technology.

B. PHASE I FEASIBILITY STUDIES

The four companies cited above were each awarded a funded 3-month-duration contract for the Phase I feasibility studies (Milestone 5). The objective of the Phase I studies was to develop the individual proposed designs so that the Source Evaluation Board, working with the AAS Hard-Core Team, could adequately evaluate the technical performance and operational characteristics of the competing designs in relation to meeting the requirements of Ref. 1, Rev. 1. The studies were constrained to pedestal-mount configurations with a 73-m (240-ft) diameter reflector, with a ratio of focal length to diameter in the range of 0.25 to 0.42. The designs were required to be capable of incorporating a data system for precision antenna beam angle pointing, using optical elements for absolute angle reference and error sensing.

During the Phase I studies, two significant characteristics of the basic design were recognized. First, the alidade and backup structure would be the limiting elements on the overall antenna system stiffness and the resulting dynamic tracking and radio frequency efficiency performance. Second, the support of an intermediate reference surface from the reflector structure, to identify accurately the direction of the radio beam formed by the reflector, was determined to be a difficult design problem: calibration of the angle data system to compensate for dead load deflections of this support would evidently be required.

Throughout the 3-month Phase I feasibility studies, the project continued to appear to be technically and financially feasible, given good engineering and proper management. The intended prime contractual approach seemed a good one, and there was no apparent reason why any of the chosen study contractors, or, by the same criterion, any equally competent and experienced contractor, could not proceed with a complete design and fabrication of the prototype instrument.

It was, however, evident that a further, more definitive and specific design and feasibility effort was required to enable a sufficiently comprehensive project definition of the total antenna system as a basis for a manageable contracted task. Accordingly, the Source Evaluation Board evaluated the four Phase I designs and selected the Blaw-Knox Company, utilizing the Dalmo-Victor Division of Textron Corporation, as a major subcontractor, to perform an extended Phase Ia feasibility study of approximately one year in duration, based on a second revision of Ref. 1 (Milestone 6).

C. PHASE Ia FEASIBILITY STUDY EFFORT

The basic objective of the Phase Ia effort by the Blaw-Knox/Dalmo Victor team was to conduct a feasibility study of the best specific configuration for the design and implementation of the total antenna system. For example, in this phase the contractor team had to consider the problem of transportation to and assembly and erection of the antenna at the Goldstone site, and, for the first time in the series of studies, integrate all of the subsystems in the design of a total antenna system. Another significant phase of this design effort was an error analysis displaying system performance within specification, with each major element of the antenna assigned a reasonable error budget.

To carry out this antenna system definition and evaluation process, it was necessary to define a design concept for each of the various major components of the antenna. The basic criterion of the component designs was a good stiffness-vs-weight characteristic to minimize static and dynamic deflections. The components were then assembled into practical combinations to provide a proper antenna system design in terms of performance vs cost.

During the latter part of the Phase Ia period, after rather extensive major component engineering studies had been done, it became apparent that a reiteration of the basic configuration concept would be required. The preliminary design being used was excessively restrictive and did not allow sufficient flexibility to solve some of the engineering problems that were becoming visible.

It was therefore decided to study in detail, but at a system level, a number of variations of the basic configuration. In the process of the configuration variation studies, layout drawings of 13 promising configuration variations were prepared for consideration. A preliminary qualitative evaluation was performed, and four of the 13 variations were selected for additional investigation (Milestone 7). The configurations were restricted to azimuth-elevation mounts capable

[2] The term "alidade," which is derived from an Arabic word meaning "the revolving radius of a circle," is commonly used to denote such components in surveying instruments or telescopes. Here the term refers to a revolving support structure in an antenna.

of ±300 deg rotation in azimuth and rotation from 4 deg above the horizon to 1 deg past the zenith in elevation. The restriction to azimuth-elevation mounts seemed clearly correct by this time, since all the other gimbal arrangements previously studied would subject the reflector to variations in gravity loading about additional axes rather than only about the elevation axis, and would thus require complex correction means for dead-load deflections. The azimuth rotation limitation was selected to meet operational tracking requirements and yet maintain reasonable simplicity in the azimuth cable wrap-up mechanism.

The type of mount was restricted to a pedestal on which the azimuth rotating parts would be mounted. This mount was selected because (1) the precision angle data system for mounts with large ring foundations was complex, (2) non-pedestal types of mounts would require a new and difficult reflector structure design, and (3) the azimuth bearing for a large-diameter, ring-foundation precision antenna was expected to be a difficult and costly design. Previous work had shown that of all reflector structures analyzed for the antenna system, a design employing a 43-m (140-ft) ring girder provided the lowest deflections. This reflector also provided the advantage of quadripod mounting directly to major attach points at the backup structure. However, for completeness, a reflector design using a small-diameter support hub was examined, since this was the configuration then being implemented in the Australian CSIRO 64-m antenna design.

An investigation of azimuth bearing arrangements, prior to the configuration variation study, had resulted in selection of a hydrostatic thrust-moment bearing and a radial bearing for wind shear loads, in preference to radial roller bearings on a large-diameter king post.

In all the gearing designs considered, it was determined that sufficient gear and reducer stiffness could be obtained. Thus, gear diameter could be selected to optimize other parameters and to minimize total cost of the bull gear and reducers. The largest practicable bull gear diameter was used. Gear reducers were used in pairs to allow use of conventional anti-backlash techniques; less conventional alternative methods that were examined were abandoned as not worth the risk.

As a part of the servo system analysis, the natural frequencies of the configuration variations were analyzed and compared. Since it was anticipated that the azimuth axis would exhibit the lowest natural frequency, this axis received the most attention. A 6-degree-of-freedom model was developed for the motion about the azimuth axis. Equations of motion were developed, and appropriate lumped spring constants and inertias were determined for the elements making up the azimuth axis systems. A digital computer analysis determined the natural frequencies of the model. In all cases, it was found that the alidade structure was the limiting element in the system because of its low stiffness. The drive system could relatively easily attain the required stiffness and high natural frequency.

An investigation of optical angle data systems for the various configurations was also conducted. It was concluded that data systems for configurations not having intersecting azimuth and elevation axes and a clear and shielded line of sight from the axes' intersection to the ground along the azimuth axis were very complex. As a result, all configurations incorporated intersecting axes and an instrument tower which followed the design concept incorporated in the 64-m CSIRO antenna then being built at Parkes, Australia.

Using the results of the component and system studies, the four most attractive configuration variations were evaluated – primarily on the basis of ability to meet the required technical performance, and secondarily on cost, schedule, specific possible engineering or implementation problems, operational features, and potential for improved technical performance.

From the evaluation, a recommendation of the preferred antenna system configuration was presented to the JPL program management. The recommendation was accepted, and the Blaw-Knox/Dalmo Victor team then prepared the drawings and documentation to support the request for proposals, for the succeeding Phase II effort of the project. A model showing the planned configuration at the completion of the feasibility studies is shown in Fig. 7.

VIII. PHASE II – ANTENNA CONSTRUCTION AND EARLY OPERATION

A. CONTRACTOR SELECTION

To initiate Phase II of the project, 2-day preprocurement and preproposal conferences were held at JPL in Pasadena and at the Goldstone Complex, attended by representatives of 34 industrial companies (Milestone 8). Revision 2 of Ref. 1 was the basic requirements document for the request for proposals, in response to which three companies submitted fixed-price proposals.

The Source Evaluation Board reviewed the three Phase II proposals and concluded that all had to be rejected because none was within negotiable range of the funds available for the basic antenna structure and mechanical system ($12 million) – the average bid was about 40% more than the available amount (Milestone 9). The Source Evaluation Board also concluded that the JPL team should make an appropriate effort to modify the technical and contractual requirements to substantially reduce the proposed cost of the antenna without compromising the basic DSIF mission requirements.

For a 2-month period, the JPL technical team conducted an intensive in-house effort concurrently with discussions with representatives of the antenna industry to determine practicable means of cost reduction. Reference 1, Rev. 3, and a revised proposed contract were developed. The modifications, in brief, reduced the contractor's risk, provided for a clearly defined minimum acceptable performance in addition to desired system performance, and provided for a performance demonstration of contractor-furnished

hardware in terms of characteristics directly measurable by the contractor and verifiable by JPL.

A new request for proposals, based on Ref. 1, Rev. 3, was issued to nine firms who requested it (Milestone 10). Proposals were received from Rohr Corporation, North American Aviation, McKiernan-Terry Corporation and a joint venture consisting of Blaw-Knox Company, Dalmo-Victor Company, and Consolidated Western Steel Corporation. All proposals were considered responsive and all were within negotiable range of the funds available. The Source Evaluation Board reviewed the four proposals and presented their recommendations to NASA (Milestone 11).

The Administrator of NASA then directed JPL to negotiate a contract with the Rohr Corporation, Chula Vista, California. A fixed-price contract of slightly under $12 million for the detailed design and construction of the 64-m-diameter antenna, in accordance with Ref. 1, Rev. 4, was executed with the Rohr Corporation on June 20, 1963 (Milestone 12).

B. DETAILED DESIGN AND INITIAL CONSTRUCTION

The first task of the Rohr Corporation was to complete the detailed antenna system design and to ensure the integration of the structural, mechanical, and servo subsystems. Next, a complete error budget analysis of all major components was made. Meanwhile, on-site work for construction and other support facilities was begun (Milestone 13). Under separate contract, the existing Goldstone Complex road system was extended almost 8 kilometers (5 miles) to provide access to the new site.

The JPL AAS Project Team reviewed and formally approved the antenna system design in January 1964, and the Rohr Corporation proceeded to the final detailed design for fabrication and construction (Milestone 14). At the same time, the placement of concrete for the pedestal and the optical instrument tower foundation was underway at the antenna site (Milestone 14).

C. COMPLETION OF THE ANTENNA

In April 1964, a Data System Development Plan document (Ref. 2) defining the total project scope to implement a complete station, including operational electronics equipment and site facilities, was published (Milestone 15). At the same time, the first fabrication of steel components for the antenna structure was begun. The concrete structural work for the pedestal and instrument tower was completed in June 1964. A diesel generator building for the provision of antenna power was completed in September, and a pump house and cooling tower facility adjacent to the antenna was completed in November.

Following a trial erection at the contractor's plant, the alidade structure was disassembled, transported to the site, and erected on the pedestal (Milestone 16). After the major structure of the alidade had been completed (with a mass of almost 900,000 kilograms or 2 million pounds of steel) a trial rotation about the azimuth axis on the hydrostatic bearing was made in early December 1964 (Milestone 17). This trial rotation was done with careful instrumentation of the hydrostatic bearing to validate the design parameters before proceeding further with erection of the parts supported by the azimuth bearing. Following the hydrostatic bearing test, erection of the elevation bearings and the tipping parts was started.

By April 1965, the control room on the second floor of the pedestal was sufficiently completed that the contractor could allow beneficial occupancy of that portion of the antenna. Installation of the station radio and data handling equipment was then started (Milestone 18). This installation was done under the immediate direction of Thomas Potter, JPL, who would be the operational station manager of the completed station.

The dual-elevation gear wheels and supporting structure and the tie truss between the two elevation bearings were completed in May 1965, and the building up of the reflector backup structure was started. By the end of July 1965, with the initial placement of the reflector panels (Milestone 19), the antenna, to a casual observer, appeared finished.

An unscheduled major event occurred in August 1965. Because of an error in setting the pressure control system in the hydrostatic bearing oil supply system, one of the azimuth hydrostatic bearing pads grounded and, with the additional rotations before the trouble was found, the bearing runner and pads were damaged (Milestone 20). (This is discussed further in Chapter V.)

Through the use of the capability designed for such an exigency, the alidade and reflector were jacked up (by that time, a load of 2,270,000 kilograms or 5 million pounds), the pads removed and remachined, the bearing runner was reground in place, and the azimuth bearing was returned to operations in approximately one month. This episode was a grim reminder of the importance of incorporating methods for repair of major mechanical components into the design of the facility.

In December 1965, the tipping parts were rotated under power, and the final setting of the reflector panels was started (Milestone 21). Final electrical power hook-up, installation of safety railings, electronic equipment installation, painting, and similar tasks continued until the dedication of the antenna and the new Mars Deep Space Station in April 1966.

D. INITIAL ANTENNA OPERATIONS

The first reception of signals by the antenna was on March 16, 1966 (Milestone 22), about 3 months less than 3 years from the signing of the contract with the Rohr Corporation and 3 months more than 6 years from the initial serious study of the communications and tracking needs which the antenna was destined to satisfy.

Within the accuracy provided by the initial measurements, which were made using a radio star, the gain of the antenna was greater than the minimum performance specifications, and the noise temperature was lower than that specified. The day following the initial radio signal reception, the Mariner 4 spacecraft, which was approaching solar occultation across the solar system from earth, was acquired and tracking — providing the first measurements of a coherent radio signal distorted by passage through the Sun's atmosphere.

E. DEDICATION OF ANTENNA AND STATION

On April 29, 1966, the antenna and station were formally dedicated by Representative George P. Miller, Chairman of the Science and Astronautics Committee of the U.S. House of Representatives (Milestone 23). Speakers at the dedication (Fig. 8) included Edmond C. Buckley, Associate Administrator of NASA's Office of Tracking and Data Acquisition; Dr. Lee A. DuBridge, President of the California Institute of Technology; Dr. Robert C. Seamans, Jr., Deputy Administrator for NASA; and Dr. William H. Pickering, Director of the Jet Propulsion Laboratory.

As part of the ceremonies, signals from the Pioneer 6 spacecraft were received by the antenna, processed by the station electronics, and played to the audience through the public address system. Following the dedication, spacecraft mission support by the station was started on a routine basis (Milestone 23).

F. "SHAKE-DOWN" OPERATIONS

About a month after the dedication, the Rohr Corporation and their subcontractors moved off the site (Milestone 24), essentially completing their part of the project. The major activities remaining were the critical maintenance support and additional training of the operations personnel; performance testing; and design and implementation of needed modifications to the antenna system and supporting facilities.

In the fall of 1966, the Mars Deep Space Station was connected into the Goldstone Complex commercial power network (Milestone 25), providing power for noncritical mission support activities at a lower cost than power generated on the site.

By the spring of 1967, it was evident that the azimuth hydrostatic bearing surface runner support was deteriorating. To keep the antenna operational until a permanent correction could be made, temporary shims were installed between the bearing runner and its backing sole plate (Milestone 26).

Because of spacecraft mission support requirements — particularly those of the Pioneer 6 spacecraft, which had gone beyond the range of the 26-m antenna network but was still functioning well — the station was put on a 24-hour, 7-day schedule in mid-1967 (Milestone 27). Except for periods of major upgrading and modification, the same operating schedule has continued since that time, in support of critical or special spacecraft mission requirements of the Surveyor, Lunar Orbiter, Mariner 1967 (Milestone 28), Mariner 1969 (Milestone 33), Pioneer and Apollo (Milestones 34, 35, 37) projects.

G. MODIFICATIONS FOR IMPROVED OPERATIONS

One major modification was the replacement of the grout under the hydrostatic bearing to solve the deterioration problem previously cited under Milestone 26. This was accomplished in a 6-week period early in 1969 (Milestone 32), after engineering studies had identified the cause of the problem, and a proper correction was designed. By careful planning of the regrouting sequence, limited support of the on-going cruise-phase Pioneer spacecraft and requested backup for the Apollo project were provided during the regrouting period.

Two significant changes have been made at the Mars Deep Space Station to take greater advantage of the antenna's capability. These are:

(1) In September 1968, all of the electronics equipment, including the antenna controls, were moved from the second floor of the antenna pedestal to a newly constructed separate control building (Milestone 31). This was done to allow for the considerably expanded tracking and communications electronic equipment required for the Mariner Mars 1969 mission (a good example of the difficulty of designing to accommodate for the flexible needs of electronic support equipment within the inflexible confines of an antenna structure).

(2) A multiple-Cassegrain feed configuration and high-power transmitter were installed in February 1970 (Milestone 36) to provide for the rapid reconfiguration and maximum capability of the radio frequency support mode as well as improved transmitting capability.

As the most advanced tracking facility of the DSN, the 64-m-diameter antenna has been vital to the support of increasingly advanced deep space communication and tracking concepts. Additional milestones in support of such activity are the first measurements of the antenna's X-band capability in January 1968 (Milestone 29) and the first use of the antenna as a planetary radar receiver (Milestone 30), as well as its use as a receiver terminal in the X-band "Goldstack" radar experiments (Milestone 38) and as a high-power planetary radar transmitter terminal (Milestone 39).

Full responsibility for all maintenance and operation of the antenna was transferred from the engineering organization to the operational organization on January 21, 1971 (Milestone 40).

IX. PHASE II – PROJECT MANAGEMENT AND CONTROL

A. PROJECT ORGANIZATION

Overall program management was under the cognizance of the NASA Office of Tracking and Data Acquisition. Responsibility for the project management was assigned to JPL. Figure 9 depicts the AAS Project organization as of April 7, 1964.

Within JPL, the Assistant Laboratory Director for Tracking and Data Acquisition, Dr. Eberhardt Rechtin, was assigned the task of ensuring the project implementation and performance commitment to NASA. Dr. Rechtin was assisted by his deputy, William H. Bayley.

The AAS Project Team was established within the JPL Telecommunications Division, under Walter K. Victor, and specifically in the Communications Elements Research Section, under Robertson Stevens. The team, comprising the necessary technical and administrative personnel for performance of the JPL role, was under the direction of the Project Manager, William D. Merrick. During the project period, Mr. Merrick simultaneously held the JPL line organizational assignment of Technical Group Supervisor.

Cognizant development engineers were assigned to each major component of the antenna and were responsible to the project manager for detailed engineering direction relating to the design, fabrication, installation, and testing in their assigned technical areas. Cognizant engineers maintained close liaison with each other to ensure complete integration of the various components and accomplished tasks as required at subcontractor plants or at the site.

A resident engineer was assigned to the Rohr Corporation during the detailed design and fabrication phases, and a resident engineer was assigned to the on-site location for engineering direction and technical monitoring of the work at that location.

Overall project schedule surveillance, progress reporting, maintenance of data and records, and preparation of plans and estimates were accomplished by a project administrator.

The project team represented many years of practical experience in all critical areas of engineering and administration. The following listing shows the individuals assigned and their areas of responsibilities. All of the individuals listed below contributed to the planning for additional 64-m-diameter antennas at overseas locations, and most of the individuals are presently engaged in the implementation of Phase III of the project (see Section VI).

Ronald D. Casperson	Cognizant engineer, pedestal, instrument tower, alidade, site facilities
Horace P. Phillips	Cognizant engineer, azimuth bearings and gears
Fred. D. McLaughlin	Cognizant engineer, azimuth and elevation drives, elevation bearings
Smoot M. Katow	Cognizant engineer, reflectors and backup structure
Kenneth P. Bartos	Cognizant engineer, quadripod feedcone structure and hoist
Robert J. Wallace	Cognizant engineer, servo and master equatorial
Houston D. McGinness	Analysis engineer, servo and master equatorial
Chris C. Valencia	Cognizant engineer, optics and measurement
David Ireland	Resident engineer at Rohr Corporation
Donald H. McClure	Resident engineer on site, Goldstone Complex
Philip D. Potter	Microwave design support
Paul C. Doster, Jr.	Project administrator

In accordance with established JPL procurement policies, a full-time contract administrator was assigned to the project team and was responsible for the administration of subcontracts relating to the project. Various contract administrators worked directly with the project technical team but were under the line supervision of the JPL Procurement Division. Marvin R. McClain, JPL Procurement Division, helped to set up contract arrangements for the Phase II effort. Contract administration was also accomplished by Gerard Tembrock.

Quality Assurance engineers, under Brooks T. Morris, were assigned full time to the project during the fabrication and installation phases. The conduct of their work was such that, although they worked directly with the project technical team, their line of supervision was under the JPL Quality Assurance Division, thus enabling independent objective evaluation of overall quality assurance aspects.

The following key individuals from JPL administrative organizations were assigned to support the project technical team and worked in the Project Office:

Wallace W. Lord	Contract Management
Joseph P. Frey	Quality Assurance Management

The Communications Engineering and Operations Section, under Richard K. Mallis, supplied the Mars Site operational facilities, not directly related to the design and construction of the advanced antenna system proper, and the DSIF receiving and data handling equipment.

Assistance, as required, was provided by all administrative and technical services elements of JPL and Caltech. Bruce Rule, who had also served as a consultant for the National Radio Astronomy Observatory's 43-m antenna at Green Bank, West Virginia, the CSIRO 64-m antenna in Australia, and the U.S. Navy's 183-m antenna at Sugar Grove, actively assisted the project in a consultant capacity from 1960 through completion at the Goldstone Complex. Consultants on specific analysis areas were utilized under short-term contractual arrangements.

B. MAJOR INDUSTRIAL PARTICIPANTS

Under the system management of JPL, many industrial firms from all over the United States were involved in the project. Rohr Corporation, Chula Vista, California, was the prime contractor for Phase II design and construction. Rohr's ability to undertake and successfully execute an advanced project such as the 64-m-diameter antenna under a fixed-price contractual arrangement is worthy of special recognition.

The engineering team of Rohr Corporation was organized under the Executive Vice President in Charge of Engineering, Frank E. McCreery. The project team was led by Robert D. Hall, manager of the Antenna Division. Major subcontractors, under Rohr, were:

Holmes and Narver, Inc. Los Angeles, California	Architectural and engineering design
The Rucker Company Oakland, California	Azimuth hydrostatic thrust bearing
Philadelphia Gear Corporation King of Prussia, Pennsylvania	Gears and drives
Kaiser Steel Napa, California	Radial bearing trucks
Precision Fabricators, Inc. Paramount, California	Alidade structure
National Steel & Shipbuilding Company San Diego, California	Elevation bearings
Dalmo-Victor Company Belmont, California	Servo and control system
William J. Moran Company Alhambra, California	General construction
Hawthorne Machinery Company San Diego, California	Power plant equipment
A. S. Schulman Electric Company Los Angeles, California	Electrical installation
H. F. Mowry, Inc. Costa Mesa, California	Electrical switchgear
Kilpatrick and Company Alhambra, California	Heating and ventilating

Industrial subcontractors supporting the JPL project in the development and implementation of equipment, facilities, and technical studies for the antenna included:

Blaw-Knox Company Pittsburgh, Pennsylvania	AAS feasibility study
The Franklin Institute Philadelphia, Pennsylvania	Theoretical analysis — azimuth hydrostatic thrust bearing
Donald R. Warren Company Los Angeles, California	Foundation and geophysical studies
Dana Construction Company Apple Valley, California	Mars Deep Space Station access road
Keuffel and Esser Company Hoboken, New Jersey	Reflector surface accuracy monitoring system
Collins Radio Company Richardson, Texas	Microwave communications link
Boller and Chivens South Pasadena, California	Master equatorial mount
Data Technology, Inc. Watertown, Massachusetts	Antenna encoders
Datex Corporation Monrovia, California	Master equatorial encoders
Kollmorgan Corporation Northampton, Massachusetts	Automatic auto-collimator and star tracker
United States Army Ft. Irwin, California	Logistics support
Bendix Field Engineering Corporation Owings Mill, Maryland	Maintenance and operations

Industrial subcontractors supplying DSIF station electronic equipment for the antenna included the following (this aspect of the station implementation, which is aside from the antenna system per se, is not described in this report):

Ampex Corporation Redwood City, California	Recording subsystem
Electro Optical Systems, Inc. Pasadena, California	Tracking data subsystem

Energy Systems Inc. Palo Alto, California	Transmitter subsystem
General Electric Company Oklahoma City, Oklahoma	Ranging subsystem
Motorola, Inc. Scottsdale, Arizona	Receiver subsystem
Rantec Corporation Calabasas, California	Antenna microwave
Resdel Engineering Corporation Pasadena, California	Frequency and timing subsystem
Scientific Data Sytems, Inc. Santa Monica, California	Station instrumentation

C. SCHEDULE EXPERIENCE

A steady pace was generally maintained in scheduled activities. A total of 33 months was required for the Phase II effort from the start of subcontractor design activity until the first operations of the antenna facility. Figure 10 summarizes the schedule experience.

D. UTILIZATION OF RESOURCES

1. Funds

The estimated costs for construction of the antenna that were envisioned at the outset of the project in 1960 were very close to the costs that were actually experienced in 1966. Table 1 summarizes, in rounded figures, the final costs in comparison with the original 1961 cost estimate of $15 million for the completed antenna facility.

2. Manpower

It is estimated that 102 JPL man-years were required for the planning, design, and implementation of the antenna facility. Considering the many subcontractors and sub-tier subcontractors involved in the project and the varied types of subcontractual arrangements, it is not possible to provide an accurate count of total man-years utilized in all of the crafts and skills provided. It is estimated, however, that the number was in the neighborhood of 300 man-years in the basic design, fabrication, and construction.

E. PROJECT REPORTING AND REVIEW

Project progress reporting was continuous throughout the project and provided information in the depth required for the NASA Office of Tracking and Data Acquisition and JPL management control and evaluation. Internal JPL weekly reports were prepared, based on material from each activity location and daily observation of each technical area. These reports covered the project progress and schedule situation in narrative and tabular form. Monthly narrative letter reports were provided by JPL to the NASA Office of Tracking and Data Acquisition, based on the weekly reports and on the evaluation of monthly reports submitted by the subcontractors. Report formats were kept as simple as possible, using photographs to show the progress and status. Expensive printing and excessive detail in reporting were avoided to minimize costs.

Schedule monitoring was based on simple forms: bar and activity block charts. The more complicated and computerized scheduling methods (Program Evaluation and Review Technique, or PERT) were used beneficially during the initial planning phases of the project but discontinued shortly thereafter.

Formal design and progress reviews, involving joint representation of NASA, JPL, and major subcontractors, were conducted at critical points along the schedule path. These points were (1) at the completion of the preliminary design, (2) at the completion of the concrete pedestal prior to steel installation, and (3) prior to azimuth and elevation axis rotations.

F. GENERAL ASPECTS

The following is a general discussion of some aspects of the project that are of potential value to future projects of a similar nature.

An excellent safety record was maintained throughout the project. Safe working standards and the use of safety equipment were closely monitored, both at fabrication locations and at the site. Although there were a few minor injuries in the course of constructing this major advanced facility, there were no serious accidents and no lives were lost.

During the antenna construction phase, on-site photographic surveillance was maintained for the purpose of security, safety, and documentation of the construction procedures utilized. Time-lapse photographs were taken daily by cameras located approximately 305 meters (1000 ft) from the antenna. Still photographs were taken at varied intervals of time, in accordance with the tempo and type of on-site activity.

No major union difficulties were experienced between JPL, major subcontractors, and labor unions. Some work delays were experienced because of conflicts between various trade unions in vying for work on this new type of facility, but in each case the difficulties were quickly alleviated by the subcontractors and the on-site resident engineer.

Because of the general interest in such a project, public information was considered highly important. All public releases by subcontractors were reviewed for technical accuracy by the JPL Public Relations Office and the Project Technical Team prior to approval for release. Although there were several releases by contractors involved, there were no known embarrassments to JPL, NASA, or the California Institute of Technology, and relationships with the contractors in this area were very good. These good relationships are believed to be the result of reasonable attentiveness to this aspect of Project activity.

As previously stated, informally annotated photographs, showing construction phase progress of the Project, were forwarded on a weekly basis to selected program management personnel to help them to understand and represent the Project. This simple procedure appeared to be a very useful communications tool.

To enhance the educational value of the antenna facility and its deep space mission support activity, a small area in the antenna pedestal was set aside for use as a museum and for public viewing. Since the dedication of the antenna, many civic organizations and school groups, as well as individuals, have visited the facility: an average of 150 people a month. Over 15,000 individuals have signed the guest register at the antenna. Considering that all who visit do not sign the register, the station manager's estimate is that this figure is low and that many more people, not normally involved in aerospace activities, have made the trip back into the Mojave Desert to see the 64-m-diamete antenna facility.

Table 1. Facility construction costs

Component	Cost
Feasibility studies and preliminary design	$ 850,000
Antenna pedestal and structure	10,920,000
Antenna servo system	760,000
Site development and utilities	280,000
Power generation and distribution	380,000
Antenna feed cone and handling	260,000
Support systems	270,000
Data system (master equatorial)	270,000
Design and engineering services	520,000
Subtotal	$14,510,000
Operations support building and associated facilities	445,000
Total	$14,955,000

YEAR	ACTIVITY	MILESTONE NUMBER	MILESTONE
1960 J F M A M J J A S O N D	JUSTIFICATION AND DEVELOPMENT OF BASIC PERFORMANCE SPECIFICATIONS	1	STUDY OF DEEP SPACE COMMUNICATION NEEDS THROUGH 1970 (SECTION III-A).
		2	INITIAL JUSTIFICATION AND BASIC PERFORMANCE SPECIFICATIONS COMPLETED. FUNDING ESTABLISHED FOR 1962 AAS (SECTION IV).
		3	AAS HARD-CORE TEAM ESTABLISHED (SECTION IV).
		4	FIRST ISSUE OF REF. 1 DESCRIBING AND SPECIFYING THE PROJECT (SECTION V).
		5	THREE-MONTH PHASE I FEASIBILITY STUDY CONTRACTS BEGUN (REF. 1, REV. 1) (SECTION VII-B).
1961 J F M A M J J A S O N D	FEASIBILITY STUDIES	6	ONE-YEAR PHASE IA EXTENDED FEASIBILITY STUDY BEGUN (SECTION VII-B).
1962 J F M A M J J A S O N D	DESIGN STUDIES	7	ITERATIONS ON BASIC ANTENNA CONFIGURATION TO SOLVE SYSTEM PROBLEMS (SECTION VII-C).
		8	PREPROCUREMENT/PROPOSAL CONFERENCES FOR PHASE II DESIGN AND IMPLEMENTATION (REF. 1, REV. 2) (SECTION VIII-A).
		9	PHASE II PROPOSALS RECEIVED FROM THREE FIRMS. ALL REJECTED BECAUSE OF HIGH COST ESTIMATES (SECTION VIII-A).
		10	REVISION OF REQUIREMENTS FOR PHASE II COMPLETE (REF. 1, REV. 3). NEW REQUEST FOR PROPOSAL ISSUED (SECTION VIII-A).
1963 J F M A M J J A S O N D	DESIGN STUDIES	11	PHASE II PROPOSALS RECEIVED, EVALUATION OF SOURCE EVALUATION BOARD PRESENTED TO NASA ADMINISTRATOR (SECTION VIII-A).
		12	PHASE II CONTRACT PLACED WITH ROHR CORP (REF. 1, REV. 4) (SECTION VIII-A).
		13	FACILITY SITE WORK (ROADS, FOUNDATION EXCAVATION) BEGUN (SECTION VIII-B).
		14	JPL GIVES FORMAL APPROVAL OF ROHR ANTENNA SYSTEM DESIGN, DETAILED DESIGN BEGUN. FOUNDATION CONCRETE PLACEMENT UNDER WAY (SECTION VIII-B).
1964 J F M A M J J A S O N D	DETAIL DESIGN / FABRICATION, ERECTION	15	REF. 2 ISSUED DEFINING COMPLETE ANTENNA, STATION FACILITIES, AND ELECTRONICS EQUIPMENT. STEEL FABRICATION UNDER WAY (SECTION VIII-C).
		16	ALIDADE ERECTION BEGUN (SECTION VIII-C).
		17	FIRST ROTATION ON HYDROSTATIC BEARING. ERECTION OF TIPPING PARTS BEGUN (SECTION VIII-C).
1965 J F M A M J J A S O N D	FABRICATION, ERECTION / ACCEPTANCE TESTING	18	INSTALLATION OF ELECTRONICS IN PEDESTAL CONTROL ROOM BEGUN (SECTION VIII-C).
		19	REFLECTOR STRUCTURE COMPLETED, SURFACE PANELS INSTALLED (SECTION VIII-C).
		20	AZIMUTH BEARING DAMAGE DISCOVERED AND REPAIRED (SECTION VIII-C).
		21	ELEVATION ROTATION ACHIEVED (SECTION VIII-C).

Fig. 4. Major milestones of the 64-m-diameter antenna project, 1960-1971

YEAR	ACTIVITY	MILESTONE NUMBER	MILESTONE
1966 J F M A M J J A S O N D	FABRICATION, ERECTION — ACCEPTANCE TESTING	22	FIRST RADIO SIGNALS RECEIVED AND TRACKED (SECTION VIII-D).
		23	FORMAL DEDICATION, INITIAL ROUTINE SPACECRAFT MISSION SUPPORT (SECTION VIII-E).
		24	ROHR CORPORATION OFF SITE. PROJECT ESSENTIALLY COMPLETE EXCEPT FOR MODIFICATIONS, CLEAN-UP ACTIVITY, AND WORK TO TRANSFER STATION FULLY TO OPERATIONS (SECTION VIII-F).
	OPERATIONAL USE, MODIFICATIONS		
		25	COMMERCIAL POWER SERVICE BROUGHT ON-SITE (SECTION VIII-F).
1967 J F M A M J J A S O N D	OPERATIONAL USE, MODIFICATIONS	26	CONTOUR SHIM ADJUSTMENT OF HYDROSTATIC BEARING (SECTION VIII-F).
		27	START 24-HOUR, 7-DAY WEEK OPERATION OF MARS DEEP SPACE STATION, SUPPORTING SPECIAL REQUIREMENTS OF SURVEYOR, LUNAR ORBITER, MARINER, APOLLO, PIONEER (SECTION VIII-F).
		28	MARINER 1967 ENCOUNTER (SECTION VIII-F).
1968 J F M A M J J A S O N D	OPERATIONAL USE, MODIFICATIONS	29	FIRST X-BAND MEASUREMENTS (72-dB GAIN) (SECTION VIII-G).
		30	FIRST USE AS PLANETARY RADAR RECEIVER TERMINAL (SECTION VIII-G).
		31	MOVE INTO NEW OPERATIONS BUILDING FOR MARINER 1969 SUPPORT (SECTION VIII-G).
1969 J F M A M J J A S O N D	OPERATIONAL USE, MODIFICATIONS	32	REGROUTED HYDROSTATIC BEARING (SECTION VIII-G).
		33	MARINER 1969 ENCOUNTER, EXTENDED MISSION PHASE START, APOLLO 11 MISSION SUPPORTED (SECTION VIII-F).
		34	
		35	APOLLO 12 MISSION SUPPORTED (SECTION VIII-F).
1970 J F M A M J J A S O N D	OPERATIONAL USE, MODIFICATIONS	36	TRICONE AND HIGH-POWER TRANSMITTER FACILITY INSTALLED. INCREASED CAPABILITY CABLE WRAP-UP INSTALLED (SECTION VIII-G).
		37	APOLLO 13 MISSION SUPPORTED (SECTION VIII-F).
		38	X-BAND "GOLDSTACK" RADAR EXPERIMENT (SECTION VIII-G).
		39	FIRST USE AS PLANETARY RADAR TRANSMITTER TERMINAL (SECTION VIII-G).
		40	FULL RESPONSIBILITY TRANSFERRED TO OPERATIONS ORGANIZATION FOR MAINTENANCE AND OPERATIONS (SECTION VIII-G).
1971 J F M A M J J A S O N D			

Fig. 4. Major milestones of the 64-m-diameter antenna project, 1960-1971 (contd)

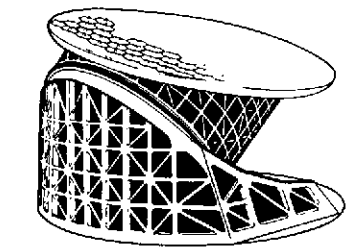

(a) ARRAY ON TRACK-OVER-AZIMUTH MOUNT

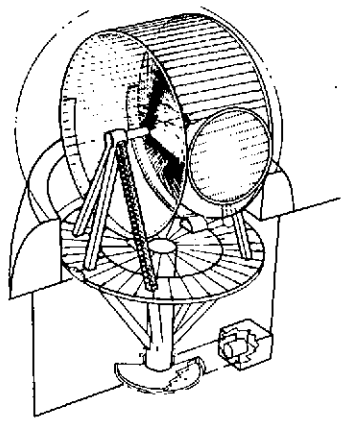

(b) HORN-LENS

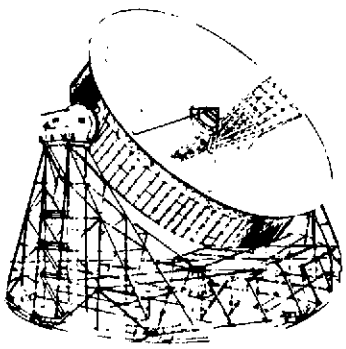

(c) MANCHESTER-TYPE MOUNT

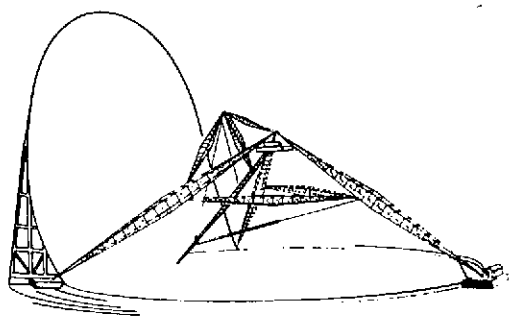

(d) EARTH BOWL (SPHERICAL)

Fig. 5. Four of 17 proposed antenna configurations

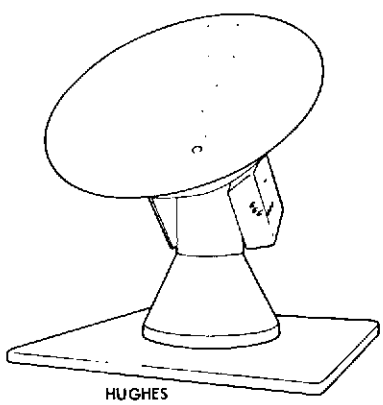

HUGHES

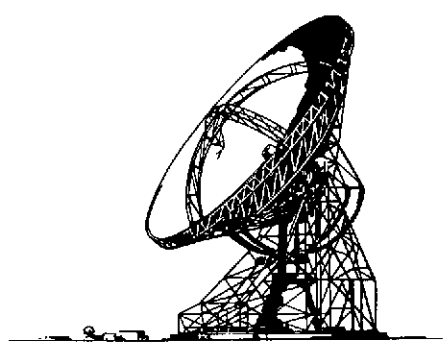

WESTINGHOUSE

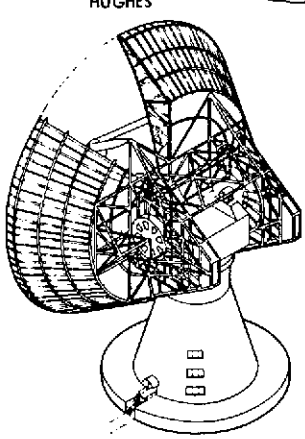

BLAW-KNOX

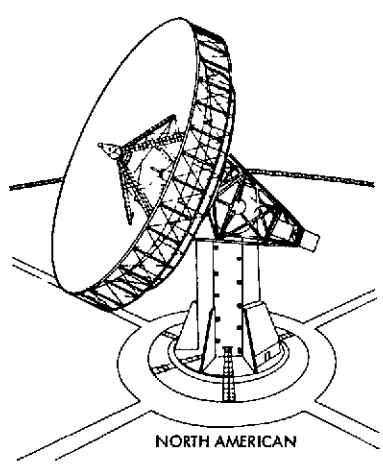

NORTH AMERICAN

Fig. 6. Antenna configurations resulting from funded study contracts

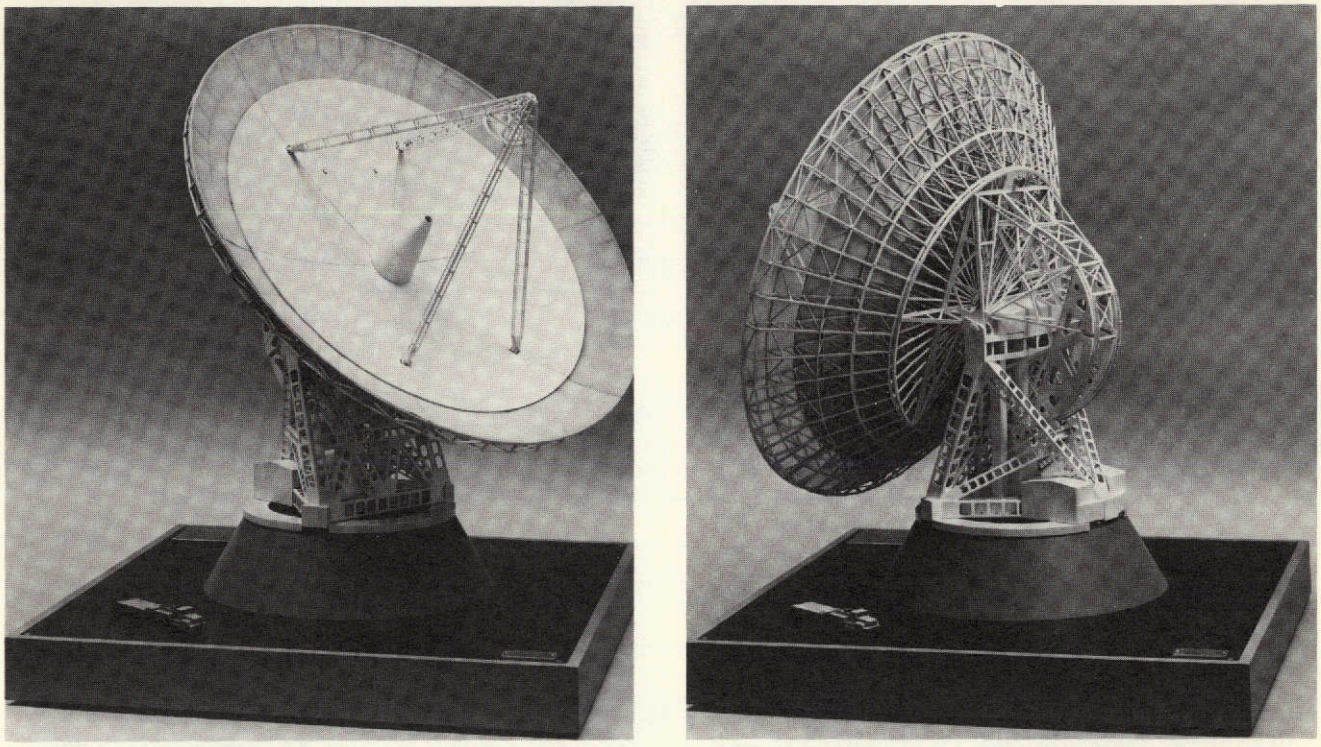

Fig. 7. Antenna model showing planned configuration at the completion of feasibility studies

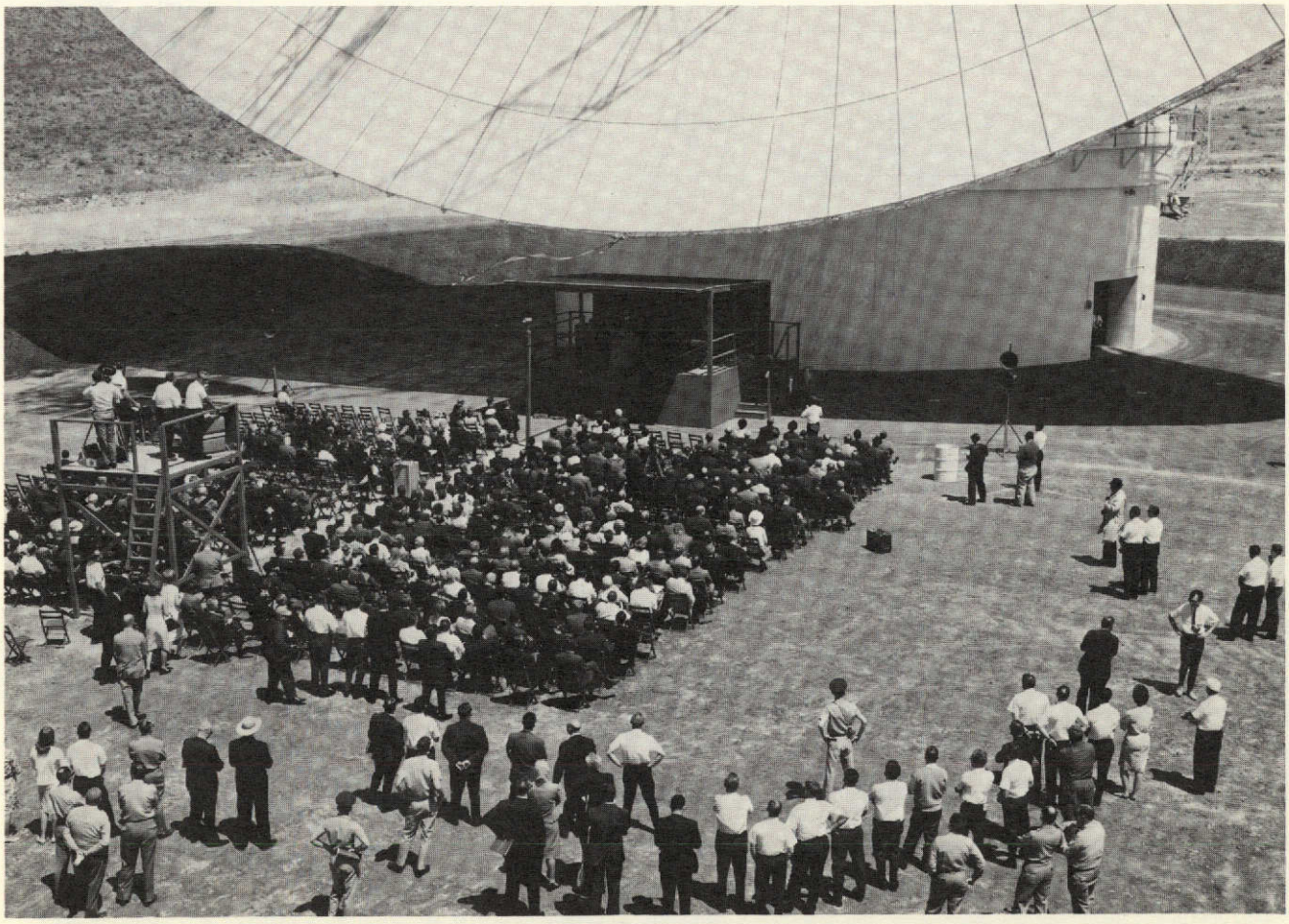

Fig. 8. Dedication of the 64-m-diameter antenna on April 29, 1966

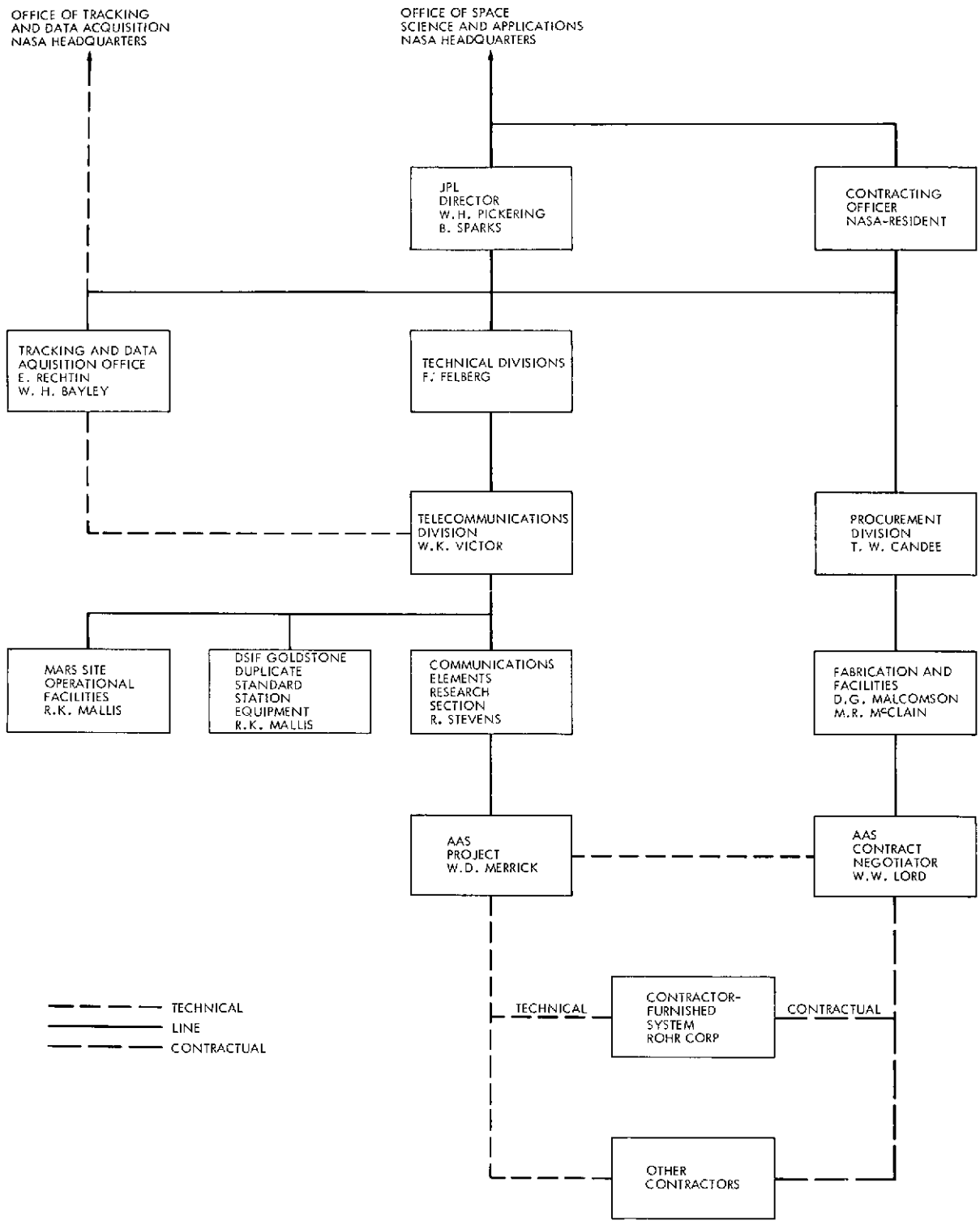

Fig. 9. The 64-m-diameter project organization for Phase II

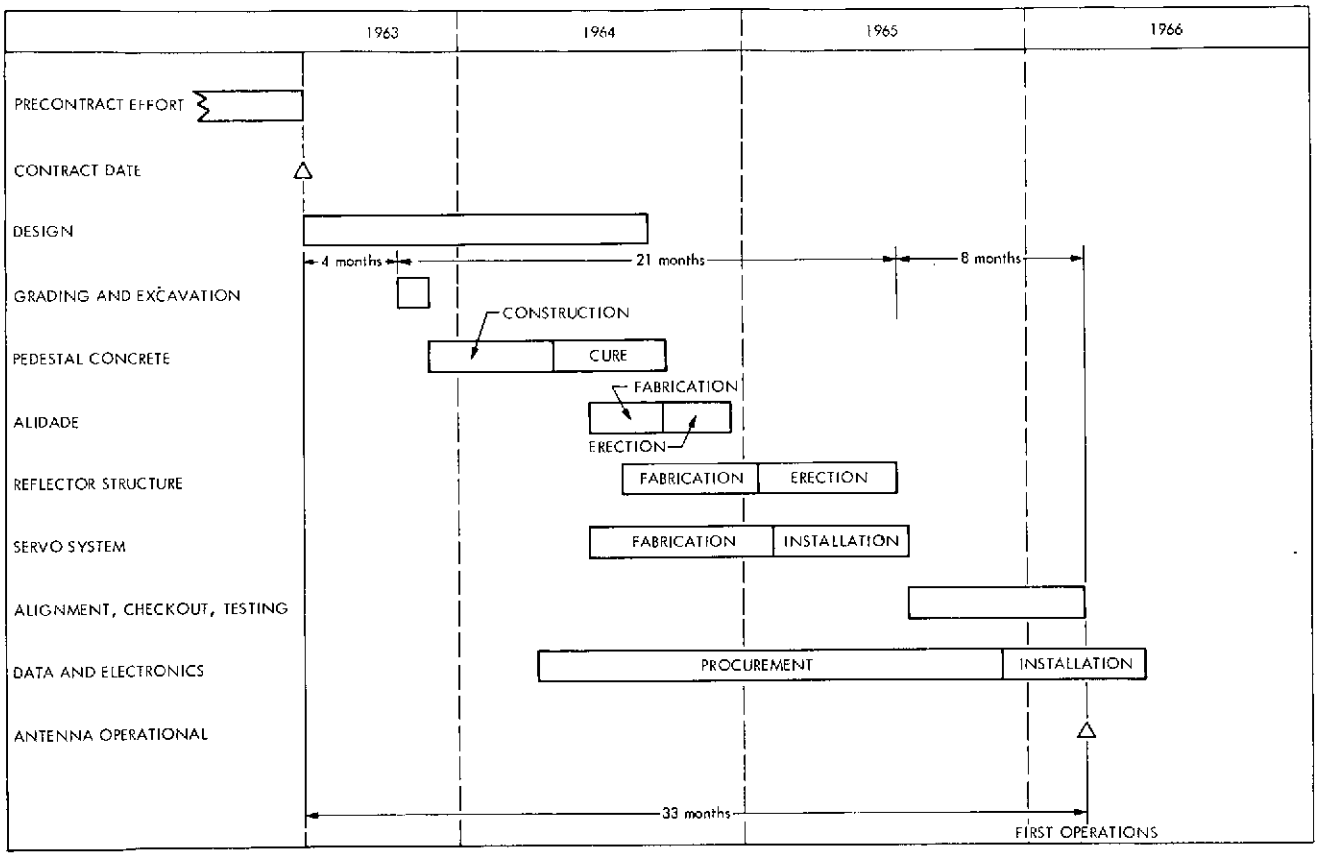

Fig. 10. Facility construction schedule experience

CHAPTER III. DESCRIPTION OF THE ANTENNA SYSTEM

In this chapter, an engineering description of the antenna system and its technical characteristics is provided. Supporting facility services are also briefly described.

I. GENERAL DESCRIPTION

The antenna has a 64-m-diameter paraboloidal reflector, with a focal length to diameter ratio of 0.42, on a fully steerable azimuth-elevation mount. The antenna uses Cassegrain microwave optics. At the normal DSN receiving frequency of 2.3 GHz, the half-power beamwidth of the antenna is 0.14 deg, the gain is 61.4 dB, and the total operating receiving system temperature at zenith can be as low as 16 K, depending on the microwave subsystem configuration. The antenna is designed to operate in the open-site environment at the Goldstone Complex and is not enclosed in a radome. The mount is capable of azimuth motion of approximately ±270 deg; its normal elevation operating range is +6 deg and +89 deg. The total weight of the antenna, including the pedestal, is 6,800,000 kg (15,000,000 lb). The steerable weight above the azimuth axis is 2,300,000 kg (5,000,000 lb).

Figure 11 shows the antenna at the time of initial operations, and Fig. 12 shows the antenna system's major components. A summary listing of the performance, operating characteristics, and specifications of the antenna system is contained in the Appendix.

II. PEDESTAL, INSTRUMENTATION TOWER, AND CABLE WRAP-UP

A. PEDESTAL BUILDING

The pedestal is a two-story, reinforced concrete building 25.3 m (83 ft) in diameter, with a diaphragm top which has a concrete collar in the center; the pedestal supports the movable structure of the antenna (Figs. 13-15). The wall thickness is 1.1 m (3.5 ft). Operational working space, equipment, and facilities are contained within the pedestal (Fig. 16). For initial operations, approximately 204.4 m^2 (2200 ft^2) of space on the second floor of the pedestal was used for the operational control room, which contained the station complement of electronics equipment (Fig. 17). In 1968, the antenna control and station electronics equipment were moved to a separate operations building to provide adequate space for the increased complement of electronics needed for advanced spacecraft mission support. The pedestal is discussed further in Chapter IV.

B. INSTRUMENT TOWER

An instrument tower supports a master equatorial optical instrument which provides the

reference for precision angle measurements of the primary reflector axis. The instrument tower is a hollow conical structure that extends through the center of the pedestal building and the alidade structure, but is isolated from both. The lower portion of the instrument tower is concrete and extends from 10.7 m (35 ft) below ground level to the top of the pedestal building. The upper portion is steel and extends to the level of the alidade top weldments, which carry the elevation bearings. The upper portion is completely enclosed in a wind and thermal shield, which is mounted on the alidade building and rotates with the alidade assembly. On top of the instrument tower wind and thermal shield is an enclosed and environmentally controlled room, where the master equatorial optical instrument is located. The purpose of the shielding and separate founding of the instrument tower is to provide a stable ground reference for the instrument. Additional information is contained in Chapter IV.

C. CABLE WRAP-UP ASSEMBLY

A cable wrap-up assembly carries water, coolants, electrical power, and electrical signals between the fixed pedestal and the rotating parts of the antenna (Fig. 18). It has a capacity of 60 large electrical (or fluid) lines. The fixed end of the cable wrap-up assembly is attached to the second floor ceiling of the pedestal; the rotating end is attached to the alidade building roof beams. The azimuth rotation limit of the cable wrap-up is ±270 deg. Details of this rather difficult design, problems encountered, and a later redesign are covered in Chapter V and Chapter VII.

III. ALIDADE AND MACHINERY

A. ALIDADE

The alidade, central structural element of the antenna, is a large, framed pentahedron constructed of heavy steel, wide-flanged structural shapes and structural plate (Figs. 19-21). The base of the alidade structure is triangular. The two top weldments of the alidade structure support the elevation bearings, which mount the antenna's primary reflector. Azimuth and elevation drive system gear reducers and an alidade building are also on the alidade. The alidade was the limiting structural element in the overall antenna system dynamics; details of the design and analysis techniques used are presented in Chapter IV.

The alidade building is used to house equipment required for the rotating structure and provides approximately 209.03 m^2 (2250 ft^2) of enclosed area for test equipment and machinery (Fig. 22). The test equipment room was designed to permit the addition of another room directly above it. With installation of a higher-power transmitter, cooling water pumps are now enclosed in a room at this location.

B. AZIMUTH HYDROSTATIC THRUST BEARING AND RADIAL BEARINGS

The azimuth bearing configuration uses a hydrostatic thrust bearing and radial roller bearings. The azimuth hydrostatic thrust bearing, set on the pedestal top, supports the full weight of the moving parts of the antenna (2,300,000 kg, or 5,000,000 lb) and permits very-low-friction azimuth rotation on a pressurized oil film. Three movable pad-and-socket assemblies float on the oil film over a stationary runner and support the three corners of the alidade base triangle (Fig. 23). The stationary runner for the bearing and the three bearing pads are completely enclosed in an oil reservoir.

Two hydraulic precharge units, an oil-conditioning network, three high-pressure power units, and associated interconnecting piping supply pressurized oil to cavities in each bearing pad to float the pads on the runner (Figs. 24-26). The hydrostatic thrust bearing presented a difficult and critical task for the project – the design and analysis are described in Chapter IV – and modifications to correct implementation difficulties are described in Chapter VII.

The azimuth radial bearing is a rolling element bearing consisting of a steel runner and a hardened wear strip mounted around the concrete pedestal collar, with the rollers mounted vertically in three truck assemblies (Figs. 27-29). The truck assemblies are attached radially to the alidade base triangle corner weldments at 120-deg intervals about the azimuth axis and project inward from the corner weldments to the radial bearing runner mounted on the pedestal collar. Each truck assembly has two rollers, supported top and bottom in antifriction bearings. The rollers bear on the wear strip attached to the runner face. The trucks are preloaded radially inward to apply sufficient force on the pedestal collar to eliminate lateral motion under maximum operating wind loads. Further discussion is contained in Chapter IV.

C. ELEVATION BEARING ASSEMBLIES

Elevation motion is provided by elevation bearing assemblies mounted on the two alidade top apexes (Figs. 30 and 31). These bearings support the weight of the antenna primary and secondary reflectors (1,100,000 kg or 2,500,000 lb), and the backup and quadripod structures. Each bearing assembly consists of two bearings, two split housings, supporting bases, a reflector support casting, associated shaft seals, and alignment and adjustment components (Fig. 32). The bearings are spherical, self-aligning roller "catalogue" items.

D. AZIMUTH AND ELEVATION DRIVES

The azimuth axis drive gear mechanization consists of four gear reducers with output shaft pinions driving on a large-diameter bull gear (Figs. 33 and 34). The azimuth gear reducers are fixed to and rotate with the alidade (Fig. 35); the bull gear is an annular ring mounted on the top of the concrete pedestal. The gear pinions walk around the stationary bull gear.

For the elevation axis drive, two semicircular bull gears are bolted to the rim faces of the elevation wheels, which are an integral part of the tipping reflector structure (Figs. 36 and 37). Gear reducers are mounted on the alidade.

The bull gears for both axes are segmented spur gears of L-shaped cross section to allow for a pinion back-up roller. Each segment is made from a forged ring gear blank welded to a mounting plate. The gear reducer has a welded steel housing, a four-stage internal gear reduction, an external final drive pinion and backup roller, and an integral pressure lubrication system (Fig. 38).

Electrically controlled hydraulic motors mounted on the gear reducers are used to drive the antenna about its axes. The support and control system uses two low-pressure and two high-pressure hydraulic power units; two control consoles; an oil conditioning network; brake assemblies; and electronic control and electrical power interfaces. Countertorque motors are mounted with the gear reducers to minimize the effects of gearing backlash. The high-pressure hydraulic system operates at 18.62×10^6 N/m^2 (2700 psi) and has 14.9×10^4 W (200 hp) available to each axis. Details of the drive gearing design are further discussed in Chapter IV and performance experience is discussed in Chapter V.

IV. TIPPING PARTS

The tipping parts of the antenna include a primary reflector backup structure, a primary paraboloidal reflector surface, a secondary hyperboloidal reflector surface, a supporting quadripod structure, a Cassegrain feed cone support, and an intermediate reference structure (Fig. 39).

A. BACKUP STRUCTURE OF PRIMARY REFLECTOR

The primary reflector structure is a 64-m-diameter paraboloidal space frame supported by a truss-type backup structure (Fig. 40). The space frame is a network of 48 rib-trusses radiating from the center hub and interconnected by a rectangular girder, intermediate rib-trusses, and ten circular hoop-trusses. The backup structure is formed by two elevation wheel trusses, supported and braced by a tie-truss (Fig. 41). Elevation wheel trusses support the elevation gear segments and counterweights to statically balance the tipping assembly about the elevation axis (Figs. 42-44). The backup structure is discussed further in Chapter IV.

B. PARABOLOIDAL SURFACE OF PRIMARY REFLECTOR

The surface of the primary reflector comprises 552 individual panels contoured from aluminum sheet and riveted to a precisely formed aluminum frame (Figs. 45 and 46). The panels are affixed to the reflector backup structure with adjusting screws which are accessible from the exposed surface of the reflector (Fig. 47); the design is such that loads in the backup structure are not transmitted into the surface panels. The panels form a solid reflecting surface over the inner half radius of the reflector and a perforated surface over the outer half radius (Figs. 48 and 49). Discussions are continued in Chapter IV and Chapter V.

C. QUADRIPOD STRUCTURE

The quadripod, which supports the subreflector, is a tubular space-frame structure of four trapezoidally shaped legs meeting in a large-apex space frame (Fig. 50). The four legs are supported at the hard points of the rectangular girder in the primary reflector structure. The quadripod also supports pulleys and/or hoists for handling the Cassegrain feed cones, the subreflector, or other heavy equipment being brought to or from the reflector. Further discussion is in Chapters IV and V.

D. HYPERBOLOIDAL SUBREFLECTOR

The subreflector is a precision hyperboloidal reflecting surface 6.1 m (20 ft) in diameter, with a 305-mm (12-in.) skirt for special optimization of the microwave feed system. The subreflector is a hub and backup space frame structure, with linear adjustment capability provided by remotely controlled electric motors and screwjack assemblies (Figs. 51 and 52). The subreflector is further discussed in Chapters IV and VII.

E. CASSEGRAIN FEEDCONE SUPPORT

The Cassegrain feedcone support is a large, three-module structure used to mount the actual feedcone and to support the radio receiver and transmitter equipment and ancillaries (Figs. 53-55). Module 1, an open-framed steel truss to allow optical surveys of the reflector surface, attaches to the center hub of the primary reflector structure. Module 2 is a framed, stressed-skin cylinder that provides a controlled environment area for microwave and electronics equipment. Module 3 is a framed, stressed-skin truncated cone that provides more controlled environment area for equipment. Module 3 also contains the Cassegrain feedcone adapter designed to permit use of any standard DSIF Cassegrain cone on the 64-m-diameter antenna (Fig. 56). Air conditioning equipment to control the environment in Modules 2 and 3 and in the Cassegrain cone is located in Module 1. The feedcone support is discussed further in Chapters IV and VII.

F. INTERMEDIATE REFERENCE STRUCTURE

An intermediate reference structure, designed to best define the true radio frequency axis of the primary reflector surface, is attached to the reflector center hub and centered on the reflector boresight axis. It is a steel truss structure. Further description of the intermediate reference structure is included in discussions of the angle data system in Chapter IV.

V. SERVO AND ANGLE DATA SYSTEM

A. SERVO AND ANGLE DATA

The servo system, for closed-loop steering of the antenna, is electrohydraulic: the inputs to the hydraulic motors that drive the gear reducers are controlled by electrically operated servo

valves (Fig. 57). Axis position and motor rate feedback are provided. The servo system input can come from the master equatorial assembly through an optical link, from radio-frequency-generated error signals, from ephemeris-controlled, computer-generated error signals, or from manual position or velocity slew commands.

A block diagram of the basic servo and angle data system is shown in Fig. 58. Key operating functions and parameters of the systems are shown in the Appendix.

Operational control and monitoring of the servo and angle data systems are provided from a console in the station control room. At this console are the controls and displays required for the servo and angle data system (Figs. 59 and 60), the hydrostatic thrust bearing, and the positioning of the antenna subreflector.

The servo control console also includes the control room displays of an area surveillance closed-circuit television system for sighting possible hazards to antenna motion, as well as a wind speed and direction display that provides information on environmental conditions.

The key to the precision pointing and angle determination capability of the antenna lies in a system consisting of the following major elements: the stable and independently founded master equatorial optical instrument, which is mounted at the intersection of the azimuth and elevation axes of the antenna; the intermediate reference surface, which is designed to accurately represent the orientation of the radio beam formed by the antenna reflector; and a precision optical link to relate the angular orientations of these two elements with each other. Further information on the antenna servo is contained in Chapters IV and V.

B. MASTER EQUATORIAL ASSEMBLY

The master equatorial assembly is a precision astronomical telescope-type mount which uses a mirror and an autocollimator to establish an optical line of site of accurately known absolute angular orientation (Fig. 61). Remotely controlled servo drive mechanisms provide rotation about its axes, and precision readouts make the orientation of the axes accessible. The motions of the mount are in hour angle and declination coordinates.

The intermediate reference structure optical assembly (Fig. 62) is mounted to the under side of the intermediate reference structure, which is attached to the reflector center hub structure. The intermediate reference structure is mounted and aligned in such a way that a collimated beam of light extending to a similar mirror attached to the rotating parts of the master equatorial assembly will coincide with the radio frequency boresight axis of the antenna reflector in any antenna attitude. Design and analysis of the master equatorial are detailed in Chapter IV.

C. ANGLE DATA ASSEMBLY

The angle data assembly uses two precision optical autocollimators – one prime and one backup. These autocollimators are mounted on the intermediate reference structure optical assembly. Each autocollimator assembly consists of optical elements that generate and project a collimated light beam onto the surface of a target mirror and then process the reflected light beam to produce analog direct current output signals proportional to the angular error between the projected and reflected light beams. This arrangement of automatic optical angle error sensing of the relative orientation of the intermediate reference structure and the master equatorial axis is used to provide closed loop tracking of the master equatorial by the antenna or of the antenna by the master equatorial depending on the desired operational mode. The angle data displays include decimal readouts of the position of the master equatorial axes in hour-angle and declination-angle coordinates, and a decimal readout in azimuth and elevation coordinates of the antenna reflector. The orientation of the master equatorial is shown in Fig. 63. Performance of the angle data system is discussed in Chapter V.

VI. SUPPORTING FACILITIES

Facility services needed to operate and maintain the antenna are integrated into the overall design. The following services and equipment are included: electrical power and distribution: heating, air conditioning and ventilating; water distribution; general and emergency lighting; fire protection; installed safety devices; sewer system grounding; and general support equipment. The isolated location of the 64-m-diameter antenna station, as well as the local terrain, is shown in Fig. 64. The antenna station plot plan is diagrammed in Fig. 65.

A. ELECTRICAL POWER AND DISTRIBUTION

Electrical power for the station was provided initially by three 500-kW diesel engine generator sets in a station power house that was designed to facilitate economical expansion. In November 1966, the station was connected to the Goldstone Complex power grid, providing a capability of 7,500 kVA at 2,400 V of commercially generated power to the site. The basic plan for power use is to utilize the more economical commercial power during periods of station operation and to use the locally generated power during critical mission periods. As of January 1, 1970, the on-site generated capability was 2000 kVA from four 500-kW engine generators.

The electrical distribution equipment for the antenna includes three electric power substations (two in the pedestal and one on the alidade); four motor control centers; two motor starters, controller and relay assemblies and high-voltage junction boxes for the 150-kW (200 hp) servo pump motors; and interconnecting cabling, wiring, and associated terminal junction boxes (Fig. 66).

Motor control center 3 is mounted in the station pump house near the pedestal, while motor control center 1 is mounted on the first floor of the pedestal building. One servo high-voltage junction box is mounted on the second floor of the pedestal building, and the other is in the alidade machinery room; the two servo high-voltage junction boxes are interconnected through the cable wrap-up assembly. The alidade machinery room also contains the servo motor pump controller assembly, relay cabinet and starter transformers, and motor control centers 2 and 2A.

Located downstream from the motor control centers are various terminal junction boxes for distribution of electrical power to specific use areas. Three-phase, 60-Hz electrical power is distributed at 120, 208, 480 and 2400 V. The electrical distribution equipment also includes circuit breakers interconnected to the servo control assembly and the angle data assembly components located in the control building control room.

B. HEATING, AIR CONDITIONING, AND VENTILATING

Heating, air conditioning, and ventilating for the antenna are provided by three contiguous networks of ethylene glycol coolant, chilled water, and conditioned air handling and distribution equipment; two evaporative cooler assemblies interconnected to domestic water distribution network at the antenna site; and exhaust fans placed in the outer walls of the alidade bilge area (Fig. 67). The cooling tower, which is part of the liquid coolant distribution networks, is mounted outdoors near the pump house. All of the equipment is high-quality commercial grade. The ethylene glycol coolant network is a closed loop consisting of two direct-driven, 15-kW (20-hp) pumps mounted within the pump house; a double-cell cooling tower; and insulated network piping and valving (Fig. 68). The network uses a coolant mixture of ethylene glycol and water. Through the network piping, the coolant network interfaces with condensers of the chilled water distribution network and with heat exchangers mounted near the hydrostatic bearing pads and the servo hydraulics.

The chilled water network is a closed loop consisting of two coolant-cooled reciprocating chillers with tube-type condensers, refrigerant compressors, associated electric motors, and control valving and gages located within the pedestal building, along with an insulated network of piping and valving (Fig. 69). Through network piping, the chilled water distribution network interfaces with three air-handling units which are mounted on the first floor of the pedestal, atop the alidade building, and in module 1 of the Cassegrain cone support structure. The nominal temperature of the chilled water is 4.4 to 10°C.

The conditioned air handling network is contiguous to the chilled water distribution network and consists of three large air handling units and associated ducting. The ducting extends to all work areas throughout the antenna structure to provide conditioned cooling or heating air for personnel and equipment. Electrical filament heaters with associated fans, controls, and thermostats are mounted within the ducting. The air conditioning, heating, and ventilating equipment also includes an evaporative cooler mounted on the roof of the alidade building and exhaust fans located in the alidade bilge area.

Because of its severe environmental requirements, the master equatorial room has a separate air-conditioning system, which includes self-contained air-conditioning networks with associated automatic controls and ducting. The two networks are independent, except for the ducting, to provide complete backup protection. Electrical filament heating components are mounted within the ducting. One of the two networks operates at all times to maintain an ambient temperature within the room of 21 ± 1°C. The operation and status of the air-conditioning equipment is monitored remotely at the angle data assembly master equatorial control panel within the operations and control building control room.

C. DOMESTIC WATER SYSTEM

The antenna's domestic water system, used for amenity purposes, consists of hot and cold water plumbing with flow-control valving and pipeline vibration isolators. The water distribution network, which is gravity-fed and interfaces with the Goldstone Complex water system, extends to the pump house, the cooling tower, the pedestal, and, via the flexible hoses in the cable wrap-up assembly, to various locations on the alidade (Fig. 70).

D. GENERAL AND EMERGENCY LIGHTING

General lighting on the pedestal and antenna is provided by standard incandescent lights, flood lamps, and quartz-iodine lamps mounted externally on the antenna structure. The pedestal building and all structural elements are sufficiently lighted so that the surveillance television cameras can be effective at night. The general lighting equipment also includes double-weatherproofed, aviation-type obstruction light fixtures, with two aviation red globes each, mounted at the perimeter of the primary reflector surface at 90-deg intervals and at the apex of the quadripod.

There is emergency lighting equipment inside the pedestal and alidade buildings and at various locations about the antenna structure. Each unit is a packaged rechargeable storage battery type with two sealed-beam, 25-W lamps. Units mounted outdoors are weatherproofed.

E. FIRE PROTECTION

Comprehensive fire alarm and fire-control water distribution networks are incorporated in the antenna facility (Fig. 71). Fire extinguishers are also mounted throughout the antenna pedestal and structure and in the pump house.

The fire alarm network includes two fire alarm stations, 29 smoke-sensitive detectors, and five manually operable fire alarm boxes. The fire alarm stations are provided with red and white indicating lights, override controls on the

antenna operation, vibrating warning buzzers, safety climbing belts, and a portable emergency electrical power pack. One fire alarm station is in the pedestal second floor near the office area; the other is in the alidade control room. The fire alarm stations are connected to the smoke-sensitive detectors and to the manually operable fire alarm boxes.

The smoke detectors are ionization-type units mounted on the ceilings and under the floors of work areas in the pedestal, on the ceilings in the alidade building, and within the air conditioning ducting. The ceiling-mounted detectors have integral red indicating lights; the under-floor and ducting detectors are interconnected to red indicating lights at the associated fire alarm station. The manually operable fire alarm boxes are mounted throughout the antenna structure.

The fire water distribution network includes ceiling-mounted fire sprinklers, fire hoses, an auxiliary pump to increase water pressure, and associated controls, piping, and valving. The fire sprinklers are located in all enclosed work spaces in the pedestal and alidade areas, and the fire hoses are mounted in steel cabinets about the antenna structure. Fire extinguishers are mounted within the fire hose cabinets and on the walls within enclosed areas. All user fire protection equipment is painted bright red and is in well-lighted locations.

The overall Goldstone Complex fire system is supervised from the Echo Deep Space Station.

F. INSTALLED SAFETY DEVICES

To protect personnel and equipment on the antenna structure, there are many permanently installed safety devices, including vibrating-type antenna rotation warning horns, electrical grounding equipment, handrails, caged stairways, and warning signs indicating hazardous areas. Emergency antenna stop pushbuttons are mounted to the electrical and hydraulic assemblies and at key locations throughout the antenna structure. An emergency stop bar is mounted to the front of the rotating stairway.

Obstruction and rotation lighting devices are mounted on the antenna structure. Standard black-line telephones are placed at key points in the pedestal and on the structure, and there is a loudspeaker network used to notify all personnel that the antenna will be activated or shut down, or of any emergency situation.

G. GENERAL SUPPORT EQUIPMENT

The antenna support equipment consists of various electrical, pneumatic, and mechanical service hoists, an electric-motor-driven air compressor assembly, and a gas-operated steam cleaner assembly with interconnecting plumbing (Fig. 72). Some service hoists are permanently mounted to the antenna structure; others are capable of being attached to selected locations about the antenna as needed.

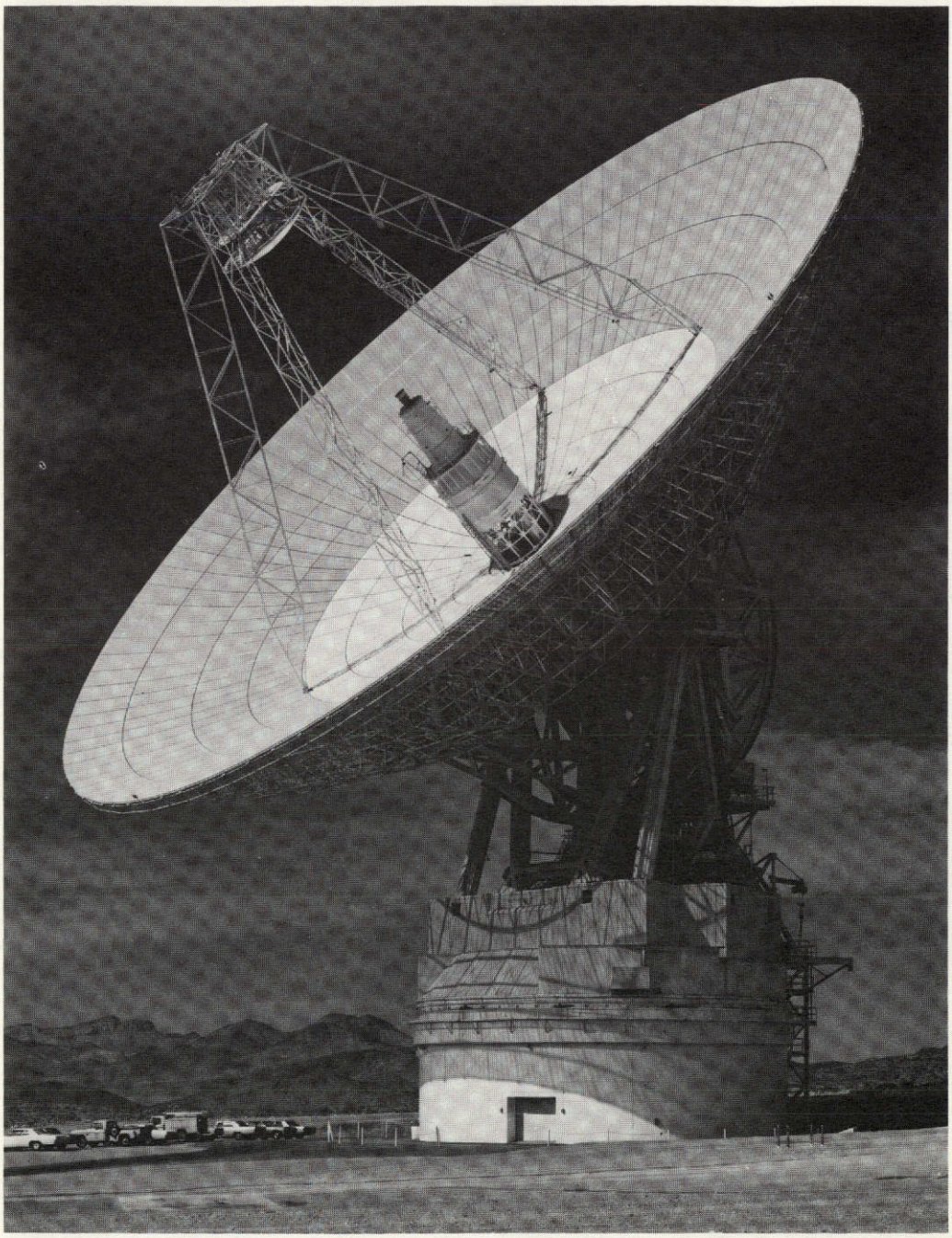

Fig. 11. The 64-m-diameter antenna at the time of initial operations

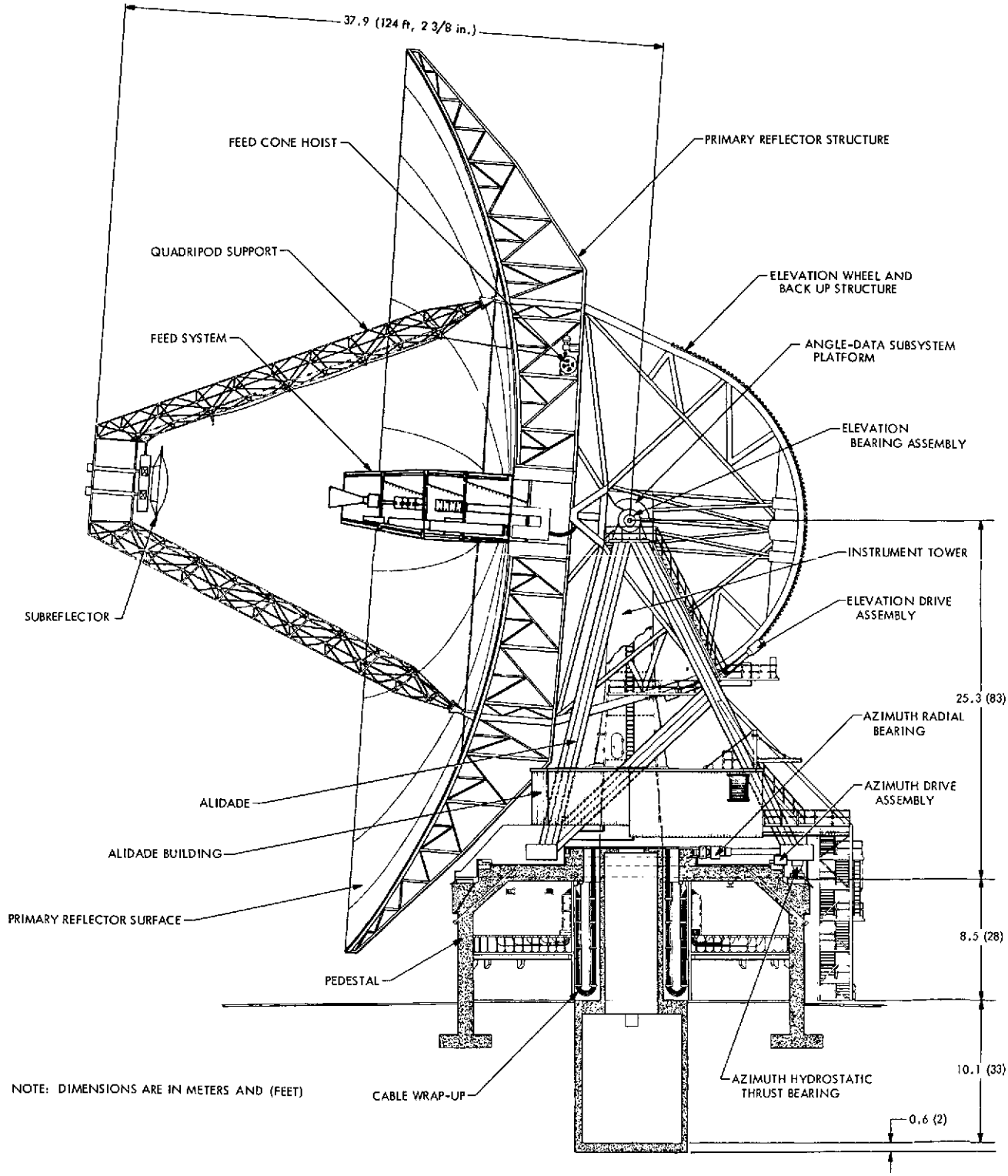

Fig. 12. 64-m-diameter antenna elevation, showing major components

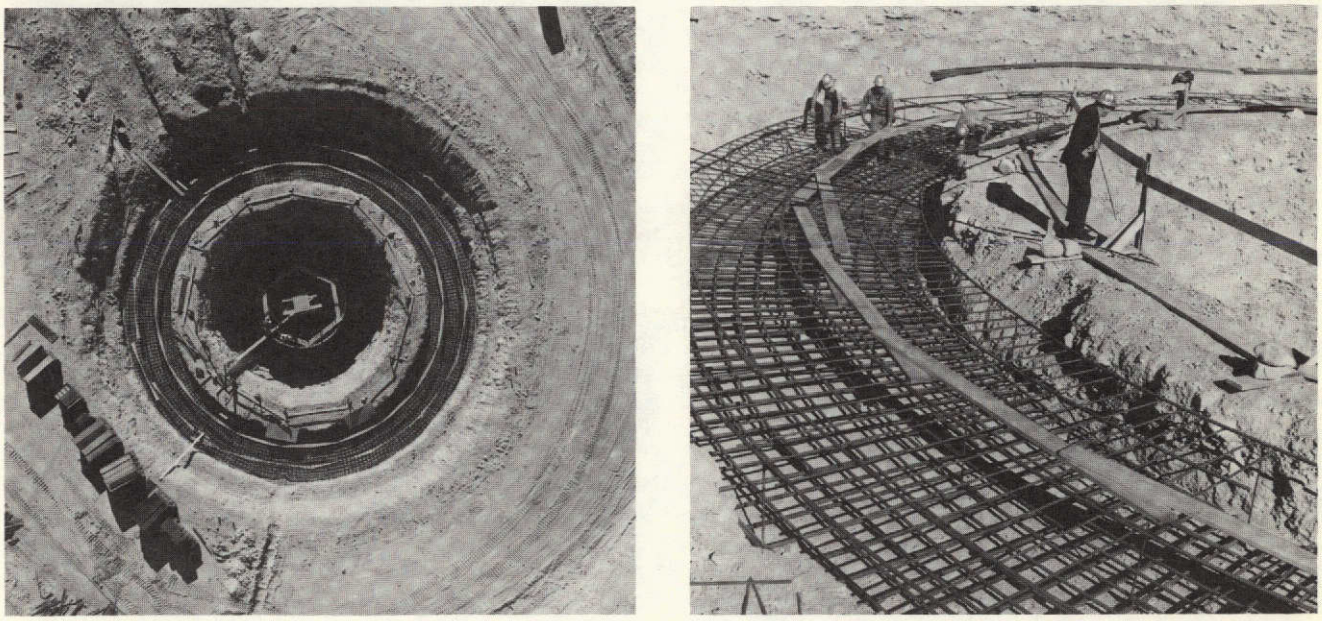

Fig. 13. Pedestal and instrument tower excavation (left) and initial reinforcing steel installation (right)

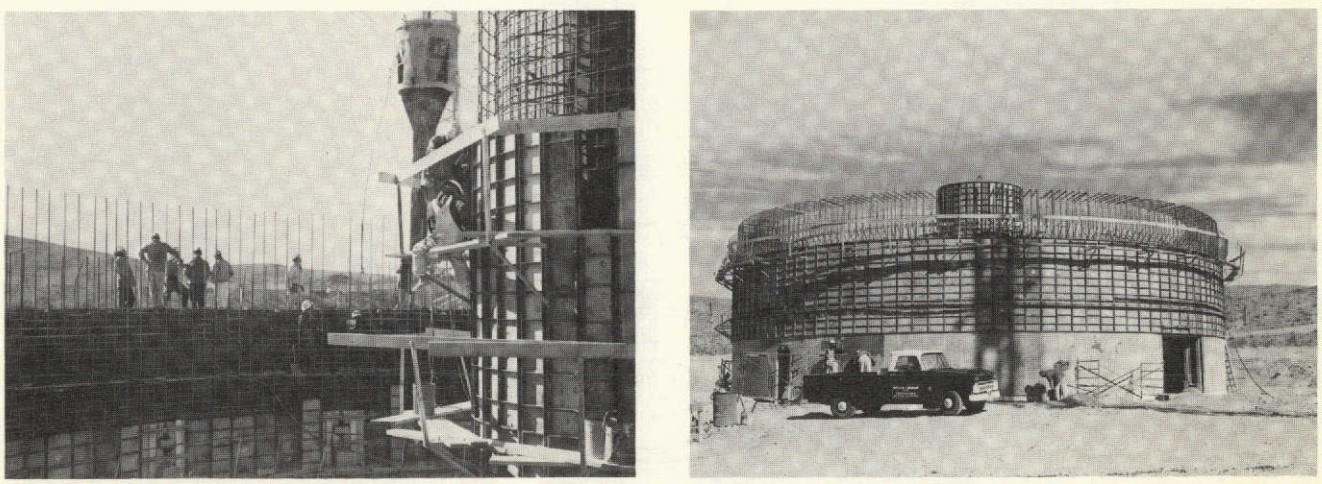

Fig. 14. Pedestal and instrument tower under construction

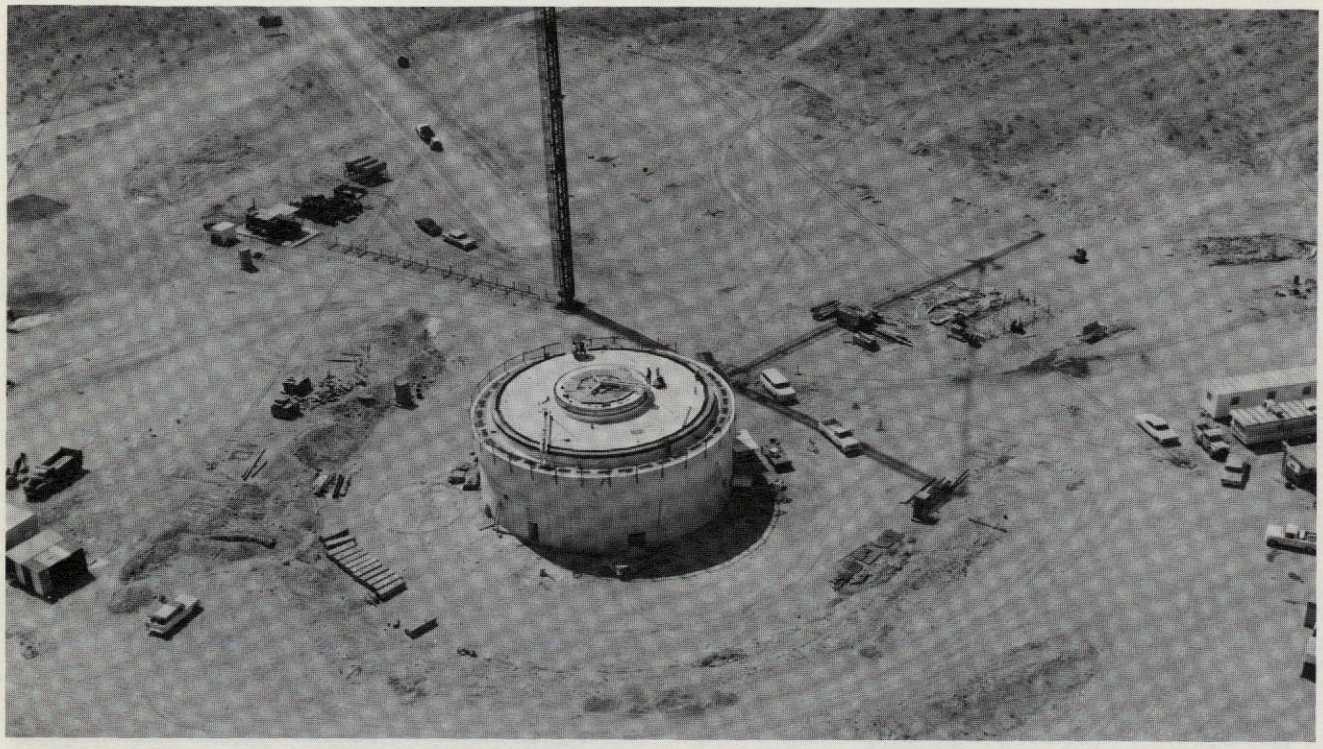

Fig. 15. Concrete pedestal building prior to the placement of heavy steel

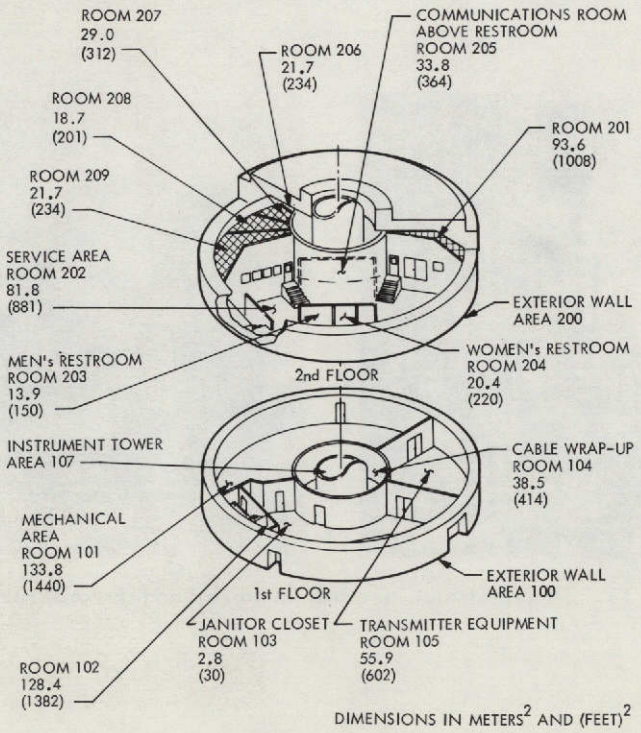

Fig. 16. Areas within pedestal building

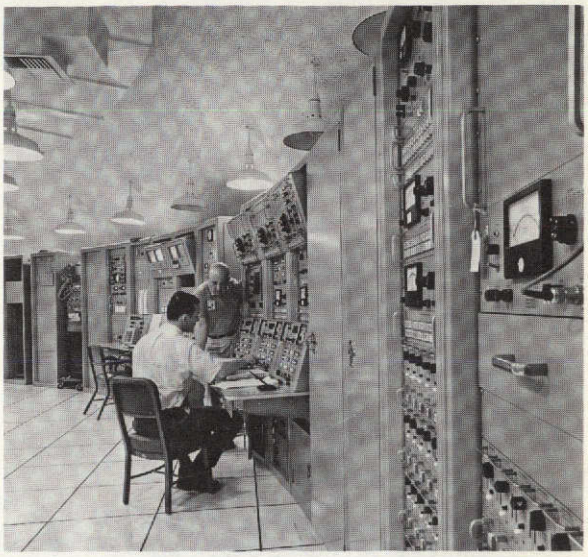

Fig. 17. Electronics equipment installed on second floor of pedestal during initial operations

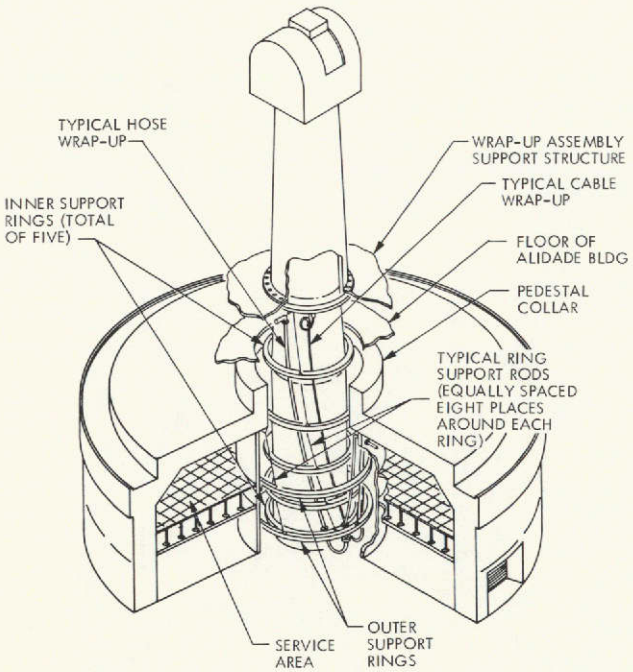

Fig. 18. Cable wrap-up assembly in relation to the pedestal, instrument tower, and alidade room

Fig. 19. Alidade during trial erection

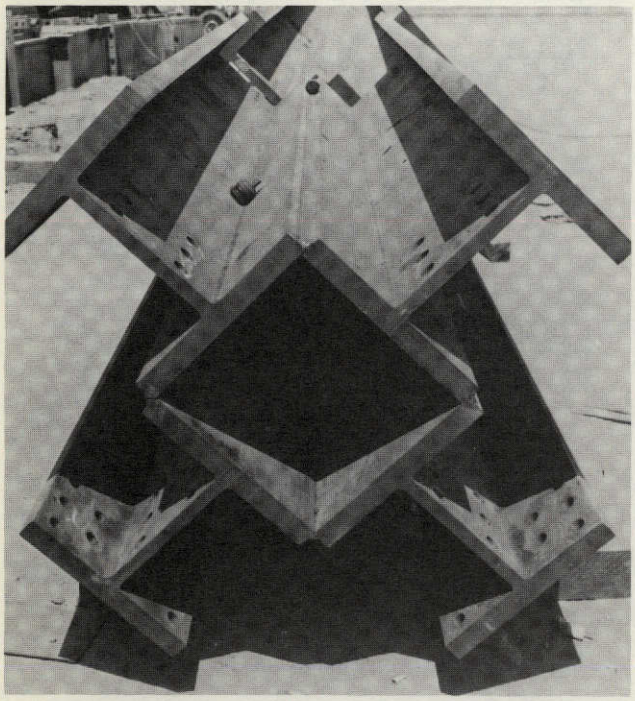

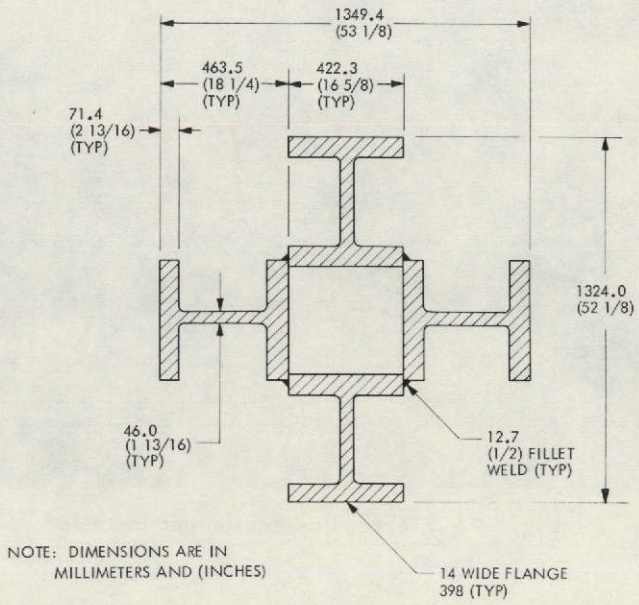

Fig. 20. Typical cross section of alidade member

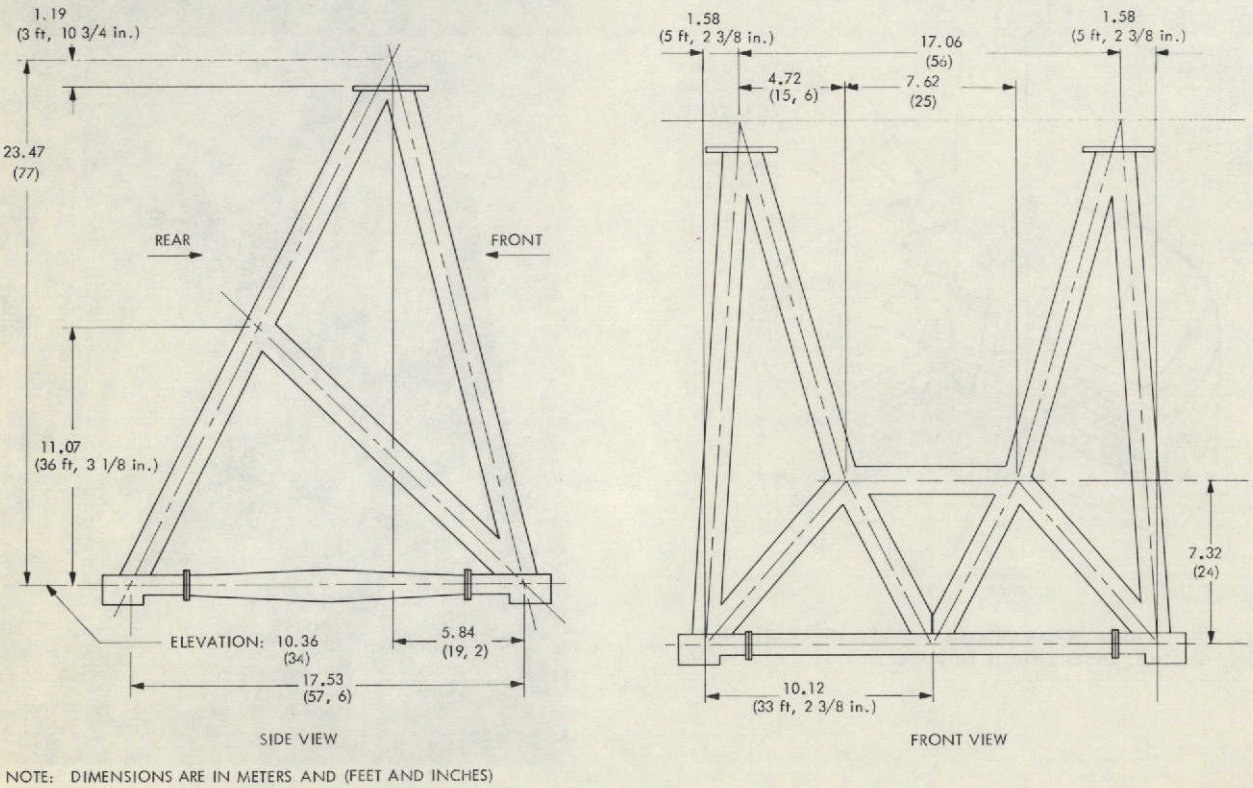

Fig. 21. Feedcone configuration during initial antenna operations

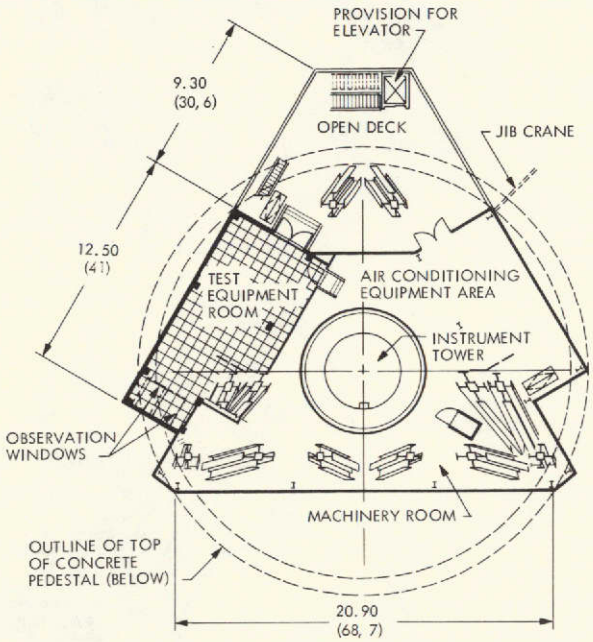

NOTE: DIMENSIONS ARE IN METERS AND (FEET AND INCHES)

Fig. 22. Areas of alidade building

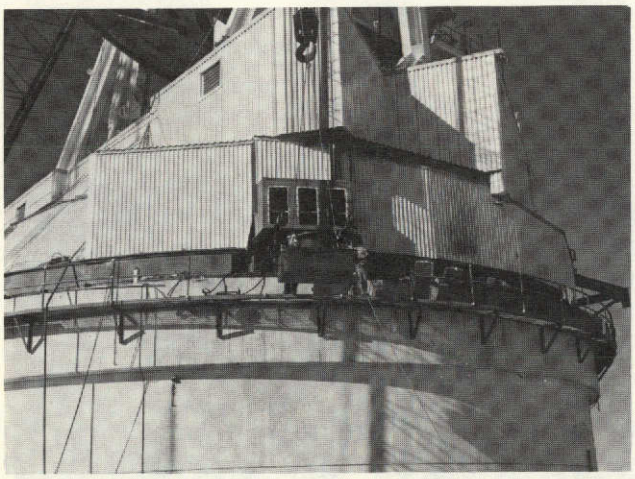

Fig. 23. View of alidade building and removal of hydrostatic bearing pad

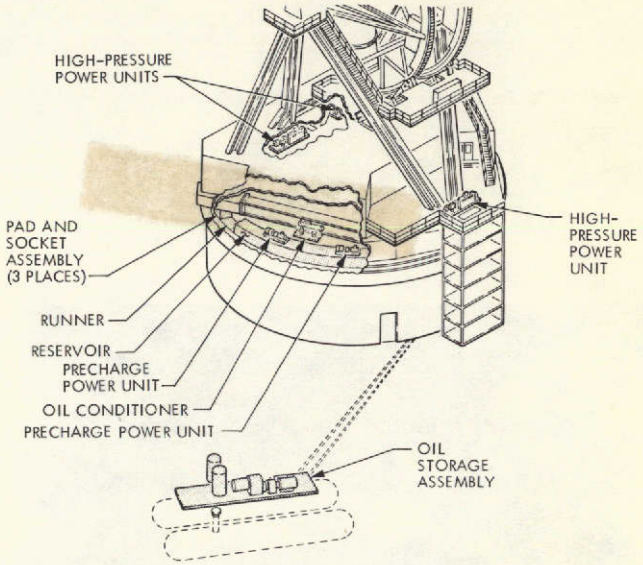

Fig. 24. Hydrostatic bearing assembly

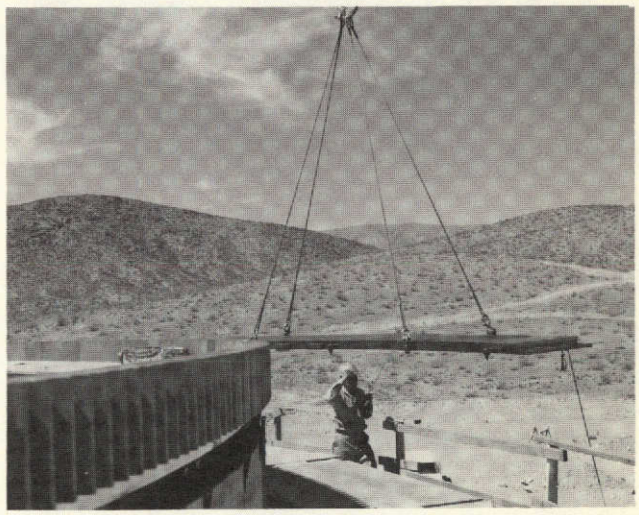

Fig. 25. Hydrostatic bearing runner being placed

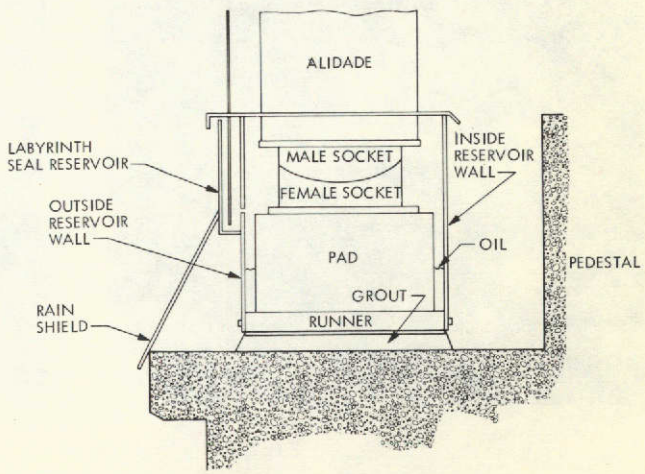

Fig. 26. Cross section of hydrostatic bearing runner and pad

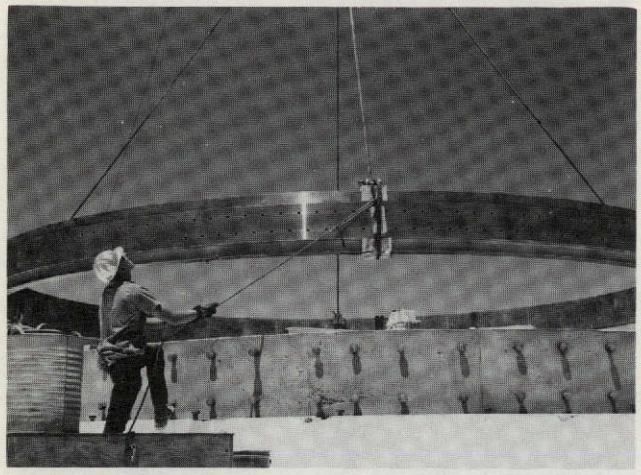

Fig. 27. Azimuth radial bearing runner being placed on pedestal collar

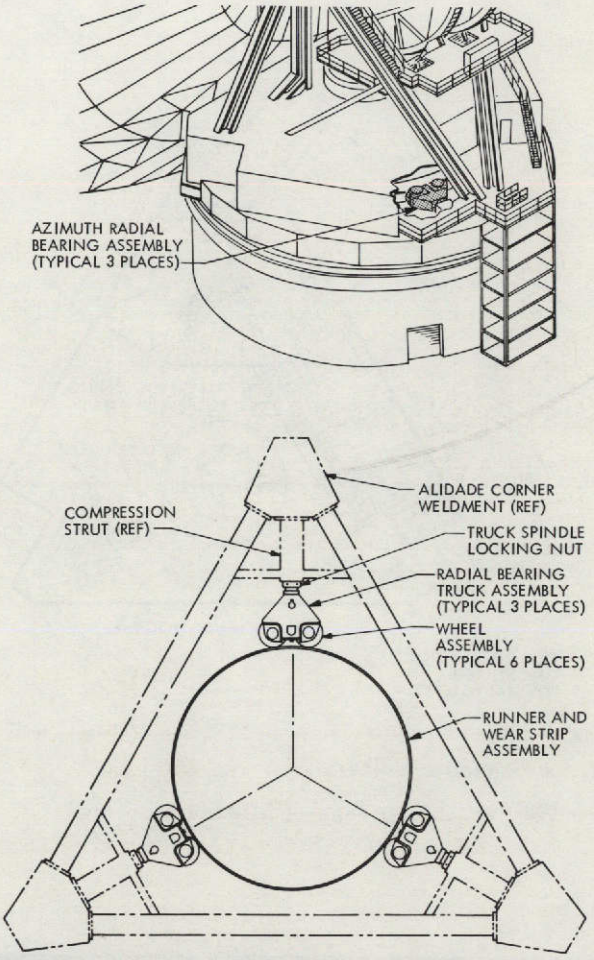

Fig. 28. Azimuth radial bearing assembly and components

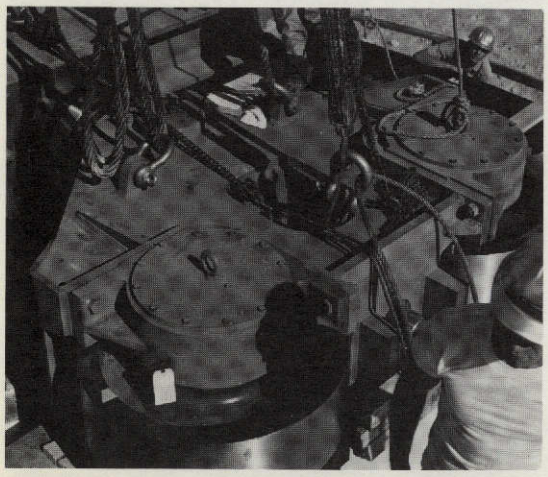

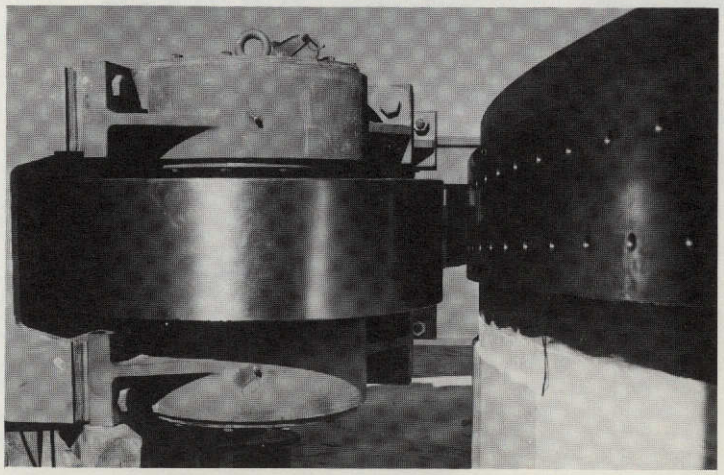

Fig. 29. Installation of the azimuth radial bearing

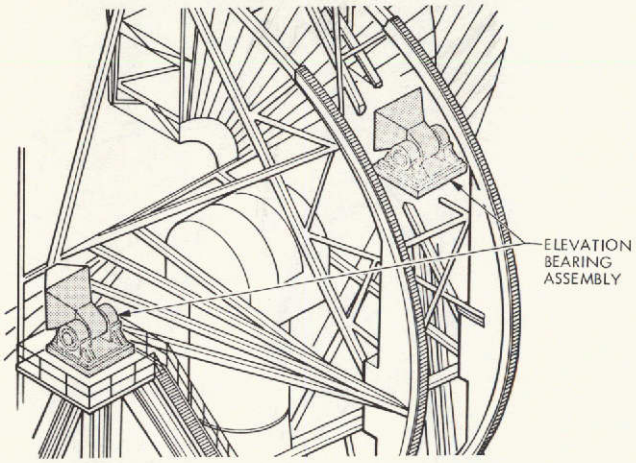

Fig. 30. Elevation bearing assembly

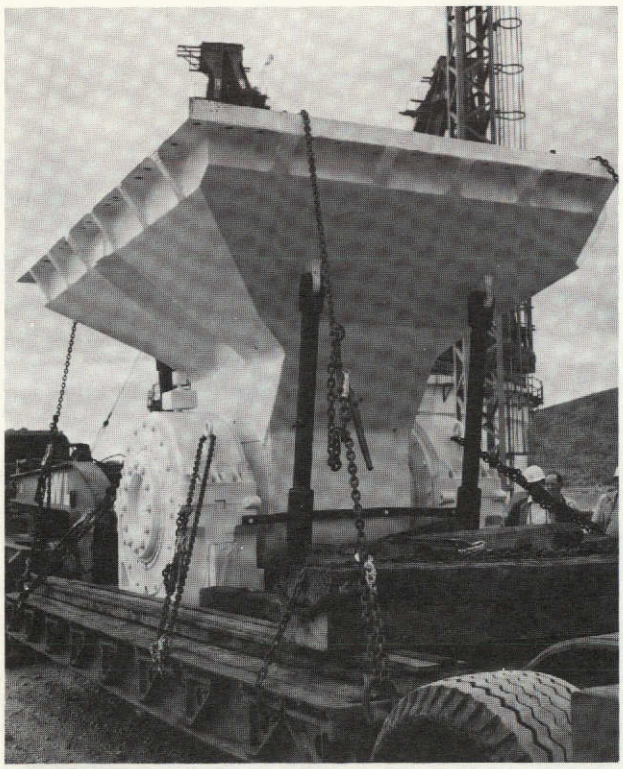

Fig. 31. Elevation bearing assembly being delivered to the work site

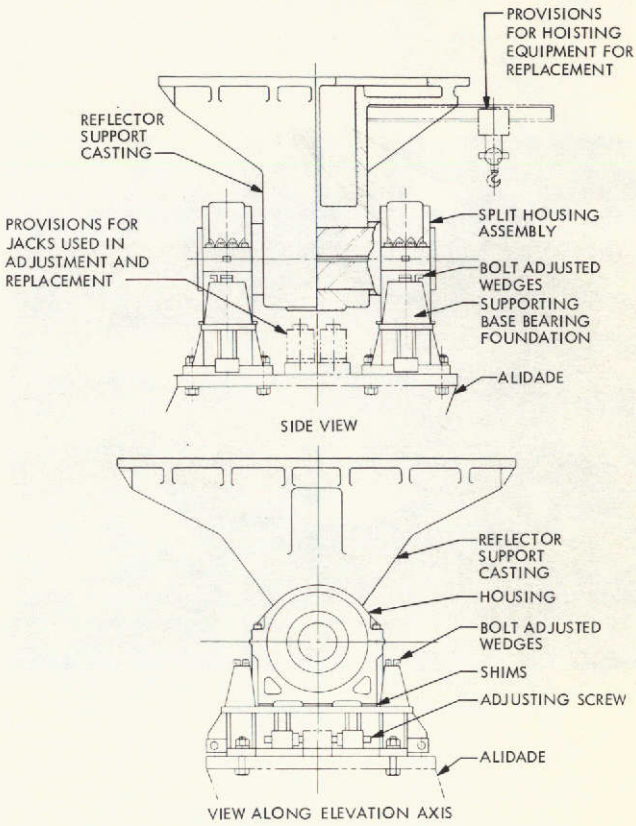

Fig. 32. Front and side view of the elevation bearing assembly

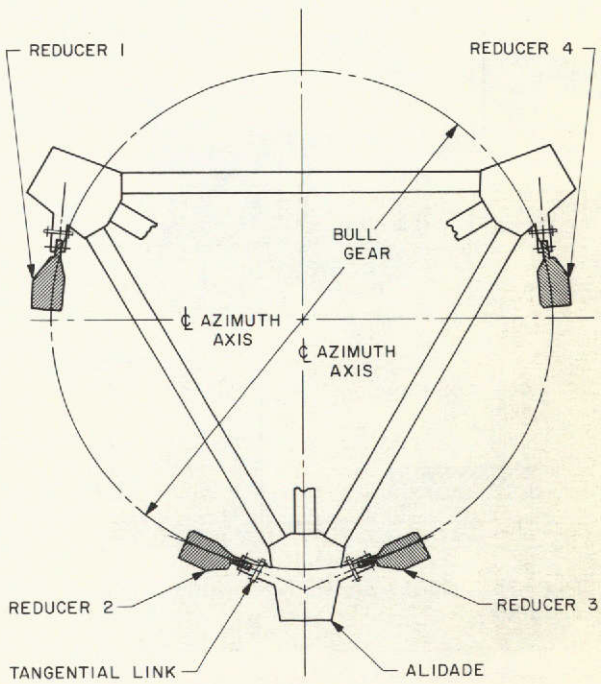

Fig. 33. Plan view of azimuth drive

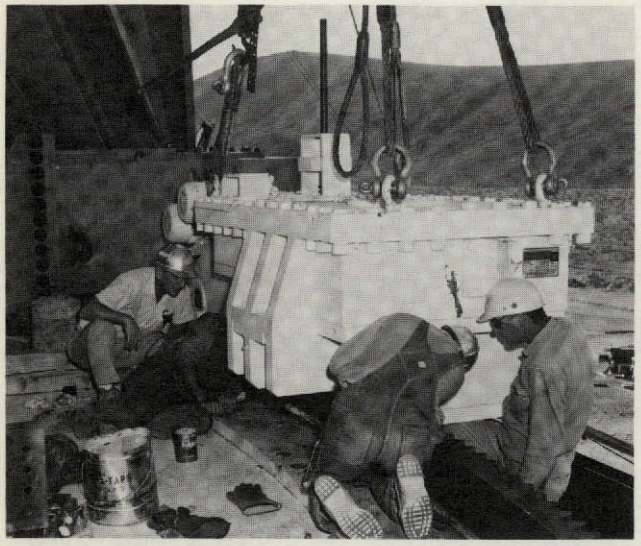

Fig. 34. Azimuth drive being installed

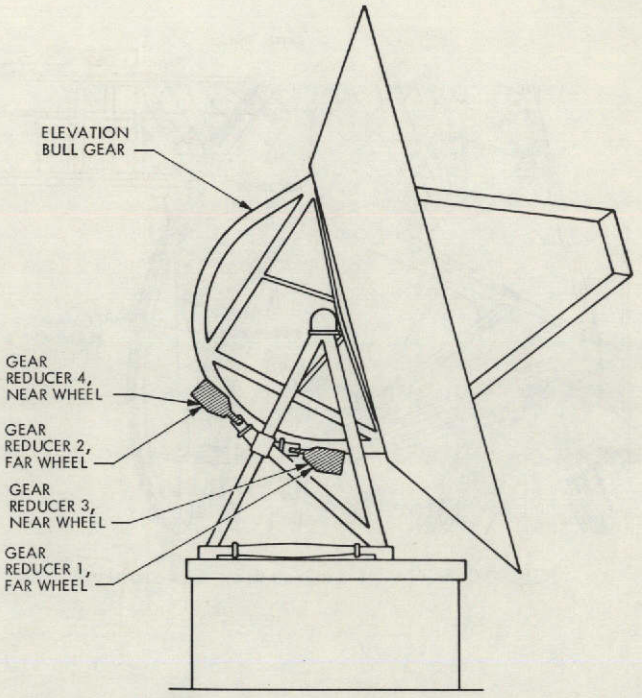

Fig. 36. Elevation drive locations

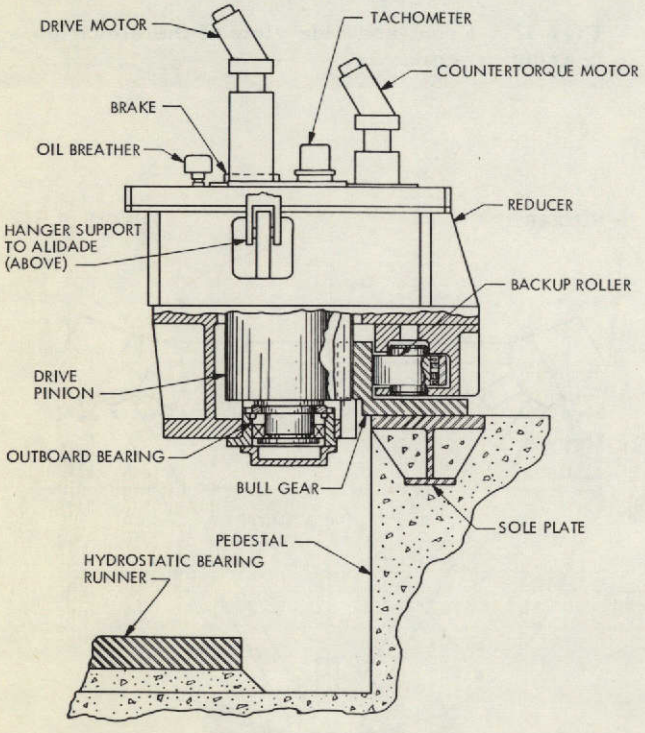

Fig. 35. Cross section of azimuth gear drive reducer

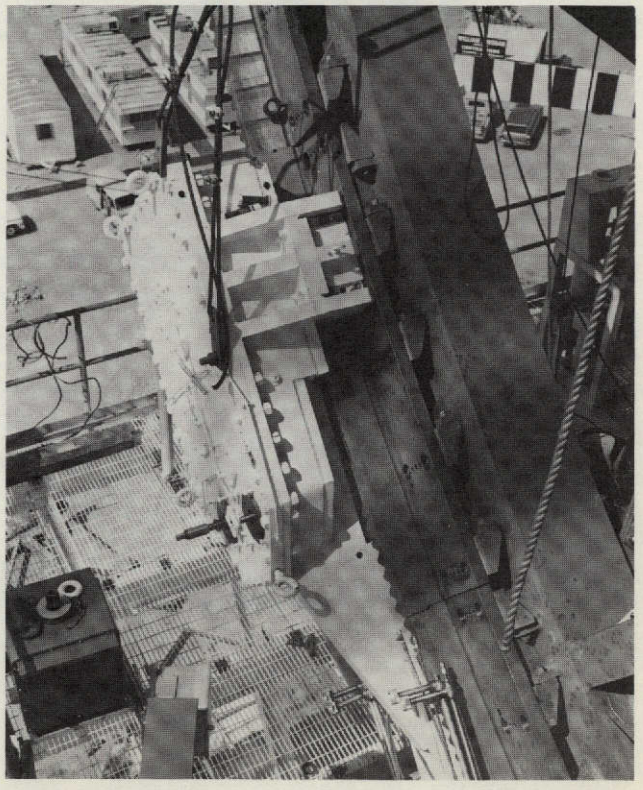

Fig. 37. Elevation drive being installed

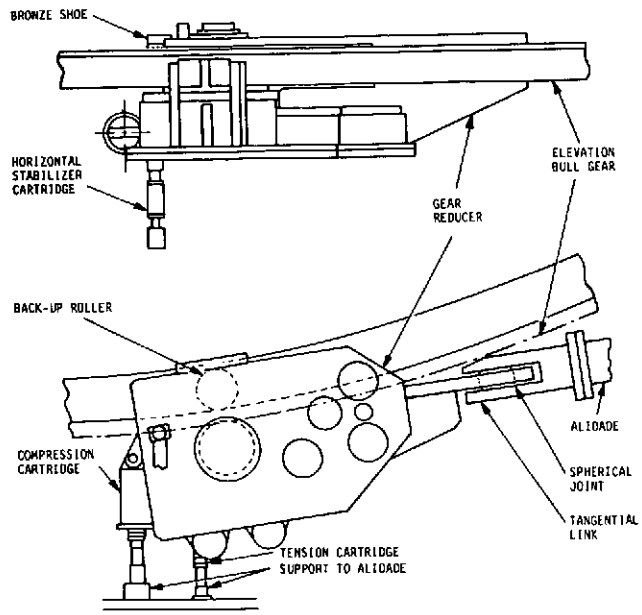

Fig. 38. Elevation gear drive reducer

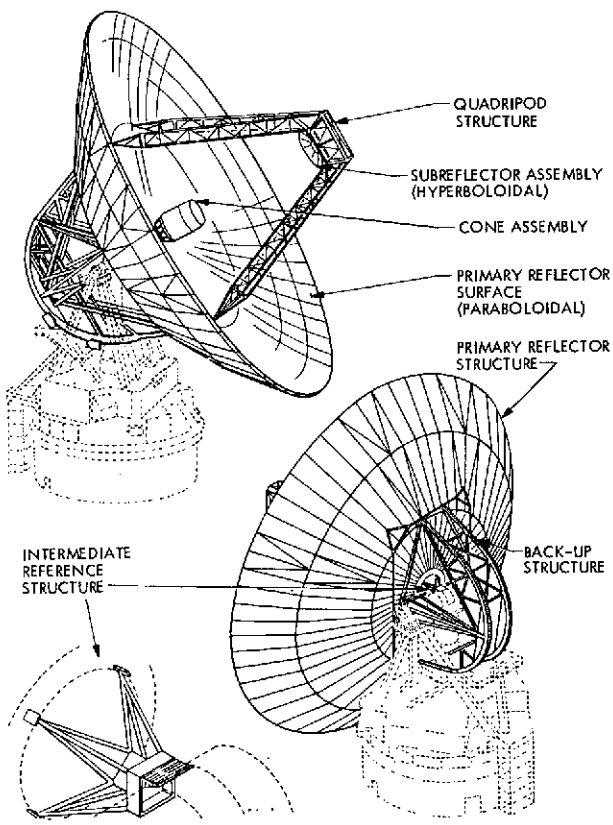

Fig. 39. Antenna tipping parts

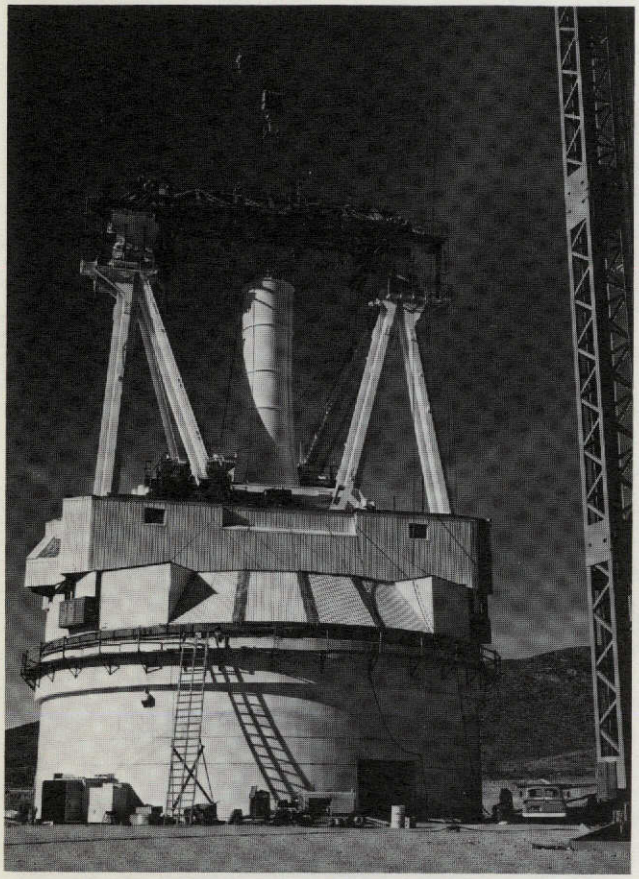

(a) Placement of the tie truss

(b) Elevation wheel being installed

(c) Lifting the center hub

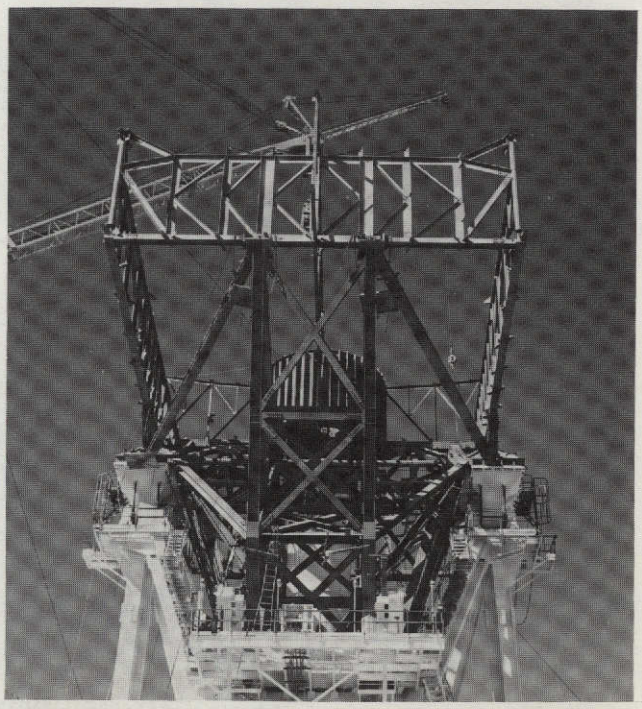

(d) Rectangular girder and center hub in place

Fig. 40. Erection of the backup structure

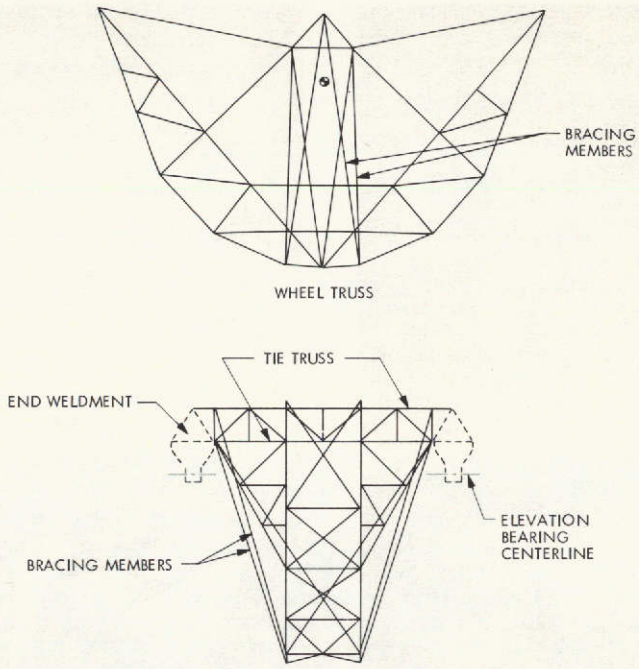

Fig. 41. General outline of elevation wheel and tie truss

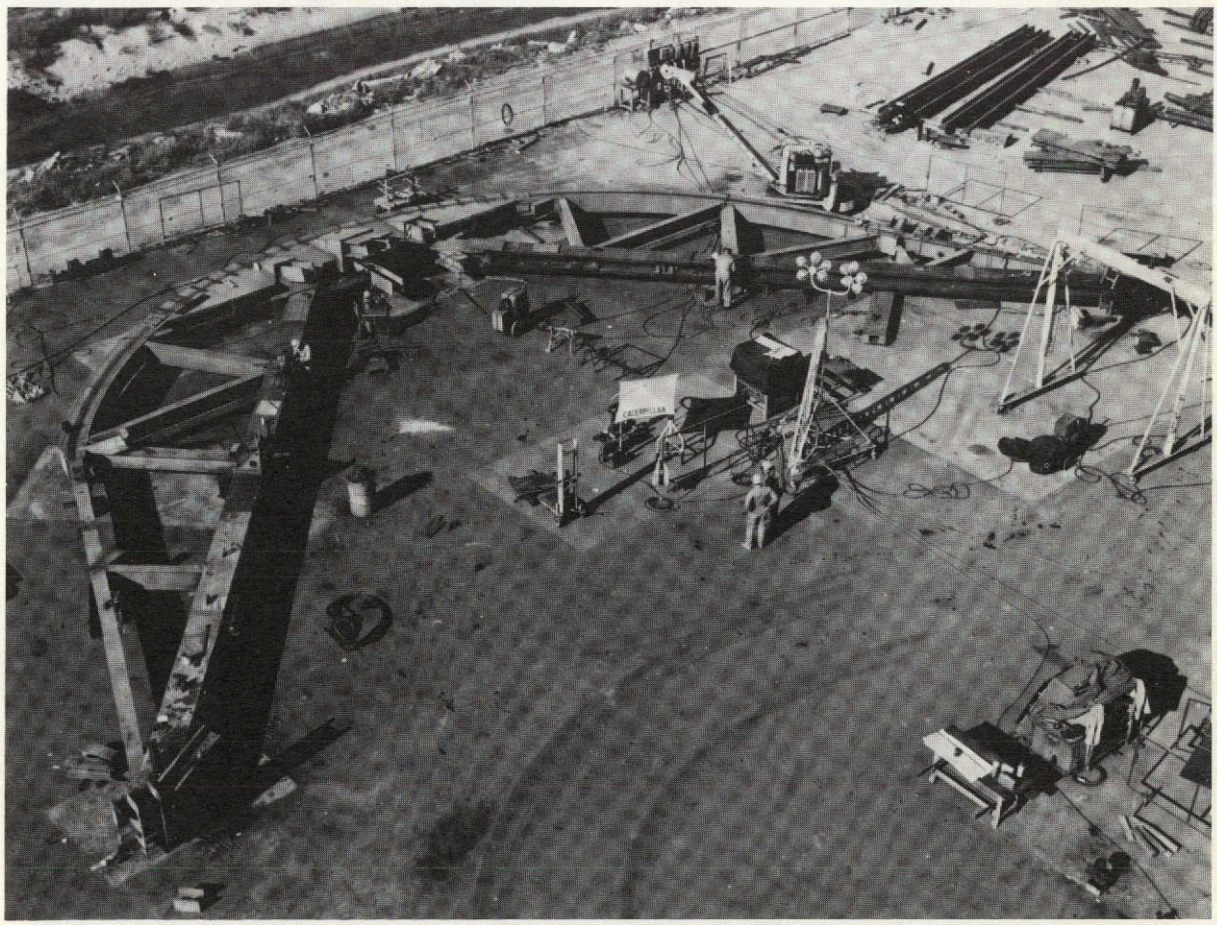

Fig. 42. Elevation wheel being fabricated

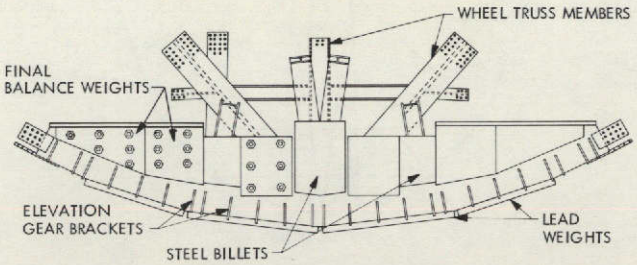

Fig. 43. Elevation wheel counterweight detail

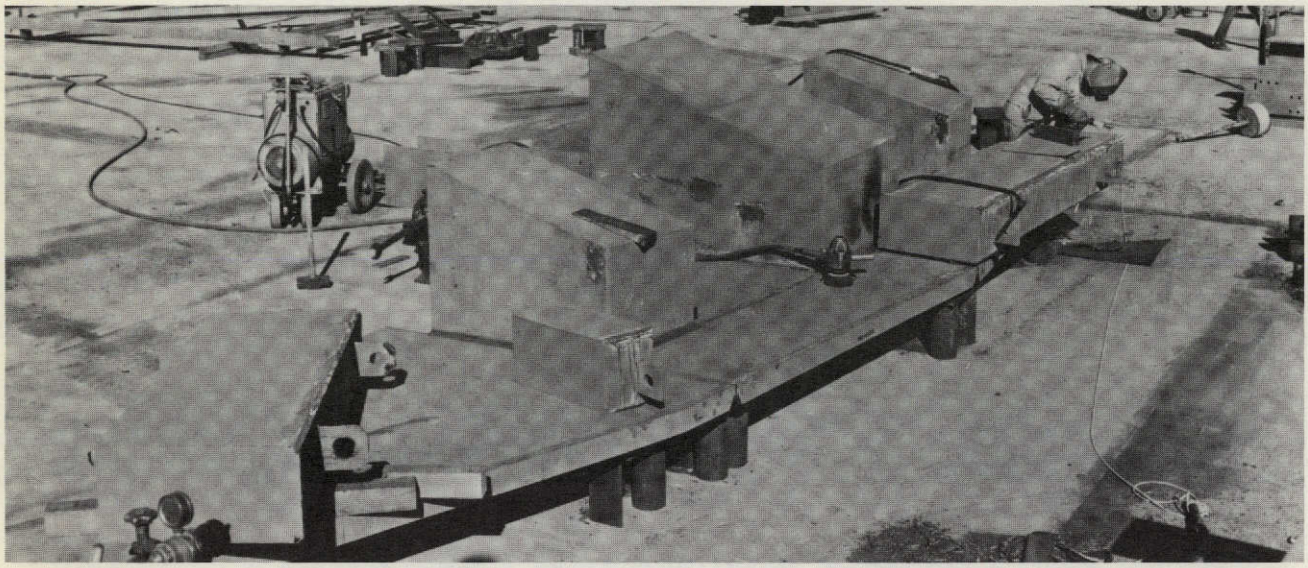

Fig. 44. Fabrication of the counterweight section

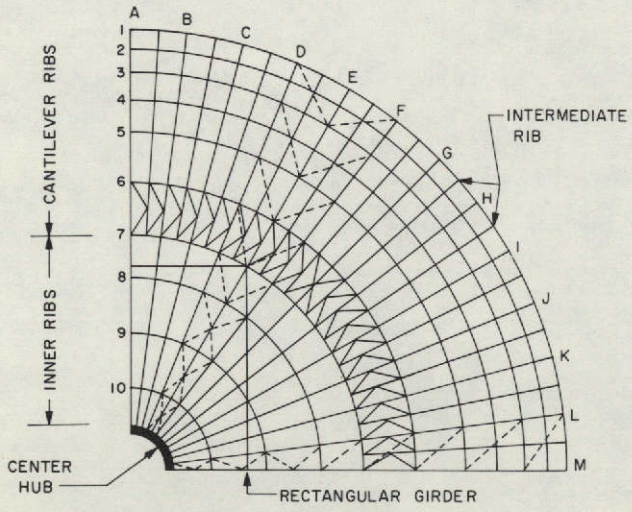

Fig. 45. Primary reflector structure, quarter reflector plan view

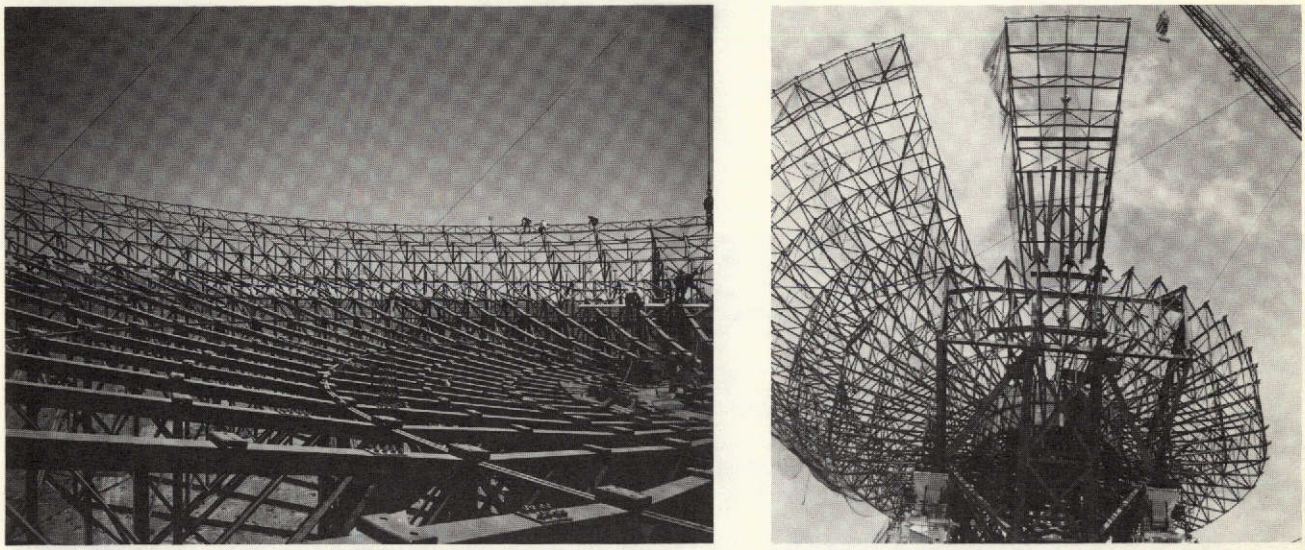

Fig. 46. Primary reflector structure during erection

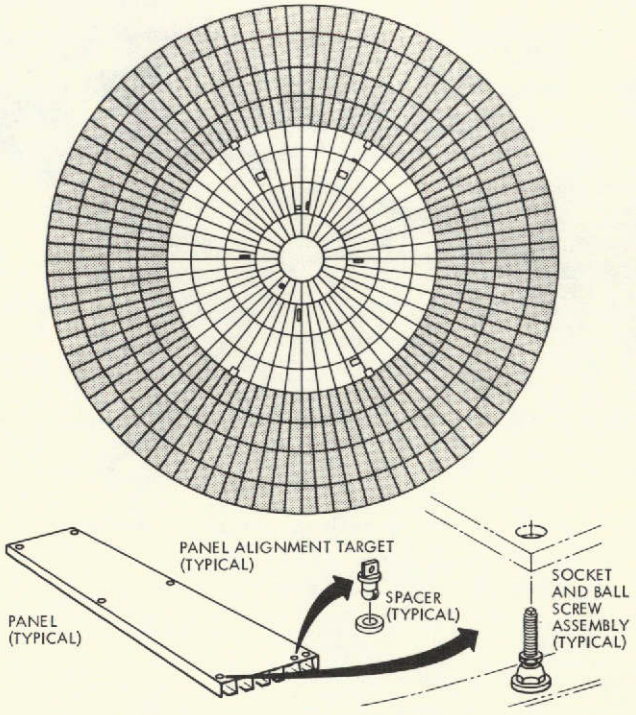

Fig. 47. Major components of the primary reflector surface

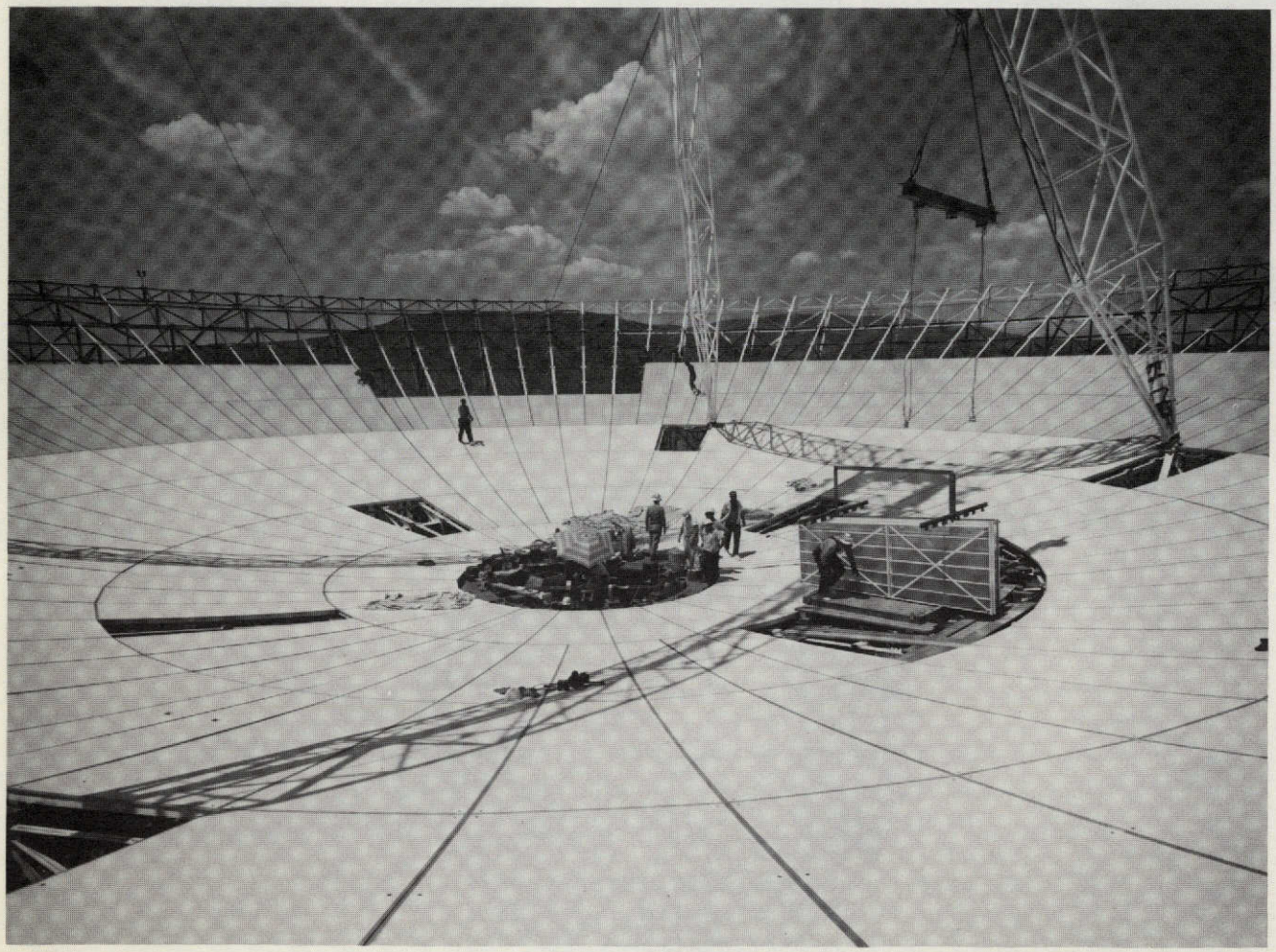

Fig. 48. Primary reflector panel installation

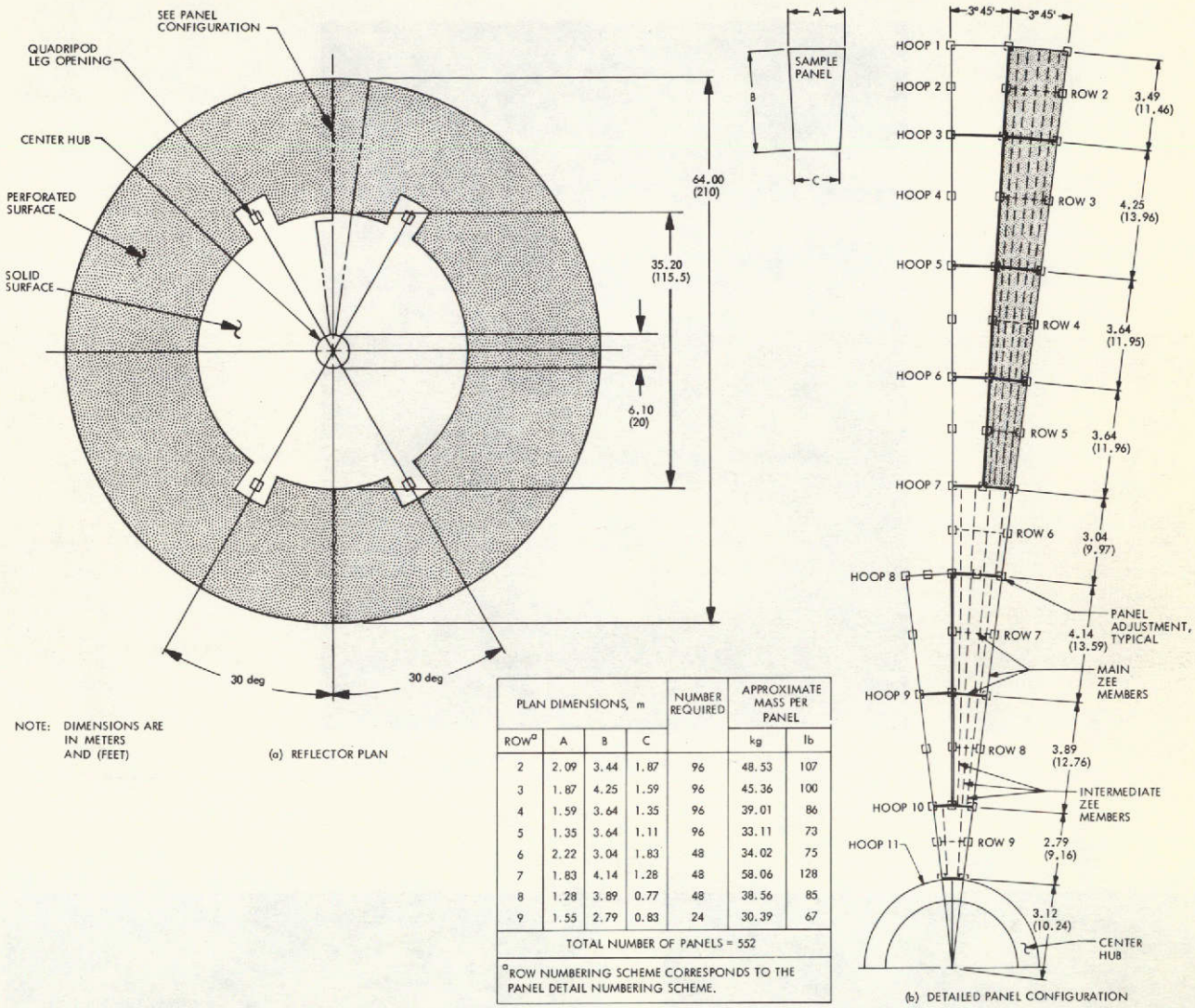

PLAN DIMENSIONS, m				NUMBER REQUIRED	APPROXIMATE MASS PER PANEL	
ROW[a]	A	B	C		kg	lb
2	2.09	3.44	1.87	96	48.53	107
3	1.87	4.25	1.59	96	45.36	100
4	1.59	3.64	1.35	96	39.01	86
5	1.35	3.64	1.11	96	33.11	73
6	2.22	3.04	1.83	48	34.02	75
7	1.83	4.14	1.28	48	58.06	128
8	1.28	3.89	0.77	48	38.56	85
9	1.55	2.79	0.83	24	30.39	67
TOTAL NUMBER OF PANELS = 552						

[a]ROW NUMBERING SCHEME CORRESPONDS TO THE PANEL DETAIL NUMBERING SCHEME.

Fig. 49. Reflector plan and detail panel configuration

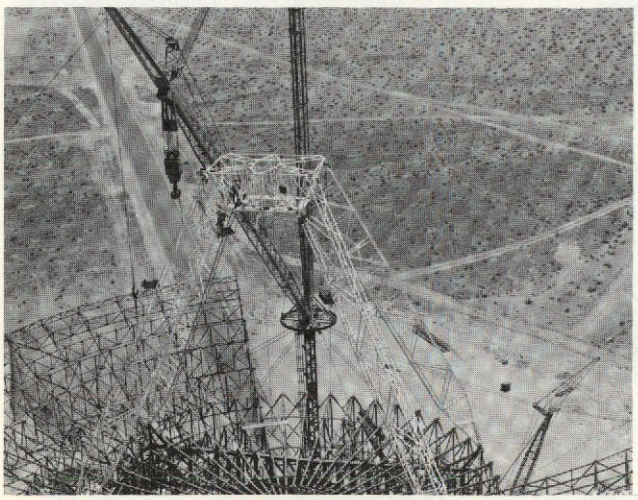

Fig. 50. Installation of quadripod

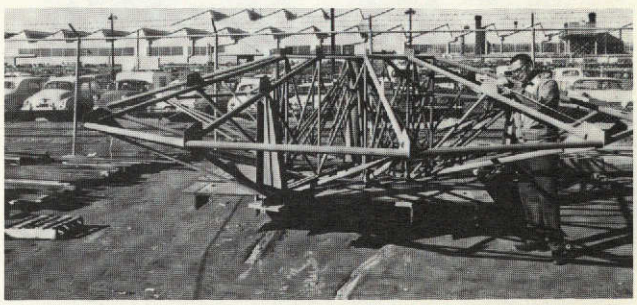

Fig. 51. Subreflector backup structure

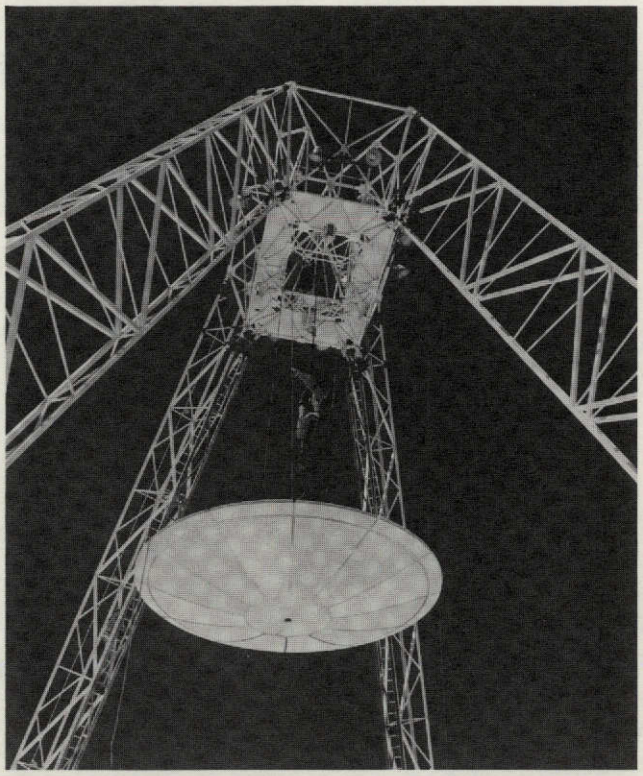

Fig. 52. Hyperboloidal subreflector being lifted into position

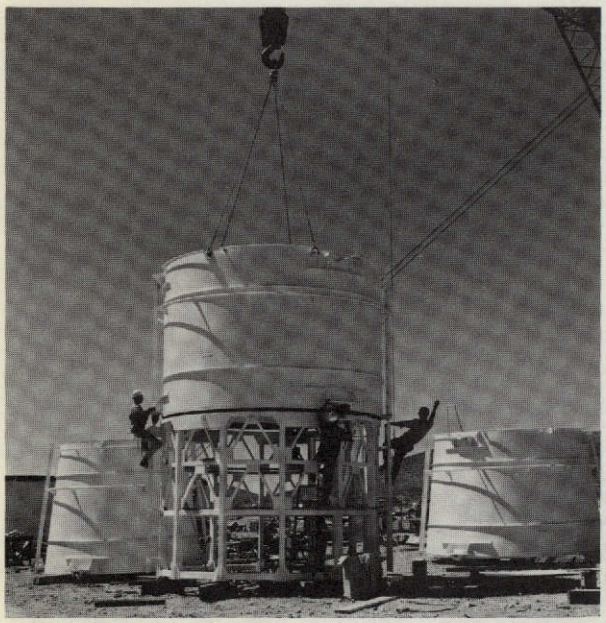

(a) Feedcone support ready for installation

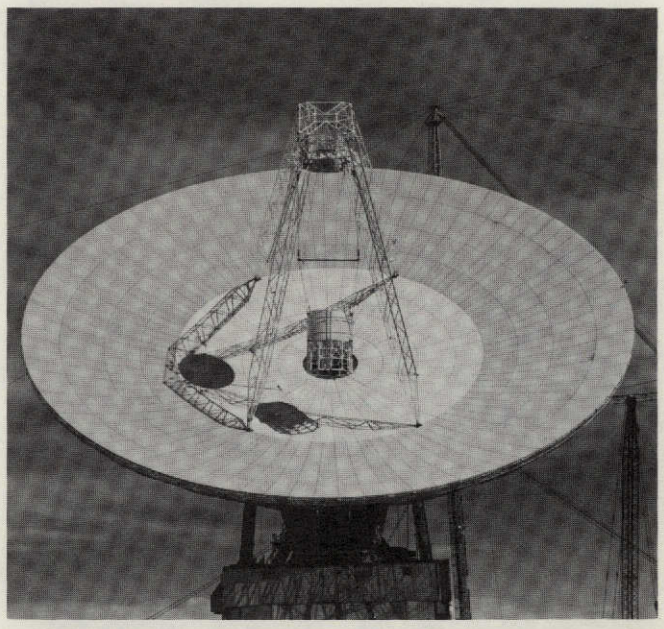

(b) Modules 1 and 2 being installed using the feedcone hoist

Fig. 53. Installation of the feedcone support

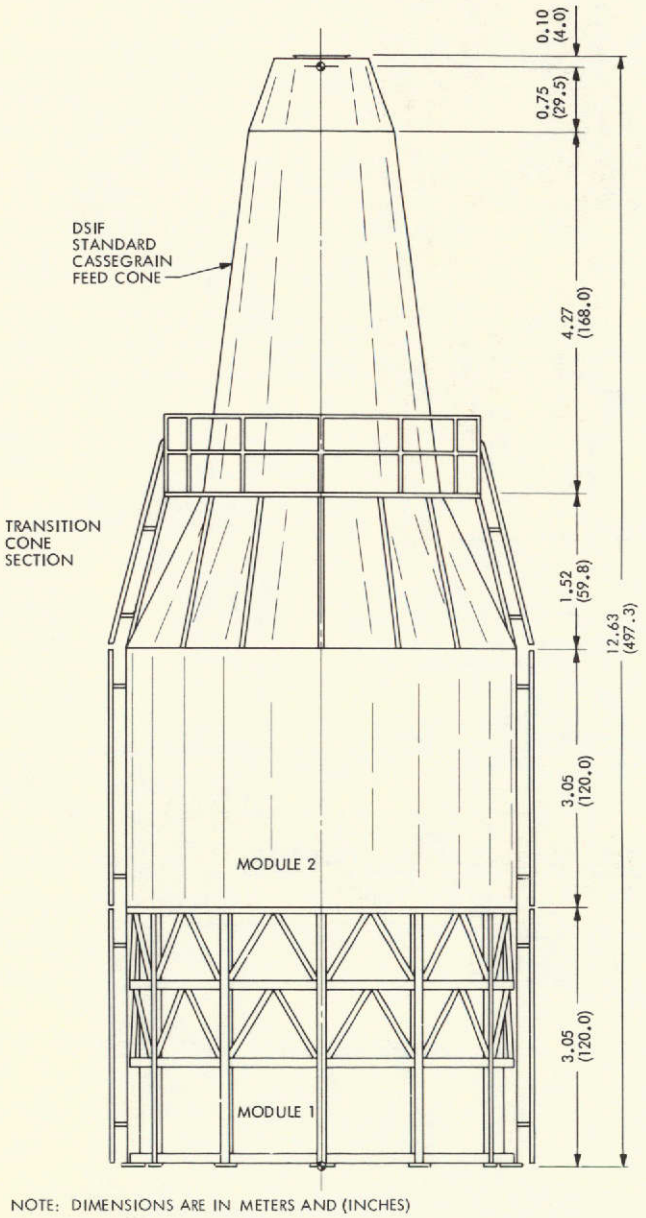

NOTE: DIMENSIONS ARE IN METERS AND (INCHES)

Fig. 54. Feedcone configuration during initial antenna operations

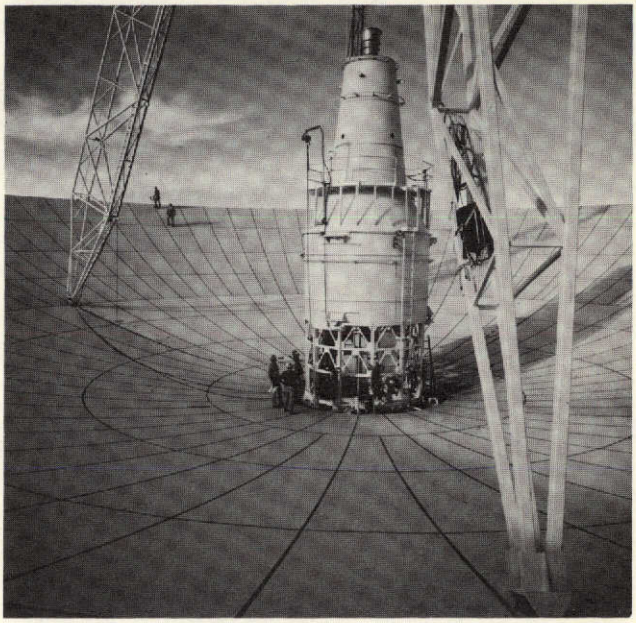

Fig. 55. Cassegrain feedcone and feedcone support in place

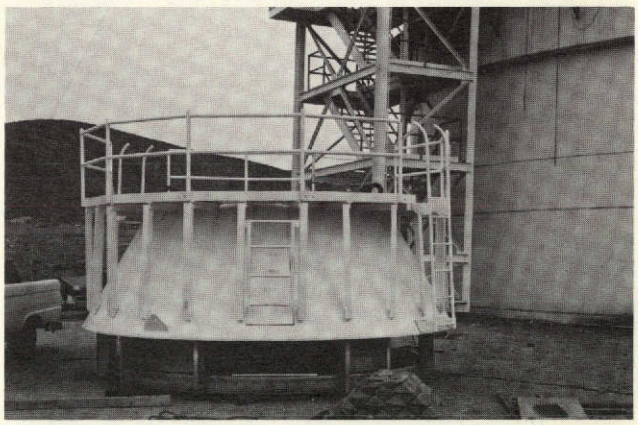

Fig. 56. Feedcone adapter for single DSN 26-m-diameter antenna

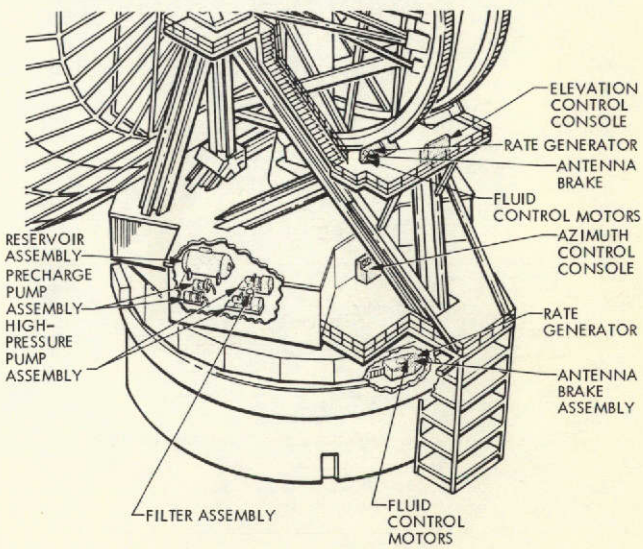

Fig. 57. Servo hydraulics assembly

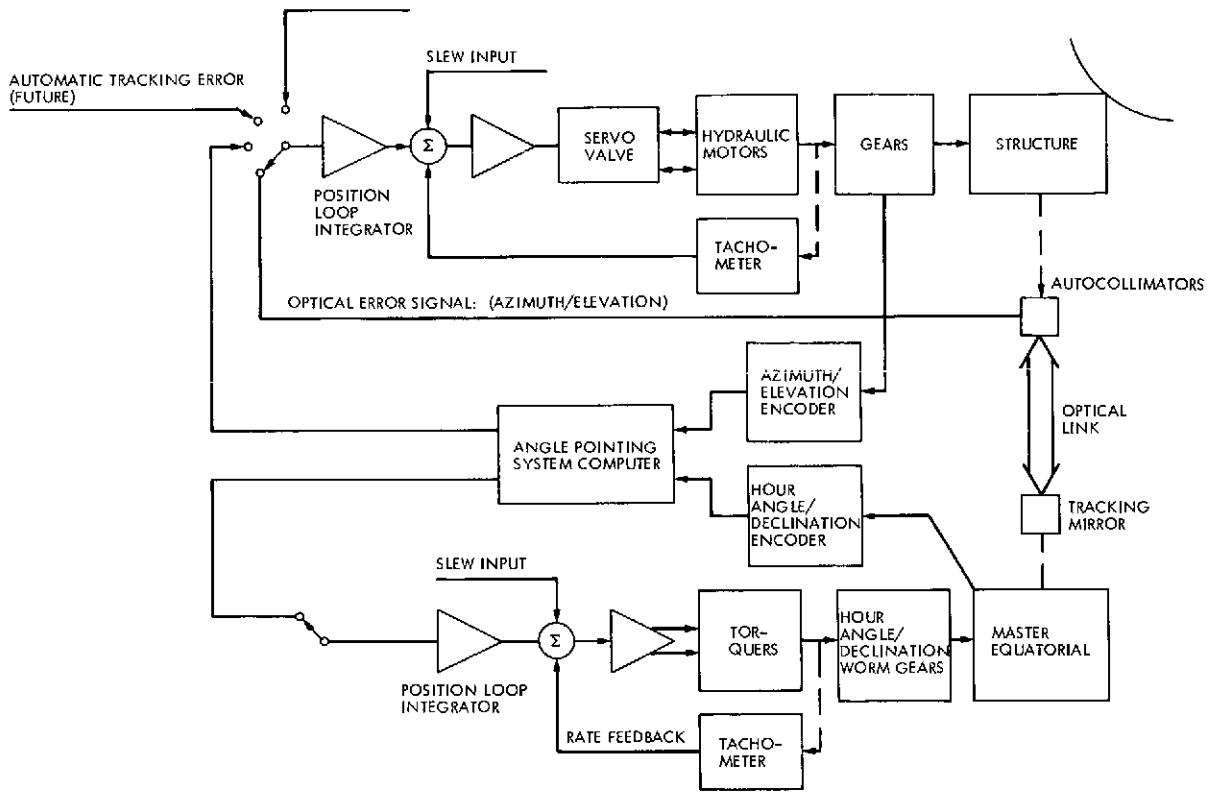

Fig. 58. Basic block diagram of servo and angle data system

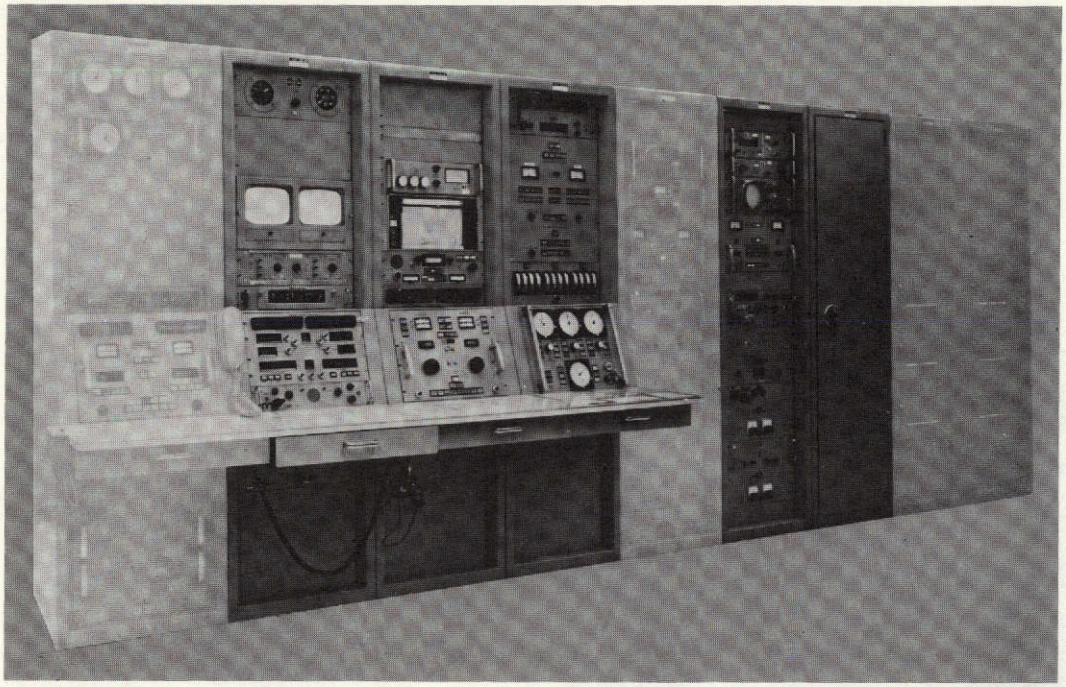

Fig. 59. Servo control assembly control room components

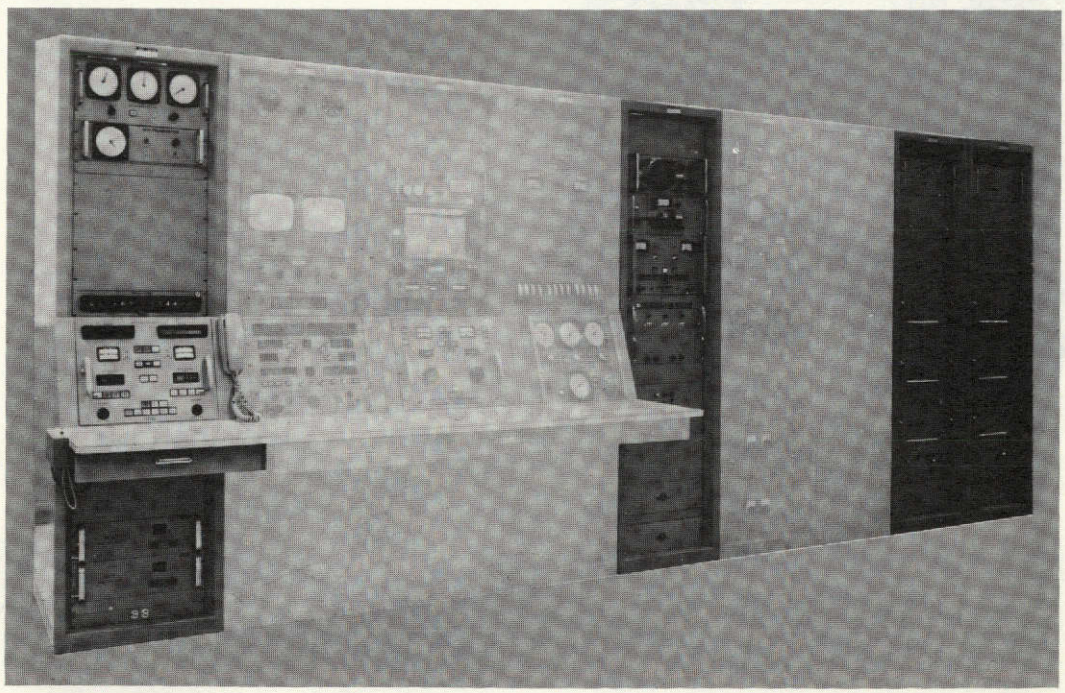

Fig. 60. Angle data assembly control room components

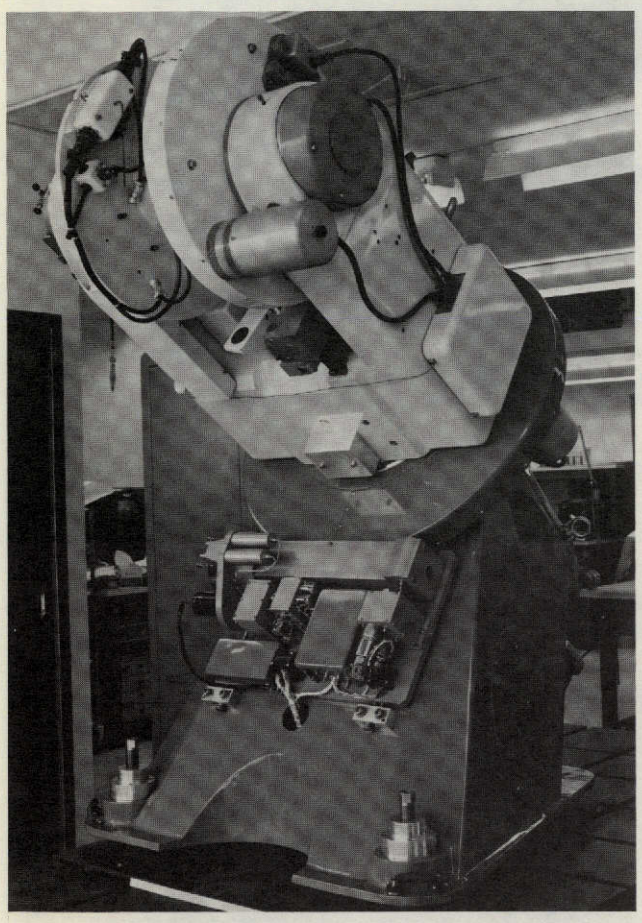

Fig. 61. Master equatorial precision instrument mount

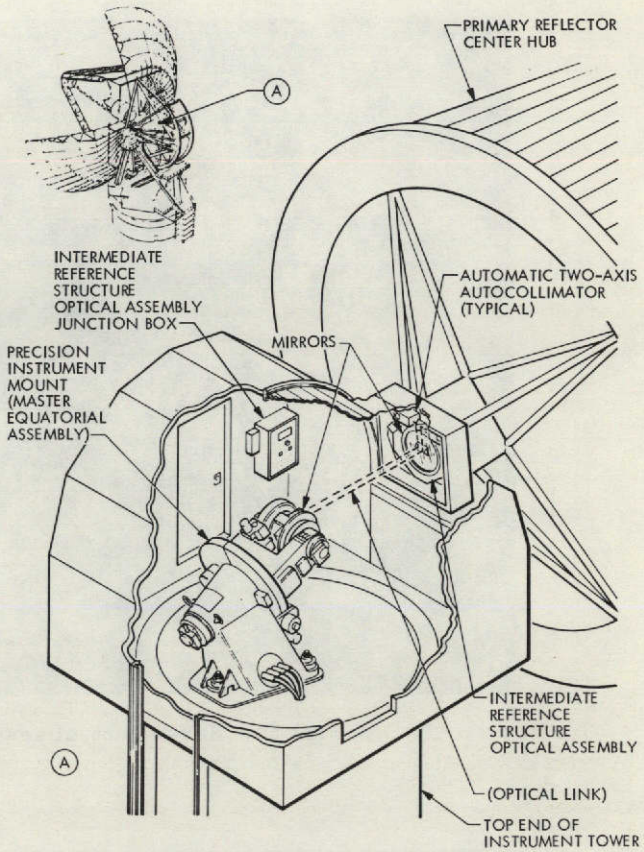

Fig. 62. Angle data system components

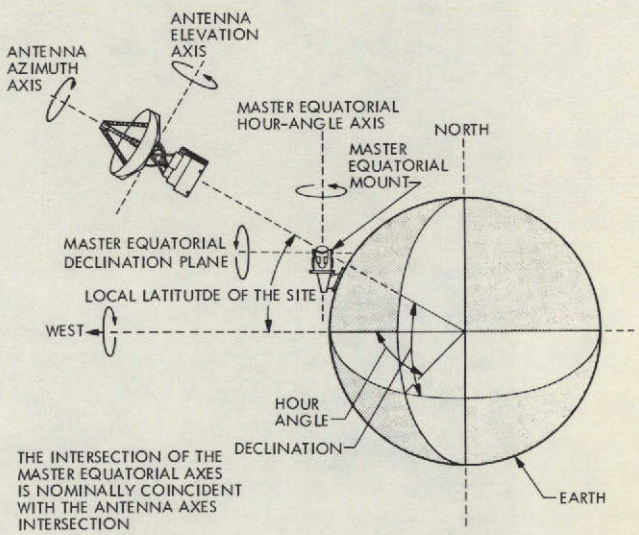

Fig. 63. Master equatorial mount orientation

Fig. 64. Mars Deep Space Station, showing local terrain

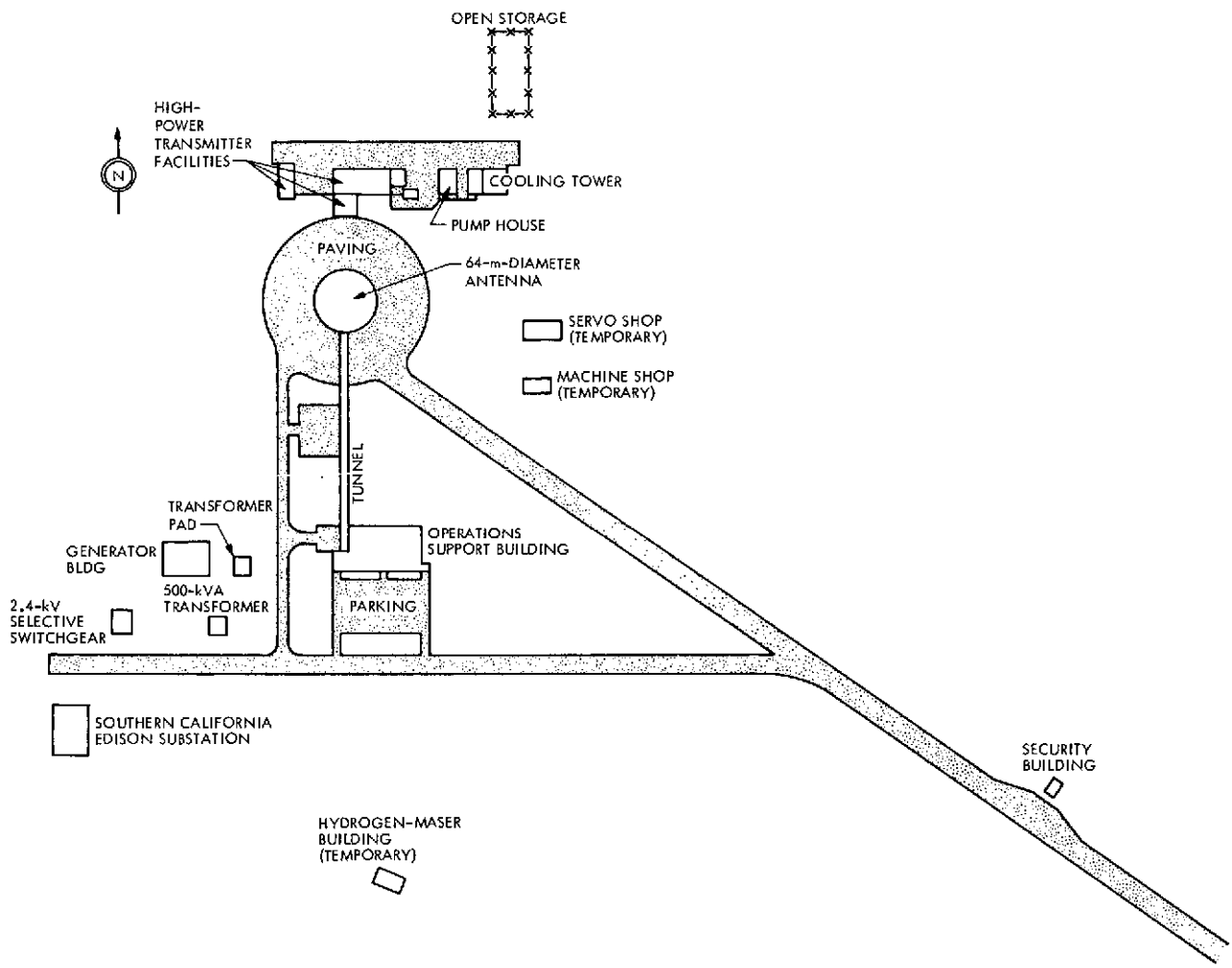

Fig. 65. Mars Deep Space Station plot plan, as of January 1970

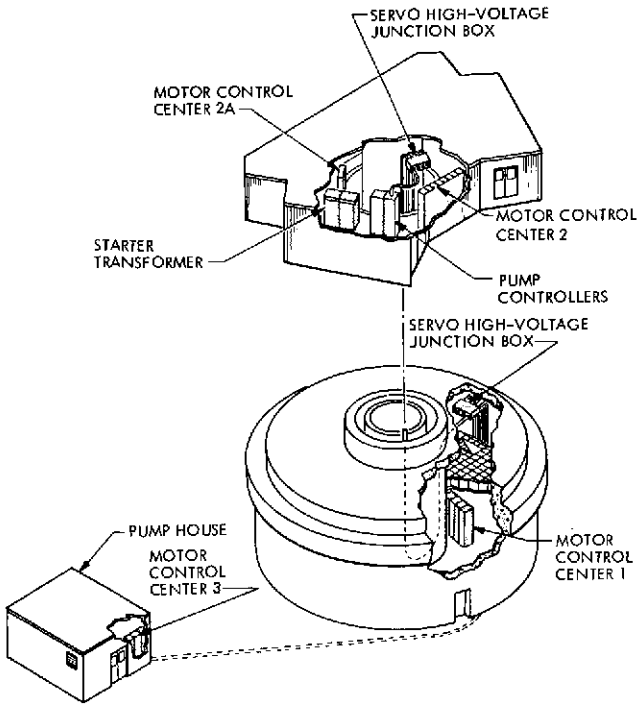

Fig. 66. Electrical distribution equipment

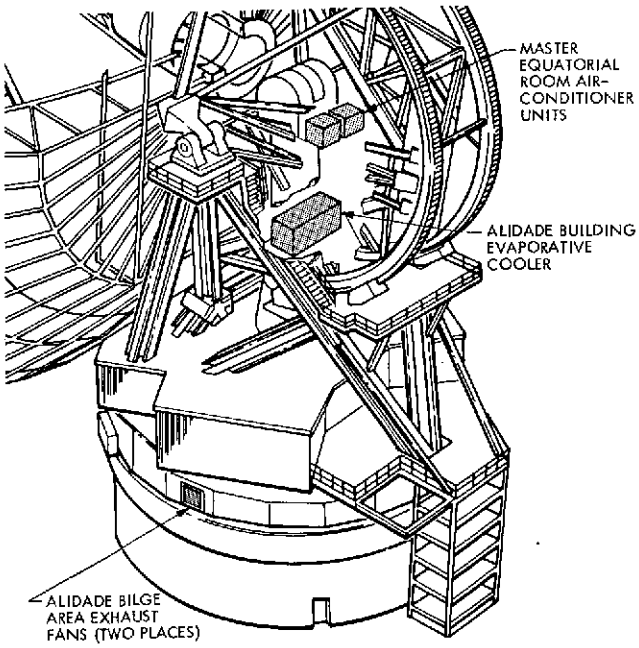

Fig. 67. Conditioned air handling network

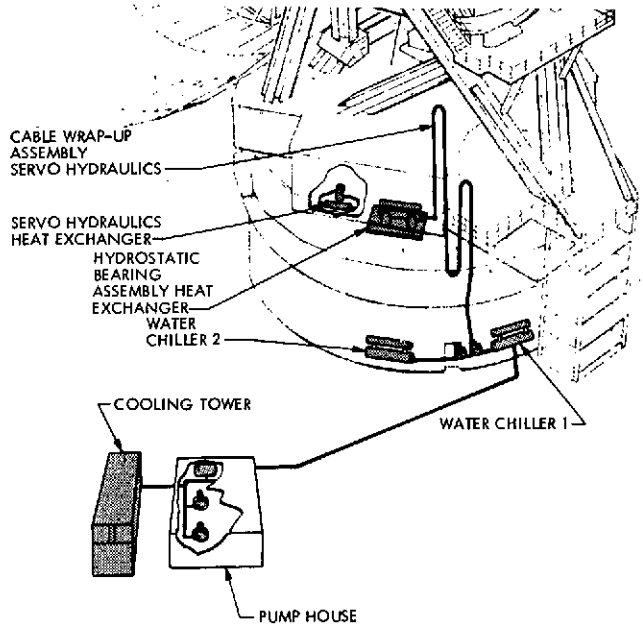

Fig. 68. Liquid coolant distribution network

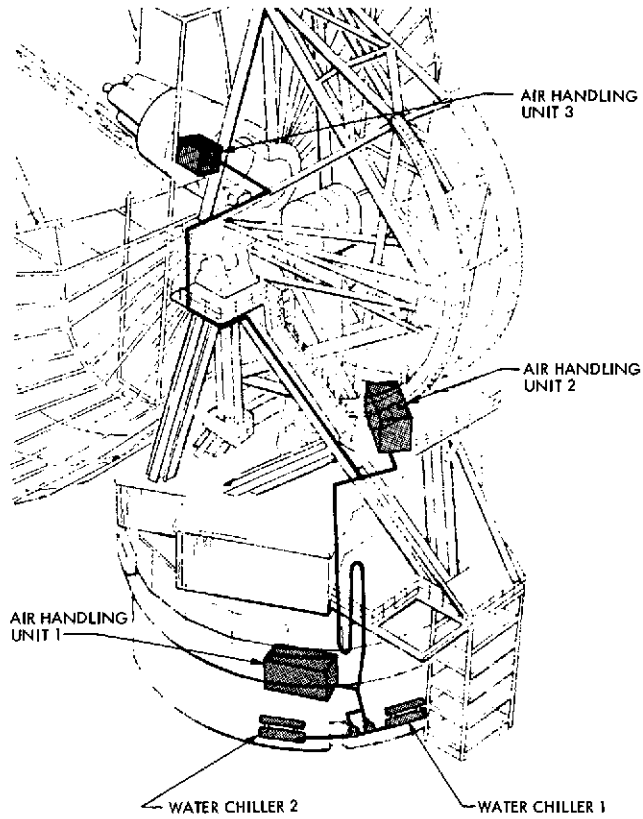

Fig. 69. Chilled water distribution network

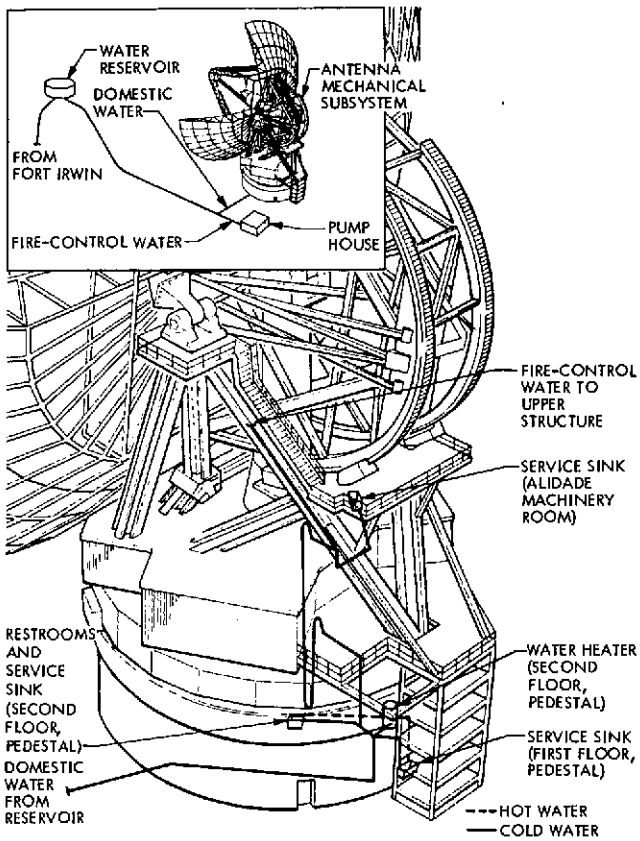

Fig. 70. Domestic water distribution system

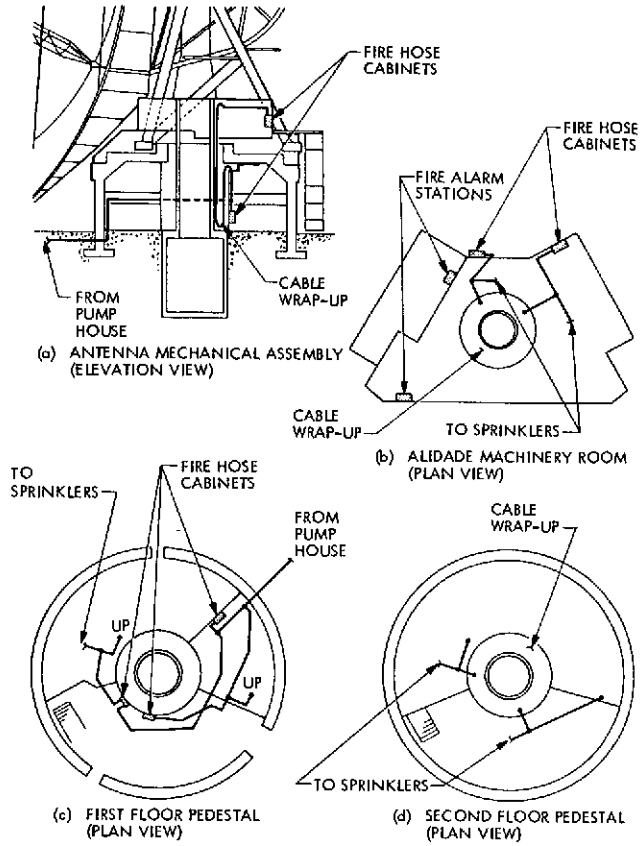

Fig. 71. Fire alarm and water distribution system

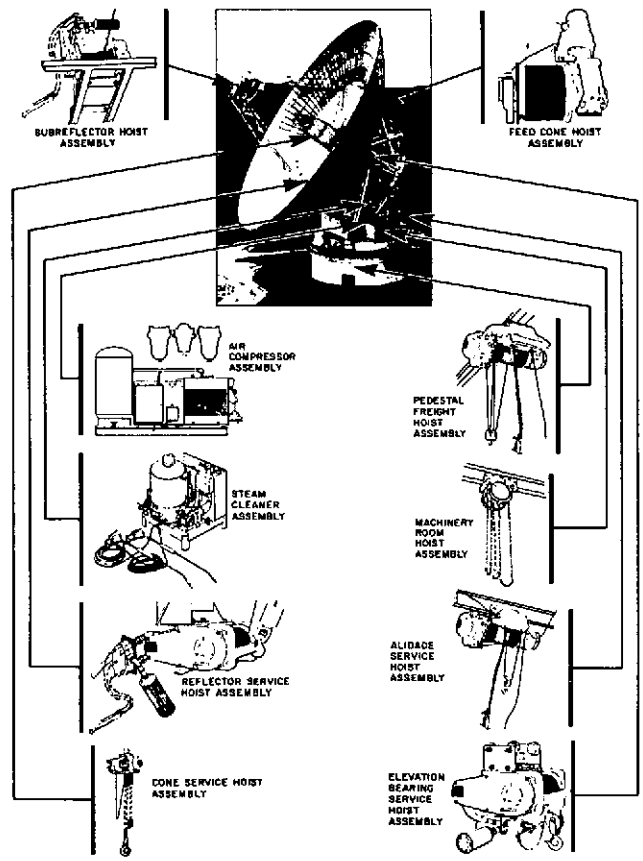

Fig. 72. Antenna support equipment

CHAPTER IV. DESIGN AND ANALYSIS OF CRITICAL AREAS

The design of the 64-m-diameter antenna presented a number of new and difficult engineering problems because of its large size, its required structural and mechanical precision in an open environment, and its required high level of radio frequency performance. This chapter discusses the overall system considerations and the related design areas of components and subsystems that warranted particular attention and analysis during the project's design phases.

I. CRITICAL SYSTEM DESIGN CONSIDERATIONS

A. BASIC ANTENNA CONFIGURATION

The selection of the antenna's basic configuration as a fully steerable single paraboloid was the first and probably the most significant system design decision.

B. TYPE OF ANTENNA MOUNT

Because the distant spacecraft to be tracked by the 64-m antenna have celestial-like motion as seen from the Earth, a polar- or equatorial-mounted antenna similar to the standard DSN 26-m antennas would have operational and technical advantages, particularly for the drive and angle data system. However, the separation of the axes inherent in the equatorial configuration increases the wind loads and gravity distortions to such extent in an antenna of the 64-m class that the design becomes very expensive to build — therefore, an azimuth-elevation mount, with intersecting axes, was selected. In fact, configuration studies made for this antenna indicated that an antenna of the 31- to 46-m class is the largest that is economically practicable for equatorial mounts.

C. DIAMETER AND STRUCTURAL TRUSS ARRANGEMENT OF THE PRIMARY REFLECTOR

The selection of the primary reflector diameter was based on a trade-off between the performance, the estimated total maximum cost of approximately $12 million for the basic antenna, and the ability to predict with reasonable accuracy, at the outset, the cost and the risk of achieving the required minimum performance. Various designs were studied with reflectors up to 76 m (250 ft) in diameter. Based on the experience in then-operating designs and available design analysis techniques, it was concluded that the performance and cost risks start to rise rapidly in the region of 67- to 73-m (220- to 240-ft) antennas. The 64-m reflector diameter was selected as providing adequate capability with acceptably low risk in design and implementation.

Studies were made of the following types of primary reflector backup structures:

(1) A radial configuration of ribs and hoops using a framework of standard tubular or structurally shaped members intersecting at work points to result in a determinant truss.

(2) A parallel configuration of ribs and hoops to form a determinant truss.

(3) A pre-tensioned configuration of ribs and hoops to form a truss resulting in tension forces in all bars under the design loads.

(4) A paraboloidal sheet supported by a cone.

The feasibility studies showed that the design approach using the standard radial rib type of truss structure with readily available structural members was still the most promising design concept. Further design and analysis were, therefore, directed toward optimizing that concept and refining the performance predictions.

The truss arrangement of the reflector structure was carefully analyzed, considering the use of a master equatorial instrument and the criterion of minimum distortion to the best-fit paraboloid at all elevation angles. Through its connection to the elevation bearings, the reflector structure could be supported by (1) a square girder, (2) a ring girder, (3) a combination of the ring and square girders, or (4) a ring girder in combination with a rectangular girder. A clearance space about the intersection of the azimuth and elevation axes was needed for the master equatorial instrument.

The truss arrangement analysis and design were done initially using the Williot-Mohr graphical analysis method,[3] since the necessary computer structural analysis programs were not readily available at that time. Deflections of the trusses were calculated and used to draw contour level maps. From these contour maps, derivations of the mean, using the original focal length paraboloid as the base, were determined and the root mean square (rms) in terms of path length errors was calculated.

On the basis of these deflection studies and the practical aspects of fabricating and erecting each type of truss arrangements, it was concluded that the ring girder in combination with a rectangular girder was the best configuration.

D. THE RATIO OF FOCAL LENGTH TO DIAMETER OF THE PRIMARY REFLECTOR

The ratio of focal length to diameter (f/d) of the reflector was a trade-off of a different sort. The early design studies of the reflector structure and its microwave optics properties indicated that a ratio of 0.25 would provide equal gain but a slightly lower system temperature than the 0.43 ratio used for all of the standard operational DSN 26-m antennas and the DSN 9-m (30-ft) and 26-m antennas used for development support. However, in order to use the Goldstone Complex 9- and 26-m antennas for various microwave and structural scale model studies supporting the design, it was decided to use the 0.43 f/d ratio. It was also recognized that some future benefit would accrue in development and operation of the 26- and 64-m antennas, if the possibility of using common feed systems existed. A common f/d ratio makes this possible on large paraboloids. This second factor has turned out to be very significant, in that standard high-performance Cassegrain cones with expensive masers and high-powered microwave installations are now used interchangeably on the 64-m and 26-m antennas.

E. THE RADIO FREQUENCY BEAM ANGLE POINTING AND READOUT SYSTEM

The design of the radio frequency beam angle pointing and readout system strongly influenced the design of the 64-m antenna. The size of the reflector structure and the precision required precluded the use of standard techniques for measurements of the axis shaft angles. To point the narrow (0.13 deg) radio frequency beam reliably to within one-tenth of its beamwidth under operating wind and thermal environment, it was considered necessary to sense the position of the reflector directly, rather than to measure it from the axis shaft angles through the structural distortions. To accomplish this reliably, a precision, equatorially gimbaled instrument (the master equatorial), mounted on a separate foundation, was positioned at the intersection of the azimuth and elevation axes, directly behind the reflector.

To support the master equatorial at the intersection of the azimuth and elevation axes, an instrument tower was required through the center of the foundation, pedestal, alidade, and reflector backup structure, effectively dividing the reflector backup structure in two.

The use of a master equatorial as the basis for beam pointing and angle readout was a trade-off that complicated the design and increased the cost of the antenna pedestal and reflector supporting structure; the decision was based on predicted system operational performance per dollar, not on cost alone.

F. POSSIBLE USE OF A RADOME

The use of a radome to protect the antenna from the wind and thermal environment was carefully considered during the early phases of the conceptual design. While it appeared that the costs, for a given aperture diameter, might nearly balance or slightly favor the radome, a higher design and implementation risk was considered to be involved. The most important consideration that led to a decision in favor of an open environment design was the predicted reduction in overall system performance as a sensitive receiving terminal, resulting from increased system temperature from the radome.

G. DRIVE SYSTEM DESIGN PARAMETERS

The planned use of the antenna to track deep space targets within a nominal ±10 deg of the ecliptic plane established certain system parameters. The latitude at the Goldstone Complex, where the antenna was to be located, is approximately 35 deg. The coverage needs required that the antenna track to within 2 deg of zenith (this capability was also satisfactory for planned overseas stations). For an azimuth-elevation mount to

[3] A method of determining the absolute displacement of truss joints, originally devised by a French engineer, Williot, in 1877, and introduced into the United States in 1894.

track to within 2 deg of zenith, the maximum azimuth tracking rate must be approximately 0.2 deg/s and the servo loop bandwidth must be at least 0.2 Hz.

The upper limit of the servo bandwidth is constrained by the lowest natural frequency of the structure; a ratio of 5:1 was considered good practice. This critical specification for the 64-m antenna design was set with a safety margin using a ratio of 7.5:1, or 1.5 Hz, for the lowest natural frequency in azimuth because of inherent uncertainty in accurately predicting the antenna dynamics.

The dominant environmental effect in the drive system design was the loading by wind forces. The calculations of forces and moments acting on the antenna because of the wind are simple in concept; they are of the form

$$\text{Force} \propto \text{air density} \times (\text{wind velocity})^2$$

$$\times \text{ aerodynamic coefficient}$$

$$\text{Moment} \propto \text{force} \times \text{lever arm}$$

However, the analytic determination of the aerodynamic coefficients as a function of wind direction and reflector aspect, as well as the determination of reflector and structure parameters such as porosity and shape and the characterization of the wind structure at the site, presented considerable difficulty, as discussed below.

H. STUDY OF WIND EFFECTS

During the initial design and study phase, a significant effort was invested in attempts to instrument the on-site wind character and in experimental wind tunnel studies of carefully scaled models of the antenna configuration to determine representative pressure distributions and aerodynamic coefficients.

The wind tunnel work accomplished was very fruitful in aiding the specification and design of the antenna; on-site instrumentation efforts at the Goldstone Complex contributed little more than a modicum of confidence in predicting the gross wind levels to be expected and in the value of using standard handbook techniques for estimated wind vs height and gust character.

By the time the design of the antenna had been developed enough for a final detailed design and implementation phase contract to be let, the determination of the basic aerodynamic characteristics was well in hand from wind tunnel measurements. The type of information obtained is indicated in Figs. 73-75.

Figure 73 presents the coefficient of reflector yaw moment (a), lateral force (b), lift force (c), drag force (d), and pitch moment (e) as a function of reflector azimuth angle with elevation angle as a parameter for the basic reflector configuration.

The plots in Fig. 73 were based on interpolation of experimental wind tunnel data on models of various reflector porosities. The actual reflector configuration that was selected after the wind tunnel test program had been completed used a 50% porosity over the outer one-half radius of the reflector and a solid surface on the inner one-half radius. From analysis of all of the data available, it was evident that the characterization shown in Fig. 73 was an adequate representation of that particular configuration. The experimental data were compared for (1) 25% porosity on the outer quarter radius and (2) 50% porosity over the entire surface. The higher porosity reduced the maximum wind force and changed the character of the wind moments. The nature of the force change is shown in Fig. 74. While the increase in porosity reduces the maximum wind torques reacting on the axis drives, the most marked effect is that on the stall characteristics; in particular, the increased porosity greatly reduces the rapidity of change in wind moment vs reflector aspect angle in the region of the critical 70-deg yaw angle. This characteristic is shown in Fig. 75.

The data for the wind-induced forces and moments were of considerable value when it became necessary, during the Phase Ia design studies, to carefully review the antenna system specifications with the necessary aim of reducing the design and implementation cost of the antenna.

The dynamics of the wind forces were also recognized as a potentially important factor in specifying the stiffness vs mass of the tipping and turning parts of the antenna structure, but, in this area, characterization of the environment was of limited quality. Despite attempts to instrument the on-site wind dynamics and a thorough review of available literature on the subject, a quantitative characterization of the actual structure of the wind at the planned 64-m antenna site, including velocity variation with height, power spectrum of gusts, and directional shifts in gusts, was not obtained. The representation that was used is sketched in Fig. 76; it is based on the time required for a 30% gust in a 13.4 m/s (30-mph) wind to envelop a 64-m-diameter reflector, plus empirical data on wind dynamics. It was possible only to develop confidence that the representation was a conservative approach.

In Chapter II, it was noted that the specifications and their validation requirements incorporated in the first requests for proposals for the Phase II final design and implementation resulted in quotations that considerably exceeded the available budget amount (along with the then-justified operational value of the antenna). The Project was faced with the need for respecifying the antenna to reduce the cost by about 30%, while still meeting the basic performance requirements. Because wind loading is a predominant factor in an open-environment antenna, it was a prime factor for attention in examining the practicality of respecification. The Project team proceeded on the basis that the antenna structure had to be designed to survive, though not to operate, under the maximum wind, ice, and seismic conditions which had any reasonable likelihood of ever occurring. This involved stress designs that

could be governed by the established American Institute of Steel Construction (AISC) code or modifications thereto, as well as a design that would provide stability against overturning.

Analyses indicated that the seismic loads, rather than the survival wind loads, were more important in terms of stability against overturning. A significant weight reduction on the azimuth bearing could be allowed before a safety factor of 1.5 on overturning would be compromised.

Ignoring the small gravity load due to the reflector panels, it can be shown that, for a particular configuration of the structural member areas of the reflector structure, the deflection of the structure due to its own gravity load is independent of the absolute value of these areas. Thus, the actual member areas and the resulting weight of the reflector structure are primarily functions of the wind load and the permissible structural deflections. Because the wind load varies as the square of the wind velocity, the weight of a particular reflector structure is a function of the square of the operating wind velocity.

As a further generalization, if the mass and inertia of the reflector are reduced, the counterweights may be reduced in the same proportion, and the stiffnesses of the lower supporting structures may be similarly reduced without compromising the resonant frequency characteristics of the total structure. The principal supporting structure affected is the alidade, and since it is also a truss, carrying its loads primarily in tension and compression, its weight may be reduced in proportion to the reflector weight reduction. Thus, the total weight of the structure for a particular configuration is fundamentally proportional to the square of the design wind loads.

Based on these facts, it was evident that a considerable cost saving in the antenna system could be realized if the operating wind velocity specifications could be reduced without compromising required operational performance. To examine this possibility, available wind loading data were analyzed in the following way. The axis torque as a function of wind velocity and wind moment coefficient for the 64-m antenna reflector is as shown in Fig. 77; the values of C_m as a function of aspect angle for the planned one-half solid, one-half porous reflector were derived from the wind tunnel data (Figs. 73a, 73b, and 75).

Through the use of these data, the ability of the antenna to operate at any aspect as a function of the wind velocity and torque capability was determined as shown in Fig. 78. The parameter K used in the plots is the axis torque in newton-meters (pound-feet) divided by the square of the wind velocity in meters/second (miles/hour); it is graphically portrayed in Fig. 79. For example, Fig. 79 shows that a drive torque capacity of 6.78×10^6 N-m (5×10^6 lb-ft) will accommodate a K-parameter of 12,295 (1800) at a wind velocity of 23.5 m/s (52.5 mph), and a K-parameter of 17,076 (2500) at a wind velocity of 20.1 m/s (45 mph). Referring to the small sketch on Fig. 78, one can see that this torque capacity on both azimuth and elevation axes would permit antenna operation at wind velocities up to 23.5 m/s (52.5 mph) over all antenna positions outside the shaded area and would permit operation at all possible normal operating antenna positions (elevation > 5 deg) at a wind velocity of 20.1 m/s (45 mph).

From these curves, it can be seen that a capability of operation at a 20.1-m/s (45-mph) wind in any aspect permits operation over a somewhat limited range of aspects at considerably higher winds. Also, a capability to move to stow in a 26.8-m/s (60-mph) wind along any path implies an ability to move to stow along a selected path at considerably higher wind velocities.

As a result of the more detailed consideration of the wind environment effects on the antenna operation, the specifications were revised downward to allow a considerably less costly design. The original and revised wind environment requirements are given in Table 2.

The revised values represented a reduction in environmental capability; however, the probability of actually losing tracking capability involves the simultaneous occurrence of a maximum wind and an unfavorable antenna position and was considered to be sufficiently small. As discussed, winds considerably over the maximums specified can be sustained over a large fraction of the solid angle coverage.

As a result of the respecification, the survival wind conditions as shown in Table 2 for survival at stow or at any other position were not changed. Wind forces for these conditions result in the maximum stresses in the members of the reflector trusses. However, these forces were reduced in the specification (Ref. 1, Rev. 3) by increasing the porosity of the reflector surface panels to 50% throughout (Ref. 1, Rev. 2 specified 25% porosity only in the outer 25% radius).

Ultimately, Rohr Corporation, the antenna contractor, chose to design and fabricate using solid panels for 50% of the radius and porous panels outside this radius, based on a compromise between fabrication cost and "footprint" load – since the solid-panel design enables a higher "man's walking load" at stow position for maintenance purposes.

I. STUDY OF SEISMIC EFFECTS

Seismic loading on the antenna was considered from the early conceptual design phase. Upon conclusion of studies, it was determined that seismic loading was not actually constraining because the design that was evolved to meet other criteria inherently satisfied the requirements to survive reasonable expectancies of seismic loading.

The 64-m antenna requires a relatively high resonant frequency structure to meet servo drive requirements under the specified wind environment. The design of such a structure for erection in a locale subject to seismic activity requires consideration of the potential seismically induced loads because structures with high resonant frequency tend to have low damping and hence must be designed for a high percentage of gravity loads

applied laterally. Dr. G. W. Housner of the California Institute of Technology was retained as a consultant on seismic loading of the 64-m antenna.

On the basis of configuration drawings and data on mass distribution for the antenna, Dr. Housner made an early study regarding earthquake hazards to the antenna. The following is a summary of the results of his study.

The site of the antenna is located with respect to the major Southern California earthquake faults as shown in Fig. 80 — it is 32.2 km (20 miles) from the Garlock fault and 136.8 km (85 miles) from the San Andreas fault.

The San Andreas fault is sufficiently far away that if an earthquake occurred there, the high-frequency components in the ground motion at the Goldstone Complex would be much attenuated and would not present a particular hazard to the antenna structure. Appreciably more severe shaking would be experienced by the antenna structure if a strong earthquake originated along the Garlock fault. The antenna structure could also be shaken severely by a weaker earthquake originating close to this site.

The antenna structure is proportioned so that it will remain seated on its pads so long as the horizontal acceleration of the center of mass does not exceed about 25-35% g. For accelerations larger than these, it would uplift (slightly) and bang on the base rail. Whether or not the center of mass would exceed 30% g acceleration during an earthquake would depend upon the intensity of ground shaking and upon the natural frequency of vibration of the structure. Initial calculations indicate that the frequency of the fundamental lateral mode of the antenna structure is in the range of 3 to 10 Hz. For a natural frequency below 6 Hz, the acceleration of the center of mass could exceed 30% g if the center of the earthquake were relatively close.

There is a small probability that the structure will rock on its base some time during its life. There is no danger that the superstructure will overturn, but there may be strong banging on the base rail. It would probably require a major modification in design, with an appreciable cost increase, to ensure against rocking on the base in the event of a strong earthquake nearby. In general, the stability and earthquake resistance of the configuration appear good.

Dr. Housner recommended that the structure be designed to be capable of withstanding an equivalent, constant, lateral acceleration of 25% g using ordinary allowable stresses; that the problem of brittle fractures should be carefully considered in the antenna design and implementation; and that the original estimates of natural frequency of lateral vibration should be calculated on the final design and the results reviewed with respect to the seismic criteria.

The recommendations were followed, although, as noted, the attention to seismic criteria did not constrain or dictate the design. (Since the antenna has been in operation, the site has been subjected to four minor earthquakes, the largest being of order 4.5 on the Richter Scale, with no problems and no banging on the base.)

J. SITE SELECTION AND LOCATION

Several possible sites at the Goldstone Complex were examined for the 64-m antenna, with consideration being given to logistics support, radio frequency interference susceptability, and detailed coverage masking. To augment these investigations, a contract was placed with Donald R. Warren Co., Los Angeles, to conduct a comprehensive study of tentative sites with respect to foundation conditions. Twelve possible sites were initially investigated; five were eliminated during the first cursory examination, and the remaining seven were investigated thoroughly, particularly with respect to the rotational stability of the optical reference tower.

After considering the criteria for the location of the 64-m antenna, a specific site was selected at the Goldstone Complex, which is located approximately 5 km (3 miles) north of Goldstone Dry Lake; its geodetic coordinates are: ϕG = 35°25'33.34"N; λG = 243°06'40.85"W; Z = 1031.8 m above mean sea level; geodetic height = 22 m; height above ellipsoid = 1010 m.

From an overall viewpoint, the site selected was a compromise. Although it was not a bedrock location and hence posed certain foundation problems with respect to seismic loadings, the location was established as providing excellent founding.

The results of the foundation investigations, as they relate to the pedestal and instrument tower analysis and design, are further discussed in Section II-A of this Chapter.

In selecting the specific site location for the antenna, it was necessary to consider the operational problems of locating several low-noise receiving stations and high-powered transmitting stations in the relatively small Goldstone Complex geographical area. The selected location provided the best practical radio frequency isolation by distance and natural terrain barriers from the other sites at the Complex. Figure 81, a horizon mask of the selected site, shows a suitably low mask in the critical directions for a South European station overlap (125-145 deg azimuth) and protection from other Goldstone Complex sites. Figure 82 depicts the terrain features surrounding the selected site.

II. CRITICAL COMPONENT AND SUBSYSTEM AREAS

A. PEDESTAL, INSTRUMENT TOWER, AND FOUNDATIONS

As described earlier, the pedestal is a reinforced concrete structure which supports the rotating elements of the antenna, transferring all vertical, horizontal, and rotational loads from the alidade to the pedestal ring footing, where the loads are, in turn, transferred to the founding material. Figure 83 shows the pedestal and its relationship to other parts of the antenna. A circular opening is provided in the center of the

pedestal's second floor and roof deck to accommodate the structurally independent instrument tower, which supports the master equatorial instrument and serves as a reference for antenna pointing.

The principal forces from the antenna alidade which act on the pedestal are vertical forces from the azimuth hydrostatic thrust bearing pads, rotational forces from the azimuth drives, and horizontal forces on the azimuth radial bearing.

Detailed foundation investigation work in support of the pedestal and instrument tower design consisted of field tests, which included borings and seismic refraction traverses, and laboratory tests of undisturbed representative samples taken at various depths in the borings. Four borings were made to a depth of 30.48 m (100 ft), as shown in Fig. 84. Undisturbed samples obtained from these borings were tested in the laboratory for moisture content and unit weight, direct shear strength, consolidation, and triaxial shear strength. The borings showed very dense alluvial soils of considerable depth, essentially granular from the surface to a depth of about 30.5 m (100 ft). The seismic studies indicated that dense alluvial soils extend to a depth of at least 152 m (500 ft). Water was not encountered in the borings.

The soil sampling process is illustrated in Fig. 85. Typical consolidation data is shown in Fig. 86. Through the use of conventional analytical methods, the design characteristics listed in Table 3 were developed. These values were within the limits set by pointing accuracy and servo compatibility requirements.

Beyond the usual foundation requirements for a structure, the pedestal design involved several other problems unique to large antennas and to the 64-m antenna in particular. The pedestal configuration, including diameter, height, wall thickness, and loading points, required careful integration of the varying requirements of isolation of the instrument tower, stability against overturning of the alidade, rotational stiffness in support of pointing accuracy, and compatibility with the flatness and elastic deflection requirements of the hydrostatic thrust-bearing runner.

A high degree of isolation was required between the pedestal and instrument tower so that movements of the instrument tower in response to dynamic loadings on the pedestal would be within acceptable limits. This was the governing factor in the design of the pedestal configuration.

To ensure that long-term settlement of the instrument tower would not occur and disturb the pointing reference, the instrument tower foundation is a "floating" silo type; i.e., the dead load of the tower is approximately equal to the weight of the soil excavated (weight of the tower is 5.54×10^5 kg (1,200,000 lb); the estimated weight of the excavated soil is 5.89×10^5 kg (1,300,000 lb). This technique imposes the same pressure on the bearing soils at the foundation base as were imposed by the overburden and thereby effectively eliminates long-term settlement caused by consolidation of the founding materials due to an increase in bearing pressure.

The hydrostatic bearing supports the dead weight of the antenna; however, there is no provision in the configuration for hold-down devices to prevent the alidade from lifting off one bearing pad under overturning loads due to wind or seismic forces. With the pedestal diameter used, the structure supported by the azimuth bearing is stable under maximum design wind or seismic loads. The safety factor at stow position and a wind velocity of 53.7 m/s (120 mph) is 1.42 to 1.00. Use of a smaller diameter pedestal would have made it necessary to include hold-down devices, at an increase in cost and complexity.

The pedestal and foundation are within the servo control loop in the precision pointing mode and hence are a part of the overall dynamic system as seen by the servo. Therefore, the compliance of the pedestal and foundation, as well as the load-carrying capacities, became a part of the design requirements.

The elastic properties of the pedestal concrete are a major part of matching the hydrostatic bearing runner and pad deflections, as will be described in the hydrostatic bearing discussion to follow. A related problem was that creep of the pedestal concrete under the bearing load during construction could cause unacceptable permanent depressions in the runner surface which would adversely affect bearing operations. The hydrostatic bearing pad and runner and the pedestal were designed so that their theoretical vertical deflection curves matched within 0.0254 mm (0.001 in.). To meet this requirement, a specific modulus of elasticity in compression of the pedestal concrete of 34474×10^6 N/m^2 (5.0×10^6 psi) after 28 days cure, with a coefficient of variation of less than 10%, was specified. To ensure uniformity, rigid quality control of the concrete raw materials and batching was specified.

The conventional approach in the design of mass concrete structures, such as dams, is to determine the modulus of elasticity obtained using concrete made from available aggregates and adapt the structural design as required. The specification of a modulus of elasticity for the pedestal material, unusual in concrete design, was essential to assure the required compatibility of the pedestal and the hydrostatic bearing, both for the initial antenna and for future replication at overseas stations.

The possible permanent distortion of the hydrostatic bearing runner surface, resulting from creep of the concrete under the load of the three bearing pads set in a fixed position on the pedestal during the construction phase, was an engrossing question. A 0.076-mm (0.003-in.) maximum was established for the deflection of the runner under a pad due to creep of the concrete under loads to be encountered during antenna construction, before the time at which azimuth rotation became possible. This problem was analyzed in consultation with Prof. J. M. Raphael of the University of California. As a result of these studies, the following steps were taken in the design and erection of the pedestal to minimize the creep problem.

(1) The pedestal was designed with extra thickness to lower the stress due to the bearing loads.

(2) Special aggregates were found in the area and used in the construction.

(3) A low water-cement ratio was used.

(4) Concrete temperature during placement was limited to not more than 21.1°C (70°F).

(5) A high cement-aggregate ratio was used.

(6) An additive was included to improve the workability of low-slump concrete.

(7) Placement and vibration of the concrete were carefully controlled.

(8) A long wet cure was provided, followed by a special coating to inhibit moisture loss and consequent drying shrinkage.

(9) Loading of the runner through the bearing pads was delayed as long as practical to allow extended cure.

(10) Care was taken to assure that after each alidade azimuth motion, the pads were left in different positions, spreading the possible creep over a variety of locations.

To verify that the cure and stability of the pedestal were occurring in consonance with the assumptions of the design and the planned loading sequence, the pedestal curing process was monitored. The technique used and the results obtained are presented in Chapter V.

B. AZIMUTH HYDROSTATIC THRUST BEARING

At the time JPL embarked on selection and design of a suitable thrust bearing for the 64-m antenna, recent work had extended the design basis for hydrostatic bearings. Some of the work had been done directly on bearings applicable to large antennas.

The thrust bearing for the 64-m antenna was to be many times larger than any that had been built, and previously unsolved problems in bearing stability, runner design, and reliability were encountered. As it developed, the design and analysis were carried out with no real difficulties in the basic design, although some difficulties were encountered in detailed construction of the bearing, as discussed in Chapter V.

The principle of the hydrostatic bearing, in its simplest form, is shown in Fig. 87. Oil, under pressure, is fed into the pad recess and is forced out in a very thin film across the sill between the pad and the runner. The pressure in the recess and under the sill acts upward on the pad, literally floating it on high-pressure oil. If the flow is maintained constant, the pressure in the recess will be that required to force the constant flow out under the pad sills. An increase in the load on the pad causes the pad to move closer to the runner, reducing the oil passage area and causing the recess pressure to rise until equilibrium is reached. The characteristic of this change is such that the bearing is extremely stiff against changes in the applied load. The load capacity of the bearing is limited only by the available hydraulic pressures, the physical size of the bearing, and the physical properties of the components. Multiple recesses are used to improve stability and reliability.

If the pad moves slowly along the runner, the only resistance is that required to shear the oil at the rate of motion of the pad. Thus the friction is very low and is completely viscous and free from the stick-slip characteristics of other types of bearings.

In the 64-m antenna configuration, the runner of the azimuth thrust bearing is mounted on the top of the pedestal wall, and a bearing pad at each of the three corners of the alidade base triangle supports the alidade, as shown in Fig. 88. The pads are actually floating elements between grease-lubricated spherical seats on the alidade and the bearing runner on the pedestal. Spherical seats permit the pad to adjust to any unevenness of the runner, which cannot be made perfectly flat.

Problems in the following areas were involved in the design of the hydrostatic bearing:

(1) The stability of the pad in following an uneven runner surface — would the pad follow an uneven surface or would it tend to fall from an unstable or metastable condition and drag one corner or one edge?

(2) The stiffness of the bearing against varying loads. High stiffness is required to maintain a high natural frequency of the antenna structure in support of the required servo bandwidth. High stiffness is required not only in the bearing, but also in the structural connection to the alidade.

(3) A uniform film height under all areas of the pad, achieved by matching deflections of the pad and runner. Badly mismatched deflection curves would leave an escape path for the oil in one area of the pad, while the film height in another approached zero, thus compromising both the stiffness and the reliability of the bearing.

(4) Operational reliability achieved by maintaining the bearing operational after failure of one pump, motor, or other flow source element.

(5) The construction of the large-diameter bearing runner. The design permitted a maximum out-of-flatness of 0.076 mm (0.003 in.) over any pad length (1.524 m or 60 in.). Exacting manufacturing and construction methods were required to achieve this.

Work on the problems outlined above was started in earnest during the Phase Ia design

study. The Friction and Lubrication Laboratory at Franklin Institute in Philadelphia, a center for research in fluid film bearings, was contracted to design a flexible program for a digital computer to analyze the pressure and flow characteristics of a multiple-recess hydrostatic bearing pad with nonuniform film height and with any of several practical flow source patterns. This was an extension and expansion of work initiated at JPL by Dr. Senol Utku in the summer of 1962.

The computer program, developed by Dr. Vittorio Castelli of the Franklin Institute and Columbia University, provides solutions of the Reynolds Equation for two-dimensional flow between the bearing pad and runner. Pressure patterns and then flow patterns are developed for a unit pressure in each recess, with zero pressure in the remaining recesses and at the edges of the pad. Because the Reynolds Equation is linear in pressure, these pressure patterns can be superimposed, based on the characteristics of the flow source to each recess, and the total pattern of film height and pressure patterns can be developed for specified conditions of loading and flow source characteristics.

The Reynolds Equation is expanded in difference form and solved for pressures by relaxation over a grid on which the pad geometry and film height are defined. As noted, this solution is carried out for each recess on the basis of unity pressure in that recess and zero pressure in the other recesses. Flow from that recess is determined from the film height and in the pressure gradient around its periphery. Negative flows in the other recesses required to maintain zero pressures therein are also calculated. The pressure/flow relationships for each recess are then combined to give the pressures at the grid points for specified characteristics of flow sources.

The computer program allows for three possible flow source systems:

(1) A common pressure source feeding all recesses in one pad through specified capillaries. The capillaries regulate the flow to each recess, minimizing the tendency of the recess with the lowest pressure to have the largest flow. This arrangement has the virtue that the film height is independent of oil viscosity, but suffers in lower bearing stiffness and reduced righting moment to force the pad to follow an uneven runner.

(2) Flow sources feeding diametrically opposed recesses in pairs, with capillaries regulating the flow to each recess. This is similar to the arrangement under (1) above, except that loss of a pump leaves the pad in a balanced condition.

(3) Fixed flows to each recess, provided by separate fixed-displacement pumps or by a single pump with pressure-compensated flow control valves governing flow to each recess. This arrangement is not balanced in the event of failure of flow to one recess, and the film height is a function of viscosity. However, it does provide the stiffest bearing.

In addition to the flow source type, the program input includes the pad geometry; film height, either directly or in the form of constants applicable to specified mathematical functions; a defined pad tilt; and control commands for various processing and printout options.

The program outputs in nondimensional form are pad loads; recess flows; recess pressures; coordinates of the center of pressure; and, if desired, pressures and film heights at all grid points. The nondimensional output data are converted to engineering units on the basis of the physical dimensions of the bearing pad, the oil viscosity, and the actual oil supply characteristics. This program was also used in evaluating the stiffness and stability characteristics of the various configurations considered.

The next step in the analysis of the bearing was to match the deflection of the pad and runner; that was done in three steps:

(1) An analysis program was developed for the deflection of the bearing runner due to the pressure pattern under the pad.

(2) An analysis program was developed for the deflection of the pad due to the pressure pattern under it, and resisted by the spherical bearing connecting it to the alidade.

(3) A link program was developed in which the hydrostatic bearing program, the runner deflection program, and the pad deflection program were run iteratively, in the following way: assuming that the runner and pad are flat, the pressure pattern under the pad is computed; then deflections for the pad and the runner are calculated, a new (nonuniform) film height is determined, and the process repeated, calculating new pressures and new deflections. This process was found to converge after a reasonable number of iterations.

The deflection of the runner resulting from the pressure pattern under the bearing pad was analyzed in two parts: that due to the deflection of the runner as elastically supported by the concrete haunch, and that due to the deflection of the concrete haunch as an elastic beam supported on the pedestal. In the analysis, the foundation modulus was determined following Biot (Ref. 3), and the conventional flexure equations were solved by iteration using the computer program developed for the purpose.

The computer program for calculating the pad deflection was based on conventional elasticity equations, assumed a central support reaction representing the spherical seat connecting the pad

to the alidade corner weldments, and used the pressure distribution calculated from the hydrostatic bearing program.

The analysis outlined above was carried out for the deflection along the long and short dimensions of the pad. In the latter case, the relative deflections were very small and did not constrain the design.

The final bearing design included the following characteristics:

(1) The pads, made of carbon steel, were 1.016 m (40 in.) wide, 1.524 m (60 in.) long, and 0.508 m (20 in.) deep. There were six recesses in the bottom of each pad (Fig. 89), with the center two slightly larger than the corner recesses.

(2) The runner was also carbon steel, 127 mm (5 in.) thick. Analysis showed that the runner did not play a major part in the deflection problem and that thicknesses ranging from 102 mm (4 in.) to 203 mm (8 in.) would be acceptable. The 127-mm (5-in.) dimension was chosen on the basis of its manufacturability and because it provided space for an acceptable joint design (Fig. 90) between adjacent segments.

(3) The pedestal concrete was required to have a Young's modulus E of 3.5×10^{10} N/m^2 (5×10^6 psi). This, with the 508-mm (20-in.) thick pad, gave design deflection curves for the pad and runner which matched within 0.0254 mm (0.001 in.) over the entire pad area.

(4) The oil viscosity was 114×10^{-6} m^2/s (525 SUS), approximately equivalent to that of SAE 40 motor oil. Oil flow was to be 4.7×10^{-4} m^3/s (7.5 gallons/minute). Recess pressures, in normal operation, were 5.5×10^6 (800 psi) for the corner recesses and 6.9×10^6 N/m^2 (1000 psi) for the two center recesses.

(5) Theoretical film height on an ideally flat runner was 0.2032 mm (0.008 in.). In failure modes, with the oil supply to the two center recesses or to diagonally opposed corner recesses stopped, a minimum of 0.1270 mm (0.005 in.) film height was predicted.

(6) Check valves, installed at the oil entry to the pads, prevent oil from flowing out through the supply line in case of a failure (such as a ruptured hose). In this case, the oil from the adjacent recesses flows through the inactive recess, creating a pressure within that recess tending to maintain film height on the pad. This feature is the key to the operational ability of the bearing under failure mode conditions.

After the design was completed, a one-fifth scale model of the pad and segment of the runner was constructed, representing the elasticity of the pad and runner with aluminum material and the foundation with a large block of Plexiglas (Fig. 91). Capacitance probes were mounted in the runner, which was movable so that all of the pad could be surveyed for film height. A hydraulic power supply, with pressure-compensated flow control valves providing a fixed flow to each recess and a metered hydraulic jack for applying load, was provided. The test results from this model verified the design predictions. The model was also used to test the development and lubrication requirements on the spherical seat between the pad and the alidade corner weldment.

The oil supply system was made up of conventional hydraulic components schematically arranged as shown in Fig. 92. This system can be broken down into three principal sections:

(1) A precharge unit, which draws oil from the hydrostatic bearing reservoir; passes it through filters and then through a heater and a heat exchanger for temperature control; and supplies it to the high-pressure skids. The oil temperature is controlled as a means of controlling the viscosity. Since the bearing does no net work, all of the pump power must ultimately be dissipated as heat in the heat exchanger. The heater is used only to warm the oil when starting the bearing after a shutdown period.

(2) Three high-pressure skids, one for each bearing pad, take oil from the precharge section, filter it, and supply it at a constant flow rate to the pad recesses.

(3) The accumulator system, which, in the event of electric power failure provides a supply of high-pressure oil to maintain bearing operation while the brakes are stopping the azimuth motion.

Redundancy is built into the system in the form of duplicate precharge pumps and filters and duplicate accumulators. The high-pressure pumps are driven by motors driving pairs of pumps supplying diagonally opposite recesses on the pads. Thus, if there is a pump or other flow failure to any recess, the motor for that pump can be stopped and the pad will be left with a symmetrical supply and pressure pattern.

In recent years, since the design of this bearing, major advances have been made in applicable analytical techniques. More sophisticated and capable computer programs for the analysis of the flows and pressures under a hydrostatic bearing pad are now available, and the finite element approach to the analysis of continuous structures would provide an improved approach to analyzing the deflections of the pad and the runner. Details of the analytical methods described in this report are given in Refs. 4 and 5.

C. ALIDADE

The primary design considerations in the alidade were that it provide high stiffness in support of the pointing accuracy and the high natural frequency requirements; that the detailed design reflect the demands of manufacturability and transportability; that control against brittle fracture be assured through proper specification and laboratory test of steel composition and grain size; that it permit an independently founded instrument tower; and that it support the antenna drive system.

The stiffness requirements were established in the dynamic analysis and were set with respect to loads applied at the elevation bearings, the azimuth and elevation drive points, and the azimuth radial and thrust bearings. These requirements were met in the idealized structure as well as in the detailed design of the various joints within the structure. The design problem was unusual in a large structure, in that deflections, rather than stresses, were the governing criteria. In general, the member stresses in the alidade were 25 to 50% of those normally encountered in large structures.

The selected basic configuration of the alidade was a pentahedron supported at the three lower corners and supporting the elevation bearings on the two upper corners. This configuration adapts well to the requirement for a large-diameter azimuth thrust bearing and to clearance requirements for dual elevation bull gears, allowing placement of the instrument tower at the vertical centerline of the antenna. The basic configuration was depicted in Figs. 19-21 of Chapter III.

The initial design of the alidade was carried out by conventional graphical and analytical methods. The final design analysis, including the spring constants relating to the structural dynamics, were calculated on an IBM 7094 computer using the JPL-developed STIFF-EIG program and the STAIR programs (Refs. 6 and 7).

The applied loads on the alidade are shown in Table 4.

The azimuth and elevation gear drives are connected to the alidade through tangential links, with spherical joints permitting the gear drives to move slightly in following the azimuth and elevation bull gears. The elevation drive connections are made into a heavy box section between the rear upper members. The elevation bearing loads are carried by the elevation bearing support weldments, and the azimuth thrust and radial bearing loads are carried into the base triangle corner weldments. Care was taken in the design of each of these weldments to ensure that the applied load is carried through the weldment to the reaction point by adequate members in direct compression or tension. In the elevation drive, a relatively small bending moment is introduced by a slight offset of the tangential links. The horizontal beam carrying this load was designed to keep the resulting bending deflection within acceptable limits.

The base triangle is made up of the corner weldments, which are conventional plate structures, and welded rectangular box sections. The other main alidade members are made up of four 356-mm (14-in.) wide-flange (WF 300) sections welded in a box section as shown in Fig. 20 of Chapter III. This section was selected after studies of more conventional box and tubular sections showed that difficulties would be encountered at the joints where several members come together at different angles.

In the detailed design, all field connections were made with ASTM A325 high tensile bolts designed to carry the actual stress capacity of the members. This provided a considerable margin of safety for the relatively low stresses actually encountered. The largest members used were about 12.2 m (40 ft) in length and weighed a maximum of 45,000 kg (50 tons), permitting highway transportation from the fabrication plant to the construction site.

D. AZIMUTH AND ELEVATION GEAR DRIVES

Azimuth and elevation motions of the antenna are driven by servo-controlled hydraulic motors mounted on and driving through high-reduction-ratio gear drives.

In addition to the usual design problems of capacity and life, the gear drive design involved very stringent stiffness requirements and backlash control, along with extremely smooth operation at low speeds. There were also the problems of manufacturing and installing the very-large-diameter bull gears. In general, conventional design approaches were used, the detail arrangements being the only unusual aspect of the drives.

The economics of size and the stiffness requirements of the drives indicated that large-diameter bull gears should be used. The achievable runout of these large gears when mounted on the structure precluded conventional fixed gear reducers because of tooth mesh problems. Instead, an arrangement was developed in which the gear reducers were connected to the alidade by struts with spherical bearings, permitting movement of the drives while following the bull gears. The separating forces of the gear teeth are taken by a hardened roller mounted on the gear reducer and bearing against a machined surface on the inner diameter of the bull gear. Only the tangential tooth load is transmitted through the connection to the alidade. The dead weight of the gear reducers is supported by auxiliary connections to the alidade which permit the reducers to follow eccentricities in the bull gear.

The basic detailed characteristics of the drives are listed on Table 5. Each gear drive consists of four internal meshes plus the final mesh between the gear box output pinion and the bull gear. All gear teeth are at a 25 deg pressure angle and are rated in accordance with AGMA standards for a minimum operational life of 22,000 h.

A countertorque system is employed to eliminate the effects of backlash in the antenna drive system (Fig. 93). For each axis, each of the four gear reducers has a drive motor and a countertorque motor on the input shaft, and a single output pinion. The drive (D) motors are connected in parallel across the servo control valve. The

countertorque (CT) motors are connected in series to a pressure-regulating valve which provides a constant pressure across these motors, and hence a constant torque output. The countertorque motors are piped so that two provide continuous clockwise torque, while the other two provide continuous counterclockwise torque. Two reducers oppose each other with the constant torque from the countertorque motors. As shown in Fig. 93, Reducer 1 opposes Reducer 2, and Reducer 3 opposes Reducer 4, as indicated by the arrows.

For the condition of no external load on the antenna, the drive motors produce no torque, and the only contributors to torque are the countertorque motors. The output of the opposed reducers is balanced, and there is no net torque on the axis.

With the application of external loads on the antenna, all drive motors drive in the same direction, sharing the load. Two of the CT motors are also driving in this direction and add driving torque. The two remaining CT motors are dragging (acting as pumps) and absorbing torque. The torque on the antenna axis is thus equal to the torque from four D motors plus the torque from the two CT motors aiding, less the torque from the two dragging CT motors.

For most operating wind torques, the dragging CT motors exert more torque than their companion D motors; hence, their reducer output pinions will oppose the driving motion. The driving pinions bear on one side of the gear teeth, and the dragging pinions bear on the opposite side.

If the direction of the antenna rotation is reversed, the dragging pinions and the driving pinions exchange roles simply by the reversal of the driving motors, and there is no lost motion due to backlash.

For very high axis torque, the drive motors overcome the CT motors, and all four pinions assist motion. In this case, the anti-backlash capability is lost.

Stiffness calculations for gear drives have generally been notable for their optimism. On the 64-m antenna, the gear manufacturer performed the calculations for the gears, shafts, and bearing, and contracted with the Franklin Institute for a very thorough analysis of the gear reducer housings. Each gear reducer was tested for stiffness, backlash, and breakaway friction and was subjected to a run-in test. The test method and the results obtained are presented in Chapter V.

E. TIPPING PARTS — REFLECTOR, QUADRIPOD, AND SUBREFLECTOR

The effects of environmental loads were an important consideration in the analysis and design of the reflecting surfaces and supporting structures. Such loads distort the antenna surfaces and/or geometry, resulting in losses in radio frequency gain/aperture efficiency and beam pointing.

Gravity forces change in direction relative to the axis of the tipping parts when elevation angle changes are made, resulting in distortions of the structural shape. Distortions are also created by variable forces from changes in wind velocities and differential changes in the temperatures of the parts.

1. Reflector Structure

To minimize unrecoverable loss of reflector aperture efficiency resulting from gravity-induced distortion, the design of the reflector truss structure was optimized so as to maintain a paraboloidal reflector shape as the structure deflects, at the expense of a changing focal length or production of small, predictable beam-pointing errors. The focal length change can be compensated by a straightforward systematic focusing adjustment, and calibrations can be applied to negate the pointing errors.

Early in the design studies, the need was recognized for an analysis method for accurate and rapid calculation of deflections of a complex structure under various environmental loads. The need was also recognized for a suitable method for best-fitting a paraboloid to a set of deflections from an original different paraboloid — a method that could output the characteristics of the deflected surface in terms of an rms error from the new best-fit paraboloid and could output the necessary origin and axis location data of the new paraboloid to compute the radio frequency boresight direction. The analysis of radio frequency aperture efficiency performance as affected by the irregularities of the actual large reflector surface is based on the rms deviation from a design surface. This follows the approach of Ruze (Ref. 8). Use of this criterion will be illustrated in later discussion on the radio frequency analysis and performance (Chapter V).

By 1961, during the feasibility study period, the STIFF-EIG computer program (Ref. 6) had been developed at JPL for static and dynamic analysis of spacecraft structures. Trial use on idealized or equivalent 26-m antenna reflector structures with a reduced structural member count produced useful demonstration calculations of deflections and stresses. The program's solution algorithm limited its size capacity to the analysis of structures with fewer than 130 deg of freedom, with the use of the IBM 7094 computer.

A sufficiently accurate analysis representation of a single quadrant of the tipping assembly of the 64-m antenna required a solution capacity for 750 joints with 3 deg of freedom per joint, a total of 2250 deg of freedom to analyze a pin-jointed quarter segment. This capability was provided by the STAIR computer program (Ref. 7) developed by the Lincoln Laboratory of the Massachusetts Institute of Technology; the program was obtained by JPL in trade for STIFF-EIG.

Through the use of the STAIR program, data representing one quadrant of the reflector backup structure filed the core of the 7094 computer when only three loading conditions were computed per run. A half-structure limited the loading conditions to one, with double the computing time. A practical balance between final solution accuracy and computer costs was attained by assuming quadrant symmetry — although the 90 deg open structure between the elevation wheels (for

clearance of the optical tower) diluted the validity of the quadrant symmetry assumption.

During the early design study phases, a computer analysis program was developed that provided a minimum rms error criteria best-fit paraboloid to a set of data representing an arbitrarily, but modestly, distorted paraboloid. Using that program, a paraboloid is best-fitted (rms error minimized) to the three component deflection vectors computed using the structural analysis program. The outputs of the best-fit program are the root mean square of the residual errors between the best-fit paraboloid and the actual distorted surface, plus the position of the best-fit paraboloid vertex and the orientation of its symmetry axis. These outputs allow for calculating the antenna gain (or aperture efficiency) of the reflector as a function of frequency and for calculating its boresight axis.

The initial minimum rms paraboloid fitting program was modified and upgraded (Ref. 9) subsequently to include (1) error contour level plot output, (2) focal length change of the best-fit paraboloid in relation to an original undistorted paraboloid, (3) capability to directly input data from field measurements of an actual antenna reflector, and (4) best-fitting with partial data of assumed symmetrical structures.

The capability to input field data was an important aspect of the analysis capability, because the specification of the antenna to the design and construction contractor was in terms of directly measurable mechanical or structural properties of the antenna. For the reflector structure, that meant measurements of the mechanical distortion of the completed reflector as a function of environment (gravity) loading, not measurements of its radio frequency performance: it was JPL's problem to translate the reasonably definable mechanical measurements into actual antenna performance.

Some typical results of the analysis by the STAIR program and the treatment of field measurements on the reflector structure, as well as the use of the rms best-fitting program, are presented in Figs. 94 and 95. These figures show the computer-organized rms error contour plots at horizon and zenith attitudes for the reflector structure, as analytically computed and as determined from field theodolite and chain measurements for the gravity loading difference from a 45-deg reflector alignment elevation.

Because the change in relative direction of the gravity force results in deflections of the reflector structure, it was necessary that the surface panels be set to a desired true paraboloid shape at some mean elevation angle in order to minimize the maximum distortion at other elevation angles. A 45-deg reflector alignment elevation angle, selected on an engineering judgment basis, resulted in a satisfactory distortion pattern at horizon and zenith look elevation angles. Rather fortuitously, the change in distortion at horizon look has been found to be slightly less than at zenith look, resulting in best antenna performance in the most used sky coverage ranges of elevation angles.

Figures 94 and 95 also give the rms error of the distorted surface from the rms best-fit paraboloid and the change in focal length of the new best-fit paraboloid in relation to the original (45-deg elevation angle) paraboloid. A comparison between computed and measured data for the error contours, total rms error from best-fit paraboloid, and change in focal length attests to the serviceability of the analysis technique developed for design and acceptance testing of the reflector structure of the antenna. At both attitudes, the processed field-measured error data are smaller in magnitude than those from the analytical computations (see Figs. 94 and 95). Recently, these differences have been reduced to a very small amount through use of an improved structural computing program (NASTRAN) which allows inclusion of joint stiffness and through improvements in accuracy of processing the field data (Ref. 10).

In addition to gravity loading, the other significant environmental factors, wind and temperature, had to be considered in the design analyses.

For wind loading, pressure coefficients were obtained from the wind tunnel test data previously discussed. The pressure coefficients are converted at a particular wind velocity to concentrated loads applied at the structure joints, and the distortions calculated with the STAIR computer program. Thermally induced distortion results from differential expansion of the structure due to temperature differences within the structure caused by unequal exposure to the sun. The inputs to the computer analysis were the temperature differences of the truss elements.

The analysis techniques used to predict wind and thermal distortion of the reflector structure, and hence allow calculation of radio frequency performance degradation under the environment, are displayed here by the application to a specific case: the reflector axis is at the horizon; the direction of a 13.4-m/s (30-mph) wind is 120 deg yaw angle from the reflector axis; the Sun is 90 deg from the reflector axis.

The temperature differences for this case were applied to all ribs outside the main girder on one side only, representing a condition with the sun shining at a right angle to the reflector axis. The temperature difference at the outside chord of the ribs exposed to the sun was assumed to be at +5.6°C (+10°F); at the diagonals of the rib trusses, because of partial shading, to be at +2.8°C (+5°F); and at the top chords next to the surface panels, in the shade, to be at 0°C (0°F) — tests using special painted steel parts showed that for the reflector structure, properly painted, a 6°C (10°F) difference between the sunlit and the shaded portions is a reasonable design assumption.

The results of the temperature loading distortion computations are shown in Fig. 96a; the contours represent the distortion from the original unloaded paraboloidal surface (defined by the reflector panel attachment points). The plane of the main girder line dividing the rib and hoop trusses under the temperature load from the

unloaded (shaded) ribs is also indicated in Fig. 96a.

Similar data showing the calculated distortion from the assumed wind loading are shown in the contour plot of Fig. 96b. Figure 96c shows the error contours representing the vectorial addition of the distortions from wind and temperature loading and the horizon-look gravity distortions. When the sum of the wind, temperature, and gravity distortions of Fig. 96c is best-fitted by a paraboloid using the rms program, the residual errors are as shown by the error contours in Fig. 96d; the figure also shows the resulting overall rms error between the distorted surface and the best-fit paraboloid, as well as the change in focal length of the best paraboloid relative to the original undistorted paraboloid.

It has not yet been possible to implement and process field measurements on the reflector to compare directly with these temperature and wind distortion calculations.

The techniques developed to compute the approximate pointing error contribution of the reflector structure and to relate the field measurements of the structure are described below.

The discussion below concentrates on the pointing errors in the vertical plane (elevation angle error). The major cause of elevation angle error of the reflector is the change in gravity-induced deflections as the reflector is elevated or depressed. The reflector pointing errors in the horizontal plane conceptually result mainly from wind forces. On the basis of the computations of wind-induced reflector distortions just discussed, the pointing errors due to the wind environment should be significant. However, as noted, it has not been possible so far to develop practical field instrumentation that could provide experimental data to support a meaningful comparison with the calculation. Also, during the several years of operational experience on the antenna at S-band frequencies using radio frequency beam pointing controlled by ephemeris command, no significant systematic wind-induced tracking errors have been identified.

It is recognized that there are compensating deflections of the subreflector, similar to the gravity case but more difficult to calculate (and at present uncalculated), that in concept act to reduce the resulting wind-induced radio frequency beam pointing errors. Although the matter of wind-induced error evidently does not significantly affect S-band operations, the planned use of the 64-m antenna at X-band and higher frequencies to the limit of the antenna performance capabilities, makes it important that this behavior be understood on a sound engineering basis. Analytical and experimental work in this area is being continued.

As an example of calculation and comparison with field data of the reflector elevation angle errors, the error from the baseline setting at 45-deg elevation angle to zenith look will be considered; comparable results were obtained for the 45-deg to horizon look range, with the exception of somewhat wider error tolerances in the field data made below 20-deg elevation angle.

The deflections of the paraboloid from the paraboloid best-fitting rms program provided data for computing the radio frequency boresight direction of the paraboloid. Figure 97 shows the best-fit paraboloid data for gravity deflection at zenith look, with the surface panel attachment points defined or set to a perfect paraboloid at 45-deg elevation. The fit to the STAIR program–computed deflections in terms of reflector axis orientation and origin and focal length is shown in Fig. 97a, and the fit to the field data is shown in Fig. 97b.

2. Reflector Surface

In the preceding analysis of the reflector backup structure, the calculations do not account for errors in manufacturing or for errors that result from environmental loading of the reflector surface panels.

The radio frequency reflecting surface is formed by panels spanning and supported by the work points or nodes of the reflector backup structure. Reflector panels were fabricated by riveting a contoured sheet of 2.36-mm (0.093-in.) thick aluminum to contoured, rivet-jointed frames of Z-section aluminum angles. The basic reflector panel design was in production for Rohr Corporation's 26- to 30-m (85- to 98-ft) antennas, and straightforward calculations based on their performance for that application showed that the design was adaptable for use on the 64-m antenna.

The approach to validating the reflector panel and framing design was largely empirical and experimental. To demonstrate that no structural stability problem for the "free" flange side existed for the surface panels loaded from the back side, a shop test of an experimental panel was made using common bricks simulating the air loads on a panel supported on its normal fasteners. Critical wind conditions were simulated at speeds up to 53.6 m/s (120 mph) at stow position and 31.3 m/s (70 mph) into the back of the reflector. The test showed that analytical answers from the aluminum handbook equations were conservative for the flange buckling case, and, in fact, an X-shaped bracing provided on the back of the panels was found to be redundant.

On the basis of the shop tests, the maximum deflection of a panel was predicted to be approximately 0.762 mm (0.030 in.) under an air loading of 203.0 N/m^2 (4.25 lb/ft^2), corresponding to the antenna at 120 deg yaw in a 13.4-m/s (30-mph) wind. Considered as approximately a 2.5 sigma loading condition, the 0.762 mm (0.030 in.) figure is equivalent to 0.305 mm (0.012 in.) rms; a negligible addition, by the panels, to the rms deflections of the reflector support structure from environmental loads. Also, the basic dead weight of the panels is less than 95.5 N/m^2 (2.0 lb/ft^2), so that the panel deflections due to the change in gravity load direction produce negligible distortion.

The panel fastenings must resist large axial forces from the wind loads acting normal to the surfaces of the panels and modest side forces developed from gravity and from wind loads on the webs of the beams used in the panel frames. Also, with changes in ambient temperature,

differential expansion occurs between the aluminum surface panels and the steel in the reflector structure. Therefore, a controlled flexibility in the side force direction is essential in the panel fastenings to prevent high stresses in the panels.

The design requirements of this fastener were satisfied with a corner fitting aluminum casting riveted to two Z-beams meeting at a corner. Through a threaded bushing in the outer leg of this casting, there is a stainless steel, ball-ended screw, rotatable through a hole in the surface skin and held in a socket tightly screwed to the top chord of the reflector structure's rib.

As with the reflector structure, the panels were specified to the design and fabrication contractor on the basis of their measurable structural/mechanical characteristics rather than their radio frequency performance. The empirical techniques were straightforward but required careful execution. The finished panels were set up in a measuring fixture with support points exactly on the design paraboloid, and errors from the true paraboloid were measured normal to the plane described by the support point corners. The measured error readings of each panel and for the total of all readings were reduced to an rms error per panel and for the entire set of panels. Based on numerical analysis, an rms error for the complete set of panels was computed and was assumed to describe the distortion of the entire reflecting surface as a random error which was added to the rms error of the support points of the reflector backup structure for purposes of analyzing and predicting the radio frequency performance of the total reflector. The results of these analyses and measurements on the completed antenna are described in Chapter V.

3. Quadripod and Subreflector

The design of the quadripod to support the hyperboloidal subreflector was a trade-off of its radio frequency aperture blocking characteristics and its structural stiffness and strength as a crane-like beam for hoisting the Cassegrain feed cones into place. (The radio frequency considerations and analysis are discussed below in Subsection I, Microwave Optics.) The quadripod configuration was also required to mate with suitable hard mount points in the reflector backup structure in such a way that the quadripod loading would not act to distort the reflector paraboloid.

The hyperboloidal subreflector design was straightforward; it used aluminum surface panels mounted on a steel supporting truss, which was mounted by means of an adjustable focusing fixture to the apex structure of the quadripod. The adjustable feature was provided to allow optimization of the microwave optics as the elevation angle is changed; the adjustment is not used for normal S-band operations, but for X-band operations it corrects for an otherwise significant performance degradation—since the focusing adjustment of the radio frequency feed system is made from a remote console in the control room.

The deflections under gravity loads of the quadripod and subreflector connections were analyzed using a computer program (Structural Analysis and Matrix Interpretive System, or SAMIS) (Ref. 11), which allowed for including member stiffness and connection rigidity as well as axial properties of the structure. The SAMIS program was also used to calculate the gravity deflections of the primary feed horn mounted in the Cassegrain cone. These calculations, along with the STAIR program analysis of the reflector backup structure to determine the distortions of the quadripod feed mounting points, allowed the calculation of the quadripod's gravity-induced error contribution to beam pointing.

Figure 98 summarizes these deflections in terms of shifted reflector focal position calculations for the conditions previously presented in the example for the reflector structure – namely, the gravity-induced distortions at zenith look for assumed perfect alignment of the quadripod and its support, and for the subreflector and primary feed, at a 45-deg elevation. These computed results are shown in Fig. 98a; similar data based on analysis of field theodolite and chaining measurements are shown in Fig. 98b. The agreement between analysis and field measurements is qualitatively good and quantitatively adequate.

4. Computation and Field Data Analysis to Predict Radio Frequency Beam Pointing Errors

Gravity-induced radio frequency beam pointing errors result primarily from deflections of the main reflector structure and of the quadripod support structure. The configuration of the 64-m antenna design is such that these two error sources largely compensate for each other, resulting in a relatively small net beam pointing error.

The calculation and reduction of field measurements for the reflector structure and the quadripod/subreflector/primary feed distortions under gravity loading were combined to estimate resulting radio frequency beam errors from the complete microwave optics supporting structural assembly. In this process, which is depicted in Fig. 99a (computed) and Fig. 99b (analysis of field data), a ray from the deflected position of the hyperboloid's secondary focus is reflected from the vertex of the best-fit paraboloid at an angle of reflectance equal to 0.82 times the angle of incidence (this multiplying factor assumes a uniform radio frequency illumination of the paraboloid). For the computed case, the intermediate reference surface (IRS) mirror position, which is taken as the mechanical representation of the radio frequency beam axis, was assumed to be fixed to the reflector structure's center hub.

To summarize from the presentation in Fig. 99: the radio frequency boresight error, with respect to the IRS mirror, produces angle errors of +0.020 and +0.004 deg, respectively (the + error produced is in the direction to cause the beam to point below a commanded elevation angle).

It is expected that improved agreement can be achieved between the wholly calculated and the measurement-based pointing errors with the use of the NASTRAN analysis program (Ref. 10) now available, which allows analysis of large structures involving beams with bending rigidity and

plates. Future improvement of the field measurement precision is also anticipated. The methods described for the analysis and validation of the 64-m antenna are considered adequate to provide an accuracy of approximately 0.020 deg in predicting radio frequency beam pointing, a barely adequate level of precision.

The calculations described above were made by JPL; calculations made by the antenna design and construction contractor (Rohr Corporation) to show a design capable of meeting the specifications are given in Ref. 12. Data from radio frequency beam measurements are discussed in Chapter V.

F. STRUCTURAL DYNAMICS

The dynamic properties of the antenna structure are integral to the closed-loop servo steering system and directly affect the radio frequency beam pointing capability in tracking a moving target or operating under the influence of a dynamic environment. To satisfy the dynamic pointing requirements in what is considered to be a straightforward and conservative manner, a relatively high lowest natural frequency was required of the structure. Because designing authentically to a high lowest natural frequency is a difficult and uncommon requirement for very large structures, the matter was given considerable attention — a thorough analytical and modeling structural dynamics activity was begun with the Phase I design studies and carried through to the completion of design.

The structural dynamics studies aimed to provide:

(1) An adequately representative model of the structure from which dynamic characteristics, in the form of transfer functions and spring constants and inertias, could be obtained for use in the servo system design.

(2) An insight into the relationships between the structural configuration and detail design and the structural dynamic characteristics, with a method of readily analyzing the effects of design changes on the system dynamics.

At the outset, the basic problem in the structural dynamics analysis was that of reducing the complex structure to a lumped-parameter spring-mass model of a size which could be handled with available computation methods and yet was large enough to represent satisfactorily the characteristics of the structure. The problem was complicated by the variety of driving and readout points involved in the various modes of servo operation, each of which had to be available in the model for determining the needed transfer functions.

During the Phase I design study, the various contractors made simplified dynamic models of the structure, characteristically of 5 to 8 degrees of freedom, for which natural frequencies were computed by available numerical methods. In the later Phase Ia study, a more complete model was developed, with an eigenvalue computing program allowing 50 degrees of freedom and capable of providing the natural frequencies of the structure and the related mode shapes.

Difficulties encountered in the use of this eigenvalue program led to a JPL-funded study using an analog simulation. This simulation involved a detailed modeling of the lower structure (alidade, pedestal, and drives) and a representation of the reflector in terms of its normal modes. The results of this study indicated that a lowest natural frequency of approximately 2 Hz could be achieved, based on the Phase Ia study configuration. The validity of the analysis methods was tested by calculating the lowest vibrational modes of the 26-m Az-El antenna at the Goldstone Venus Station and then comparing the results with field measurements performed on the antenna — a rather difficult and exciting task. The comparison was modestly satisfying.

The specification for the final antenna design (Ref. 1, Rev. 4) required computer studies to determine the significant frequencies and the transfer functions applied to the drives and wind disturbance characteristics of the antenna, based on models of at least 15 degrees of freedom for each axis. These studies were required to be kept up to date as the design proceeded and included the following specific tasks:

(1) Development of a lumped-parameter model for azimuth and elevation motion.

(2) Determination of transfer functions from the drive motors to the reflectors for azimuth and elevation motions at elevation angles of approximately 5, 45, and 85 deg.

(3) Determining the transfer functions of wind disturbances on the antenna position at reflector elevations of 5, 45, and 85 deg.

(4) Studying the lower natural frequencies and mode shapes of the elevation and azimuth models independently and with the two models coupled together by the cross-coupling in the design configuration.

(5) Developing simplified models for use in control system analog studies.

In the final design specification (Ref. 1, Ref. 4), a minimum natural frequency of 1.5 Hz was established for the antenna structure, under conditions with the drive motors locked and including the compliances of the soil, concrete, structures, and drives.

The final design lumped-parameter models used for elevation and azimuth motions are shown in Figs. 100 and 101. These models have 15 and 16 degrees of freedom, respectively, and contain the information for the desired transfer functions; the parameters of the models are given in Table 6.

The actual spring and mass parameters were based on idealizations of the structure to achieve a lumped-parameter representation. The dynamic equations were based on combinations of

the springs and masses shown, together with appropriate physical dimensions and kinematic relationships. As a final step, equations of motion were written for each mass, and the actual dynamic matrices were developed by the use of Lagrange's equations.

A difficult part of developing satisfactory dynamic models was the approximation of the reflector and the related tipping structure by a lumped-parameter model of reasonable size. The reflector model was developed by first calculating its natural frequencies, using the JPL-developed STIFF-EIG program, and then developing lumped-parameter models with the equivalent total mass and lower natural frequencies, and with the same input impedance at low frequencies as the reflector. The complete tipping structure was beyond the capabilities of the STIFF-EIG Program, which is limited to approximately 180 degrees of freedom. The problem size was reduced by noting the essential symmetry of the structure and reducing the analysis to one quadrant of the structure with symmetric and antisymmetric boundary conditions on the radial edges of this quadrant, which are the planes of symmetry.

Utilizing the conditions of forces and displacements applicable to symmetric and antisymmetric planes of symmetrical reflector structures (Ref. 13), the model of the reflector structure can be reduced to one-fourth size. Further reduction was obtained by eliminating one-half of the ribs and transferring one-half of their weight and relative stiffness to each of the two adjacent ribs. With these reductions, the reflector could be analyzed by the STIFF-EIG program.

Because of the symmetry conditions, there is no cross-coupling between azimuth and elevation motions in the analysis model. For the real structure, the possibilities of cross-coupling arise from variations in member properties from friction, and from within the servo electronic and hydraulic circuits. Sensitivity analysis of reduced models indicated that cross-coupling arising from small structural variations had no significant effect on the poles and zeroes of the system transfer functions. An analysis was made of the possibility of stability problems arising from friction-induced cross-coupling, and these were shown to be negligible. Cross-coupling within the servo circuits was minimized by careful detail design, including accumulators in the hydraulic supply lines to the servo valves, large-diameter hydraulic drain lines, careful cable shielding, and well-regulated power supplied.

As the final design was nearing completion, spring constants and masses for the dynamic model were refined, and the lowest resonant frequencies and mode shapes were calculated. These calculations showed that the lowest frequency was related to a low transverse compliance at the elevation bearing connection to the tipping structure. A design modification was made, and this problem was eliminated. When the final design was completed, spring constants and masses were finally recalculated and inserted into the model to assure that the minimum resonant frequency criteria would be met.

Final transfer functions for the servo system analysis were obtained from the dynamic model matrices. For the azimuth and elevation axes, they included the following:

(1) Rotation of the reflector core representative of the intermediate reference structure as a function of drive motor motion.

(2) Rotation of the drive pinion as a function of drive motor motion. The drive motor pinion is a measure of the azimuth data box input.

(3) Free rotor deflection across the drive spring as a function of motor motion. This is a measure of the impedance of the antenna as seen by the drive motor.

G. SERVO DESIGN AND ANALYSIS

The servo system design for closed-loop steering of the antenna was a critical problem. After the structural characteristics within the servo loop and the wind forces acting on the servo loop had been characterized, however, the development of the design was straightforward.

Closed loops for position and rate control were needed to satisfy the performance requirements: the effects of wind loads are counteracted primarily by a stiff servo position loop, while friction and deadband errors are reduced by a wide-band servo rate loop.

The position loop bandwidth is constrained by the lowest significant natural frequency of the structure. A position loop bandwidth of 0.2 Hz was required to maintain an acceptable tracking error over the range of target dynamics. This led to the design specification of a 1.5-Hz lowest significant natural frequency in the antenna structure. This very conservative 7.5 to 1 margin between the lowest structural natural frequency and the position loop bandwidth was specified because, at the time, we had a low confidence factor in our ability to accurately predict the natural frequency of such a large complex structure — normally, a 4-to-1 margin would suffice. The position loop was analyzed to determine the error due to wind gusts. Using the empirical model of the wind power spectrum that was presented in Fig. 76, the error due to wind environment was estimated. For example, for a 13.4-m/s (30-mph) mean wind velocity, the parameters of the wind spectrum are (see Fig. 76),

$$\omega_1 = \frac{13.4\ \text{m/s}}{64\ \text{m}} = 0.21\ \text{rad/s}$$

$$\omega_2 = 2\ \text{rad/s}$$

The resulting angle error θ is then determined by evaluating

$$\theta\ \text{rms} = \left\{ \int_{-\infty}^{\infty} \left|Y(j\omega)\right|^2 S_{T_\omega}(\omega)\, d\omega \right\}^{1/2}$$

where S_{T_ω} is the power spectrum of the wind. Substituting the Laplace operator s for j_ω,

$$Y(s) = \frac{s}{\left[\omega_c K \frac{s}{\omega_c} + 1\right]\left[\frac{s^2}{\omega_n} + 2\left(\frac{s}{\omega_n}\right)\zeta + 1\right]}$$

where

ω_c = servo corner frequency

K = effective spring constant of the antenna structure below its lowest resonant mode

ω_n = lowest antenna structure resonant frequency

ζ = antenna structure damping factor in the neighborhood of ω_n

Evaluation of the integral based on the design parameters yields a 3σ maximum error for wind gusts of a 13.4-m/s (30-mph) mean velocity of 0.008 deg.

The position loop compensation is a modified Type 2 system. An integration network is combined with a lead-lag network to provide adequate phase margin at the frequency specified for closing the loop. This type of compensation provides a maximum loop gain and is stable over the expected variation of error signal gain slope.

The rate loop was designed with a wide bandwidth to minimize the position loop phase shift and the effects of component friction and deadband. The rate loop is closed using dc tachometers, which are coupled to the first reduction stage of each gear box. The four tachometer voltages are averaged and compared to the rate command voltage, or integrated position error signal within the servo amplifier. A block diagram of the rate loop is shown in Fig. 102, and a plot of typical closed loop amplitude and phase characteristics is shown in Fig. 103.

To help achieve the desired bandwidth and gain in the rate loop, an evidently unusual technique was employed. Inertia disks totaling five times the reflected antenna inertia were added to each drive motor shaft. The primary effect of this inertia is to lower the hydraulic resonant frequency, which allows higher rate loop gain. The inertia also acts to decrease the pole-zero frequency spacing of the structural resonances as measured at the drive point by the tachometers. This second characteristic reduces the phase and gain variations on the rate feedback signal as the structural resonances are excited.

Lead-lag compensation with the lead corner at 2 Hz is used to provide the phase margin required to close the rate loop above the hydraulic resonance. The hydraulic resonance is at 1.1 Hz in the azimuth axis and 1.2 Hz in the elevation axis. The rate loops are closed at 4 Hz or above in both axes. In concept, the bandwidth of the loop is limited only by the phase delay of the servo valves and could be set at 6 to 10 Hz. However, in the actual system, a 30-Hz resonance between the motor and the tachometer limits the loop bandwidth.

During the final design phase of the antenna, the detail design of the rate loop was tested and verified by an analog computer simulation. This simulation included the lowest four vibration mode frequencies of the composite structural model, the gear boxes, the drive motors, and the servo valve characteristics. The simulation was done in two stages: first as a linear system and then with the major nonlinearities included.

A servo-valve-controlled hydraulic system was chosen to drive the antenna after a careful comparison was made with several other types, including dc electric motor generator sets, eddy-current clutches, and servo-pump-controlled hydraulics. The servo-valve hydraulic configuration was selected on the basis of over-all technical performance and operational experience with similar systems on the DSIF 26-m antennas.

The detailed design and implementation of the servo drive system were controlled by the torque and dynamic speed range requirements — the system was required to operate smoothly through the angle velocity range of 0.5 deg/s to 0.001 deg/s. Basically, standard commercial components were used; however, certain critical characteristics had to be specially tailored or selected: for example, maximum allowable motor friction and minimum internal leakage; servo valve bandwidth, flow gain, and null leakage; and tachometer noise level and linearity.

H. MASTER EQUATORIAL DESIGN AND ANALYSIS

The angle data system of the 64-m antennas, which includes the master equatorial instrument, is used to control the pointing direction of the radio frequency beam. The reasons for adopting the master equatorial, along with a discussion of its basic functions, have been covered in Chapters II and III.

The distribution of tolerances within the allowable radio frequency beam pointing error was one of the major tasks of the preliminary design. The initial division was to allocate 0.015 deg to the basic antenna and the balance (~0.008 deg, assumed to be independent and uncorrelated) to the angle data equipment, including the master equatorial. The antenna portion of the error is between the radio frequency beam position and the reference structure located behind the reflector. The antenna error sources include wind and thermal effects, deadload deflections of the primary and secondary reflectors, the field alignment tolerances of the total reflector assembly, and the antenna servo tracking error. The angle data equipment error sources include the structural-mechanical deflections of the master equatorial, the encoders, the autocollimators, the alignment of the master equatorial with the Earth axis, the alignment of the antenna-mounted optical equipment with the reflector datum plane, and the master equatorial servo tracking error.

Initially, in the design of the total antenna system, it was planned to provide compensation

for the reflector deadload errors as a function of elevation angle. However, as the design evolved, it was found possible to virtually balance the error contributions of the primary reflector with the secondary reflector rotation and translation so that this complication was eliminated. The initial error budget for the angle data system, including the master equatorial, is shown in Table 7.

With such a rigid specification on the master equatorial instrument, it was decided that a careful preliminary analysis of the configuration concept should be carried out. The configuration that was analyzed is shown in Fig. 104.

The pointing vector, normal to the plane mirror mounted at the center of the declination shaft, can be specified by an hour angle ψ and a declination angle θ. On a perfectly aligned and rigid instrument, these two angles correspond, respectively, to the angular displacement of either end of the polar shaft and to the angular displacement of either end of the declination shaft. On an actual instrument, however, the mirror pointing vector does not correspond exactly to the displacement of the shaft ends, and it is this discrepancy or error angle that was considered. The analysis evaluated the contributions to this error angle caused by gravity loading, shaft bearing runout, orthogonality alignment of the two shafts, and temperature gradients in the structure. From Fig. 105, it may be seen that the error angle ϵ between the mirror and the shaft ends is

$$\epsilon = \left[(\phi \cos \theta + \zeta \sin \theta)^2 + \eta^2 \right]^{1/2} \qquad (1)$$

It was assumed that the structure was symmetrical about the polar axis and statically balanced about both axes; therefore, it was necessary to consider only asymmetrical gravity loads, since only those loads contribute to an angular deflection at the center line of the declination shaft. Since the polar shaft is round, its contribution to the error angle is independent of the hour angle ψ and can be compensated. Therfore, the structure was assumed fixed at the juncture of the polar shaft and yoke.

Because the stiffness of the yoke in planes yz and xz is different (see Fig. 106), the error caused by gravity loading will vary with the hour angle ψ. Under the additional assumptions that no moment can be transferred through the declination shaft bearings, and that each leg of the yoke is a prismatic beam, formulas were developed on the basis of conventional static structural analysis techniques for the angular deflection components ϕ, η, and ζ for two hour angle positions, namely, for the case where the declination shaft is parallel to the ground (ψ = 90 deg), and for the case where the declination shaft lies in a vertical plane (ψ = 0). For intermediate values of ψ, intermediate error angles would be obtained. The detailed development of the error formulas is presented in Ref. 14.

If the two shafts of the master equatorial instrument are supported by antifriction bearings, there will be an error component caused by runout of the inner races and another caused by the epicyclic action of nonuniformly sized rolling elements.

The concept that there is a line, within a bearing-supported shaft, which does not move in space during rotation of the shaft is based on the assumption of a perfectly circular inner race. This concept does not apply to real bearings because no inner race is perfectly circular. A more realistic concept assumes that the inner race is elliptical and that there is a finite variance among the diameters of the rolling elements. These latter assumptions yielded the following angular error component for the runout of each shaft:

$$\epsilon = \frac{2\Delta d + (a + b)}{\ell} \qquad (2)$$

where $2\Delta d$ is the difference between the diameters of the largest and smallest rolling elements, a and b are the semimajor and semiminor axes, respectively, of the elliptically shaped inner race, and ℓ is the spacing between the two bearings.

The inner race radial runout as listed in most bearing catalogs corresponds to the numerator of Eq. (2). For the best grade ball bearings of the size appropriate for the master equatorial, this value is approximately 5.1×10^{-3} mm (200 μin.); specially prepared or selected bearings can be slightly better.

If the two legs of the yoke are at different average temperatures, an angular error will be produced. The electronic equipment mounted on the declination shaft and the drive motors mounted on the yoke (see Fig. 104) constitute heat sources. By suitably insulating the mounting of these power units and providing a temperature controlled environment, it was estimated that the effective temperature difference between the legs of the yoke would not be greater than 1.7°C (3°F). For those conditions, the resulting error angle is

$$\phi = \frac{\Delta T \, \alpha L_2}{L_3} \qquad (3)$$

where α is the coefficient of linear expansion, L_2 and L_3 are given in Fig. 106, and ΔT is the average temperature difference between the yoke legs.

It was necessary that the declination shaft be very nearly perpendicular to the polar shaft. In boring the yoke for the declination shaft bearings, a relative offset error would inevitably result. In order to limit this component of angular error to, say, 2 seconds of arc, the relative offset error could not exceed 0.0089 mm (0.00035 in.) for a 914-mm (36-in.) wide yoke. It did not seem reasonable that this kind of offset tolerance could be obtained on a yoke of the size under consideration. Therefore, it was necessary to incorporate an adjustment of one bearing position.

This adjustment can be achieved by making the outer diameter of one bearing eccentric with respect to its center. Such a feature can be accomplished in several ways, all of which offer certain difficulties. It was quite important that the radial deflections of the bearings at each end of the declination shaft be nearly the same, or an additional error component would exist. The adjustable bearing had to be very carefully designed.

If the relative offset error of the declination shaft bore can be limited to 0.102 mm (0.004 in.), and this eccentricity built into the adjustable bearing, a very sensitive orthogonality adjustment is possible. If the smallest practical adjustment of the eccentric bearing is taken as 2 deg, the maximum residual orthogonality error is

$$\phi = \frac{0.00012}{L_3} \tag{4}$$

A preliminary design configuration study of the master equatorial established that a yoke of the width and depth shown in Fig. 107 was large enough to provide for mounting the autocollimator and tracking mirror. In order to obtain a numerical estimate of the angular error components, the foregoing analyses were applied to this particular representative design. The material chosen was steel; the polar bearings were spaced 559 mm (22 in.) apart; the concentrated mass weight $\underline{W}$ was 9.07 kg (20 lb); the dimension $\underline{R}$ of Fig. 106 was 305 mm (12 in.); and other necessary parameters were computed from the dimensions of Fig. 107.

By the application of the structural distribution relationship developed in Ref. 14, the following error angle components, in seconds of arc, that were caused by gravity loading were obtained for the representative design configurations:

$$\phi_{\psi=0} = -0.63$$

$$\eta_{\psi=0} = 0.18$$

$$\zeta_{\psi=0} = 0$$

$$\phi_{\psi=90} = 0.03$$

$$\eta_{\psi=90} = 1.28$$

$$\zeta_{\psi=90} = 0.067$$

which, properly consigned, give total errors of

$$\epsilon_{G_{\substack{\psi=0\\ \theta=0}}} = 0.66$$

$$\epsilon_{G_{\substack{\psi=90\\ \theta=66}}} = 1.28$$

The bearing runout errors were estimated from Eq. (2) by setting the numerator at 5.1×10^{-3} mm (200 μin.). For the polar shaft, the error may be in the direction of ϕ or η and is

$$\phi \text{ or } \zeta = 1.87 \text{ arc seconds}$$

For the declination shaft, the error may be in the direction of ϕ or ζ and is

$$\phi \text{ or } \zeta = 1.14 \text{ arc seconds}$$

From Eq. (3), the temperature gradient error is, for the assumed temperature difference,

$$\phi = 2.17 \text{ arc seconds} \tag{5}$$

From Eq. (4), the orthogonality error is

$$\phi = 0.69 \text{ arc seconds} \tag{6}$$

By properly combining all of the errors above and substituting them into Eq. (1), the following maximum total angular errors for the representative design are found:

$$\epsilon_{\substack{\psi=0\\ \theta=0}} = 6.50 \text{ arc seconds} \tag{7}$$

$$\epsilon_{\substack{\psi=90\\ \theta=0.65}} = 6.03 \text{ arc seconds} \tag{8}$$

The error component from one part of the bearing runout error, namely, that from a variation of rolling element size, is a random error. The temperature gradient error is also random. The other errors are systematic, in the sense that they could be repeated.

The numerical errors given above were developed, as stated, for the preliminary configuration design of the master equatorial to obtain an early validation of compatibility of the master equatorial concept with its allocated error budget. An unanticipated benefit was that the analysis gave improved insight into some of the design trade-offs which benefited the final design. Analysis of the final design by the contract supplier of the master equatorial instrument was done routinely, following the methods discussed above.

I. MICROWAVE OPTICS

At the time the basic microwave optics configuration was being defined for the 64-m-antenna as a Cassegrain geometry, the application of the particular feed type in microwave paraboloidal

antennas was just beginning; also, the design and use of antenna feeds to provide very low receiving system noise temperature was a new technology. This section outlines the techniques used to accomplish the design and predict the performance of the initial feed system for the antenna.

1. Design Criteria

The primary criterion of the microwave optics design for the 64-m antenna was to maximize the ratio of antenna gain to system noise temperature (that ratio was termed the figure of merit) at the S-band receiving frequency. Secondarily, it was necessary to maintain a low sidelobe level at angles within a few degrees of the antenna axis in order to permit tracking close to the sun without undue increase in the apparent antenna noise temperature. The forward-looking spill-over at the hyperboloidal secondary reflector, resulting in the significant aperture blockage by that reflector, presents a basic problem with Cassegrain feeds for such an application and caused considerable concern during the early design phase. However, despite that inherent weakness and the limited prior design and application of the type of feed, it seemed that for very large (in wavelengths) paraboloidal reflectors, Cassegrain optics could, when properly optimized, provide a combination of high aperture efficiency, extremely low antenna noise temperature, and acceptable near-in sidelobe level control.

The microwave optics design was studied theoretically and experimentally by the four Phase Ia study contractors. In addition, an experimental effort under Dr. Peter Foldes of the RCA Victor Co., Ltd., in Montreal, Canada, was sponsored by the Jet Propulsion Laboratory. The latter contract was specifically aimed at empirically determining the optimum geometry and any other parameters significantly affecting the antenna structural design.

Simultaneously, an analytical study was done at JPL to evaluate the radio frequency design. Particular emphasis was placed on improved figure-of-merit feed design, optimum subreflector size, the performance factors which vary with f/d ratio, and the efficiency of the antenna when it is operated in the simultaneous-lobing, angle-tracking mode.

2. Basic Feed Parameter Definition

The size range of the hyperboloidal secondary reflector and the primary feed, defining their principal interaction with the antenna structural design, was resolved in the following rather simplistic way.

The geometry of a typical Cassegrain system is represented in Fig. 108. Using standard ray tracking techniques, the effect of the subreflector on the secondary pattern sidelobe level may be predicted approximately.

In this approximation, the dish aperture field is given as a linear superposition of the field, without blocking, onto a negative field which exactly cancels the field over the subreflector region and is zero elsewhere. The system secondary pattern is derived as a linear superposition of the diffraction patterns of the two aperture distributions. The spurious sidelobe envelope, therefore, corresponds to the diffraction pattern of a circular aperture the size of the subreflector. In the case of the 64-m-antenna with a reasonably sized secondary reflector, the first null of this diffraction pattern is about 2 deg removed from the main beam axis, which is the closest to the sun that the antenna was specified to track. Thus, the first sidelobe level of the blocking aperture had to be considered; its main beam could be neglected for this consideration. Under these conditions, the maximum subreflector size is approximated by

$$d = \left(\frac{\eta\alpha}{\pi^2 G}\right)^{1/4} (D\lambda)^{1/2}$$

where (see Fig. 108)

η = overall efficiency

α = desired sidelobe level relative to isotropic

G = (assumed) first sidelobe level of blocked aperture relative to its main beam

D = diameter of primary reflector

λ = wavelength of operation

Assuming the values tabulated below for the parameters defined above, a maximum subreflector size based on the criterion of the near main beam sidelobe level may be determined as follows:

η = 0.65

α = 10 dB

G = -17.6 dB

D = 64 m (210 ft)

λ = 0.131 m (0.429 ft) (2295 MHz)

d = 7.0 m (23 ft) (the maximum size of the subreflector)

The actual diameter of the subreflector was selected as 6.1 m (20 ft) to provide ease of quadripod support design — note that the area of the secondary reflector is small (~1%) relative to the primary reflector and hence the basic aperture efficiency is a weak function of the secondary reflector size.

Having established the basic dimensions of the secondary reflector, the next step in defining the microwave feed interface with the antenna structure was that of identifying the approximate size of the primary feedhorn.

It can be seen from Fig. 108 that the feedhorn at F' can have a maximum size d_{max} without introducing further aperture blockage beyond that caused by the secondary reflector. From inspection, it can be seen that

$$d_{max} = d\left(\frac{FF'}{OF}\right)$$

The angle γ subtended by the subreflector, as seen from the horn, is given by

$$\gamma = \frac{d}{FF'}$$

The minimum feedhorn width, d_{min}, for a 10-dB illumination taper on the subreflector, is given by

$$d_{min} = 2\frac{\lambda}{\gamma} = 2\lambda\frac{FF'}{d}$$

The ratio β of the maximum allowable feed size to the minimum necessary size is thus given by

$$\beta = \frac{d_{max}}{d_{min}} = \frac{d^2}{2f\lambda}$$

where f = dish focal length OF. For the subreflector diameter of 6.1 m (20 ft) and focal length of 18.3 m (60 ft), β is equal to 7.8. From this approximate analysis, it was evident that there was a very substantial flexibility available to the feed system design within the antenna configuration constraints — there was the freedom to use a large (in wavelengths) primary feed aperture with controlled illumination to efficiently illuminate the subreflector and, hence, the paraboloid. Thus, at the early stage of the antenna configuration design, the d_{max} dimension of the horn calculated from the relations discussed above was assigned with good confidence that a satisfactory specific feed configuration could be designed within that constraint.

As noted in the introductory comments, the planned Cassegrain configuration for the 64-m antenna represented a new type of microwave system to JPL at the time. To provide validation of the design concepts and to evoke practical design constraints, a Cassegrain experimental project, in support of the 64-m antenna microwave work, was undertaken. In this project, a high-performance shaped-beam Cassegrain system was designed for use at 960 MHz, which was then JPL's space communication operating frequency, on a 26-m (85-ft) antenna at the Goldstone Complex. One important problem in low-noise Cassegrain feed system design, which is aggravated by the small size (in wavelengths) of the subreflector on a 26-m antenna at 960 MHz, is spill-over at the edges of the primary reflector. Such spill-over allows earth's radiation to contribute significantly to the system temperature. To improve the situation on this early design, a "beam shaping" skirt was devised and installed on the rim of the secondary reflector. This feed system, which included an integrally mounted liquid-helium cooled-maser amplifier, was used extensively in actual operational support of deep space missions. This work with shaped-beam subreflectors resulted in a very practical design that produced significantly improved figure-of-merit performance over a conventional geometric optics based design — a simple shaped-beam subreflector design was ultimately used for the 64-m antenna.

A design study program was then initiated to define a suitable feed system for the 64-m antenna, using techniques similar to those used in the 26-m antenna Cassegrain project.

To test the specific 64-m antenna feed system concept, a 9-m (30-ft) diameter antenna and quadripod at the Goldstone research and development (Venus) station were modified to be a precise one-seventh scale model of the intended 64-m antenna microwave configuration — it was operated at K_u-band, the scale model frequency corresponding to S-band on the 64-m antenna. A long-distance antenna range at the Goldstone Complex (Tiefort Mountain antenna range) was utilized for far-zone gain, boresight, and pattern determination at the K_u-band frequency.

These K_u-band model feed studies provided direct support in several areas. With the configuration established for the experimental gain and pattern data, a simple determination was made of the aperture blocking by the quadripod and secondary reflector structure and its support. A light was placed at the focal point of the antenna and the photograph shown in Fig. 109 was obtained.

A simple analysis of the photograph shows the structure outline blocks 6.255% of the available aperture. Assuming that the percentage of intercepted energy equals the percentage of shaded area of the aperture,

$$\frac{\eta'}{\eta} = (1 - B)^2$$

where η'/η is the reduced aperture efficiency factor from the blocking and B is the fractional area blocked. To estimate the quadripod effect, $B = \sigma A$ was used, where A is the optically blocked area and σ is defined as an average radio frequency opacity. Considering the relatively modest wavelength size of the quadripod cross section at the operating frequency, the opacity was estimated as 0.8. These simple measurements and calculations were helpful in the initial aperture efficiency predictions.

The model study work included correlation of measured data with calculations of (1) aperture efficiency radiation patterns based on primary feed illumination and (2) aperture efficiency and pattern distortion as a function of antenna structural and reflector surface deformations. The results indicated that the available methods of calculating total antenna performance in terms of primary feed pattern data with degradations by mechanically measurable reflector surface distortions were of acceptable accuracy. As noted, we used the method of Ruze (Ref. 8) in relating reflector surface mechanical errors to radio frequency performance — the method was then becoming recognized as a useful practical approach to that key matter.

3. Techniques for Radio Frequency Performance Prediction of Specific Microwave Configuration

The aperture efficiency and gain of the 64-m antenna system with the planned microwave configuration with carefully calculated. The method used was based on experimentally determined full-scale primary feed radiation patterns (which could be easily and accurately obtained on the experimental antenna pattern range); from those data, the hyperboloid and then the paraboloid patterns were calculated. Figure 110 shows the experimental primary feedhorn patterns used as input for the calculations of the secondary reflector patterns using the Rusch scattering program. The scattering program generates the fields from the hyperboloidal subreflector; this process has demonstrated very good agreement between experimental and calculated patterns (Fig. 111). The amplitude and phase patterns of the hyperboloidal subreflector/primary feedhorn combination were then used as input to a JPL-developed paraboloidal antenna efficiency computation program. Results of these calculations are summarized in Table 8. The total presented in the table gives the calculated antenna system gain available at the maser preamplifier input port.

The contribution of the antenna and feed system to the total receiving system noise temperature was calculated on the basis of the pattern parameters.

Table 9 summarizes the calculation of antenna noise temperature, defined at the feedhorn output. Later measurements confirmed this value with an estimated accuracy of ±1 K (3σ).

Table 2. Original specifications and as-built relationships

Operating conditions	Wind velocity				Dynamic wind pressure			
	m/s		mph		N/m^2		lb/ft^2	
	Original	As-built	Original	As-built	Original	As-built	Original	As-built
Precision I	0 to 13.4	0 to 13.4	0 to 30	0 to 30	0 to 110.1	0 to 110.1	0 to 2.30	0 to 2.30
Precision II	13.4 to 20.1	13.4 to 20.1	30 to 45	30 to 45	110.1 to 248.0	110.1 to 248.0	2.30 to 5.18	2.30 to 5.18
Precision III	20.1 to 29.1	—	45 to 65	—	248.0 to 441.0	—	5.18 to 9.21	—
Drive to stow (any path)	31.3	22.4	70	50	587.0	307.4	12.26	6.42
Survival at stow	53.6	53.6	120	120	1763.4	1763.4	36.83	36.83
Survival at any position		31.3		70		587.0		12.26

Table 3. Pedestal concrete design characteristics

Characteristic	Value
Ultimate compressive strength of soil	2.87×10^6 N/m^2 (60,000 lb/ft^2)
Allowable stress on soil	9.57×10^5 N/m^2 (20,000 lb/ft^2)
Pedestal rotation under maximum operating wind loads	
About a horizontal axis	4.4 arc seconds
About a vertical axis	0.13 arc seconds
Instrument tower rotation under maximum operational wind loads	
About a horizontal axis	1.9 arc seconds
About a vertical axis	0.06 arc seconds
Maximum soil pressure beneath the pedestal footing	
Under maximum operating wind load	3.11×10^5 N/m^2 (6,500 lb/ft^2)
Under maximum survival wind load	8.61×10^5 N/m^2 (18,000 lb/ft^2)
Under maximum design seismic load	3.86×10^5 N/m^2 (8,070 lb/ft^2)
Predicted foundation settlement (occurring during construction)	
Pedestal	1.52 mm (0.60 in.)
Instrument tower	0.71 mm (0.28 in.)

Table 4. Loads on the alidade

Load	Value
One-half weight of tipping structure	5.78×10^6 N (1.3×10^6 lb)
Maximum load at elevation bearing assembly (dead load plus 53.6-m/s (120-mph) wind)	7.12×10^6 N (1.6×10^6 lb)
Maximum load on hydrostatic bearing pad (dead load plus seismic)	11.56×10^6 N (2.6×10^6 lb)
Maximum load from radial bearing (seismic)	4.3×10^6 N (0.97×10^6 lb)

Table 5. Gear drive data

Characteristic	Azimuth	Elevation
Maximum drive torques at axis		
13.4-m/s (30-mph) wind	4.08×10^6 N-m (3.01×10^6 lb-ft)	4.23×10^6 N-m (3.12×10^6 lb-ft)
22.4-m/s (50-mph) wind (maximum operating)	9.63×10^6 N-m (7.10×10^6 lb-ft)	10.68×10^6 N-m (7.88×10^6 lb-ft)
31.3-m/s (70-mph) wind (survival at any position)	18.03×10^6 N-m (13.3×10^6 lb-ft)	20.74×10^6 N-m (15.3×10^6 lb-ft)
Gear ratios		
Gear box internal ratio	610/1	514/1
Bull gear/pinion ratio	47/1	56/1
Total ratio	28,724/1	28,730/1
Bull gear data		
Pitch diameter	21.3 m (70 ft)	25.3 m (83 ft)
Tooth data	88.9-mm (3-1/2-in.) circular pitch 247.7-mm (9-3/4-in.) face 25 deg spur gear 245-285 Brinell hardness	

Table 6. Parameters of dynamic models

(a) Masses

Mass	Element represented	Axes of motion[a]	
		Elevation	Azimuth
A	Pedestal	4	5, 6
B	Alidade, lower half	2, 3, 4	1, 5, 6
C	Alidade, upper half	2, 3	1, 5, 6
D	Drives	3'	—
E	Reflector core	2', 4	1', 5'
G	Feed	2'	1'
H	Quadripod	2'	1'
N	Counterweight	4'	5'
P	Masses in reflector simulation	3'	6'
Q		3'	6'
R		4'	5'

[a]Primes indicate tipping structure.

(b) Springs

Spring	Element represented	Axes of displacement[a]	
		Elevation	Azimuth
K^A	Soil	4	5, 6
K^B	Pedestal, azimuth bearings, alidade base, and azimuth drives	2, 3, 4	1, 5, 6
K^C	Alidade	2, 3	1, 5, 6
K^D	Elevation drives and supports	3, 3'	—
K^E	Top of alidade, elevated bearings, and tie truss	2, 3	1, 5'
K^G	Cone and feed support	2'	'
K^H	Quadripod legs	2'	1
K^N	Elevation wheels	4	5'
K^Q	Springs in reflector simulation	4	6'
K^R			5'

[a]Primes indicate tipping structure.

Table 7. Angle data system error budget

Element	Error, deg
Autocollimator	0.001
Master equatorial mount	0.004
Angle encoders	0.002
Master equatorial servo	0.003
Predicts	0.006
Alignment	0.002
Rss	0.008

Table 8. Calculated 2295-MHz aperture efficiency and gain

Item	Efficiency, %	Gain, dB
Theoretical maximum	100	+ 63.75
Illumination factor[a]	76.8	- 1.15
Quadripod scattering[b]	86.8	- 0.62
Surface tolerance[c]	98.4	- 0.08
Dissipation loss[d]	96.6	- 0.15
Total	65.4	+ 61.75 ±0.27 (3σ)

[a]Includes spillover and subreflector blocking.
[b]Assumed 80% opaque.
[c]Initial estimate; 1.52 mm (0.06 in.) RMS.
[d]S-band multifrequency feedcone, loss to preamplifier input.
[e]Estimated tolerance, primarily due to quadripod opaqueness uncertainty.

Table 9. Calculated 2295-MHz antenna noise temperature

Item	Zenith antenna noise temperature, K
Direct spillover to ground, 0.3%	0.8
Quadripod scattering to ground[a]	2.8
Atmospheric and extra-atmospheric noise	6.0
Losses	Negligible
Total	9.6

[a]Assumed 80% opaque; isotropic scattering.

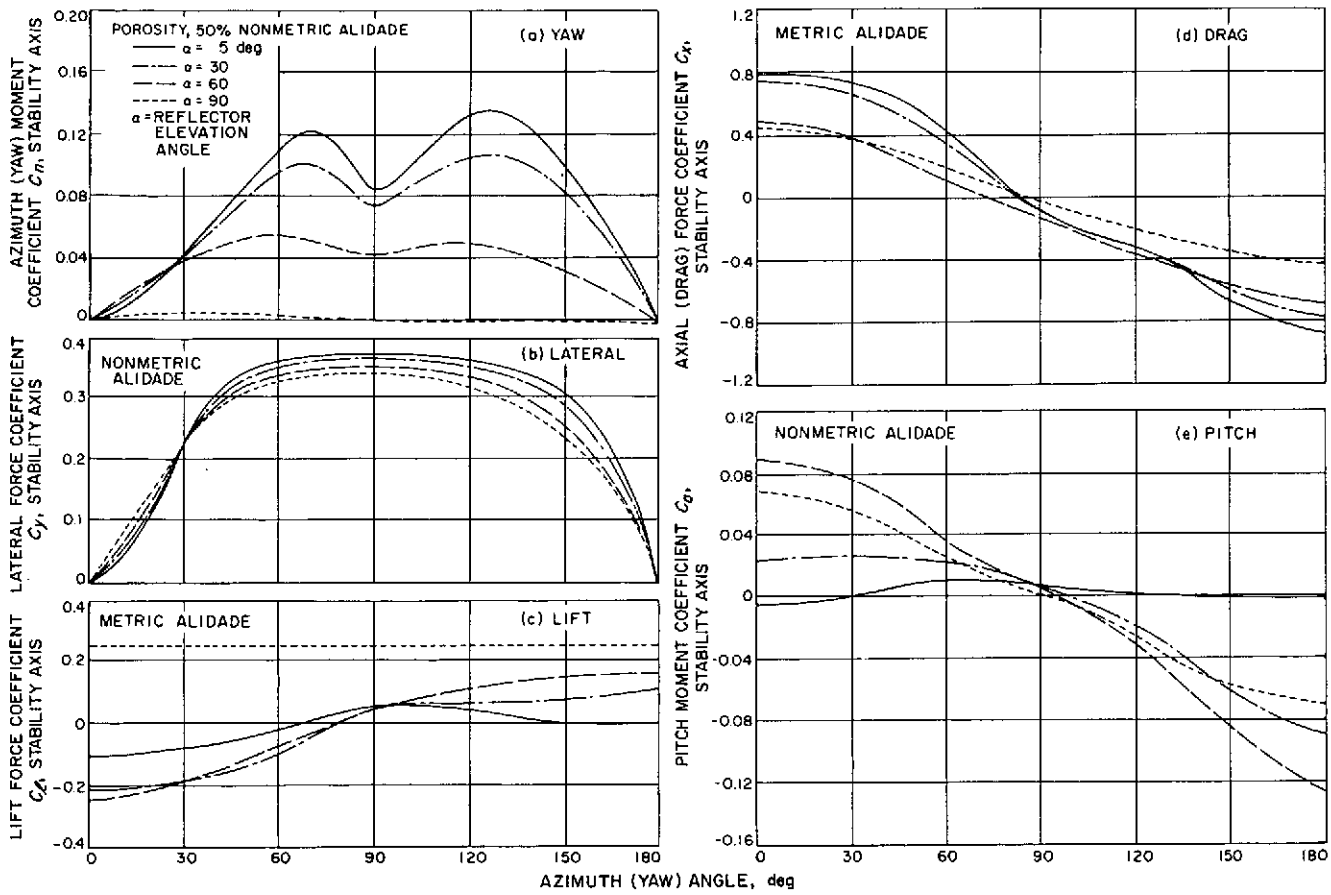

Fig. 73. Estimated moment coefficient for basic configuration

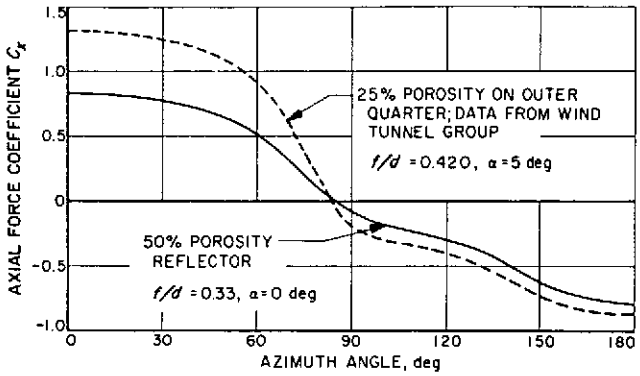

Fig. 74. Comparison of axial force coefficient for 25% porosity on outer quarter and 50% porosity over entire surface

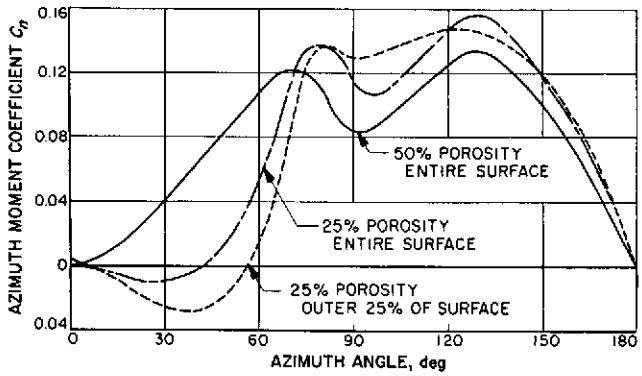

Fig. 75. Comparison of effects of porosity on azimuth torque, α = 5 deg

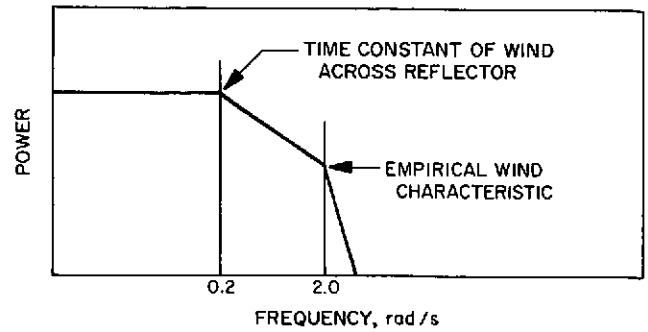

Fig. 76. Proposed wind power spectrum

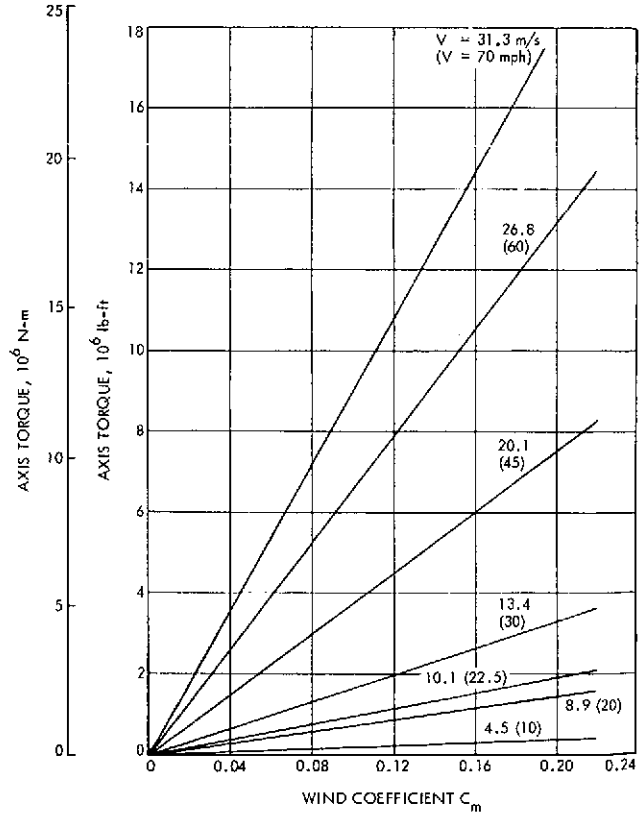

Fig. 77. Wind torque vs C_m as a function of wind velocity

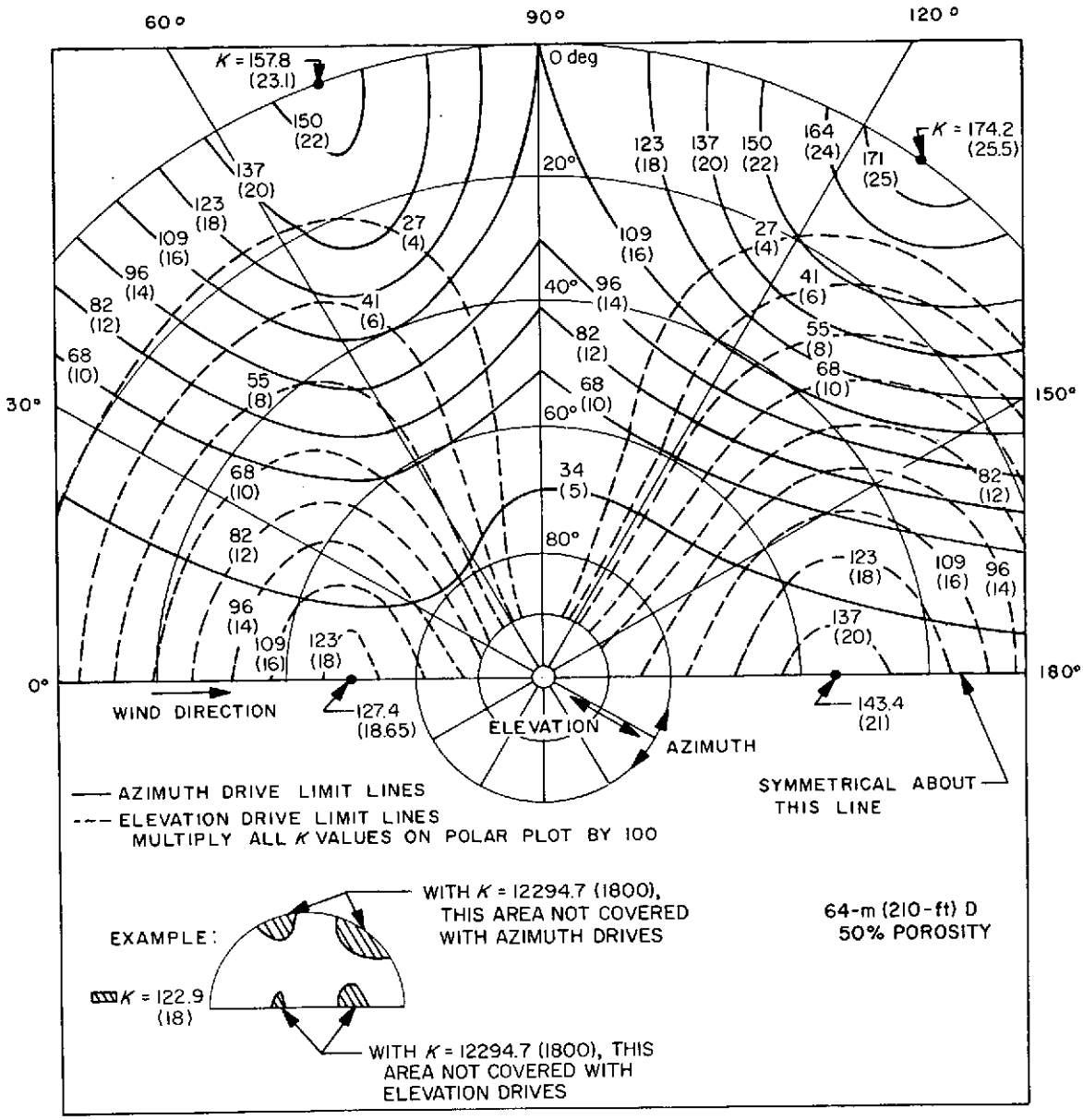

Fig. 78. 64-m antenna torque limits

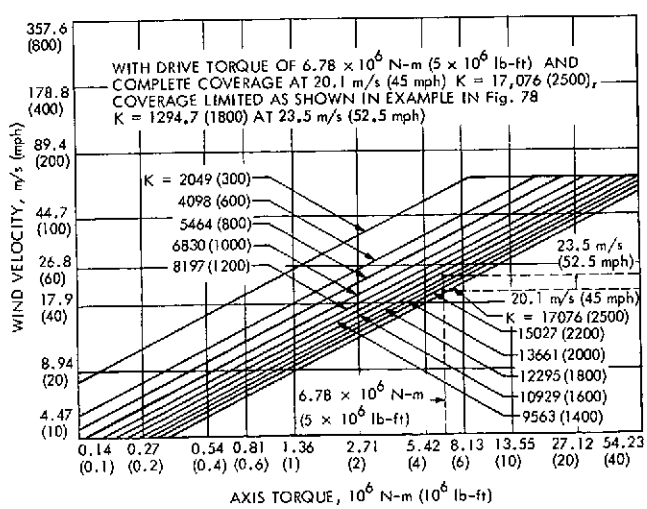

Fig. 79. K-factor for torque limits

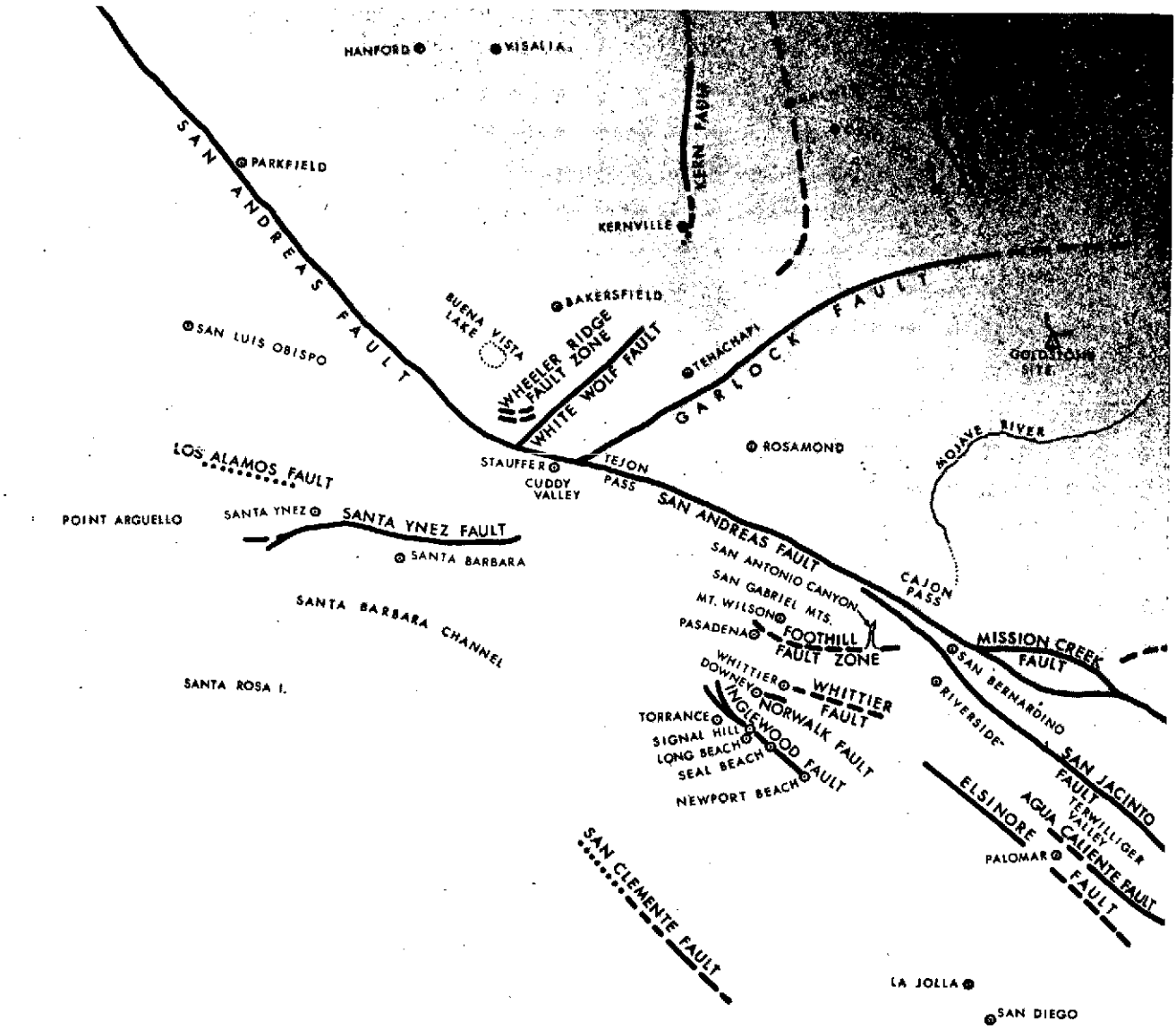

Fig. 80. Major earthquake faults near the Goldstone area

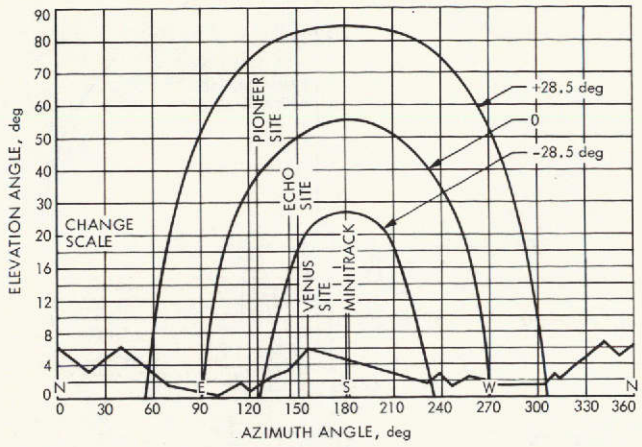

Fig. 81. Mars Deep Space Station horizon mask, ground level + 1.5 m (5 ft)

Fig. 82. Terrain mask at Mars Deep Space Station

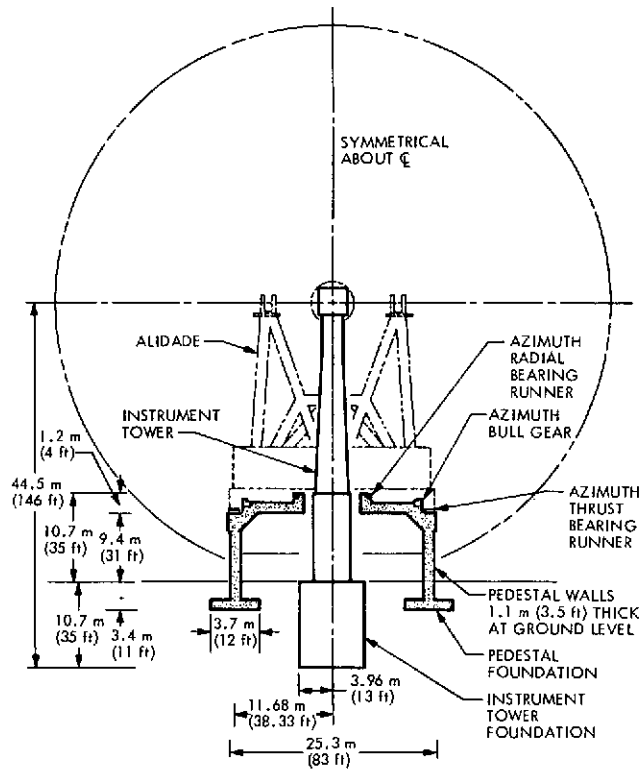

Fig. 83. Pedestal and instrument tower in relation to the antenna structure

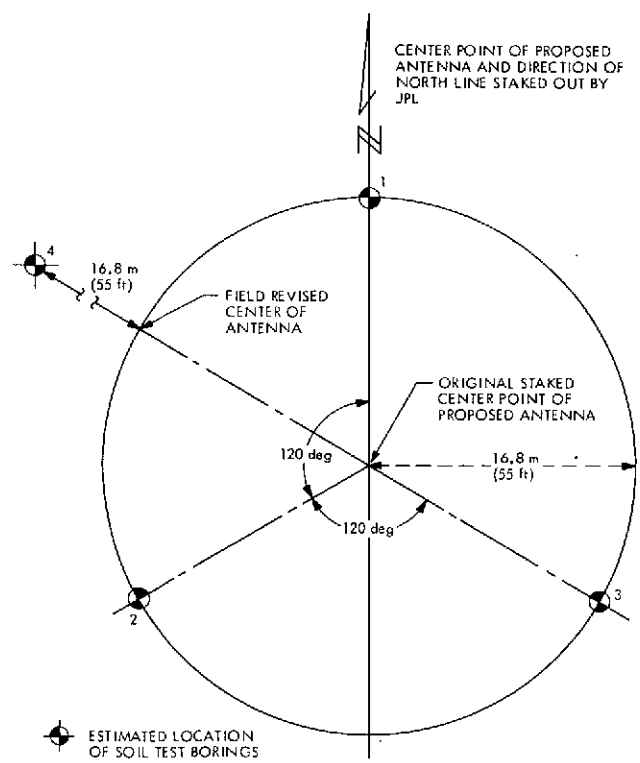

Fig. 84. Soil test borings at selected site

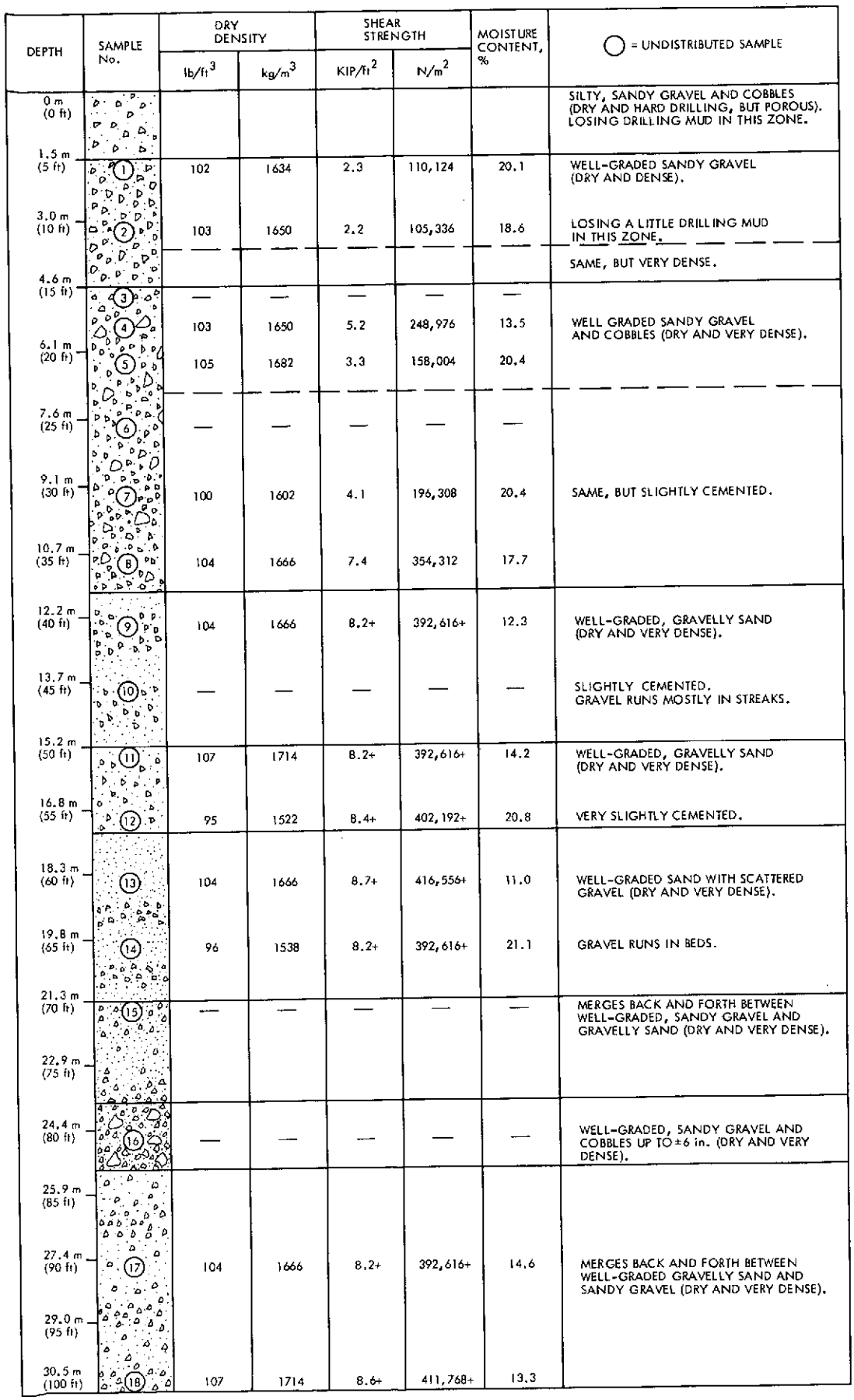

DEPTH	SAMPLE No.	DRY DENSITY lb/ft³	DRY DENSITY kg/m³	SHEAR STRENGTH KIP/ft²	SHEAR STRENGTH N/m²	MOISTURE CONTENT, %	◯ = UNDISTRIBUTED SAMPLE
0 m (0 ft)							SILTY, SANDY GRAVEL AND COBBLES (DRY AND HARD DRILLING, BUT POROUS). LOSING DRILLING MUD IN THIS ZONE.
1.5 m (5 ft)	①	102	1634	2.3	110,124	20.1	WELL-GRADED SANDY GRAVEL (DRY AND DENSE).
3.0 m (10 ft)	②	103	1650	2.2	105,336	18.6	LOSING A LITTLE DRILLING MUD IN THIS ZONE.
							SAME, BUT VERY DENSE.
4.6 m (15 ft)	③	—	—	—	—	—	
	④	103	1650	5.2	248,976	13.5	WELL GRADED SANDY GRAVEL AND COBBLES (DRY AND VERY DENSE).
6.1 m (20 ft)	⑤	105	1682	3.3	158,004	20.4	
7.6 m (25 ft)	⑥	—	—	—	—	—	
9.1 m (30 ft)	⑦	100	1602	4.1	196,308	20.4	SAME, BUT SLIGHTLY CEMENTED.
10.7 m (35 ft)	⑧	104	1666	7.4	354,312	17.7	
12.2 m (40 ft)	⑨	104	1666	8.2+	392,616+	12.3	WELL-GRADED, GRAVELLY SAND (DRY AND VERY DENSE).
13.7 m (45 ft)	⑩	—	—	—	—	—	SLIGHTLY CEMENTED. GRAVEL RUNS MOSTLY IN STREAKS.
15.2 m (50 ft)	⑪	107	1714	8.2+	392,616+	14.2	WELL-GRADED, GRAVELLY SAND (DRY AND VERY DENSE).
16.8 m (55 ft)	⑫	95	1522	8.4+	402,192+	20.8	VERY SLIGHTLY CEMENTED.
18.3 m (60 ft)	⑬	104	1666	8.7+	416,556+	11.0	WELL-GRADED SAND WITH SCATTERED GRAVEL (DRY AND VERY DENSE).
19.8 m (65 ft)	⑭	96	1538	8.2+	392,616+	21.1	GRAVEL RUNS IN BEDS.
21.3 m (70 ft)	⑮	—	—	—	—	—	MERGES BACK AND FORTH BETWEEN WELL-GRADED, SANDY GRAVEL AND GRAVELLY SAND (DRY AND VERY DENSE).
22.9 m (75 ft)							
24.4 m (80 ft)	⑯	—	—	—	—	—	WELL-GRADED, SANDY GRAVEL AND COBBLES UP TO ±6 in. (DRY AND VERY DENSE).
25.9 m (85 ft)							
27.4 m (90 ft)	⑰	104	1666	8.2+	392,616+	14.6	MERGES BACK AND FORTH BETWEEN WELL-GRADED GRAVELLY SAND AND SANDY GRAVEL (DRY AND VERY DENSE).
29.0 m (95 ft)							
30.5 m (100 ft)	⑱	107	1714	8.6+	411,768+	13.3	

Fig. 85. Typical results of borings made at the selected site

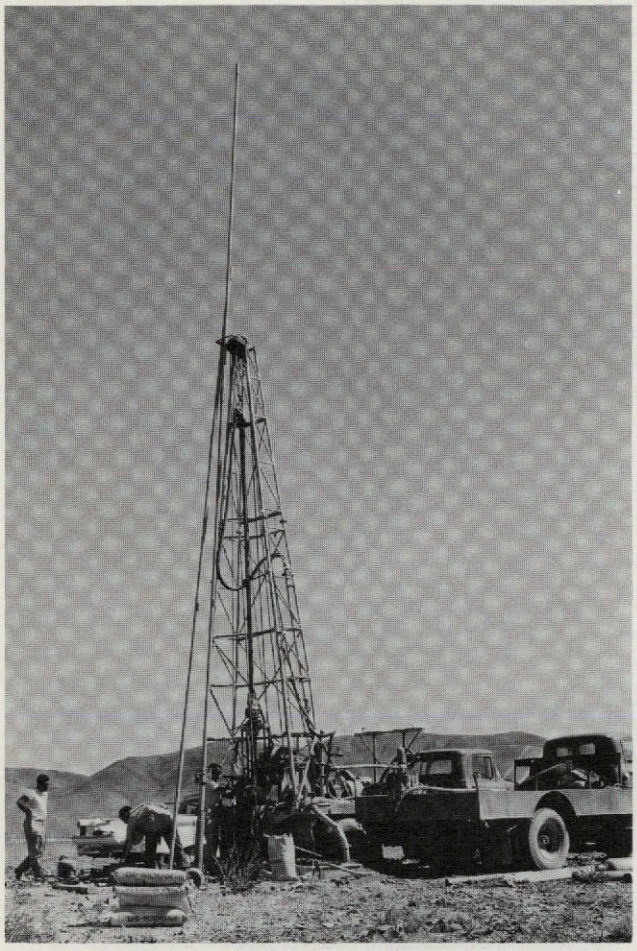

Fig. 86. Soils investigation

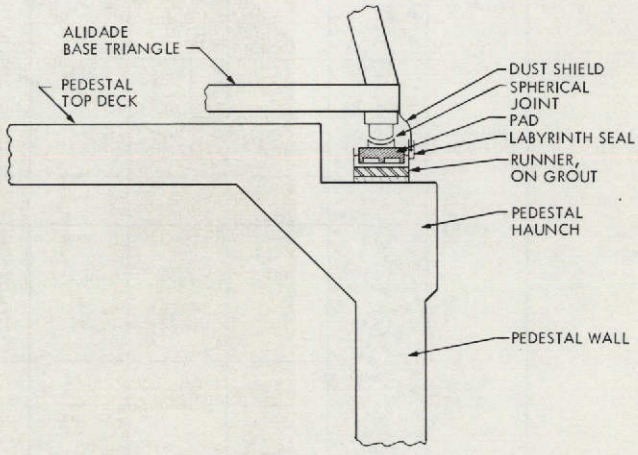

Fig. 88. Azimuth hydrostatic thrust bearing, general arrangement

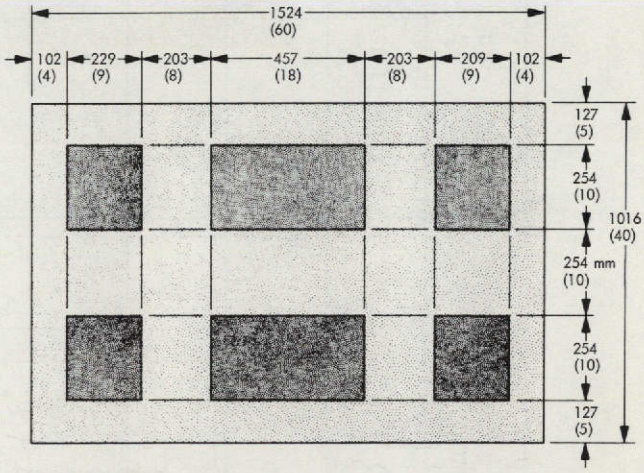

Fig. 89. Recess pattern of hydrostatic thrust bearing pad

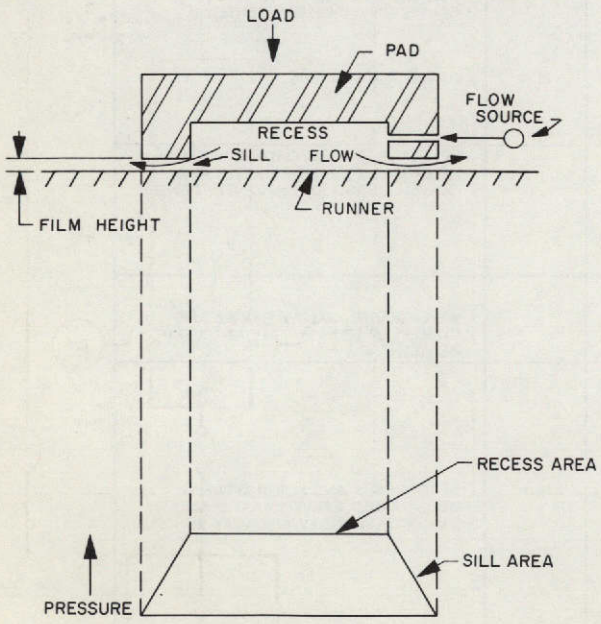

Fig. 87. Basic hydrostatic bearing and pressure pattern under pad

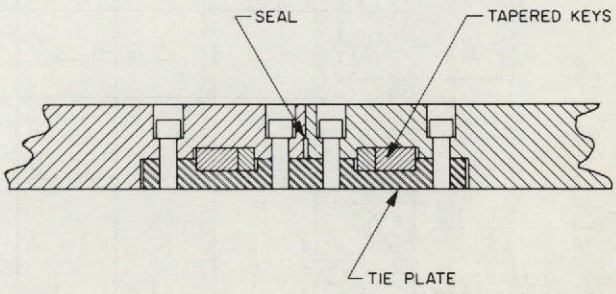

Fig. 90. Hydrostatic thrust bearing runner joint

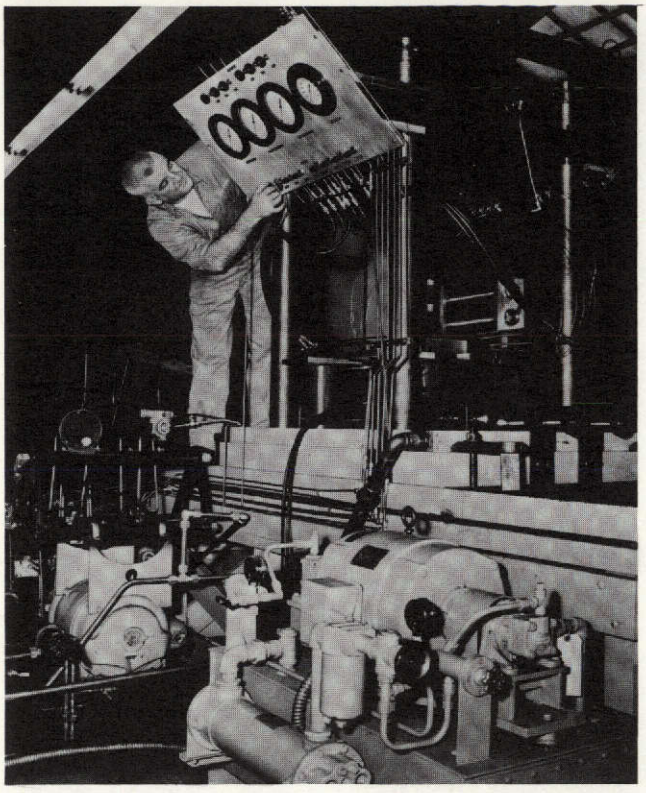

Fig. 91. Hydrostatic bearing model and test stand

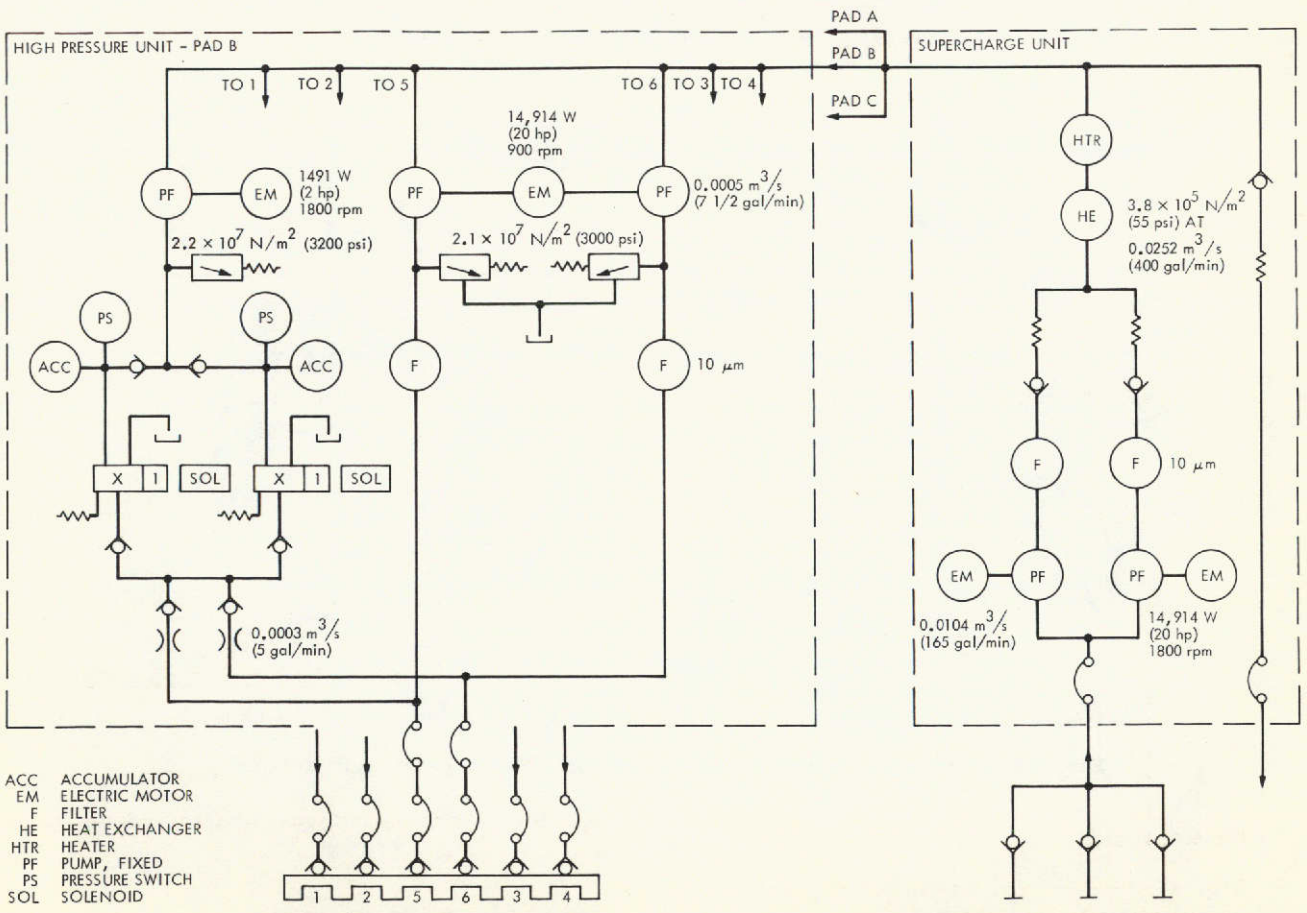

Fig. 92. Hydrostatic bearing hydraulic power system

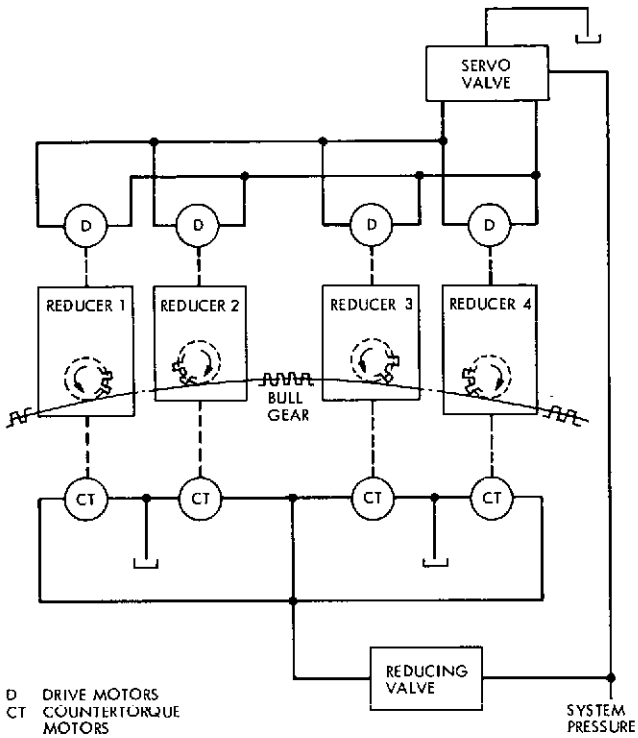

Fig. 93. 64-m antenna countertorque system

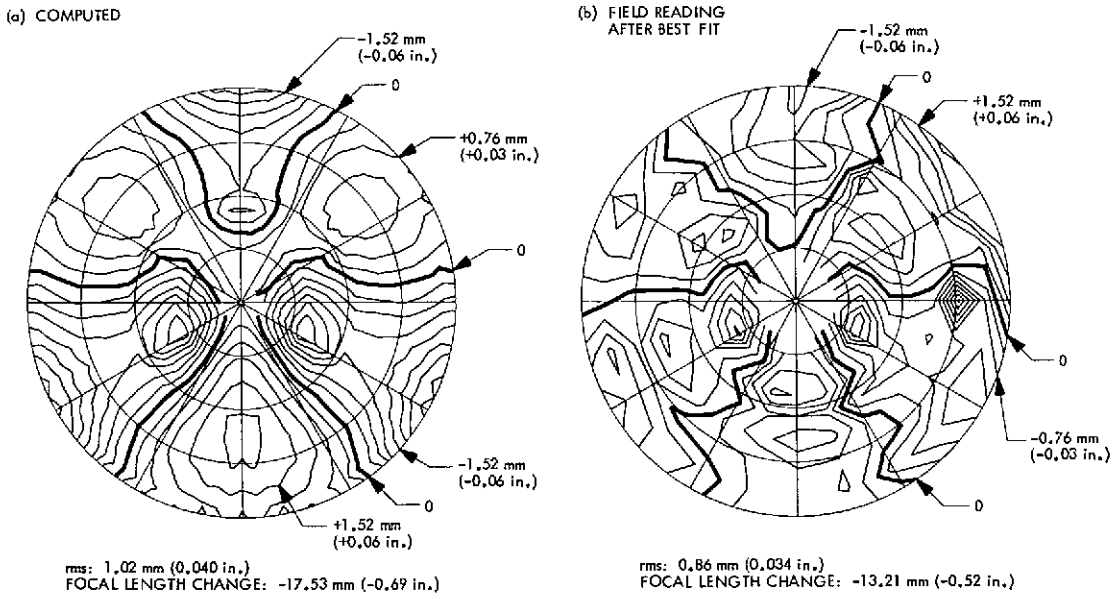

Fig. 94. Horizon-attitude contour maps of 1/2-RF-pathlength errors

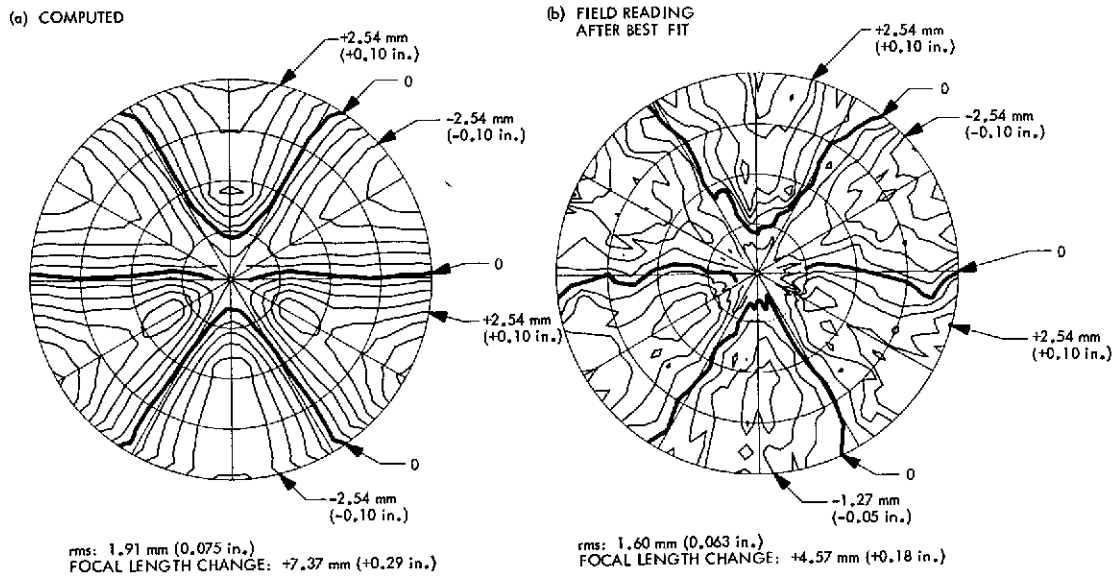

Fig. 95. Zenith-attitude contour maps of 1/2-RF-pathlength errors

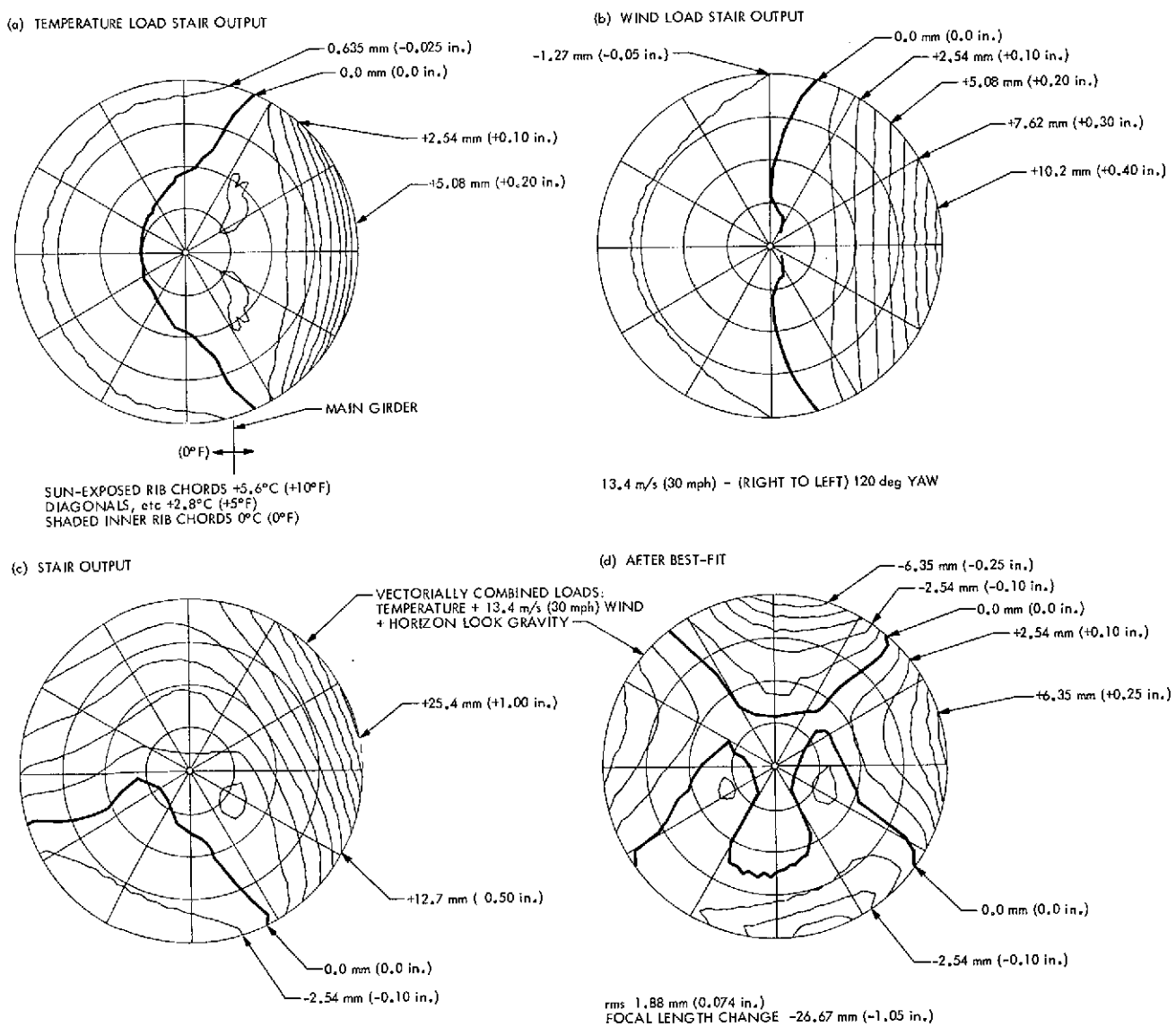

Fig. 96. Contour map of 1/2-RF-pathlength errors, with wind and temperature loads

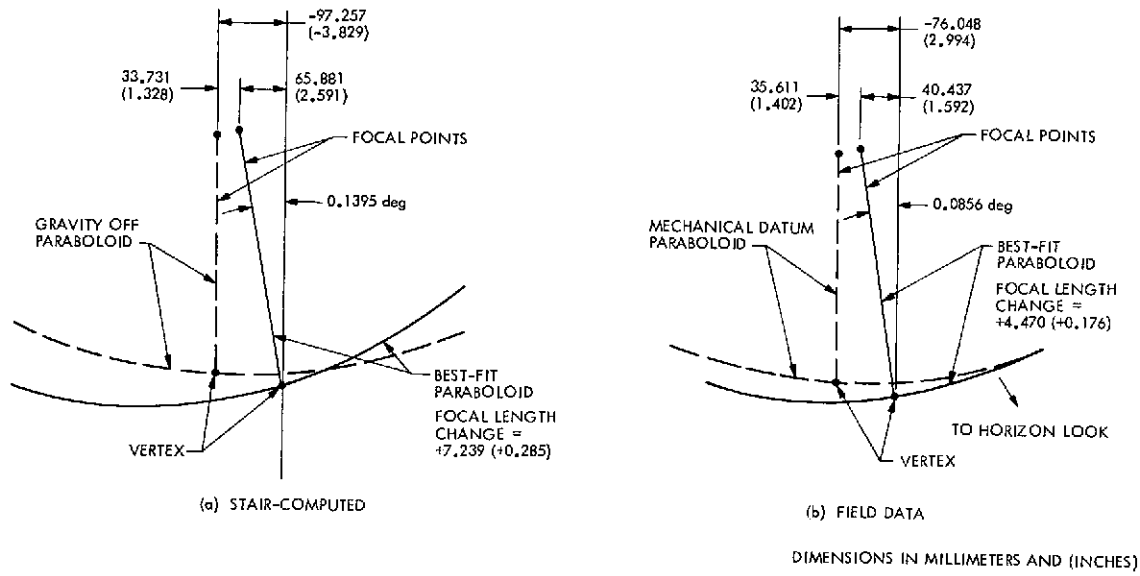

Fig. 97. Best-fit paraboloid data for reflector structure

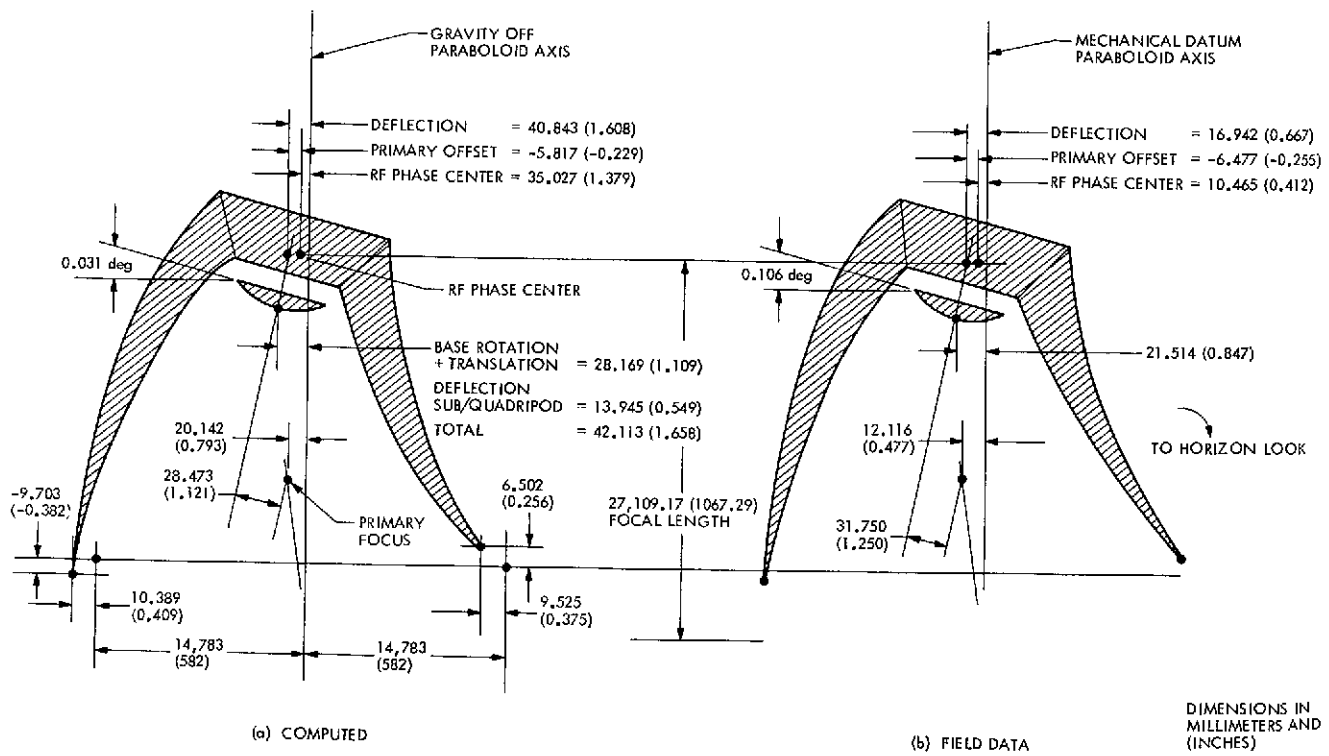

Fig. 98. Subreflector quadripod gravity deflection data at zenith look, surface panels set to perfect paraboloid at 45-deg elevation angle

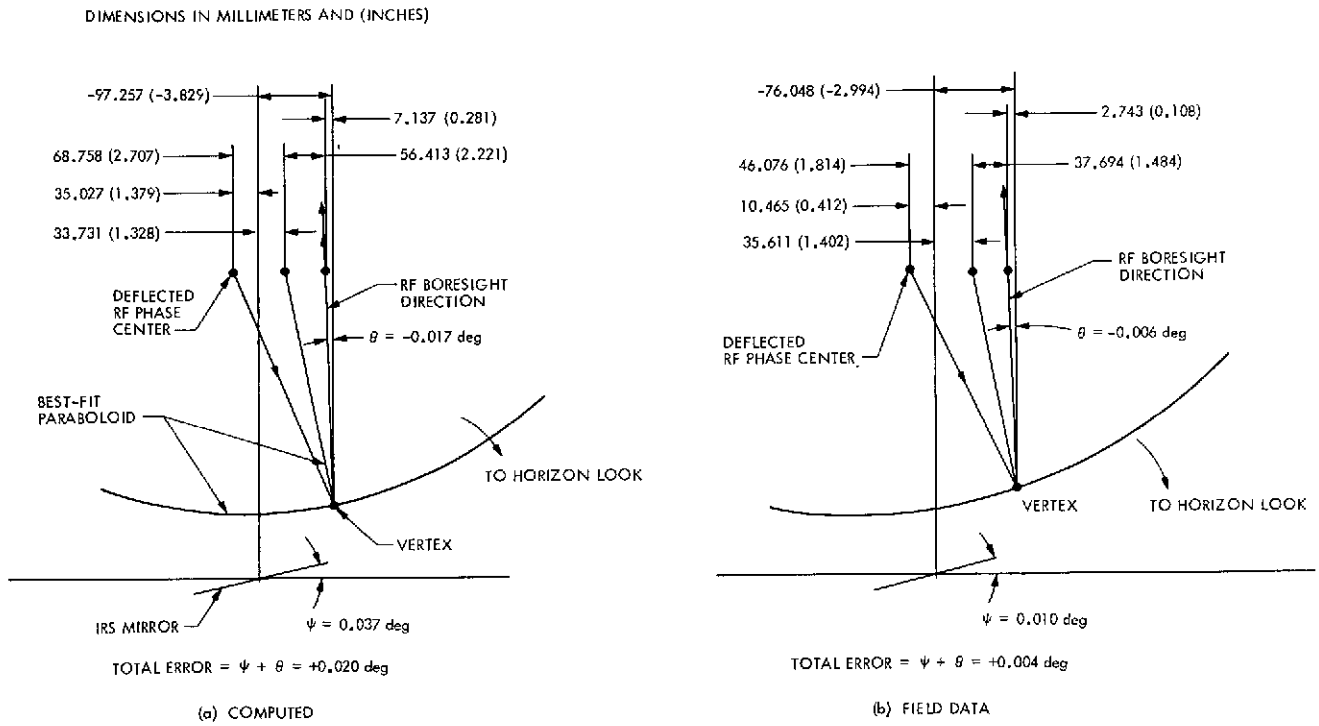

Fig. 99. Radio frequency beam boresight direction error at zenith look, zero setting at 45-deg elevation angle

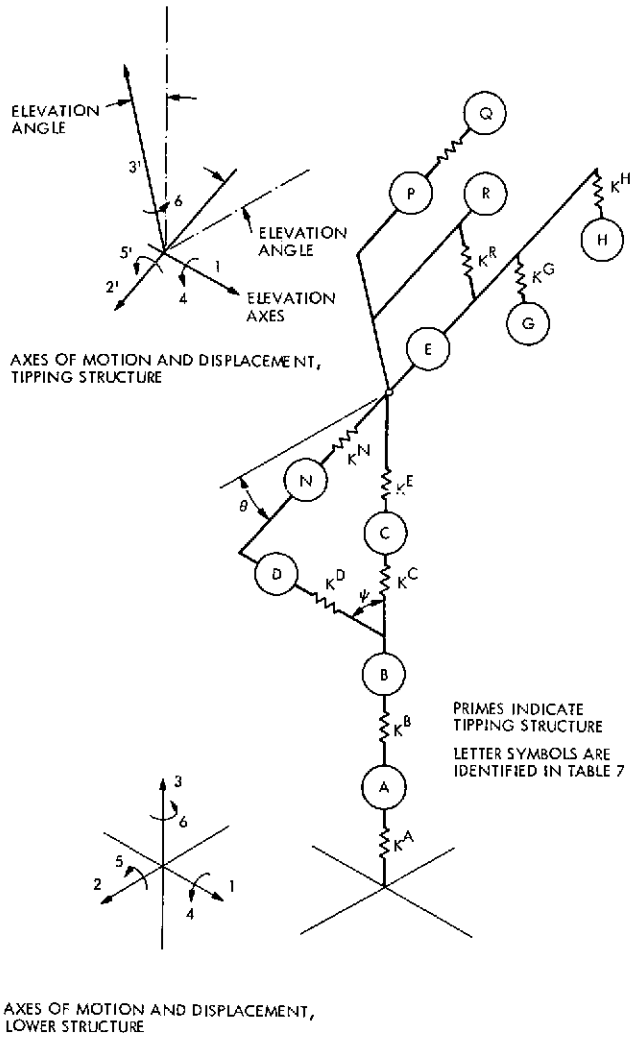

Fig. 100. Final design dynamic model (elevation)

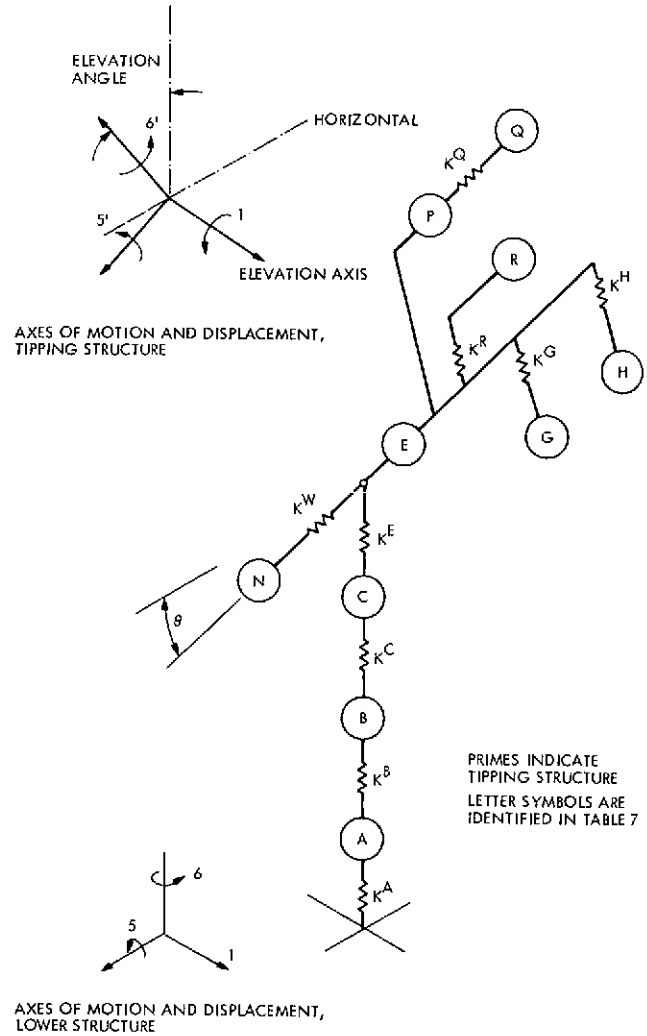

Fig. 101. Final design dynamic model (azimuth)

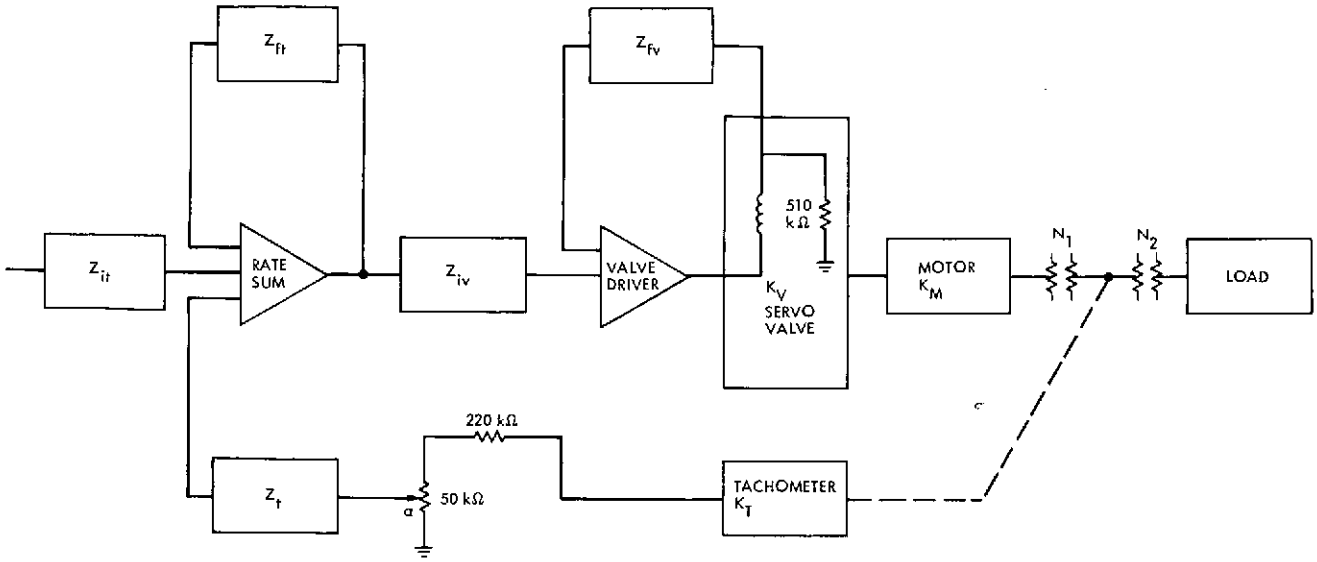

Fig. 102. Block diagram of rate loop servo

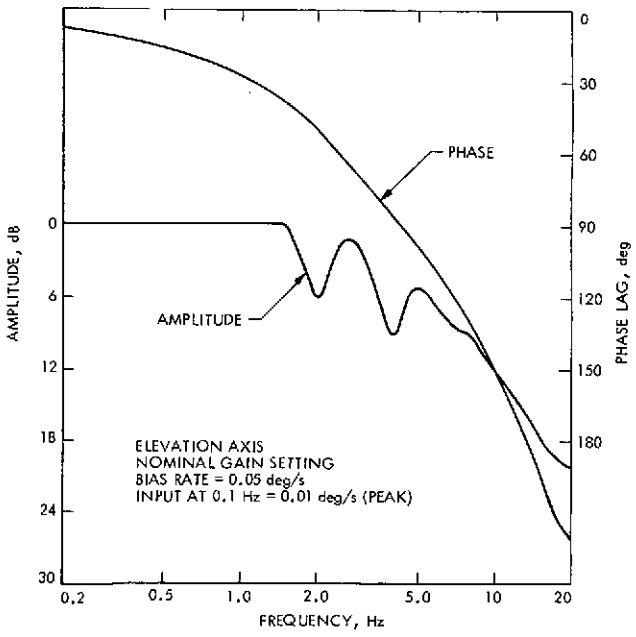

Fig. 103. Typical closed rate loop amplitude and gain

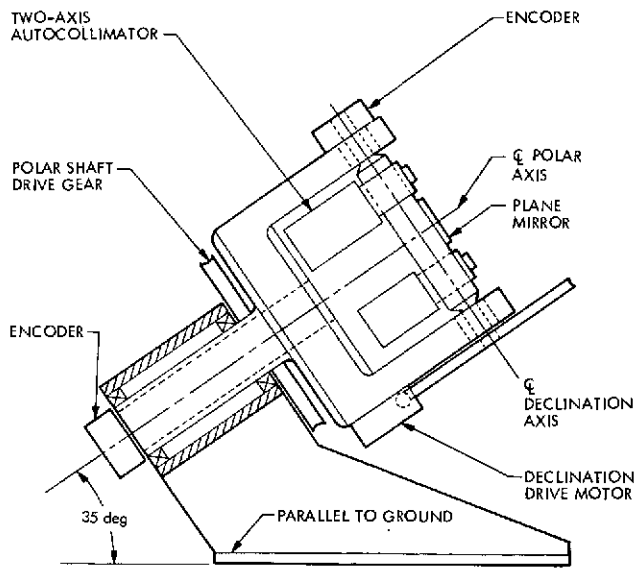

Fig. 104. Assembly view of master equatorial instrument

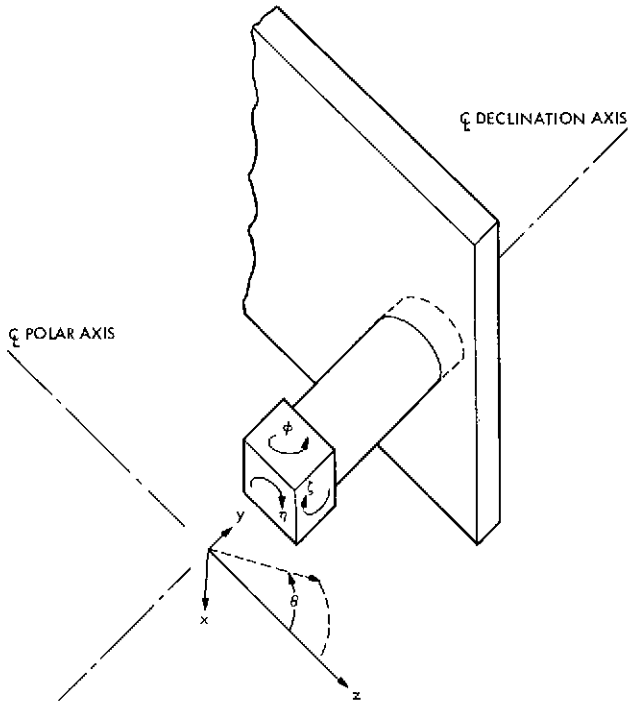

Fig. 105. Orientation of error components

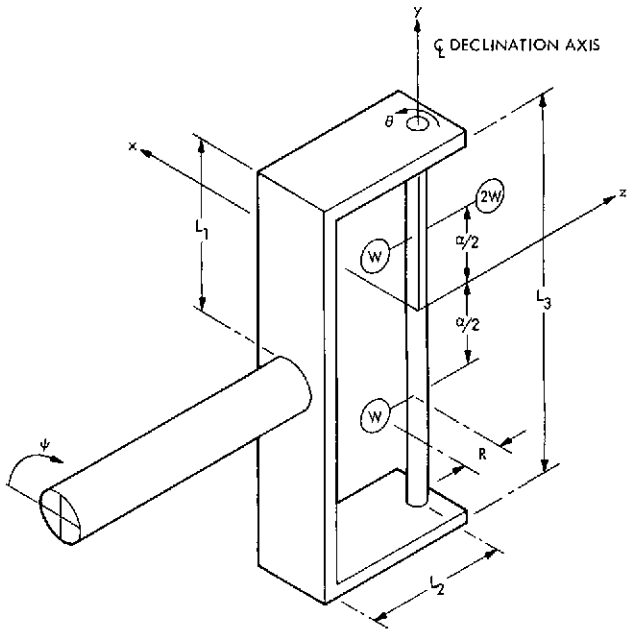

Fig. 106. Schematic of master equatorial yoke

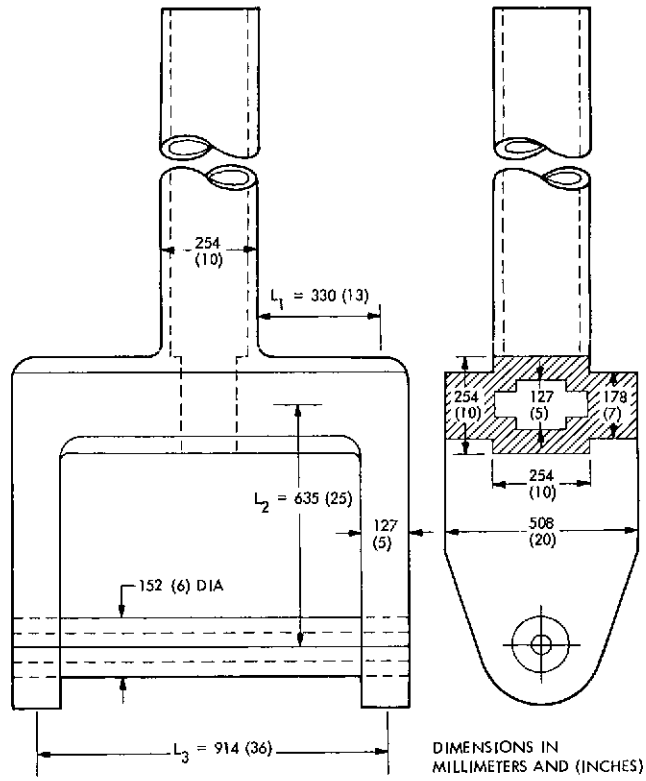

Fig. 107. Configuration yoke for master equatorial instrument

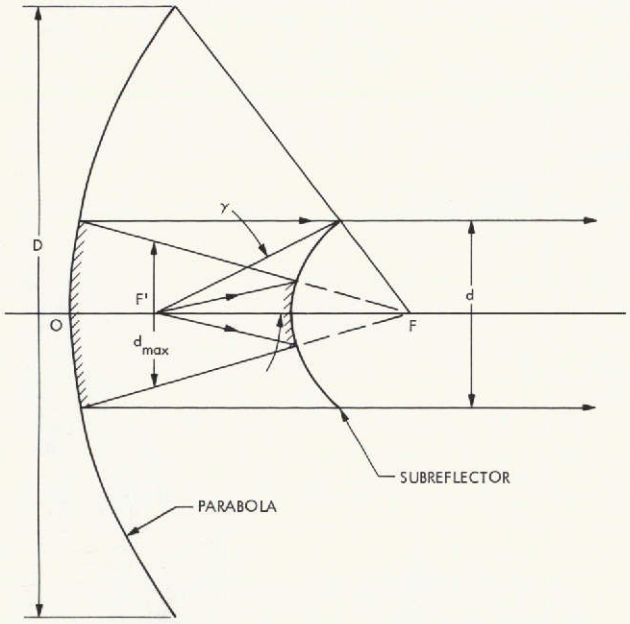

Fig. 108. Cassegrain system

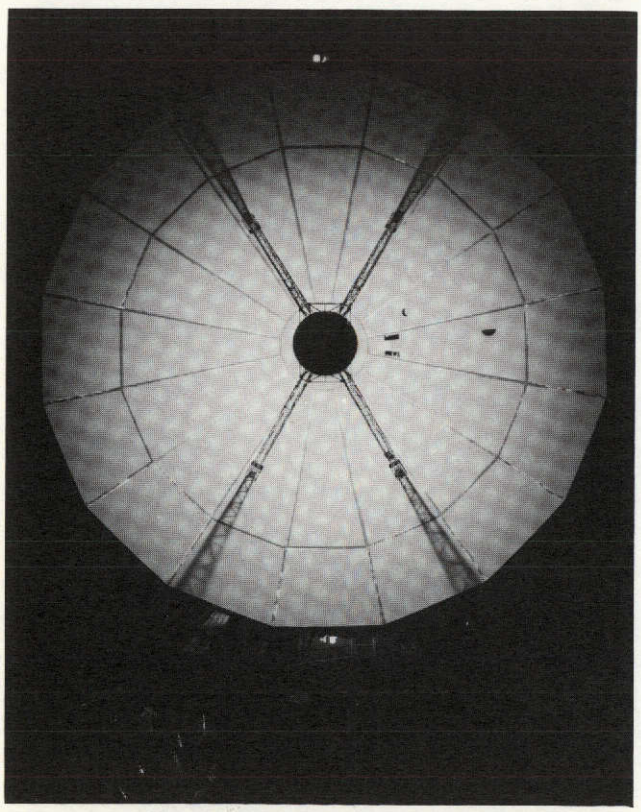

Fig. 109. 64-m-diameter antenna model quadripod

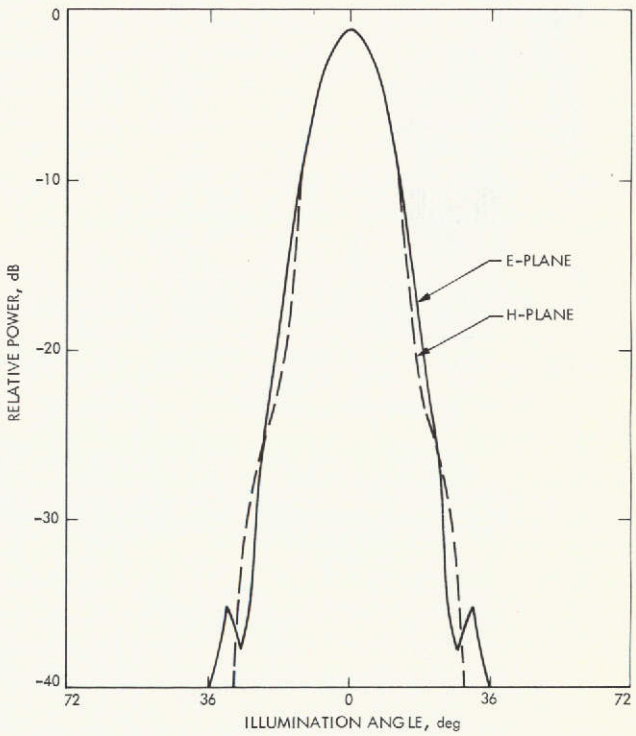

Fig. 110. Broadband dual-mode horn radiation pattern, 2295 MHz

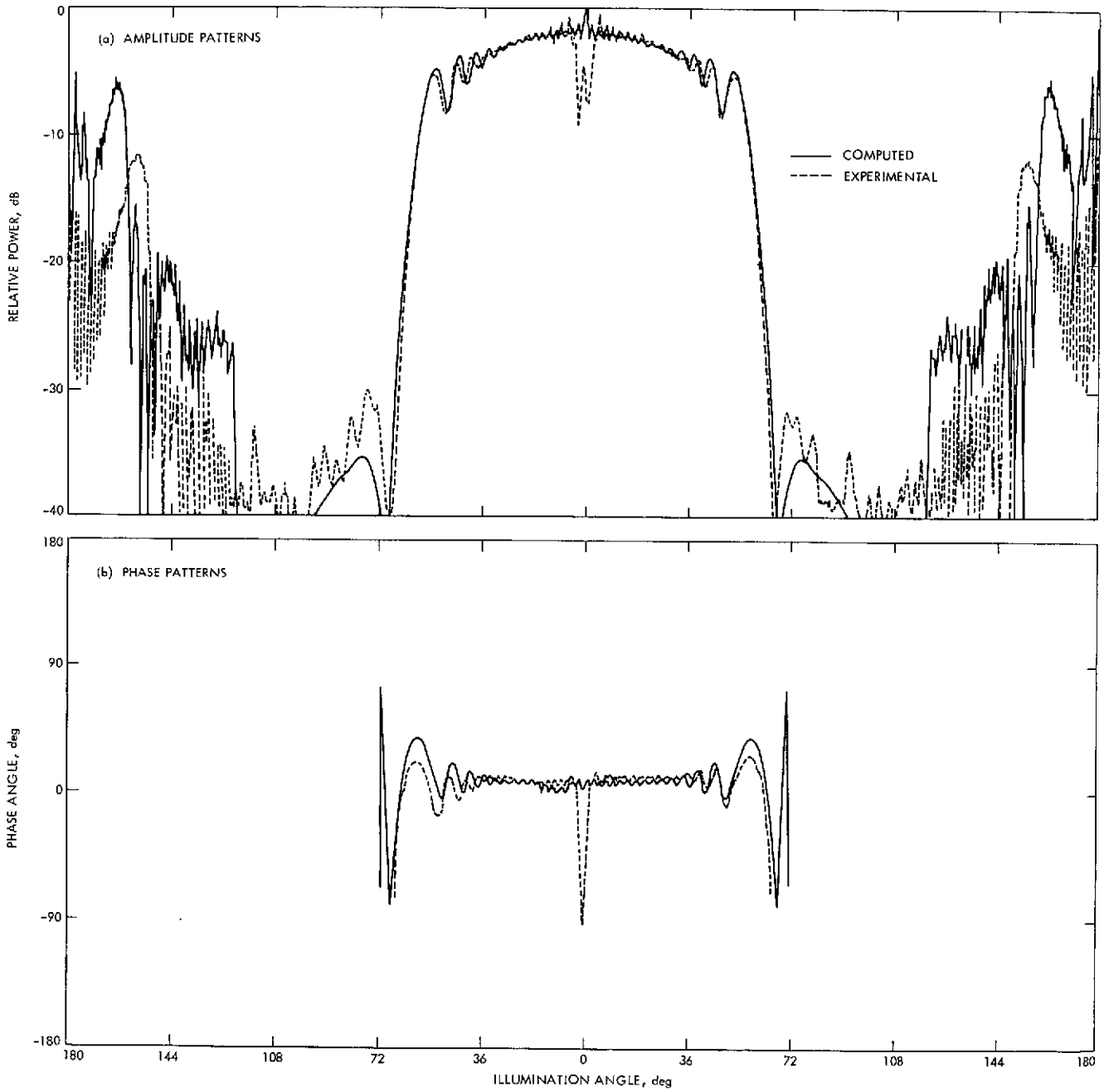

Fig. 111. Comparison of computed and experimental patterns of feed horn/ hyperboloid combination; (a) amplitude and (b) phase

CHAPTER V. ANTENNA PERFORMANCE

The performance of the 64-m antenna as an operating instrument is reviewed in this chapter. The principal system capabilities of the antenna, aperture efficiency, system temperature, and beam pointing accuracy are presented. Performance both at S-band and at an experimental X-band frequency is presented and compared with the original specifications.

I. PERFORMANCE REQUIREMENTS

A. GENERAL DISCUSSION

The significant measure of the antenna performance is its operation as a complete system under field environmental conditions.

Of prime importance are the RF aperture efficiency, noise temperature, and beam pointing performance of the antenna. In this chapter, performance is evaluated from data on RF signal strength and pointing against radio star and spacecraft signal sources, and these results are correlated with measured and calculated mechanical errors of the reflecting surfaces, supporting structures, and mechanical devices.

The narrow RF beam requires high precision boresight pointing – the pointing system includes the servo drive system, gear boxes and drive units, azimuth and elevation bearings, and deflections of the Cassegrain geometry support structure. Performance characteristics of these elements are discussed.

The actual system performance in support of assigned spacecraft tracking and ground radio science missions has proved to be well within original performance specifications. Information is included on reliability and performance of the major elements of the antenna.

The particular value of the performance data at the X-band frequency (8.4 GHz) as compared with that at the originally specified S-band frequency range (2.2 GHz) is that at the higher frequencies the system performance is much more sensitive to reflector surface errors, pointing distortions, etc., and the data are therefore more powerful in defining the antenna performance capability.

Tests or performance data on some major assemblies of the completed antenna are available. In several cases, the test data to show specification compliance of a major assembly had to be taken prior to installation on the antenna or during the construction of the antenna.

B. OVERALL PERFORMANCE SPECIFICATIONS

The system specifications, as established at the outset of Phase II, are set forth in detail in Section III of Ref. 1, Rev. 4. A summary of specifications, calculations, and measurements is included in the Appendix of this Technical Memorandum.

In meeting the mechanically oriented specifications established by JPL for the 64-m antenna, Rohr Corporation established major milestones for the following tests: surface accuracy, pointing accuracy, reflector deflection

surveys, locked rotor frequency, hysteresis, and alidade stiffness. Table 10 summarizes the results of the tests as determined upon completion of Rohr Corporation's work in 1966. Measurements were made using a dummy feedcone and a simulated load.

The following sections are discussions of performance investigations conducted during engineering tests and operations.

II. POINTING ACCURACY PERFORMANCE

The procedures used to calibrate the radio frequency beam boresight errors from computed structural data, as well as the comparison with reduced field-surveyed data, have been described in the previous chapter. This chapter presents data on operational boresight error data obtained from actual radio star tracking performance.

Antenna pointing calibrations have been obtained by tracking radio star sources of sufficiently well known ephemeris and determining the beam-pointing error as a function of mechanical pointing. Representative results of such a calibration track are shown in Fig. 112. For this particular sample, the absolute pointing error measured in the declination/hour angle coordinate system of the master equatorial is less than 0.015 deg for the range of local hour angle of ±60 deg.

A noteworthy characteristic of the data plotted in Fig. 112 is that the peak-to-peak variation is very small (±0.003 deg). Although the data are offset in hour angle and declination, there is no systematic error pattern related to angular position. It is this straight-line characteristic that suggests the net of the elevation plane deflections is less than that calculated.

Figure 113 is an accumulation of boresight error data taken over a 3-year period (1967-1970). The data on the top two plots are errors in the hour angle and declination coordinates of the master equatorial instrument. The lower plot represents the magnitude of the error in beam coordinates computed from the hour angle and declination component errors of each point.

In practice, because of restricted time availability, pointing data are only taken after a component change to verify performance, so these data include the effect of bias errors from configuration changes as well as other error sources. Figures 114 and 115 show the distribution of the boresight error data in beam coordinates. These plots show that the 3σ value of data is less than the 0.020 deg specified for the antenna system.

The data plotted in Fig. 113 were taken in all types of temperature and wind environments up to 20.1-22.4 m/s (45-50 mph) wind. A detailed study of the data indicates no systematic effect on pointing error as a function of wind velocity. As stated, this result was unexpected and further studies were conducted.

III. RADIO FREQUENCY PERFORMANCE

A. INITIAL OPERATION

The original S-band feed system configuration that was installed on the antenna is depicted in Fig. 116. This arrangement was such that the DSIF standard Cassegrain feed cones used on the 26-m (85-ft) antennas could also be used interchangeably on the 64-m antenna.

Initially, relatively crude measurements of radio star flux and comparison of the Pioneer 6 signal levels with the DSIF 26-m (85-ft) systems were used to verify the 64-m radio frequency system gain.

The block diagram of the original feedcone radio frequency system is shown in Fig. 117; the equipment provided a receive-only total operation noise temperature, at zenith, of 27 K at 2295 MHz. The initial gain measurements at S-band were 61-62 dB. This feed system, which used a broad-band dual-mode horn, polarizer, and orthogonal mode transducer, was used for tracking the superior conjunction of Mariner 4 in March 1966. In the course of that mission, initial measurements of system temperature were obtained when the antenna was pointed near the sun.

B. MEASURED S-BAND PERFORMANCE USING A LONG BASE LINE ANTENNA RANGE

In contrast to the Mariner 4 signals at -170 dBmW, the Surveyor 1 spacecraft, which had soft-landed on the moon, provided the opportunity for high signal (-100 dBmW) antenna measurements. These signals were used in a high-precision gain comparison measurement. Figure 118 gives the measurement system schematic. Table 11 gives a listing of the measurement and error sources considered. Based on these data, the measured value of the antenna system gain transferred to the master preamplifier input was +61.47 dB with 3σ error of ±0.40 dB. The antenna system initially provided 0.7 dB more performance in figure of merit (gain/system temperature) at the operational S-band frequency than the design goal in Ref. 1, Rev. 4.

It was also possible to measure antenna radiation patterns in four selected planes down to the unity gain (isotropic) level, using the Surveyor signals. Figure 119 shows the elevation plane pattern confirming the expected 0.14-deg total half-power beamwidth.

An experimental S-band feed system (called the Ultra-cone) was designed as a minimum system temperature listen-only feedcone suitable for use on the Venus Station's 26-m (85-ft) antenna during the Mariner 5 Venus encounter in 1967. This feedcone was modified to include a diplexing capability and was installed on the 64-m antenna in March 1968. Based on the advanced capability demonstrated in terms of low total (zenith) operating temperatures of 17 and 28 K, listen-only and diplexed, respectively, a commitment to the Mariner 1969 Project to support a high-data (16.2 kilobits/s) experimental video data system experiment was possible.

Further improvements in the feedcone system were completed in time for the Mariner 6-7 Mars encounter video playback operation which provided total (zenith) operating temperatures of

16 and 22 K, primarily a result of an improved diplexing filter. The 16 K system noise temperature, in the listen-only mode, consisted of 9.6, 2.2 and 4.2 K for the antenna, dissipative loss, and preamplifier input noise contributions, respectively.

IV. ANTENNA COMPONENTS

The following is a discussion of the performance of the structural, mechanical, and electronic components of the 64-m antenna mechanical system with respect to the specifications established at the start of Phase II of the project (Ref. 1, Rev. 4). This discussion, in combination with that contained in Chapter IV, "Design and Analysis of Critical Areas," completes the discussion of antenna components from design inception through initial operations. Modifications for improved capabilities, not within the scope of the initial specifications, are discussed in Chapter VII.

It has not been possible to confirm the performance of the antenna through testing under all extremes of the environmental requirements of the established specifications. The following comments, drawn from operational experience, are the best available indicators of the success in achieving the intent of the environmental specifications.

Insofar as the performance of the antenna structure and its related mechanical components are concerned, there have been no discernible adverse effects in operating in winds up to 20.1 m/s (45 mph) (actually, gusts to near 35.8 m/s (80 mph) have reportedly been experienced during operation), in driving to stow in 24.6 m/s (55 mph) winds, and with the structure stowed in winds to 38.9 m/s (87 mph). Similarly, no adverse effects have resulted in operation through the temperature range from -15.5 to 49.4°C (4 to 121°F). However, operation in the higher temperature ranges did lead to the redesign and replacement of a heat exchanger for the hydrostatic bearing.

Low-temperature operation led to an oil cavitation problem in the elevation reducer lubricating system. This was temporarily resolved by operating the lubricating pumps at all times, and was finally resolved by installation of immersion oil heaters. The problem was a secondary one, since one obvious solution would be the substitution of a lighter oil. The heater installation was selected as more practical, since each reducer has a near 0.2-m^2 (50-gal) capacity.

A truly extreme rainstorm, 152 mm (6 in.) of rain in less than 1/2 hour, forced one halt in operation. Accumulation of water in the hydrostatic bearing reservoir, flooding in other structure and operational areas, all in combination with high winds, led to the shutdown.

Snow has accumulated to a depth of 200 mm (8 in.) with no evidence of damage to the structure.

As in the case with the environmental specifications, life expectancy and reliability requirements of the established specifications have not generally been subject to direct test for compliance. The reliability and maintainability of the 64-m antenna, under very heavy operational use, have proved excellent. With the exception of the azimuth hydrostatic thrust bearing, which is discussed in detail later in this chapter, no special problems of reliability have been encountered. The overall maintainability of the antenna has proved similar to that of the conventional DSIF 26-m (85-ft) antennas.

The operational experience shown in Table 12 is included as a measure in confirming the success of the design effort in achieving a reliable and dependable instrument.

The 15-h downtime was a loss due to low film height during the time in which difficulties were being experienced with the hydrostatic bearing. The 3.6-h downtime was logged against the replacement of a hydrostatic bearing film height transducer; other similar events have taken much less time. The antenna has supported many critical mission spacecraft operations wherein any interruption in support could have had very serious impact on the mission objectives. For such critical occasions, special maintenance, training, and other precautionary measures are normally undertaken. Under those conditions, the 64-m antenna has never failed to meet the mission support requirements.

A. PEDESTAL AND INSTRUMENT TOWER

The pedestal concrete was specifically required to have modulus properties that would match the hydrostatic bearing pad deflection patterns in order to provide suitable structural stiffness to be compatible with the antenna system resonant frequency requirement. To make sure that these requirements were met, during the construction phase, test cylinders were made from each concrete batch and tests were made for 7- and 28-day compressive strengths and for the elastic modulus at 28 days. Average elastic modulus for all of the cylinders was 35232×10^6 N/m^2 (5.11×10^6 psi) and the coefficient of variation was 7.4%, within the 10% specified. To determine that excessive distortion of the pedestal would not occur in construction and compromise the hydrostatic bearing runner flatness, the curing of the pedestal concrete was carefully monitored. To observe the drying rate, the weight loss of samples of the concrete was measured. Two 152 × 305 mm (6 × 12 in.) cylinders, made from the pedestal concrete mix, were prepared. One was coated in the same manner as the pedestal, the other was left unpainted. Each was weighed daily as a measure of the loss of moisture due to evaporation. Figure 120 is a graph of the results which are interpreted as showing a satisfactory drying rate for the painted cylinder, the sample representing the drying condition of the pedestal.

To monitor the internal strain of the pedestal due to creep during construction and due to operating loads, approximately 50 Carlson extensometers were permanently placed within the concrete walls and roof deck by fastening them to the reinforcing steel before placement of the concrete. They were set to measure radial, tangential, and vertical deformations. Special care was required to avoid damaging the extensometers during concrete placement. Continual

readings, made for a period of about 2 years, indicated no adverse dimensional stability problems. Drying shrinkage of the pedestal concrete was determined to be essentially complete at 4-1/2 months after placement.

To allow determination of radial tilt occurring during the curing period, four sets of three brass level buttons were inserted in the pedestal haunch where the hydrostatic bearing runner is supported. No detectable tilt occurred during the monitoring period.

Regarding the suitability of the founding in relation to seismic design consideration, the only pertinent information to supply is that since the antenna has been in operation, the site has been subjected to four minor quakes, the largest being of order 4.5 on the Richter Scale, with no problems and no banging on the base.

No modifications have been required on the pedestal, pedestal foundation, or instrument tower foundation.

The instrument tower was designed to have a resonant frequency ≥4 Hz with a 1000-kg (2200-lb) weight (representing the master equatorial equipment) mounted on its top. The tower's deflection was to be less than 2 seconds of arc, due to coupled loads resulting from 20.1-m/s (45-mph) wind load on the antenna structure.

The instrument tower foundation modulus was determined experimentally by jacking against the pedestal. Using that value and with the actual weight of the master equatorial equipment (approximately 1000 kg), the lowest natural frequency was calculated to be 4.5 Hz, well above the minimum specification. Angular excursion of the instrument tower due to reflected wind loading has been measured at less than 1.0 arc seconds, well within specification.

Thermally induced excursions of the instrument tower have been found to produce minor pointing inaccuracies caused by tilting of the master equatorial support base. The total excursion, measured over a 36-hour period, was 6.7 arc seconds. These deviations have not caused problems in operating at S-band frequencies. However, reliable around-the-clock operations at X-band or higher frequencies will require a suitable method to reduce these excursions.

The instrument tower is insulated with rigid foamed-in-place polyurethane approximately 51 mm (2 in.) in thickness. Polyurethane was selected because of its good thermal properties. It is rated as incombustible by standard ASTM test procedures used for rating building materials and was therefore considered acceptable for the designed use. Under certain conditions, however, vigorous burning can be sustained with generation of dense toxic black smoke.

This hazardous property became known to JPL after an insulation fire occurred during the construction of the antenna. However, due to the difficulty and expense of removing the windshield surrounding the instrument tower to expose the insulation for removal, the decision was made to retain the insulation and accept the minor fire damage risk. (The tower insulation for the overseas 64-m antennas was redesigned, with a fibrous glass insulation being substituted.)

B. CABLE WRAP-UP

The cable wrap-up was required to be capable of carrying various power, signal, control, fluid and gaseous services between the fixed pedestal and the rotatable alidade. The system was to be low drag on the antenna motion and not generate detectable electric noise. The design was to permit ±300 deg rotation about the azimuth axis from southeast as installed at the Mars DSS. The minimum capacity was to be equivalent to four 76.2-mm (3-in.) diameter hoses and fourteen 76.2-mm (3-in.) diameter cables.

All specified design and performance parameters were met at the outset. Under extended operations, however, several adverse conditions were found:

(1) Under high pressure, the coolant line swivels would bind and cause twisting of the hoses.

(2) User personnel installed various nonstandard-sized cables into the wrap-up to conveniently support the needs of short-term projects and frequently would leave the cables in position for the next experiment. Over a period of time, this caused the mechanism to become unbalanced and to bind up during rotation.

(3) The point of rotation of the supporting mechanical structure and the supported electrical cables and water hoses did not coincide, causing differential motion and resulting in excessive wear and binding.

Because of these problems, the rotation of the cable wrap-up was limited operationally to 270 deg in each direction from neutral, and frequent inspections of all cables, hoses, and connections were found to be required. Over a 3-year period, there was no antenna downtime caused by mechanical failure of the wrap-up. There were, however, failures in water hoses and in power and signal cables.

The cable wrap-up was redesigned and modified to provide increased capacity (water, power, and signal) for a higher-power transmitting capability and multi-feedcone capability and, at the same time, correct the deficiencies discussed above. A detailed discussion of this modification is contained in Chapter VII.

C. ALIDADE

Reference 1, Rev. 4 required that the alidade be a pentahedron, all-steel space frame structure. It was required that very careful attention be given the design of the structure to minimize the possibility of brittle fracture in the very large sections of the alidade. The stiffness of the alidade structure and the bearing and drive

supports had to be compatible with specified minimum antenna system resonant frequency requirements.

Control against brittle fracture was accomplished by specification of steel composition and grain size which were confirmed by laboratory test of samples of the steel used.

During fabrication, all welding was preplanned and thoroughly inspected by X-ray, magnetic particle, or dye penetrant as required by specification. No cracked welds were found in the alidade structure, nor have any been found in subsequent inspections.

After erection at the site, structural tests as described below were performed to assure that critical stiffness requirements were met and that all joints were properly made:

(1) To determine alidade stiffness, a beam and hydraulic jack were mounted between the elevation support weldments on the alidade. The jack then applied incremental loads to spread the weldments apart, with loads measured by the oil pressure in the jack and displacements measured by a dial indicator between the end of the beam and the elevation bearing support weldments.

The maximum load applied was 188,600 N (42,000 lb), for which the measured displacement was 3 mm (0.157 in.). The design displacement for a 222,411-N (50,000-lb) load, calculated by the STIFF-EIG program, was 4.775 mm (0.188 in.). Interpolating on a straight-line basis, it was calculated that the design displacement for a 188,600-N (42,000-lb) load would be 4 mm (0.159 in.).

(2) To test the hysteresis of the alidade structure in azimuth, the brake on one azimuth drive was locked while measured torque increments were applied to the drive shaft of a second azimuth gear drive, by a cable and system of pulleys. The third azimuth gear drive brakes were released so that they did not contribute to the structure. This had the effect of twisting the base triangle, the azimuth radial bearing, and the gear drives.

Clockwise loads on the input shaft were applied incrementally from zero to 190 N-m (0 to 140 lb-ft), and then reduced in the same increments to zero. The process was then repeated for counterclockwise loads for one full loading cycle. Two full loading cycles were run.

The resulting hysteresis plot of input shaft rotation vs input torque is shown in Fig. 121. At the initial loading, the stiffness appears low because of the nonlinearity of the gear tooth and bearing deflections and seating in of the contact surfaces. The apparent increase in stiffness, as unloading begins, is due to the friction in the drives tending to maintain the tension in the structure as the load on the input shaft is reduced. Regions of the curve away from either extreme show good agreement with the design value of stiffness. The structural integrity of the system is demonstrated by the repeatability of the data over two cycles of loading.

(3) The elevation hysteresis test was similar to the azimuth test, with the brake of one elevation box set while the shaft of the other box engaging the opposite elevation bull gear was rotated. This test twisted the tipping structure as well as the alidade. The test results are shown in Fig. 122. The comments on the azimuth test also apply in this case.

After jacking and hysteresis tests, all components returned to position and no slippage was detected in any joint; nor had any structural yielding occurred. The absence of slippage or yielding was validated by before-and-after measurements of punch marks, which were placed at joints with a fixed position, double center punch.

No structural modifications to the alidade proper have been required since construction. A number of minor bracketry, platforming, and access modifications have been made to support added air coolant and fire water lines and signal and power cables.

D. AZIMUTH HYDROSTATIC THRUST BEARING

It was specified that the operation of the hydrostatic thrust bearing be demonstrated by continuous movement of the antenna from one extreme azimuth position to the other (±300 deg). Acceptance of the bearing was based on proper operation as a component of the overall antenna system. A required demonstration of the azimuth hydrostatic bearing was maintenance of a minimum safe 0.076-mm (0.003-in.) film height in a failure mode with one motor driving and two pumps nonoperational.

First azimuth rotation of the 64-m antenna, with partially complete alidade, was accomplished as specified during the construction phase, providing assurance that the bearing operation on the completed antenna would be satisfactory.

As was previously mentioned, when the antenna was practically complete as a structure, there was an accident in which one corner of the rear pad of the hydrostatic bearing grounded. This caused the pad to rotate, breaking the antirotation link and rupturing the reservoir wall. All of the pads were removed and damage was found on the rear and on the right front pads. This was repaired by welding and remachining.

The damaged runner surface was welded and refinished in place, and the bearing was returned to operation by the contractor. Investigation showed that the accident was due to a misetting of the high-pressure relief valves, permitting some of the high-pressure oil supply to bypass the bearing.

At the time of antenna completion, the azimuth hydrostatic thrust bearing functioned as specified with acceptable film heights.

During the initial operational use of the antenna, monitoring of the hydrostatic bearing film height (the thickness of the oil film between the runner and the pad) indicated decreasing film heights, evidently due to deterioration of the flatness of the bearing runner. This situation required periodic corrective shimming between the runner and sole plate to maintain the antenna in operation. Meanwhile, the cause of the deterioration was studied, and adequate instrumentation for precisely measuring the runner profile was developed and proven.

To determine the cause for the low film height, tests were conducted on a full-scale mockup of a runner section. Corings were made of the grout under the actual runner, and a small section of the sole plate under the actual runner was removed.

It was found that the deterioration was a result of changes in the runner level due to oxidation of the sole plate at its interface with the grout. The oxidation of the sole plate was traced to an electrical potential across the interface and to oxidizing agents present in the grout. The grouting material supporting the sole plate and bearing runner surfaces was a proprietary nonshrinking grout consisting of a rich concrete mixture to which iron filings and an oxidizing agent had been added. Normal concrete shrinks as the entrapped water is absorbed in crystallization or is lost by permeation and evaporation. In the grout mix, the iron filings, in the presence of moisture, are oxidized and expand to compensate for the shrinkage due to water loss. This expansion normally stops with the dissipation of the free water, the material being sealed to prevent entry of further moisture. On the 64-m antenna bearing, the sealing was evidently not effective, apparently because of "breathing" caused by the runner deflections as the pad passed over an area. Moisture then continuously entered the area between the sole plate and the grout, reactivating the oxidizing agent, which attacked the bottom of the sole plate. The iron oxide formed was much less dense than the metallic iron, and the increased volume caused a vertical displacement of the runner. This displacement was actually as much as 1.5 mm (0.060 in.) in local areas, causing a runner distortion which could not be compensated for by the strong righting moments inherent in the pad design.

The nonuniform vertical displacement also resulted in very low film heights in local areas. The theoretical film height of the bearing is approximately 0.200 mm (0.008 in.) on an ideally flat runner. Film heights of 0.127 to 0.150 mm (0.005 to 0.006 in.) are acceptable; but, during this period (late 1968), film heights of definitely less than that acceptable minimum were fairly regularly encountered and required shimming in local areas to restore proper bearing operations. However, the rate of deterioration slowly accelerated to the point that areas corrected by shimming would often show deterioration within a few weeks.

By early 1969, JPL had identified a suitable different type of grout and technique for placing it; an improved sole plate design had been developed; and necessary precision instrumentation had been provided for releveling the runner. At that point, a program was undertaken to remove all of the old grout and sole plates, relevel the runner, place new sole plates, and place new grout. The task was completed in eight weeks according to a preset schedule. During the period that the bearing rework was done, the antenna was actually continued in use to support limited critical tracking commitments of Pioneer and Apollo spacecraft.

The old grout was removed by diamond tip coring tools 90 mm (3.5 in.) in diameter, with remnants of the old grout cleaned out as much as possible with air hammers. Using specially made instruments, measurements were made from the azimuth bull gear, which had been surveyed as a reference surface, to the runner surface at the inside leveling lugs. Special cross levels were made for leveling the outer surface from the inner surface. New flat ground sole plate segments were set in place with 4.7-mm (0.188-in.) parallel ground shims between the sole plates and the runner, to permit final leveling of the runner as required. New chemically inert grout was packed between the sole plate and the runner by hand, using a 1.5 to 1 sand/cement ratio and carefully controlled water content to minimize shrinkage.

All of the above-described work was carried on in three areas (between the three pads) simultaneously, always permitting a minimum of 60 deg azimuth motion usable for the critical tracking. The grout was cured for 72 hours before a pad load was applied. Corrective thin shims were installed as necessary to level the runner to provide a minimum 0.127-mm (0.005-in.) film height. This adjustment was necessary because of slight movement of the runner after leveling, due to the grout placement operation, or because the sole plates were not snug against the runner when the grout was placed.

After completion of the regrouting, the parallel ground shims were replaced with contour ground shims, thus eliminating the need for the thin laminated shims between the sole plates and the runner. The contour ground shims were anchored in place and are a permanent installation. The contour ground shims were set in place with greased surfaces. The grease served to fill any open spaces, preventing moisture entry. The grease also contained a rust inhibitor to minimize corrosion of the sole plates and ground shims.

An improved instrumentation method was developed, permitting survey of runner elevations and film heights to accuracies of the order of 0.0254 mm (0.001 in.). Figure 123 shows

a cross section of the bearing and its instrumentation.

An external rainshield between the reservoir wall and the pedestal has been installed to further reduce water entry into the bearing area.

Upon completion of the regrouting and with an oil kinematic viscosity of approximately 0.000217 m^2/s (1000 SUS), a minimum film height of 0.1143 mm (0.0045 in.) was obtained with all the pumps in operation. Since the installation of the new grout, the bearing film height and the runner profile have been recorded at regular intervals for surveillance purposes. To date, there has been no indication of the progressive deterioration previously seen. However, there are two areas, in the region of joints in the runner, that have required occasional attention.

E. AZIMUTH RADIAL BEARING

The azimuth radial bearing defines the azimuth axis and resists radial loads principally due to wind. The azimuth radial bearing was required to have friction characteristics compatible with the servo system and stiffness compatible with the overall structural minimum frequency requirements. The bearing design was specified to provide a preload system to maintain the azimuth axis definition and accommodate a temperature difference of 2.8°C (5°F) between the alidade and the pedestal within the overall temperature range specified for the complete antenna system.

Azimuth motion, employing the azimuth radial bearing, was successfully accomplished at the time of first rotation in December 1964. At the time of antenna completion, the radial bearing functioned as specified.

In the bearing design implemented, three basic misalignments can occur in the radial bearing trucks. These misalignments and methods used for correcting them are as follows:

(1) The first type of misalignment can occur in a rotation of the entire truck (Fig. 124) about the radial axis. With this misalignment, the truck will rise with one direction of rotation and fall with rotation in the opposite direction. With continued rotation, the truck will reach an equilibrium position at the top or bottom, after which its motion will be a combination of rolling and sliding. The amount of misalignment can be determined from an interpretation of a hysteresis-like curve (Fig. 125) plotted from the vertical movement of the truck as a function of azimuth travel in each direction. Specifically, a dial indicator is mounted on the truck and bearing on the top of the runner wear strip so that it will measure movement of the truck with respect to the wear strip (Fig. 126). The antenna is then rotated 120 deg clockwise in azimuth, followed by an opposite rotation of 120 deg in a counterclockwise direction. Dial indicator readings are taken at 10-deg bench marks during each direction of rotation. These data are plotted as a closed curve, as shown in Fig. 125. If the difference between the clockwise and counterclockwise data is plotted, a relatively smooth parabolic-like curve is developed. The slope of this curve at the end points, expressed in terms of inches rise per inch of circumferential travel of the truck, with appropriate sign, is the angular correction to be made in the truck alignment. With proper alignment, a maximum difference of 3.81 mm (0.015 in.) between the position of the truck in full clockwise and counterclockwise directions is achieved, which provides completely acceptable performance.

(2) The second type of misalignment is nonparallelism of the truck axles in a plane tangent to the runner wear surface (Fig. 127). This type of misalignment results in the truck moving vertically across the runner and back, eventually coming to an equilibrium position along the top or bottom of the runner, with a combination of rolling and sliding motion of the wheels. The amount of this type of misalignment, which results from mismachining of the trucks, is found by determining the angular displacement of each shaft from the true vertical for some position of the truck.

To correct for the misalignment, the truck preload is removed and the truck backed away from the runner with jacks. Removing the upper bearing end cap from each wheel, a precision (1 arc second) electronic level is placed on the end of the shaft parallel to a tangent to the runner wear surface. The level is read in that position, and then again after the wheel has been rotated 180 deg with the level in place. The midpoint of the level excursion for each axle is the angle of that axle with respect to gravity. This misalignment, then, is the difference between the midpoints for the two axles on one truck. Shims were placed between the wheel bearing boxes and the trucks to correct the alignment to an acceptable value (see Fig. 126).

(3) The third form of misalignment is for the truck rollers to be out of parallelism with the runner wear strip along a vertical line (Fig. 128). This can be determined by taking the preload off the truck, jacking it slightly away from the runner, and measuring the resulting gap at the top and bottom of the roller with feeler gauges. Adjustments are made by insertion of appropriate shims between the bearing boxes and the truck weldments to provide fully acceptable performance.

While some misalignment of the trucks of all three types described was encountered during the early shakedown periods, corrective measures have been very successful. Alignment is now checked routinely at 3-month intervals, with no serious problems occurring.

F. ELEVATION BEARINGS

Early design concepts for the elevation bearings proposed a single spherical roller bearing mounted in a one-piece housing. This arrangement, used successfully on many smaller antennas, introduced serious problems of assembly, inspection and maintenance, and replacement. The existing design, with the bearings of each assembly mounted at each end of a shaft pressed into the reflector support casting, overcomes these problems and additionally permits visual inspection of rollers and races.

The only problem encountered has been one of minor oil leakage due to reflector support casting-shaft deflection. This has led to the addition of a static seal. No structural modifications have been required.

G. AZIMUTH AND ELEVATION DRIVES

The gear drives have performed satisfactorily, with no apparent deficiencies in stiffness and strength to drive and hold the antenna under all environmental conditions encountered. Tests were performed on the complete gear reducers prior to installation on the antenna to determine compliance with design requirements.

Stiffness tests were conducted with the gear reducers mounted on a special fixture (Figs. 129 and 130) which included a short rack representing the bull gear. Loads were applied at both the input and output shafts, with measurements made of the displacement at the load points as a function of the applied load. Tests were also made on two elevation and two azimuth gear boxes to determine the gear drive housing elongation as a function of output shaft torque.

The data from elongation tests for each type were averaged and applied to all of the tested boxes of that type as a required correction to the torque stiffness measurements. Typical data are shown in Fig. 131.

Backlash was measured by applying measured torques to the gear reducer input shafts and noting the input shaft rotation between the point in clockwise and counterclockwise motion. A typical curve of the recorded data is shown in Fig. 132, indicating a total backlash of 38 deg.

Breakaway friction was measured by determining the torque required to start and to maintain motion of the unloaded gear reducer in both clockwise and counterclockwise directions. Starting torques ranged from a low of 1.13 to a high of 3.73 N-m (10 to 33 lb-in.), while the running torques ranged from 1.58 to 3.95 N-m (14 to 35 lb-in.). A summary of the data on all of the gear reducers is given in Table 13; it is interesting to note that there is as much as a 1.5 to 1.0 ratio in breakaway torques for opposite rotations of the same gear reducer.

Each elevation gear reducer was run at no load for 1-3/4 hours clockwise, and a like period counterclockwise, at input speeds ranging from 800 to 2400 revolutions/min. The azimuth drives were run at no load for 2 hours at speeds ranging from 400 to 2400 revolutions/min at the input shaft. Temperature readings were made of the sump oil, and at the upper high-speed bearing. These readings ranged from 3 to 8°C (5 to 15°F) above ambient.

In addition, elevation gear reducers Numbers 1 and 3 were run at 400, 1000, 1800 and 2400 revolutions/min at the input shaft and with output pinion loads ranging as high as 33896 N-m (25,000 lb-ft). Oil temperatures were not significantly different from those measured in the no-load tests. Efficiencies were acceptable as calculated from the input and output torque measurements. A typical curve is shown in Fig. 133.

Design studies resulted in a specified minimum gear reducer stiffness of 2.98×10^7 N-m (2.2×10^7 lb-ft) per radian at the output shaft and a maximum stiffness differential from any one reducer to another of 25%. The in-plant test results ranged from 3.12 to 3.53×10^7 N-m (2.3 to 2.6×10^7 lb-ft) per radian, showing compliance with the design specification.

One significant problem was encountered with the drive design during construction: the elevation gear reducers would not properly track the bull gear. This was largely due to improper initial installation of the reducer support cartridges and inadequate stiffness of the supporting structure. Bronze wear shoes were added to preclude the possibility of the reducers "walking off the gears," the support cartridge was more carefully aligned, and the support platform was stiffened. Following those changes, adequate performance of the elevation reducers has been obtained, and no further structural or mechanical modifications have been required.

Each gear box is fitted with a spring set, hydraulic release disc-type brake. These brakes are arranged so that high pressure in the servo supply system releases the brake and either hydraulic failure or interruption of an electric circuit by power failure or by any of a series of interlocks causes the brakes to set. Additionally, elevation stow locks are provided for use with the antenna in the zenith position when extremely high winds are anticipated. These mechanical locks have teeth which engage tooth segments mounted on the elevation wheels, separate from the bull gear.

The brakes were specified to have a torque capacity of 216.9 N-m (160 lb-ft) at the gear reducer input shaft. As installed, however, the brakes did not meet this requirement and had a capacity of only 94.9 N-m (70 lb-ft).

A decision to continue use of the lower-capacity brakes was made after careful consideration of the dynamic and static braking requirements. The dynamic stopping capability had been proved during the acceptance testing of the antenna, wherein the reflector was driven into the limits at each end of travel at the maximum slew velocity. The brakes, automatically set by

electrical interlocks at the travel limits, adequately stopped the motion. The static capacity requirement, holding the antenna in 53.6-m/s (120-mph) winds, was therefore the determining factor.

The elevation axis has the advantage of stow-locks to assist the brakes. Any windmilling of the antenna about the azimuth axis, due to the maximum winds, would not result in catastrophic failure. There was, therefore, high assurance of the safety of the structure.

In that it is desirable, from an operational standpoint, to eventually replace the brakes with those of the specified capacity, the brakes have been redesigned and meet the 216.9 N-m (160 lb-ft) requirement. The redesigned brakes are being used on the 64-m overseas antennas and are now installed on the Goldstone 64-m antenna.

H. PRIMARY REFLECTOR BACKUP STRUCTURES

Upon completion of the antenna, the primary reflector structure and its backup structure met the established specifications. The following discusses performance under environmental loads.

The attachment points on the reflector structure were set for the proper paraboloid shape at 45 deg elevation angle; at other elevation angles, the change in gravity loading on the assembly distorts the reflector structure out of the correct shape. The resulting distortion of the structure at zenith and horizon aspect angles in terms of root mean square deviation of the panel attach points on the structure from the ideal shape were computed, and the results are shown in Figs. 134 and 135 and in Table 14. The field-measured values are also shown in the same figures and in Table 15. The calculated and measured distortions were within the specified tolerance.

The reflector structure is further distorted from its paraboloidal shape by variable wind loads on the surface panels transmitted to the reflector structure and by solar differential heating and expansion of the individual members of the reflector truss structure. Direct field measurements required to evaluate these distortions have not yet been accomplished. The RF gain results at S-band during normal mission support use, with the antenna subject to these environmental loads, have indirectly indicated distortions well within specified values.

I. PRIMARY REFLECTOR SURFACE

As illustrated in Chapter III, the primary reflector surface is formed by 552 individual panels affixed through adjustable support points to the reflector backup structure. To establish the fabrication error of the panels themselves, each panel was set up in a fixture in a tape-controlled mill with a contour measurement for each 645 cm^2 (100 $in.^2$) of its surface. The measurements were made normal to the plane of the four corners of each panel (that plane established a zero reference panel); the errors between the desired paraboloid passing through four corners and the actual surface were measured to determine compliance with specifications. Using the data, the RMS error for each row and the total RMS error for the entire surface were computed. Also, the average deviation of the panels and the standard deviation about the average were calculated. Table 16 shows the summary of the results.

The majority of the panels were slightly convex to the true shape resulting from assembly of flat sheets and contoured Z-frame.

After installation and adjustment, the panels were inspected for correct locations by theodolite angle readings on the panel alignment targets. Figure 136 shows the technique employed.

The target holes are located accurately in radial distance from the antenna reflector vertex by drilling through bushings in a flexible strap gauge.

The "zero" setting of the surface panels was done at 45 deg elevation angle at night, with little wind, and the Ref. 1 requirement of 1.50 mm (0.060 in.) RMS setting tolerance was improved upon. The error in the final setting value of the panels was measured to be 0.480 mm (0.019 in.) RMS at the fastening points of the panels. It is believed that this value could be lowered without design changes, merely by a more tedious set-and-check procedure.

From the long use experience and measured performance values at higher than S-band frequencies, the particular design of the surface panels (believed pioneered by Rohr Corporation) has proved to be very satisfactory. The panels weigh less than 97.6 kg/m^2 (2.0 lb/ft^2) and are capable of supporting a 136-kg (300-lb) man walking or standing on the surface without permanent distortion.

J. QUADRIPOD, SUBREFLECTOR, AND CASSEGRAIN FEED SUPPORT

The quadripod provides for support of the hyperboloidal microwave subreflector and the feedcone handling hoist.

In regard to the latter function, a 28,100-kg (62,000-lb) load was lifted by the hoist with the antenna at the horizon look, demonstrating satisfaction of the hoisting specifications. However, prior to the test and before actual field usage of the quadripod/hoist installation, modification of the design was deemed necessary. Bar members at the quadripod apex were reinforced and a removable tie was added between the upper legs at the cable attach points. This was done following further study of the design with a refined computer analysis not previously available and coupled with strain gauge tests of the installed quadripod.

The torsional mode natural frequency of the quadripod showed a close agreement between the field measurements and computed values, but only after the computing mathematical model used in the computer analysis was upgraded by including bar members with bending rigidity at the nodes.

The computation checked by field theodolite readings showed no discernible primary surface distortion near the connection points of the quadripod legs to the reflector structure under gravity loading.

The surface of the subreflector was required to be within 1.27 mm (0.050 in.) RMS of a best-fitted hyperboloid as manufactured. As checked with a rotating template, 0.686 mm (0.027 in.) RMS was achieved.

The Cassegrain system was aligned to the computed geometry at a 45-deg elevation angle using a theodolite above the vertex of the primary surface with its axis aligned square to the datum targets in the reflector structure. Two separated cross-hairs were provided on axis of the subreflector for aligning to the theodolite's line-of-sight along the symmetric axis of the paraboloid. The IRS mirror was adjusted normal to the same line of sight. The RF boresight direction is defined by this normal to the IRS mirror when the antenna is at 45 deg elevation, since the master equatorial collimates to the same mirror.

At elevation angles away from the 45 deg setting position of the Cassegrain geometry, the deflections due to the gravity loading of the primary surface, the subreflector, and the RF feed displace the RF boresight direction from the normal to the IRS mirror. This error is described in Chapter IV of this report. Also, displacements of the operating RF phase centers from the true foci of the best-fit paraboloid and hyperboloid result in gain loss. These losses are discussed in connection with the performance of the antenna at X-band, since these offsets from gravity loading and the resulting gain losses are negligibly small for S-band.

As described in Chapter VII, the tricone subreflector was modified to include remote console controllability to provide the two lateral motions as well as the axial motions for focus. Thus, for X-band and higher-frequency use, the virtual focus of the hyperboloid system can be superimposed on the focus of the best-fit paraboloid and recover about 1.27 mm (0.050 in.) equivalent RMS distortion loss when the offset is about 68.6 mm (2.7 in.) at zenith look.

K. SERVO AND CONTROL SYSTEM

The antenna servo and control system, as installed, met all of the specified performance requirements of bandwidths, rates, tracking error, etc.

The servo electronics is the principal interface, not only between other subsystems but also between man and the machine. During the initial operations period, some changes were effected in the servo electronics equipment to improve these interfaces. Such modifications were accomplished in early 1969, during the period of azimuth hydrostatic bearing rework, to preclude additional antenna shutdown time. Changes were made in the servo electronic equipment as follows:

(1) Addition of an Optics II mode to accommodate a redundant antenna-mounted autocollimator that had been added to the IRS optical assembly.

(2) Addition of bias controls to allow front panel selection or adjustment of the elevation and cross-elevation position error bias voltages.

(3) Various minor cabling and equipment changes. These were made because of moving the equipment location from the pedestal to the new operations building.

As noted above, there was only one major equipment modification of the servo electronics. In addition, there were many minor variations and additions to the control and monitor circuits, and the design was not "frozen" until early 1970. This freeze occurred for the purposes of configuration control and the final transfer from engineering to operations.

L. PRECISION ANGLE DATA SYSTEM

Although performance of the precision angle data system exceeded specifications in all areas, certain equipment changes were made for improvement of man/machine interfaces. These changes included the following:

(1) Addition of a second autocollimator on the Intermediate Reference Structure optical assembly. This redundancy provides a backup at a critical point in the pointing system.

(2) Modification of the master equatorial angle encoders to make the on-axis synchronous assembly a one-piece unit rather than the original two pieces. This change was made to allow field personnel to interchange on-axis synchronous assemblies with no change in system accuracy. The original design required alignment tolerances of the stator and the rotor to the axis which were prohibitively close for field work.

In addition to the changes listed above, many relatively minor changes have been made. These changes were made to correct both design and fabrication errors, as well as to improve the interface characteristics of the system.

The major internal contributions to the pointing error of the Master Equatorial have been measured to be less than 2 seconds of arc (3σ). They include the declination axis runout, the hour angle axis runout and gravity deflection, the axes' orthogonality, and the temperature gradient errors. The error contribution of the on-axis encoding system has been measured at less than 7 seconds of arc (3σ).

V. PERFORMANCE OF THE ANTENNA AT X-BAND

A. INTRODUCTION

Having determined the outstanding S-band performance of the 64-m antenna, the potential of obtaining increased antenna gain by going to a shorter wavelength was investigated.

Late in 1966, a simple, well-calibrated X-band (8448-MHz) feedcone system (XCE) was constructed. This feedcone was used for detailed evaluation of the 26-m (85-ft) antenna reflector at the Venus DSS. In February, 1968, the 64-m antenna became available for a short evaluation period.

The primary purpose of the X-band test program was to evaluate performance for future programs possibly requiring an X-band data link. Additionally, an advantage of short-wavelength RF evaluations is the ability to clearly define the system surface tolerance and other structural-related effects.

Detailed information concerning radio frequency performance of the antenna at X-band is contained in Ref. 15.

B. PREDICTED X-BAND PERFORMANCE

1. RF Optics Efficiency

The RF optics efficiency fed with the XCE feedcone system was evaluated by describing the primary feed patterns (Fig. 137) and the subreflector configuration (Fig. 138) as input to the Rusch Scattering Program. The scattered patterns shown in Figs. 139 and 140 illustrate slight distortion occurring near the edge of the paraboloid (illumination angle range of 50-60 deg) caused by the optimum S-band beamshaping flange around the hyperboloid periphery. As with the earlier 26-m (85-ft) diameter reflector evaluation at X-band, the removal of the S-band flange was not considered necessary. The scattered patterns were then evaluated with the JPL Antenna Efficiency Program. Results of the above processing are summarized in Table 17 for a hypothetical dissipationless feed illuminating a perfect reflector without quadripod.

The dissipative attenuation between the antenna reference flange and the maser reference flange was previously measured as 0.150 ± 0.0018 dB, 3σ. Estimates of polarizer and feedhorn losses are 0.025 and 0.018 dB, respectively. Table 18 gives the components considered and the overall waveguide efficiency with an estimated 1σ tolerance.

The final value for the RF optics efficiency of the 64-m antenna fed with the XCE feedcone system may be obtained from Tables 17, 18, and 19 as

$$\eta_0 = 0.629 \pm 0.024$$

where the tolerance quoted is an estimated 1σ value, primarily due to quadripod blocking uncertainty.

2. Surface Tolerance Efficiency

The gain loss from the RF surface distortions or tolerance at S-band wavelength is a negligibly small portion of the total loss at the calibration conditions of about 40 deg elevation angle, with low wind loads. However, at wavelengths shorter than S-band, a clear understanding of the surface tolerances of the RF reflective surfaces in the Cassegrain system is considered necessary to visualize the ultimate performance limitations of the system.

The RF surfaces comprise the 552 individual surface panels with factory-measured distortions with respect to their mounting legs. The distortions of the surface panels' mounting points of the reflector structure are obtained by utilizing the STAIR structural computing program as described earlier. Also to be considered are the deflections of the focus of the best-fit paraboloid and the phase centers of the feedhorn/subreflector subsystem mounted on the quadripod and the vertex-mounted Cassegrain cone which results in equivalent RMS surface tolerance loss.

The discussions in this Chapter will be limited to the application of only the gravity loading case from the other environmental loading possibilities. The gravity loading is always present during the elevation angle motion of the antenna, independent of the wind loadings. Solar thermal loads also exist, in the first-order sense, for about 12 hours out of 24. However, these two latter loading effects (the wind and solar) can be added separately, as discussed in the other Chapters. Since the limited amount, consisting of four continuous day-and-night RF tests, of X-band tests were made under environmental conditions of little or no wind but with full solar thermal loadings, comparisons between the analytically computed surface tolerances and RF field test computed results can be made only if the solar thermal effects are negligibly small.

The data spread of the X-band tests results, as shown in Fig. 141, combined with Fig. 142, made throughout the 4 days on a 24-hour basis is the only indication or field test result available from which conclusions on the solar thermal load effects can be drawn. The narrowness of the band seems to indicate that the surface tolerance effects by solar thermal rays are small. Further tests at higher frequencies may be necessary to clearly detect the environmental wind and thermal load effects.

With the corners of the surface panels aligned by the adjustable mounting legs to the design paraboloid within negligible tolerance at a 45-deg elevation angle, together with the hyperboloid subsystem aligned on the symmetric centerline, only the distortions of the surface panels are present under low wind and solar thermal loads. Table 20 gives the measured errors, the total of which has been considered a constant, noise-like perturbation present to be added to the gravity and other distortions at attitudes other than 45-deg elevation.

The gravity load deflection vectors as output from the STAIR structural computing program

were evaluated by use of the RMS program, which yields the RMS of one-half the RF pathlengths of the residuals following best-fitting by a perfect paraboloid. This paraboloid assumes a new focal length as a best-fitting parameter. This RMS so computed is representative of the distortions occurring in the reflector backup structure, or panel support points only.

The computed surface distortions are in Table 14. Best-fit paraboloid translations and x-axis rotation are noted, as well as quadripod and subreflector deflections. The table clearly illustrates the effective absence of gravity effects at a 45-deg elevation angle, due to the alignment methods used. The second portion of the table shows the effect of lateral and axial misalignments of the RF feed focus, considered to be tightly coupled to the subreflector-feedhorn system, from the best-fit paraboloid focus, expressed in RMS equivalent error.

Figure 143, which shows the RMS equivalent error due to axial and lateral misalignments, was obtained based on studies conducted with the JPL radiation pattern programs which numerically evaluate the scalar far-field radiation pattern integral.

The power sum of the four key components, each expressed in RMS millimeters and inches, the lateral and axial misalignments occurring at the paraboloid focus, the paraboloid structure gravity distortion, and the constant component due to panel manufacturing error, is taken in two ways. The first sum allows for axial focusing of the subreflector, and the second constrains the system to a fixed-focused mode. The fixed-focused mode had previously been adopted for S-band operations.

Based on the work of Ruze, Fig. 144 was obtained; it relates RMS surface tolerance to surface tolerance efficiency for the wavelength of interest. From this figure, it is clear the improvement available by axial focusing is worth the effort at X-band, based on the structural computations in Table 14.

The RMS best-fitting program also outputs contour plots of the residuals after best fit. As discussed earlier, Figs. 134 and 135 show the computer organized plots of the horizon and zenith attitudes for the reflector structure, as analytically computed for the gravity loading difference from the 45-deg attitude. At both attitudes, the field-measured results are smaller than from the analytical computations. These differences were reduced to a small amount when an improved structural computing program (NASTRAN) was used in later studies with improvements in analyzing field readings.

It should be noted that the RMS computations above were based on a uniformly illuminated paraboloid, which is generally not achieved. No specific study of a possible discrepancy between results obtained above and results obtained on the basis of some form of feed amplitude weighting is available. This possible discrepancy is considered small.

3. Predicted Overall System Efficiency and Gain

By consideration of the computed RF optic efficiency and the computed RMS surface tolerance coupled with Fig. 134, a computed overall system efficiency and gain is established. Table 21 gives the results, based on accepting the axial focusing effort, which were shown to be worthwhile. Note that Table 21 includes the effect of nearly 0.2 dB dissipation loss within the XCE feedcone.

C. MEASURED X-BAND PERFORMANCE

1. Feed Performance

The XCE feedcone used for previous 26-m (85-ft) reflector evaluation was used on the 64-m antenna without change. Figure 145 shows the feed installed (February 1-5, 1968). This listen-only feed system was designed as a low-noise, total-power radiometer for observation of a few radioastronomical sources. In all cases, the system was sensitive to right-hand circular polarization.

Operating on the ground in a checkout mode, the XCE feedcone, pointing to the zenith, exhibits a 33.5 K total operating temperature. The individual noise sources are thought to be: $T_M'' = 13.7$ K at the maser input, $T_L = 13.2$ K, $T_F'' = 0.1$ K at the maser input, and $T_A' = 6.8$ K at the horn aperture, where T_M, T_L, T_F, and T_A are the maser, the loss, the follow-up receiver, and the antenna temperature contributions, respectively. Single superscripts refer to the horn aperture, while double superscripts refer to the maser input flange. When operated on the 64-m antenna, an additional 3.3 K noise temperature at zenith was observed. This additional noise is caused primarily from feed spillover and quadripod scatter towards the warm earth. A total X-band Cassegrain antenna temperature defined at the horn aperture of 10.1 K appears a reasonable estimate. Comparable S-band values are an incremental 3.6 K and a total of 9.3 K.

2. Focusing

The 64-m antenna is equipped with subreflector axial drives, and, as described earlier, structural calculations indicated that a worthwhile improvement in effective surface tolerance was available by the use of this adjustment. Focusing was the first step taken in the X-band evaluation. The "receive" system noise temperature with 3C273, considered a point source in the beam, was maximized. Figure 146 shows the RF results for the source, both ascending and descending in elevation angle -- a step considered essential because of previous long-time constant hysteresis in focal length found on a 26-m (85-ft) structure. Also shown in Fig. 146 is a single verification of focus at a high elevation angle and the structural predictions based on Table 14. The RF data were best-fitted to the structural predictions of axial misalignment.

Once found repeatable and in agreement with structural predictions, the focus data in Fig. 146 were used throughout the X-band evaluation in a

manual correction mode, with focus trimming as a function of elevation angle in approximately 1.27-mm (0.05-in.) steps being used.

3. System Efficiency Measurements

The overall system efficiency at the maser input flange was obtained using three nonthermal sources. No atmospheric corrections are included; the concept adopted here was to accept the atmosphere as a system loss, as would be observed during a deep space tracking mission, although the weakest of the three sources, 3C123, was given priority on the basis of a superior source distribution. Figure 141 shows good consistency among the three sources and good agreement with overall efficiency predictions. The curves in Fig. 141 are best-fitted to the data on the basis of least squares.

4. Radio Surface Tolerance Measurements

Based on the computed RF optics efficiency and the measured 3C123 efficiency data (Fig. 141), the surface tolerance of the reflecting system may be obtained. Because the gain loss from surface tolerance was expected to range approximately 1 to 3 dB, a determination of surface tolerance via the computed RF optics efficiency was considered a useful and accurate method. Figure 142 gives the mean and standard deviation limits for the RMS surface tolerance as determined from the radio measurements. The standard deviation limits include only the measurement scatter. Figure 142 also includes the structurally predicted RMS surface tolerance for the axial focused condition. In order to obtain the radio data in this instance, it was necessary to sort out the atmospheric loss contribution. This was done by accepting the usual flat-earth secant law, applicable above an elevation angle of about 10 deg, and by selecting a theoretical 0.036-dB atmospheric loss at zenith.

As Fig. 142 shows, the radio measurements indicate a better surface tolerance than predicted when at zenith, essentially in agreement with field-measured structural data (Table 15). The radio observed surface tolerance near horizon appears somewhat worse than expected in Fig. 142. This is a sensitive function of the selected zenith loss, however, and a fitted value of 0.055 dB at zenith with the secant dependence will force perfect agreement between predicted and radio measured RMS at 10 deg elevation. A zenith loss of 0.055 dB is further in agreement with the total operating system noise temperature measured without a source in the beam (Fig. 147).

It can be concluded that the zenith attenuation experienced approximates 0.06 dB and the surface tolerance over all elevation angles is essentially that calculated by structural means, with evidence that the structural field-measured data more accurately describes the reflector system when zenith-oriented.

5. X-Band Pointing

Throughout the tests, the Precision I mode was used to point the antenna. In this mode, the main reflector structure is optically coupled to the master equatorial, which, in turn, is controlled by the antenna pointing computer. An example of the overall RF precision achieved in this mode is shown in Fig. 148, which is a radiometer recording obtained during RF boresighting on Cygnus A. With a previously determined -0.006 deg declination offset, the approximate half-power points are balanced as +0.017 and -0.025 deg in declination, the mean of which is taken as an update to a -0.004 deg offset. Figure 148 continues the bracketing procedure in the hour angle axis where the extended source requires greater offsets for a half-power indication. Again, a change of 0.001 to 0.002 deg is discerned as accomplished in a stable manner.

Figure 149 considers absolute accuracy of the pointing system. In the absence of a thorough study of source position accuracy, the best available data was utilized in an ephemeris program and accepted as absolute, as discussed earlier. The 64-m antenna tipping structure is a self-compensated system; that is, various structural gravity deflections are opposed, resulting in very low, over-all RF boresight errors as a function of elevation angle.[4] As Fig. 149 shows, in the absence of a priori corrections (the brief test period was inadequate to define and implement specific angle bias corrections), the absolute pointing for the four sources used, spanning declinations of +2 to +40 deg, may be specified as approximately 0.010 deg peak-to-peak, with the exception of very low elevation angles. Therefore, it is highly probable to acquire a known astronomical object within the X-band half-power beamwidth (0.038 deg) without resorting to any correction terms.

Figure 149 includes third-order curves fitted on the basis of least squares. The standard deviation σ is 0.0024 deg in declination and 0.0025 deg in hour angle. It is therefore highly probable that a known astronomical object may be acquired within a tenth of the X-band half-power beamwidth, using the third-order curves as a priori corrections. Note that this performance applies for sources within declinations +2 to +40 deg, based on a five-day sample.

Drift curves of the quasar 3C273 at a 35-deg elevation angle (Fig. 150) confirm the expected 0.038-deg half-power beamwidths.

D. SUMMARY OF X-BAND PERFORMANCE

A brief RF test program at X-band, 8448 MHz, was conducted on the 64-m-diameter on February 1-5, 1968. Twenty-four hours/day radio star tracking shows the peak system gain and efficiency are 72.3 dB and 52%, respectively. The accuracy of radio star calibrations of this kind is considered to be ±0.8 dB, with high confidence. Ordered changes, due to gravity loading in the

[4] Originally, the repeatable errors were planned to be removed through use of an elevation angle-driven cam modulating the intermediate reference surface. To date, this refinement has not been considered necessary and has therefore not been made.

reflecting system surface tolerance and focal length, occurred as predicted by analytic structural models. The combined accuracy of the master equatorial pointing and reflector boresight systems were found adequate for X-band, assuming observed systematic effects are removed. The precision of the pointing system and the stability of the total structure appear compatible and of outstanding quality.

Generally, good weather was experienced during the tests, with little or no occurrence of winds in excess of 9 m/s (20 mph). The daylight hours were sunny and bright; normal thermal effects were apparently experienced. The generally dry climate experienced at the Goldstone Complex allowed a total operating noise temperature of less than 37 K at zenith.

Accepting a system surface tolerance maximum of 1.65 mm (0.065 in.) RMS as applicable over a very wide range of elevation angles, gain limit should occur in the 2-cm band. Although further use experience is needed, it is clear a significant ground capability for weather-dependent space communications or radio/radar astronomy is available at X-band using the 64-m diameter antenna.

Table 10. Major milestone test results upon completion of Rohr work on the 64-m antenna

Test	Specification requirement	Calculated result	Measured
Surface accuracy operational RMS (1 σ), mm (in.)	6.350 mm (0.250 in.)	4.674 mm (0.184 in.)	4.318 mm[a] (0.170 in.)
Pointing accuracy operational peak (3 σ), deg	0.033	0.029	0.029
Reflector gravity deflections			
Zenith to 45 deg (1 σ) (600 points optically measured)	-	2.032 mm[b] (0.030 in.)	1.524 mm[b] (0.060 in.)
45 deg to horizon (1 σ) (200 points optically measured)	-	1.880 mm[b] (0.074 in.)	1.600 mm[b] (0.063 in.)
Pointing accuracy gravity (deflection 45 deg to horizon)	-	0.0271	0.017
Locked rotor frequency			
Azimuth axis, Hz	≥ 1.5	1.58[c]	1.55
Elevation axis, Hz	≥ 1.5	1.65[c]	1.80
Alidade stiffness	-	A 188,600 N (42,400 lb) load was applied at top of alidade parallel to elevation axis. The calculated motion was 4.039 mm (0.159 in.) and the test result was 3.987 mm (0.157 in.).	
Total rotating mass	-	2,040,000 kg (4,500,000 lb) ±10%	2,309,452 kg (5,091,471 lb)

[a]Calculated values used when actual measured values were not available.

[b]Rigid-body best-fit values used.

[c]Analysis based on two 15-deg-of-freedom lumped parameter models, one for each axis.

Table 11. Gain measurement error sources

Measured difference	39.713	±0.014 p.e.
Attenuator calibration		±0.021 p.e.
Differential waveguide loss	0.0609	±0.0019 p.e.
Ellipticity		±0.008 p.e.
Pointing errors		±0.01 p.e.
Gain standard horn	21.85	±0.086 p.e.
	61.62[a]	±0.0905 dB, p.e.

[a]At feedhorn output.

Table 12. Operational experience, 1968 – 1969[a]

	1968	1969
Number of recorded equipment failures	24	27
Number of failures involving loss of antenna tracking time	8	7
Maximum time loss for a single failure	15.0 h	3.6 h
Total time loss for all equipment failures	23.6 h	6.0 h

[a]These data cover the antenna, drives, servo, and angle data system.

Table 13. Breakaway torque data, gear drives

Gear drive No.	Torque, N-m (lb-in.)			
	Breakaway		Running	
	CW	CCW	CW	CCW
	Elevation			
1	2.26 (20)	3.73 (33)	1.58 (14)	3.28 (29)
2	3.05 (27)	2.60 (23)	2.60 (23)	1.92 (17)
3	2.71 (24)	2.15 (19)	2.03 (18)	1.58 (14)
4	3.73 (33)	3.95 (35)	2.94 (26)	3.28 (29)
	Azimuth			
1	2.26 (20)	2.82 (25)	1.69 (15)	2.26 (20)
2	3.39 (30)	2.26 (20)	3.95 (35)	3.39 (30)
3	3.39 (30)	3.39 (30)	2.82 (25)	2.82 (25)
4	2.82 (25)	2.26 (20)	2.26 (20)	1.69 (15)

Table 14. Computed surface distortion of 64-m antenna from change in direction of gravity vector from 45-deg elevation

Source	Surface distortion for indicated elevation angle													
	0 deg		15 deg		30 deg		45 deg		60 deg		75 deg		90 deg	
	mm	in.	mm	in.	mm	in.	mm	in.	mm	in.	mm	in.	mm	in.
Best-fit paraboloid data														
Vertex y-coordinate	40.33	1.588	35.63	1.403	20.47	0.806	0.0	0.0	-28.47	-1.121	-61.62	-2.426	-97.26	-3.829
Vertex z-coordinate	1.77	0.070	1.12	0.044	0.53	0.021	0.0	0.0	-0.41	-0.016	-0.66	-0.026	-0.74	-0.029
Rotation x-axis, rad	0.001015		0.000894		0.000548		0.0		0.000712		0.001539		0.002427	
Focal length change	-17.60	-0.693	-11.15	-0.439	-5.16	-0.203	0.0	0.0	3.96	0.156	6.43	0.253	7.24	0.285
Quadripod apex z-deflection	-0.64	-0.025	-0.38	-0.015	-0.23	-0.009	0.0	0.0	0.10	0.004	0.18	0.007	0.25	0.010
Subreflector														
z-deflection	-1.22	-0.048	-0.71	-0.028	-0.43	-0.017	0.0	0.0	0.10	0.004	0.18	0.007	0.25	0.010
Axial indicated position	-19.55	-0.77	-12.19	-0.48	-5.59	-0.22	0.0	0.0	4.06	0.16	6.86	0.27	7.87	0.31
Lateral y-direction deflection	-27.94	-1.1	12.70	0.5	2.54	0.1	0.0	0.0	22.86	0.9	45.72	1.8	68.58	2.7
Subreflector														
Lateral offset equivalent error, rms	0.48	0.019	0.20	0.008	0.03	0.001	0.0	0.0	0.38	0.015	0.79	0.031	1.22	0.048
Axial offset equivalent error, rms	1.47	0.058	0.91	0.036	0.43	0.017	0.0	0.0	0.30	0.012	0.51	0.020	0.58	0.023
Best-fit paraboloid reflector structure														
Distortion from 45-deg, rms	1.02	0.040	0.81	0.032	0.46	0.018	0.0	0.0	0.58	0.023	1.22	0.048	1.91	0.075
45-deg 1/2-RF-pathlength, rms	(Field measured distortion used for 45-deg position)						1.22	0.048						
Total 1/2-RF-pathlength, focused axially														
Distortion, rms	1.65	0.065	1.47	0.058	1.30	0.051	1.22	0.048	1.40	0.055	1.91	0.075	2.59	0.102
Total 1/2-RF-pathlength, focused only at 45 deg														
Distortion, rms	2.16	0.085	1.73	0.068	1.37	0.054	1.22	0.048	1.45	0.057	1.96	0.077	2.67	0.105

Table 15. Measured system distortion of 64-m antenna at 0- and 90-deg elevation angle

Source	Error, RMS			
	0 deg		90 deg	
	mm	in.	mm	in.
45-deg elevation 1/2-RF-pathlength error	1.22	0.048	1.22	0.048
Reflector structure gravity deflections from 45-deg elevation	0.86	0.034	1.60	0.063
Subreflector lateral offset[a]	0.51	0.020	1.27	0.050
Total 1/2-RF-pathlength error	1.57	0.062	2.39	0.094

[a]Axially focused mode.

Table 16. Manufacturing tolerance, surface panels

Panel row No.[a]	Surface					
	RMS to zero plane		Average deviation		Standard deviation	
	mm	(in.)	mm	(in.)	mm	(in.)
1	1.09	0.043	0.43	0.017	0.99	0.039
2	1.07	0.042	0.23	0.009	1.04	0.041
3	0.99	0.039	0.41	0.016	0.91	0.036
4	0.89	0.035	0.38	0.015	0.79	0.031
5	0.81	0.032	0.61	0.024	0.51	0.020
6	0.84	0.033	0.51	0.020	0.66	0.026
7	0.46	0.018	0.10	0.004	0.46	0.018
8	0.43	0.017	0.03	0.001	0.43	0.017

[a]1 = outside Row

Total for all panels

RMS = 0.97 mm (0.038 in.)

Average deviation = 0.38 mm (0.015 in.)

Standard deviation = 0.89 mm (0.035 in.)

Ref. 1 specification

RMS = 1.52 mm (0.060 in.)

Table 17. Feed efficiency, XCE feedcone

Parameter	Value, %
Forward spillover	7.22
Rear spillover	0.20
Illumination efficiency	86.81
Cross-polarization efficiency	99.94
Phase efficiency	96.62
Subreflector blocking efficiency	96.45
Overall feed efficiency	74.86 ±0.20

Table 18. Waveguide efficiency, XCE feedcone

Component	Attenuation, dB
Antenna to maser flanges	0.150 ±0.002
Turnstile junction	0.025 ±0.025
Feedhorn	0.018 ±0.018
Overall waveguide efficiency	95.65 ±0.22%

Table 19. Quadripod efficiency, 64-m antenna

Parameter	Value, %
Blocked area A	6.255
Opacity σ	80-120
Quadripod blockage efficiency η'/η	87.88 ±2.4

Table 20. Measured surface distortion of 64-m antenna at 45-deg elevation angle

Error source	Error, RMS	
	mm	(in.)
Surface-panel setting	0.48	0.019
Primary surface-panel manufacturing	0.89	0.035
Subreflector manufacturing	0.69	0.027
Total 1/2-RF-pathlength error	1.22	0.048

Table 21. Computed system distortion, efficiency and gain, X-band[a]

Elevation angle, deg	Surface tolerance		Surface tolerance efficiency, %	Overall system efficiency, %	System gain, dB
	mm, RMS	in., RMS			
0	1.65	0.065	70.6	44.4	71.5
15	1.47	0.058	76.4	48.0	71.9
30	1.30	0.051	81.4	51.2	72.2
45	1.22	0.048	83.2	52.3	72.3
60	1.40	0.055	78.6	49.5	72.0
75	1.91	0.075	64.4	40.5	71.1
90	2.59	0.102	43.5	27.4	69.4

[a]Axially focused mode.

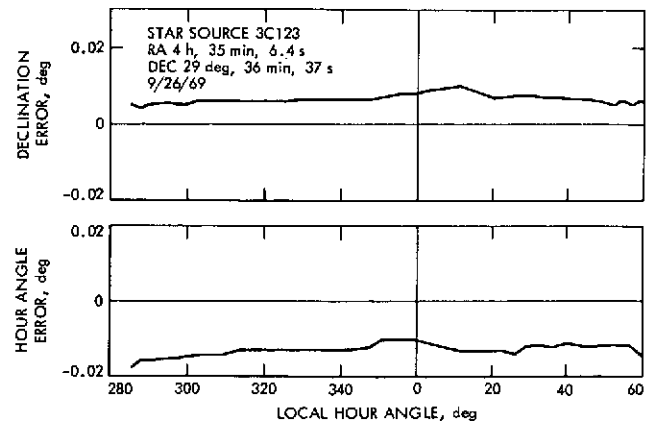

Fig. 112. Typical plot, system pointing error

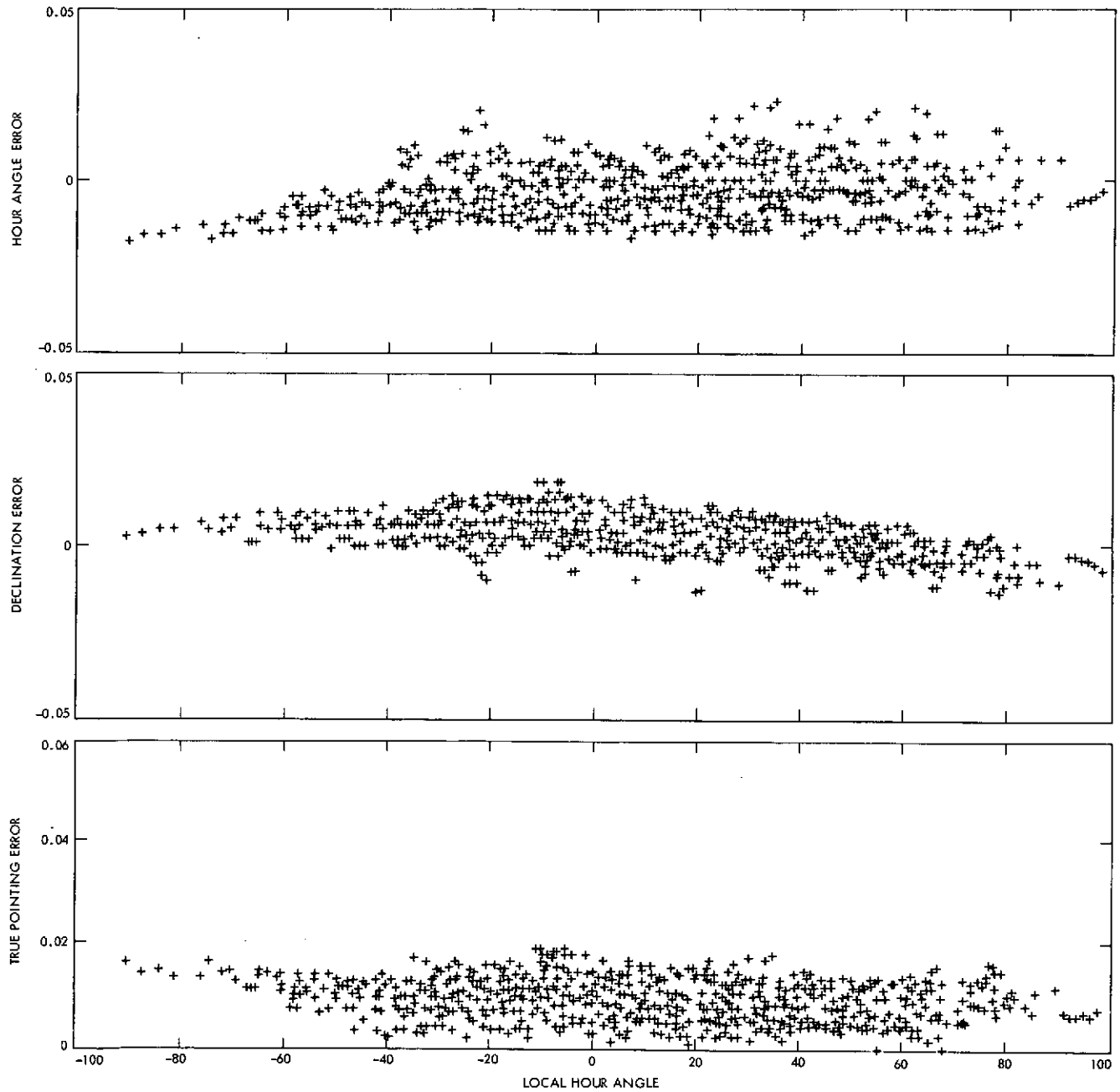

Fig. 113. Antenna pointing general data, all sources

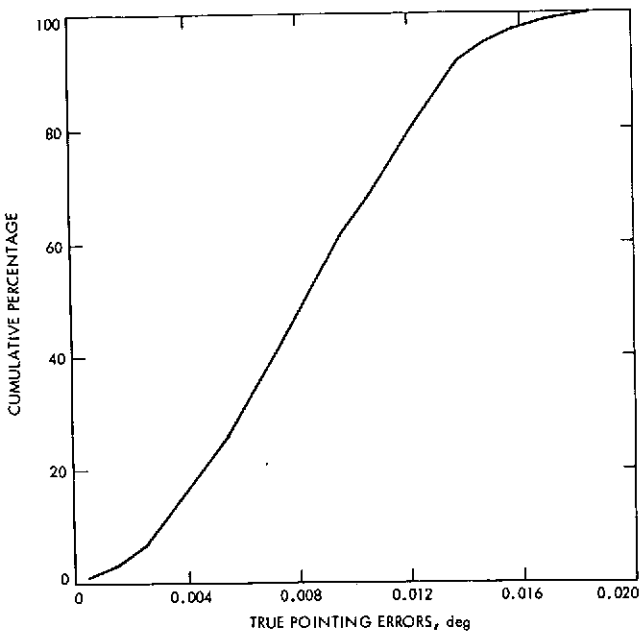

Fig. 114. Cumulative percentage of true pointing errors

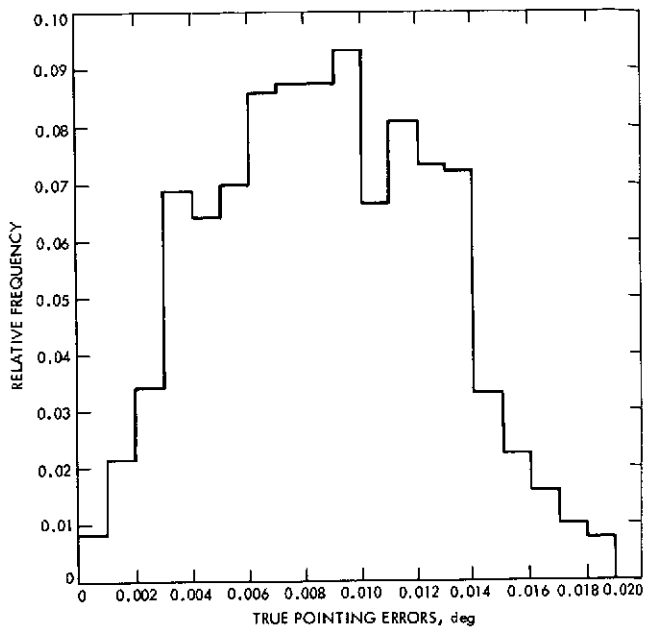

Fig. 115. Frequency distribution of true pointing errors

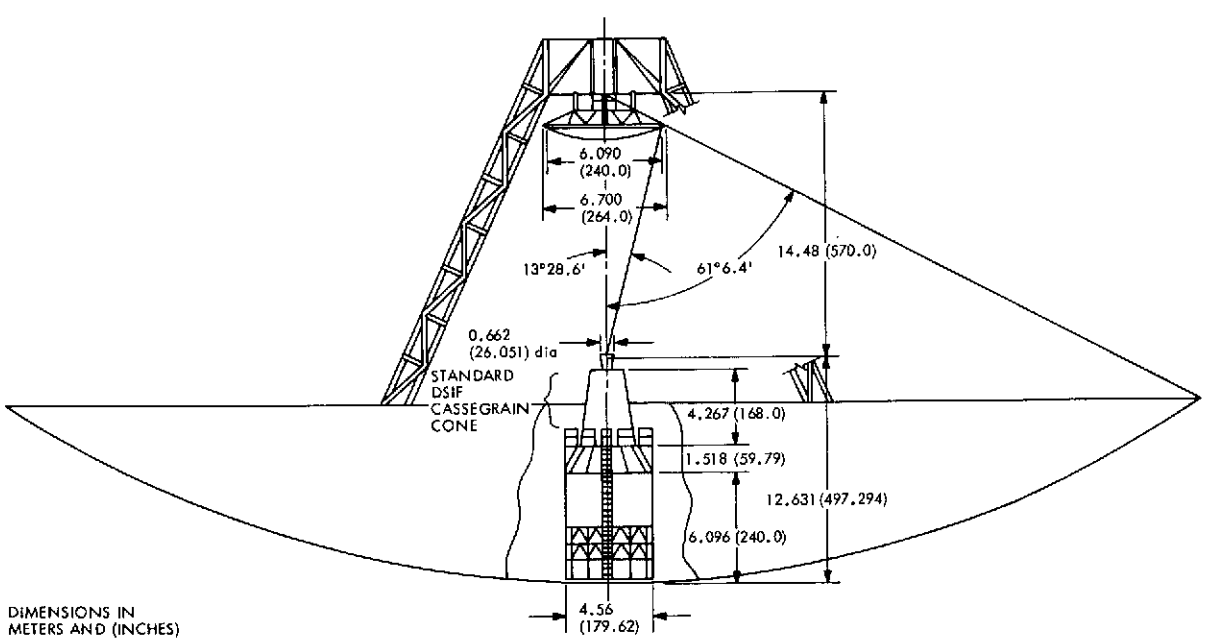

Fig. 116. 64-meter antenna original feed system configuration

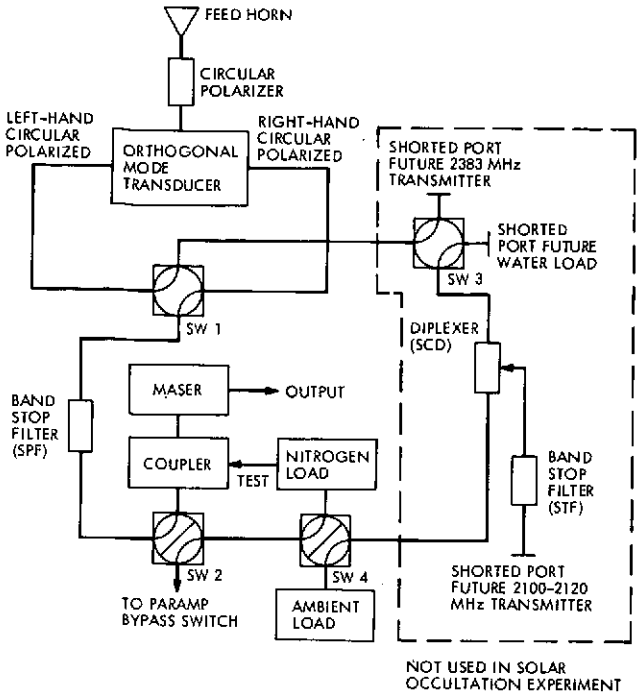

Fig. 117. Original feedcone configuration for Mariner 4 superior conjunction

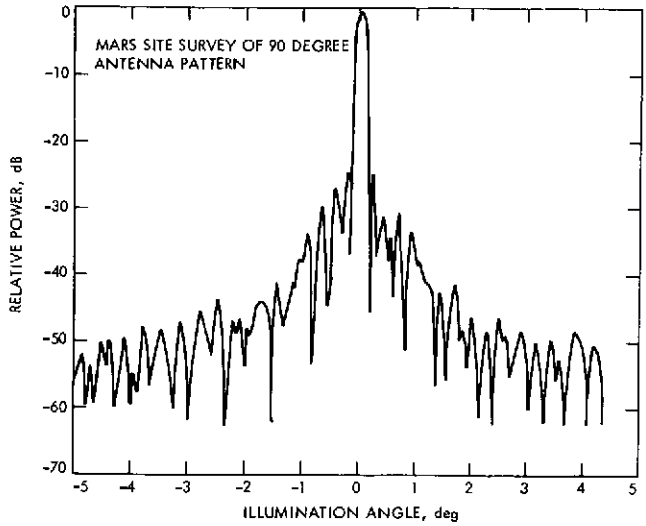

Fig. 119. 64-meter antenna elevation plane radiation patterns

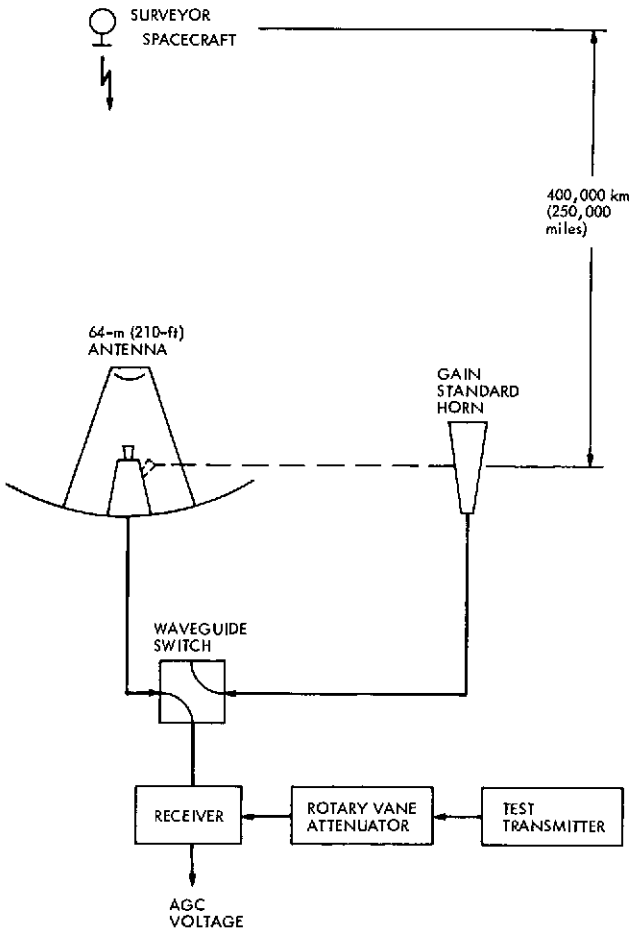

Fig. 118. Experimental gain measurement schematic

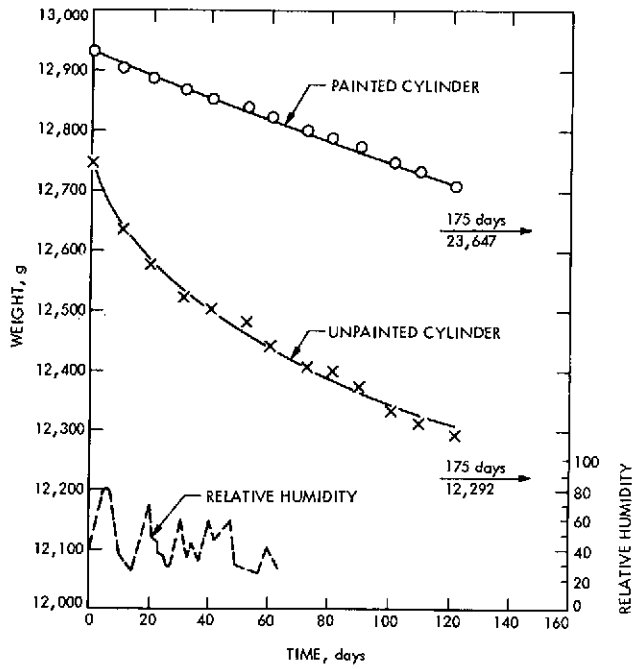

Fig. 120. Moisture loss in test cylinders

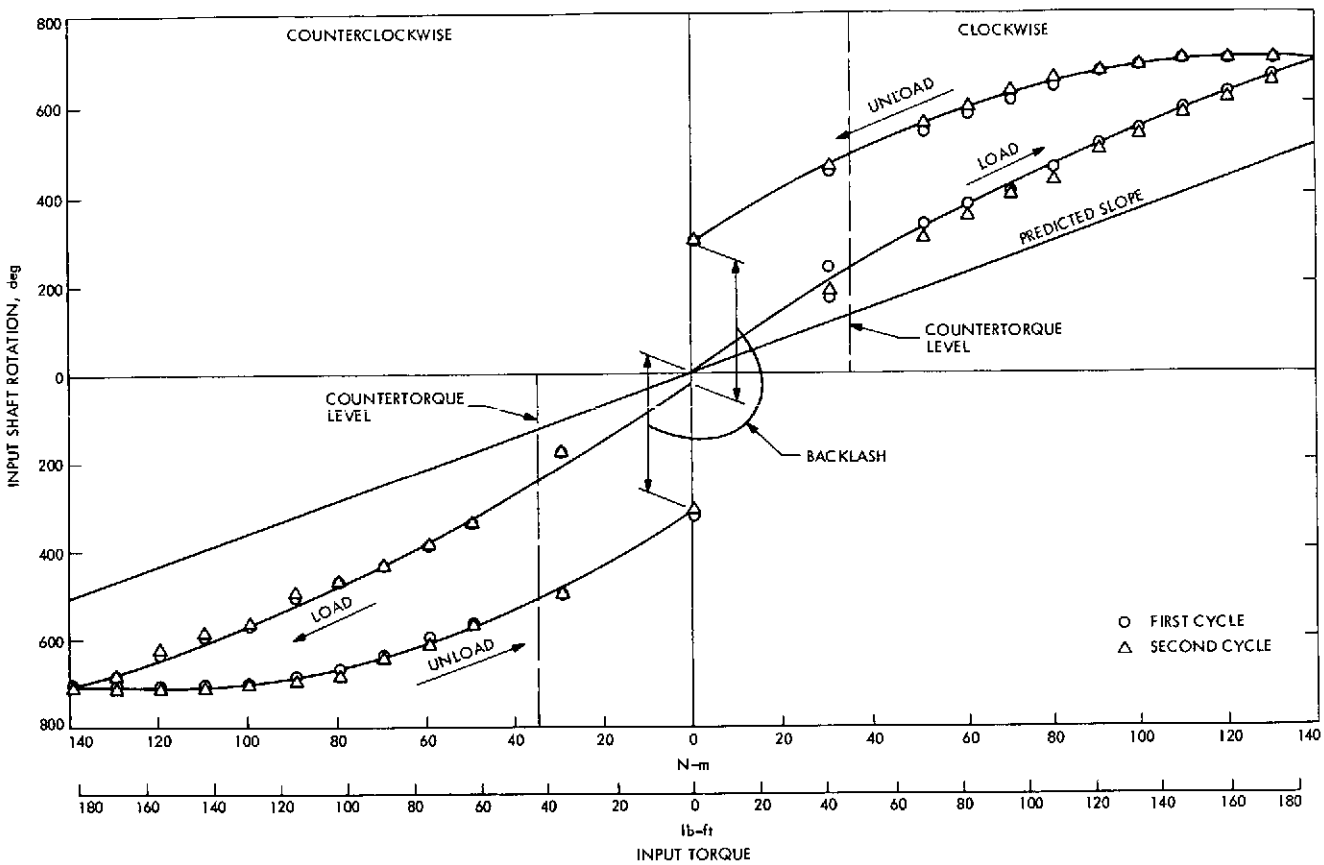

Fig. 121. 64-meter antenna azimuth hysteresis test results

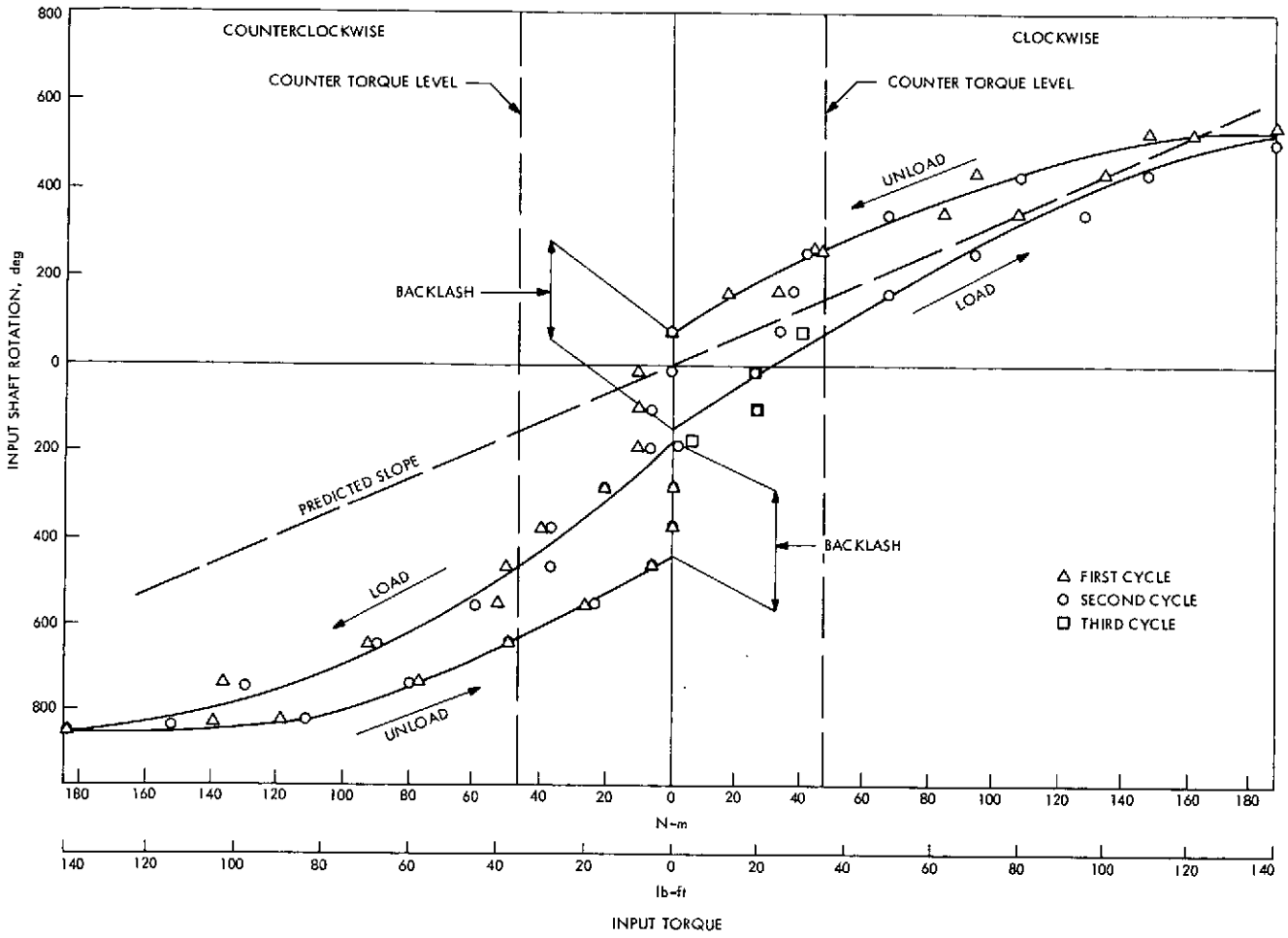

Fig. 122. 64-meter antenna elevation hysteresis test results

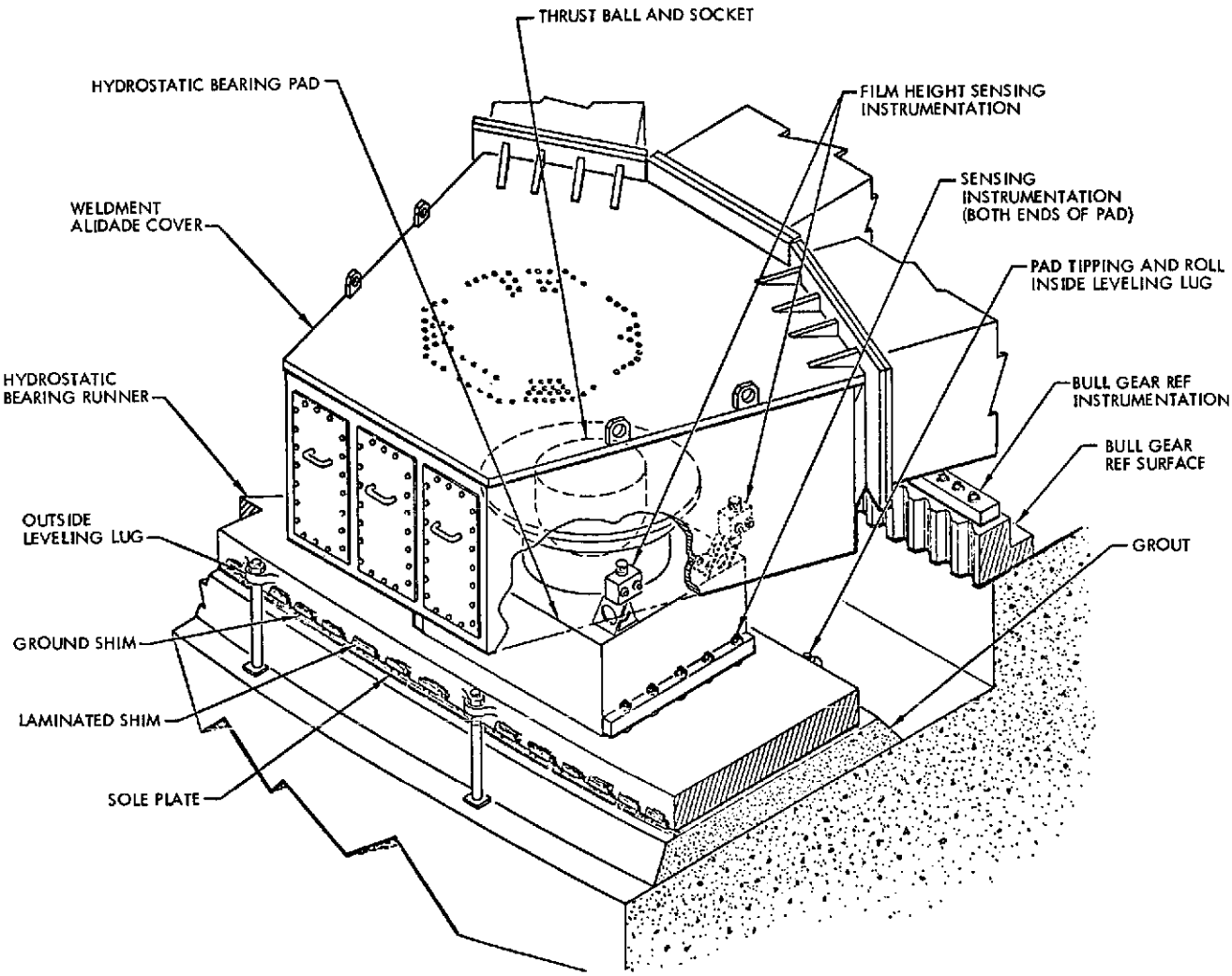

Fig. 123. Hydrostatic bearing cross section

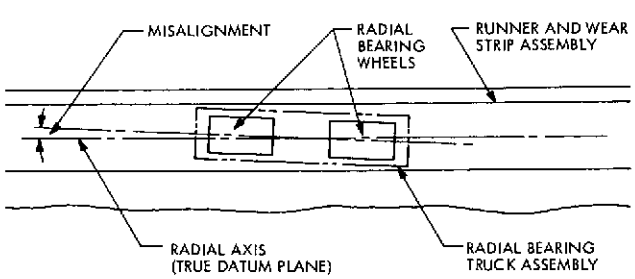

Fig. 124. Misalignment about the radial axis, radial bearing

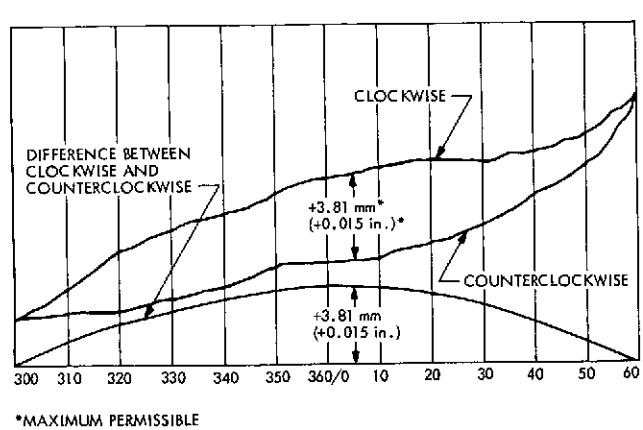

Fig. 125. Typical hysteresis curve, radial bearing

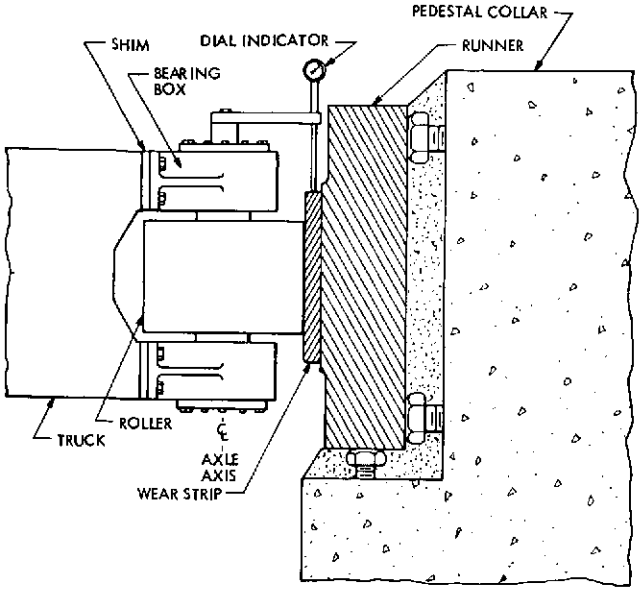

Fig. 126. Hysteresis test setup, radial bearing

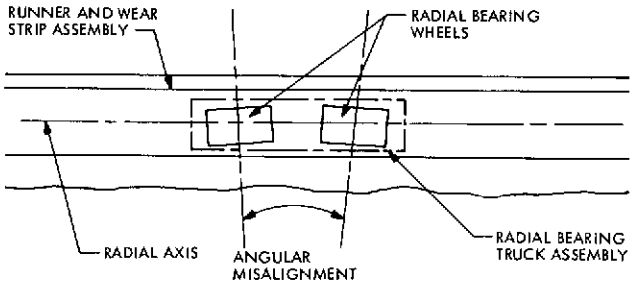

Fig. 127. Misalignment due to nonparallelism of truck axles, radial bearing

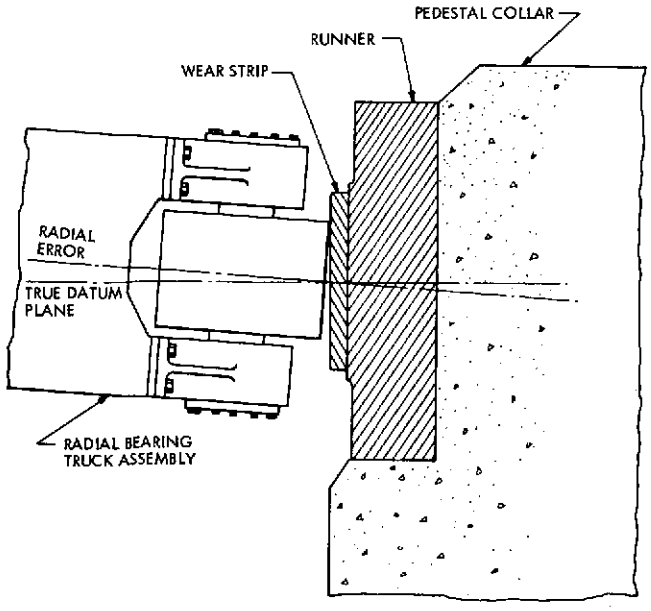

Fig. 128. Misalignment about the tangential axis, radial bearing

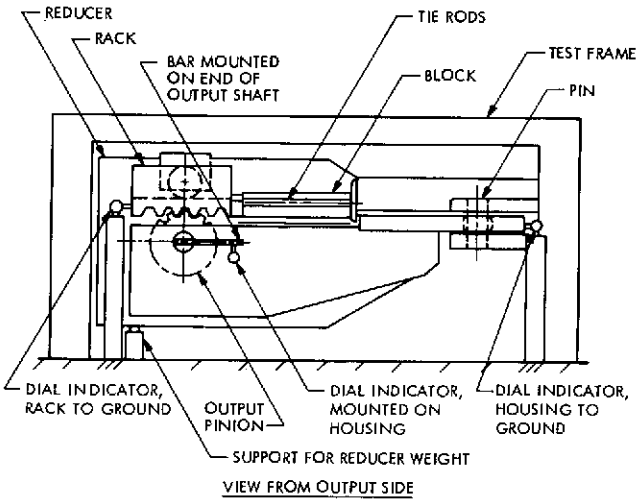

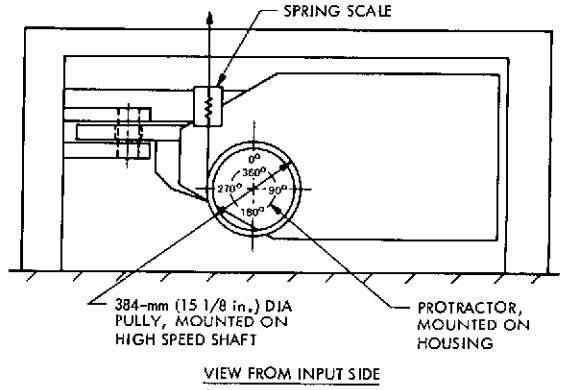

Fig. 129. Stiffness test arrangement (input shaft loaded)

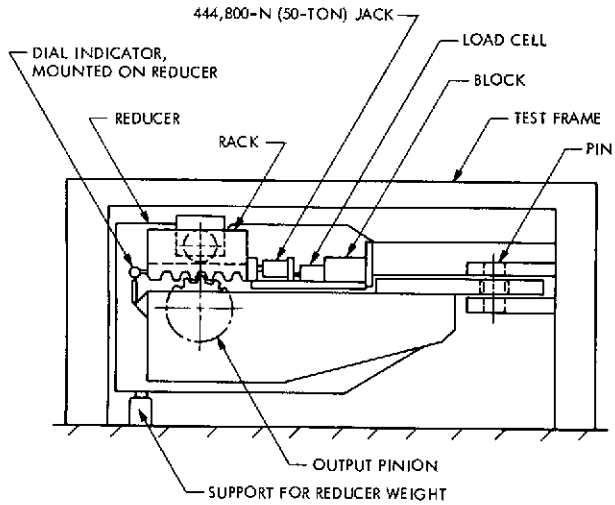

Fig. 130. Stiffness test arrangement (output shaft loaded)

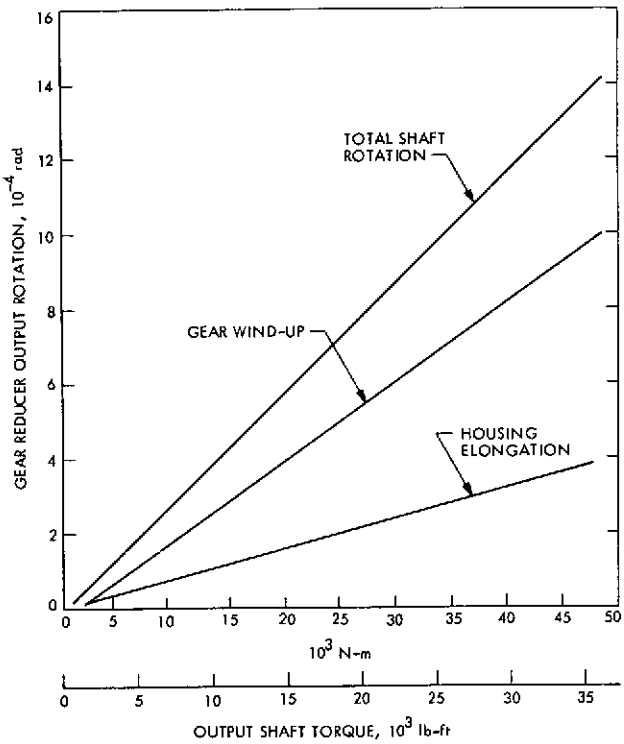

Fig. 131. Typical stiffness test data, gear drives

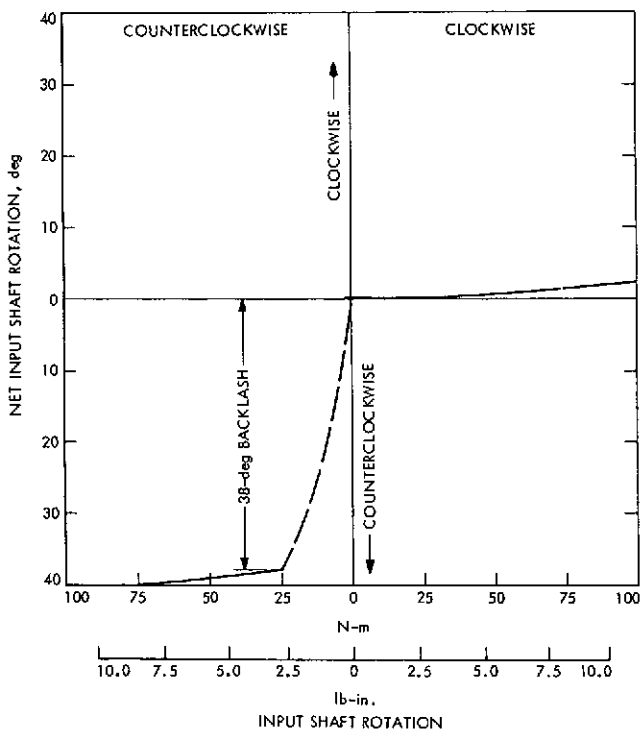

Fig. 132. Typical backlash test data, gear drives

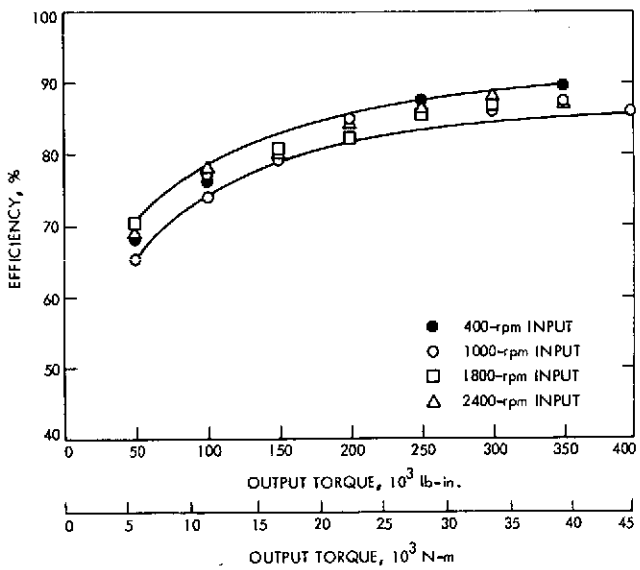

Fig. 133. Efficiency vs output torque, elevation gear drive

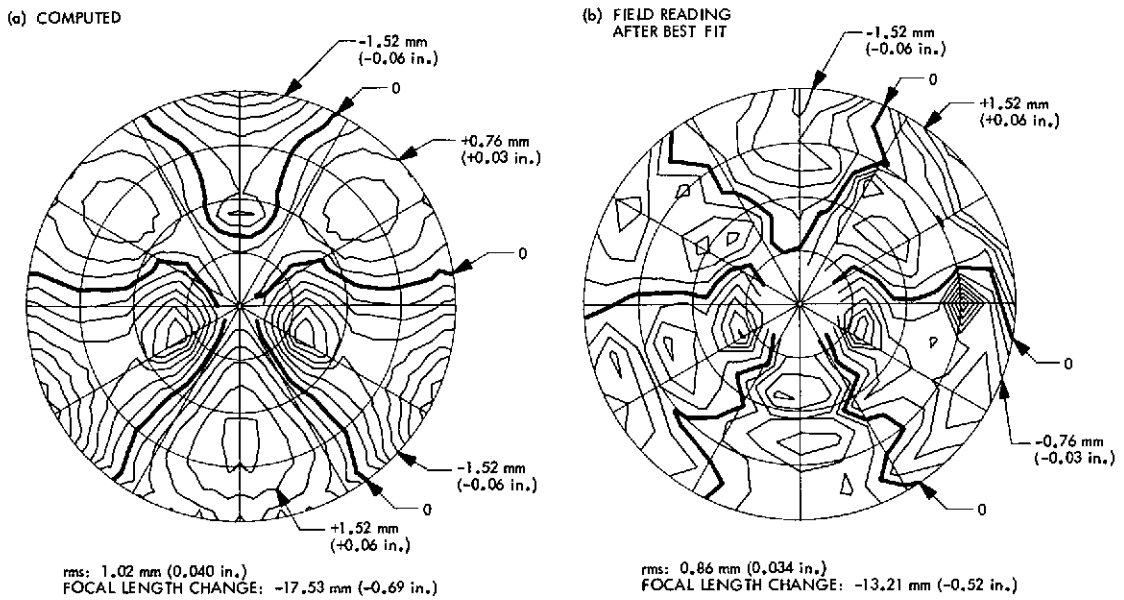

Fig. 134. Horizon-attitude contour maps of 1/2-RF-pathlength errors

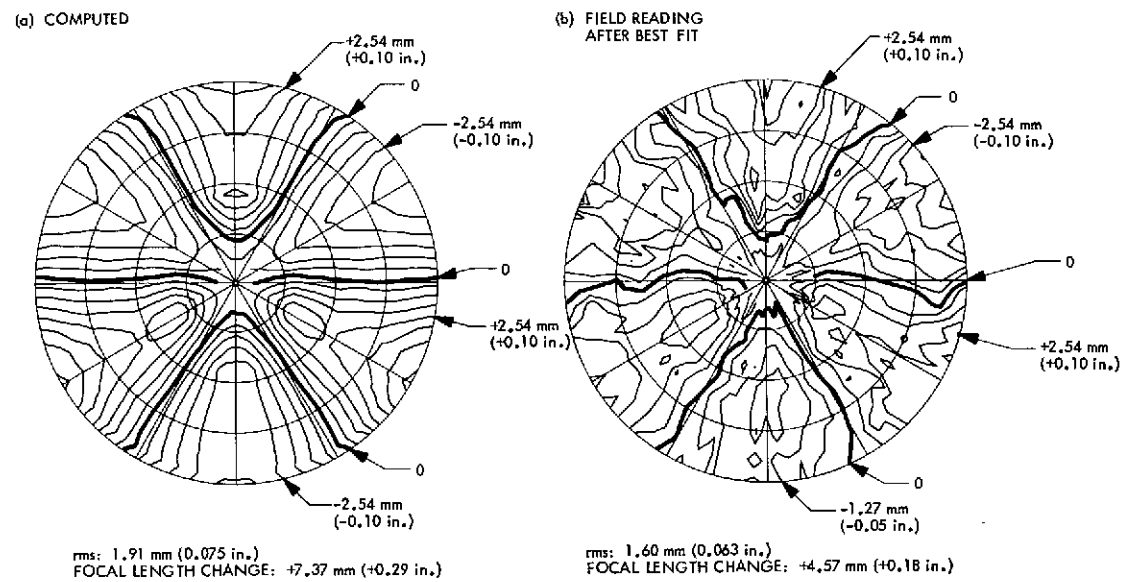

Fig. 135. Zenith-attitude contour maps of 1/2-RF-pathlength errors

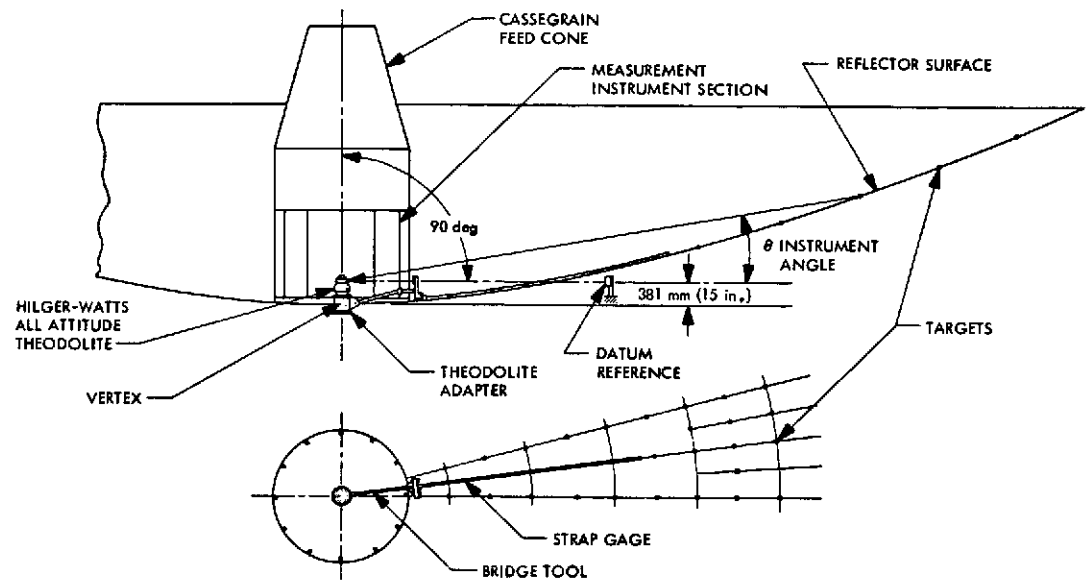

Fig. 136. Surface measuring technique, primary reflector

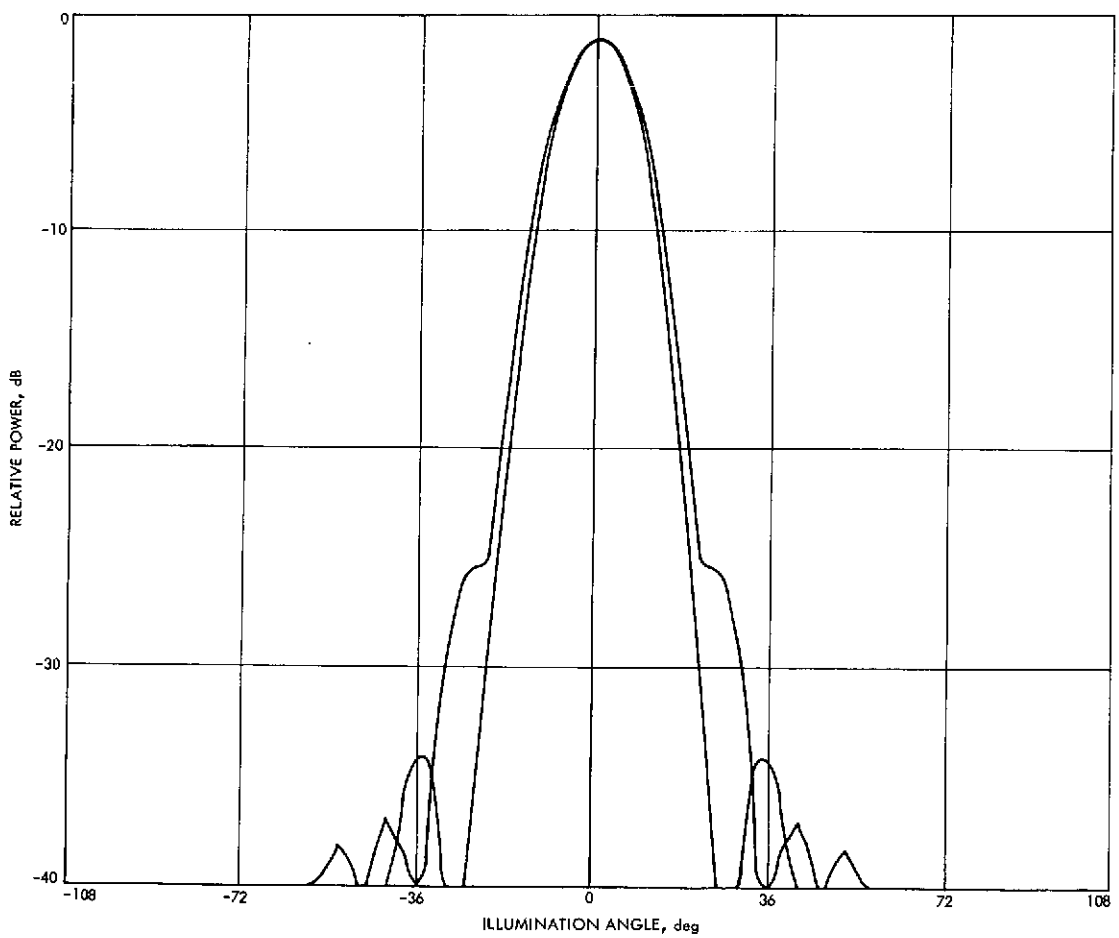

Fig. 137. Primary feed radiation patterns, E- and H-plane, 8448 MHz

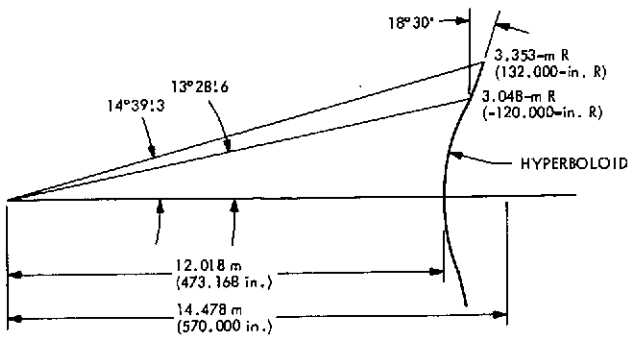

Fig. 138. Subreflector configuration, 8448 MHz

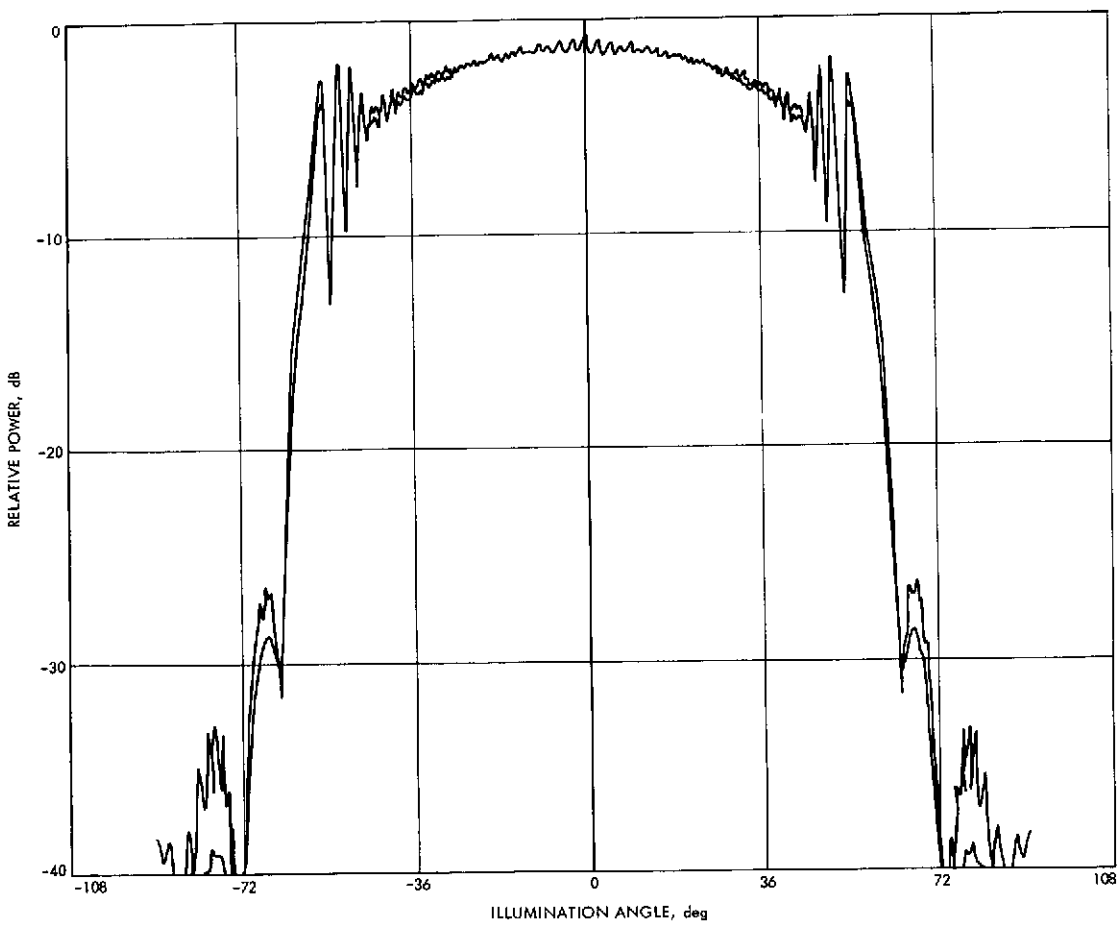

Fig. 139. Subreflector scattered radiation patterns, E- and H-plane, 8448 MHz (amplitude)

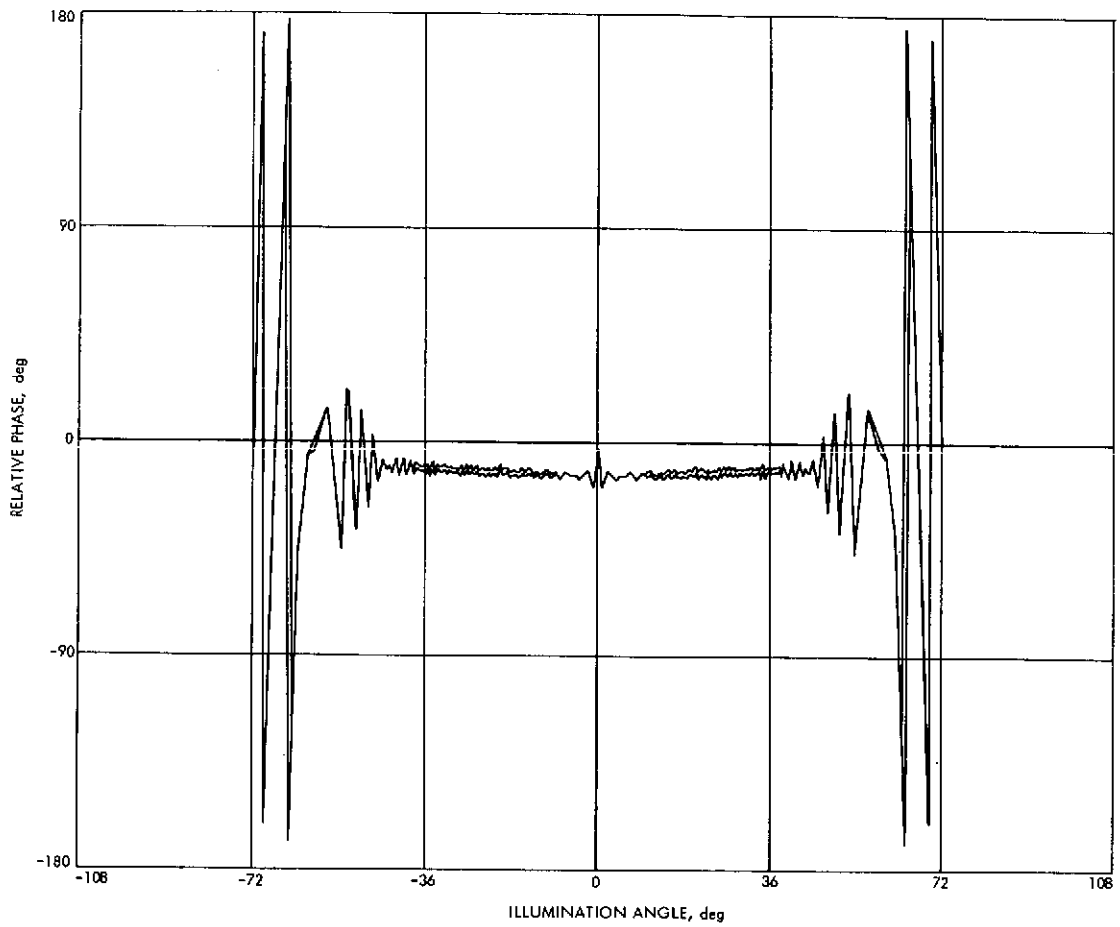

Fig. 140. Subreflector scattered radiation patterns, E- and H-plane, 8448 MHz (phase)

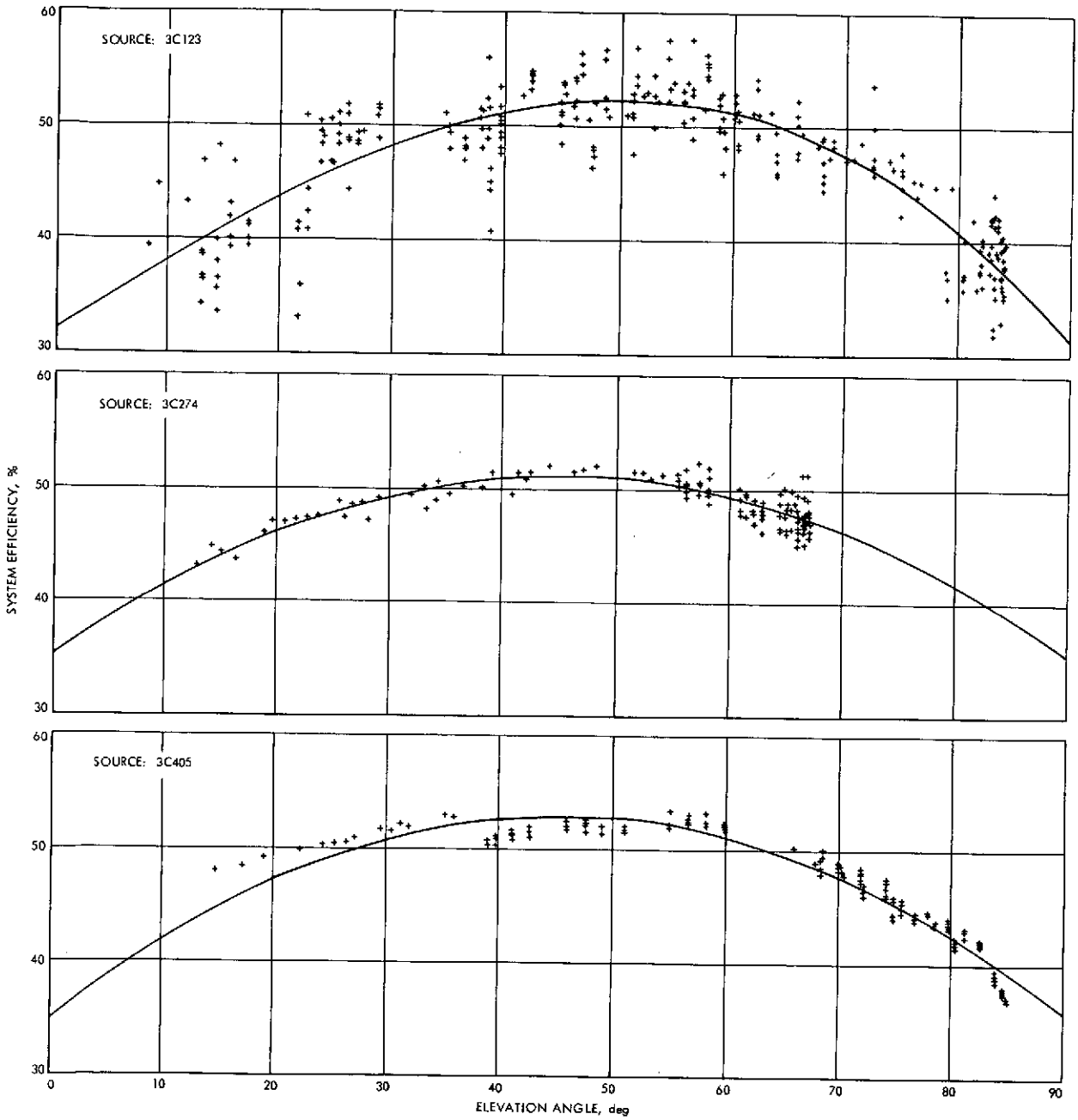

Fig. 141. System efficiency as a function of elevation angle, 8448 MHz

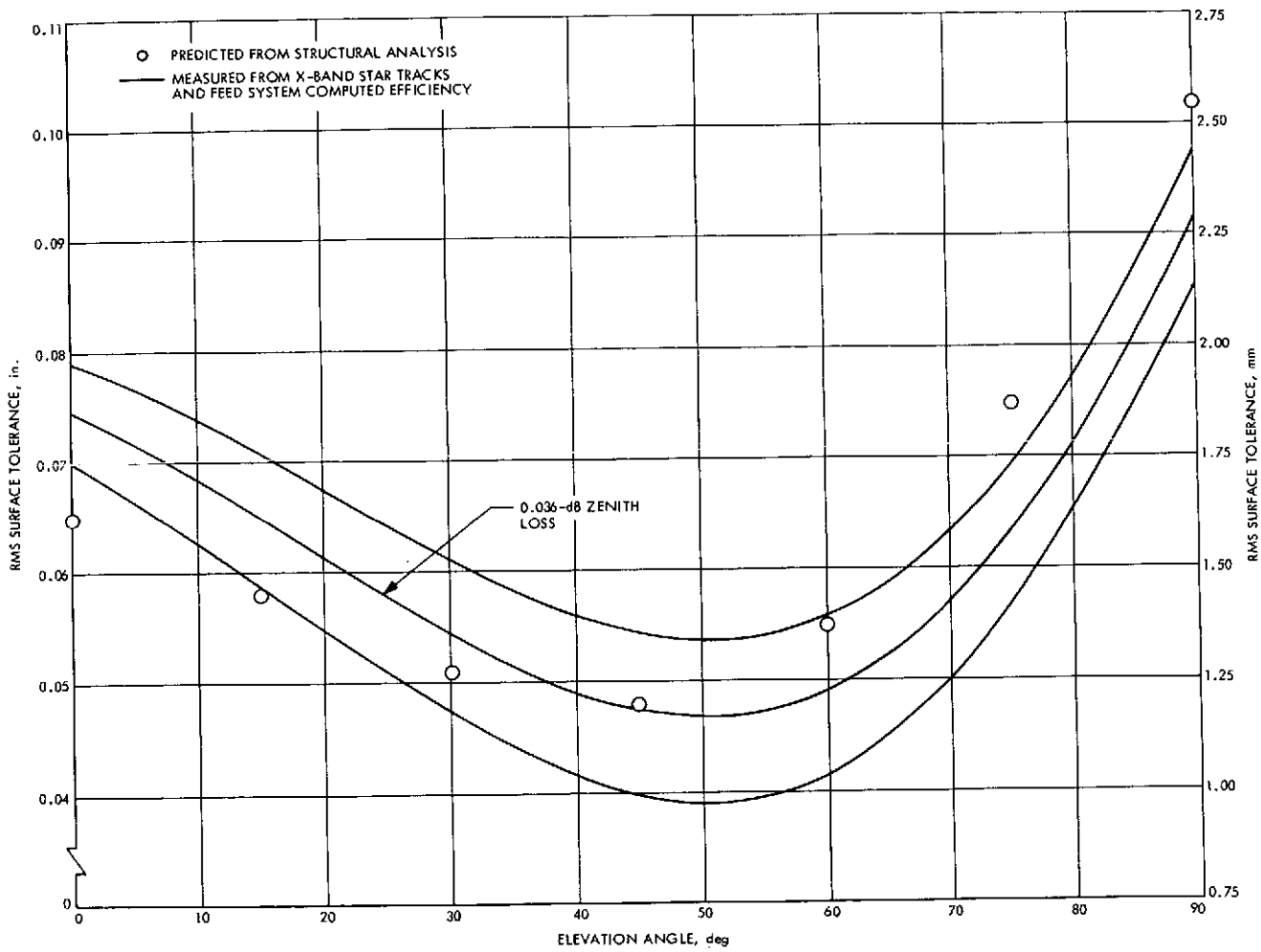

Fig. 142. RMS surface tolerance as a function of elevation angle, 8448 MHz

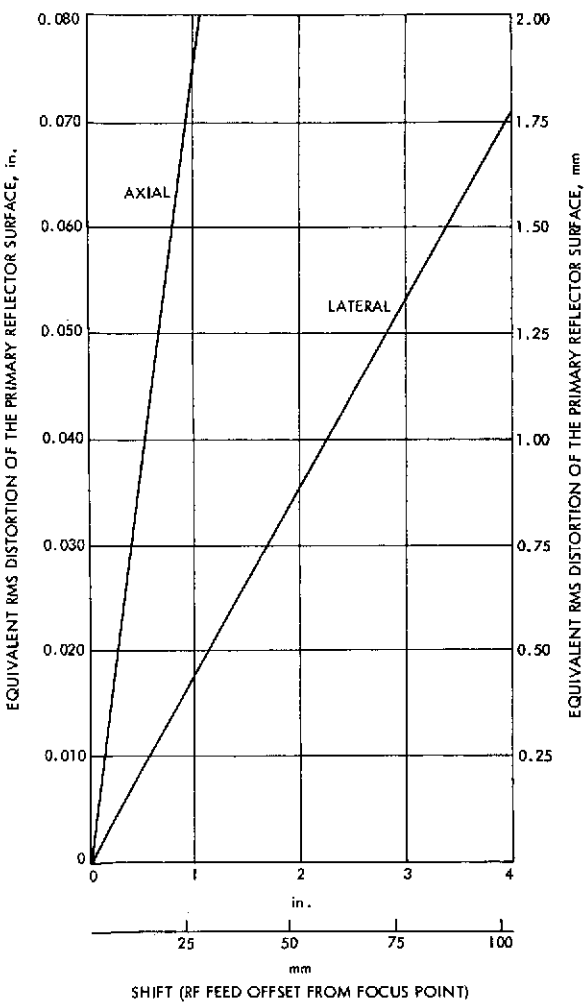

Fig. 143. Equivalent rms as a function of feed point axial and lateral shifts

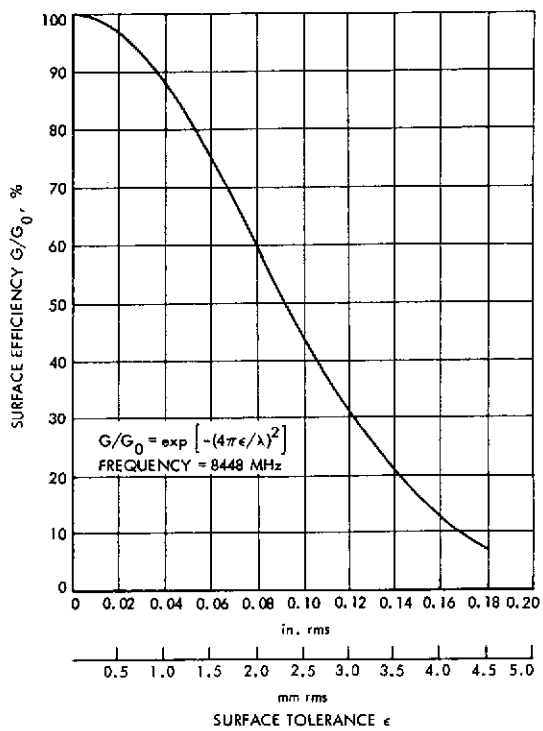

Fig. 144. Surface efficiency as a function of surface tolerance

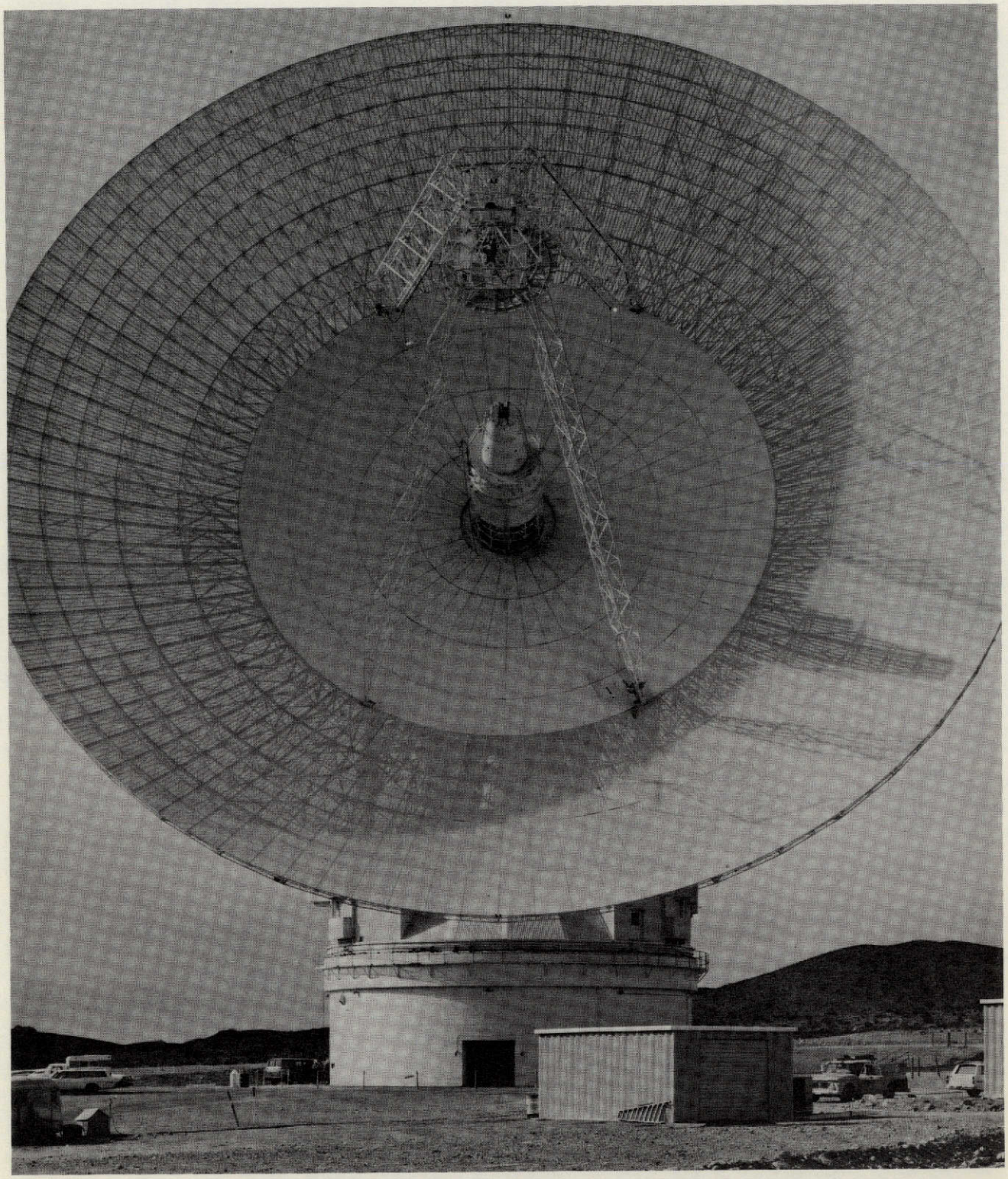

Fig. 145. 64-meter-diameter antenna with XCE feedcone installed

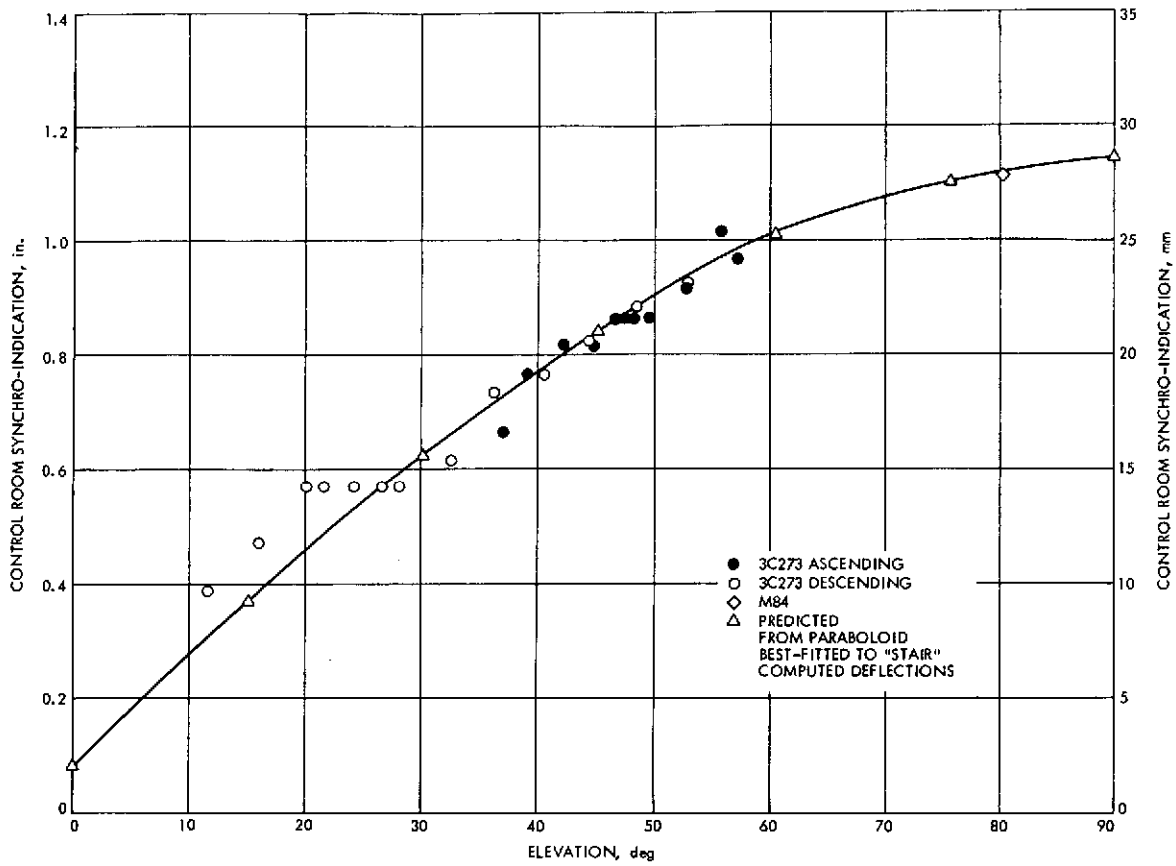

Fig. 146. Focus as a function of elevation angle, 8448 MHz

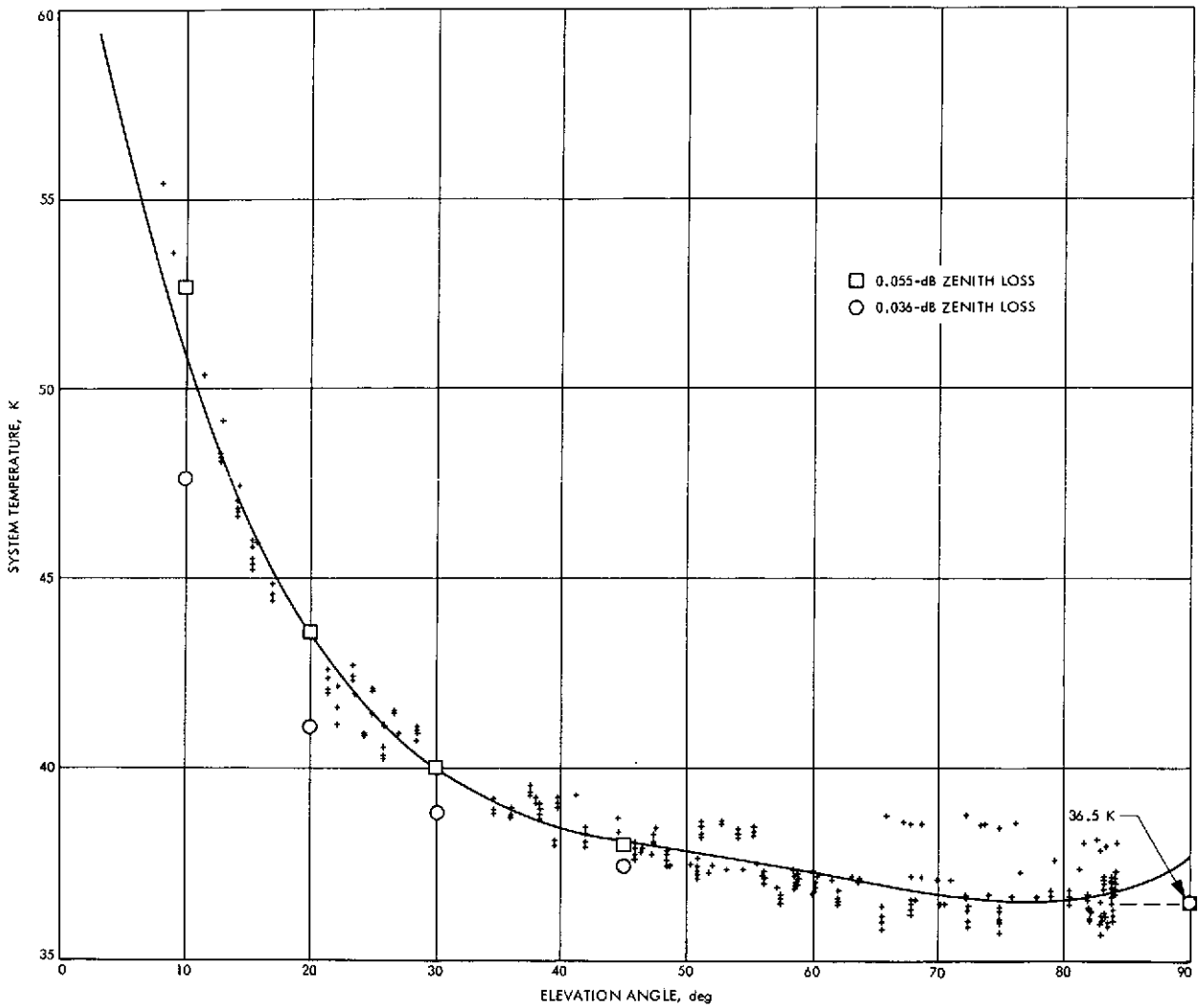

Fig. 147. Total system operational temperature as a function of elevation angle, 8448 MHz

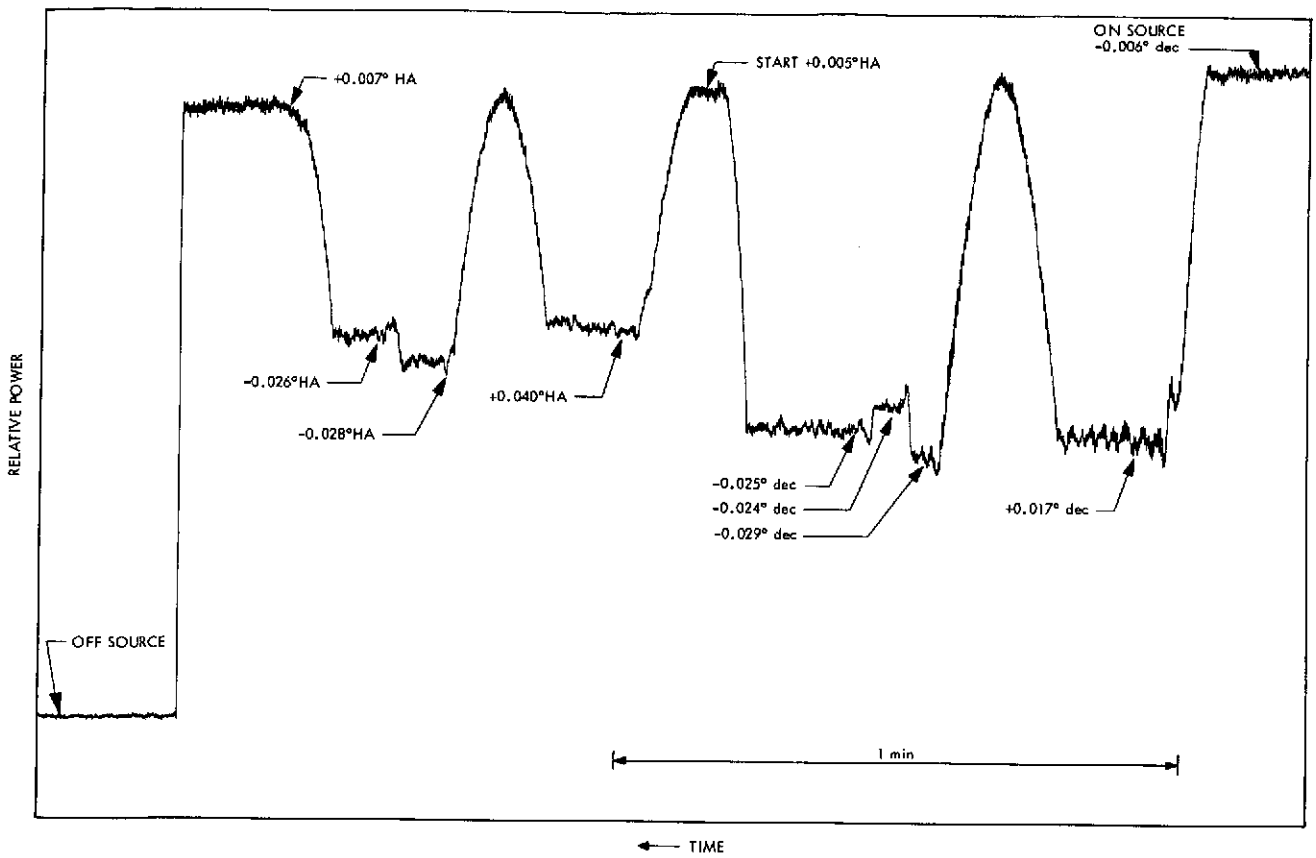

Fig. 148. Cygnus boresighting recording

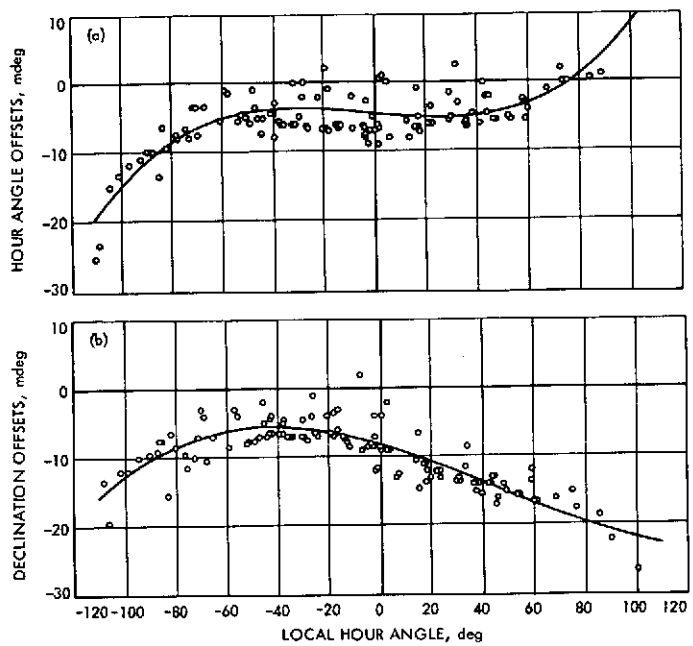

Fig. 149. Angle offsets as a function of local hour angle

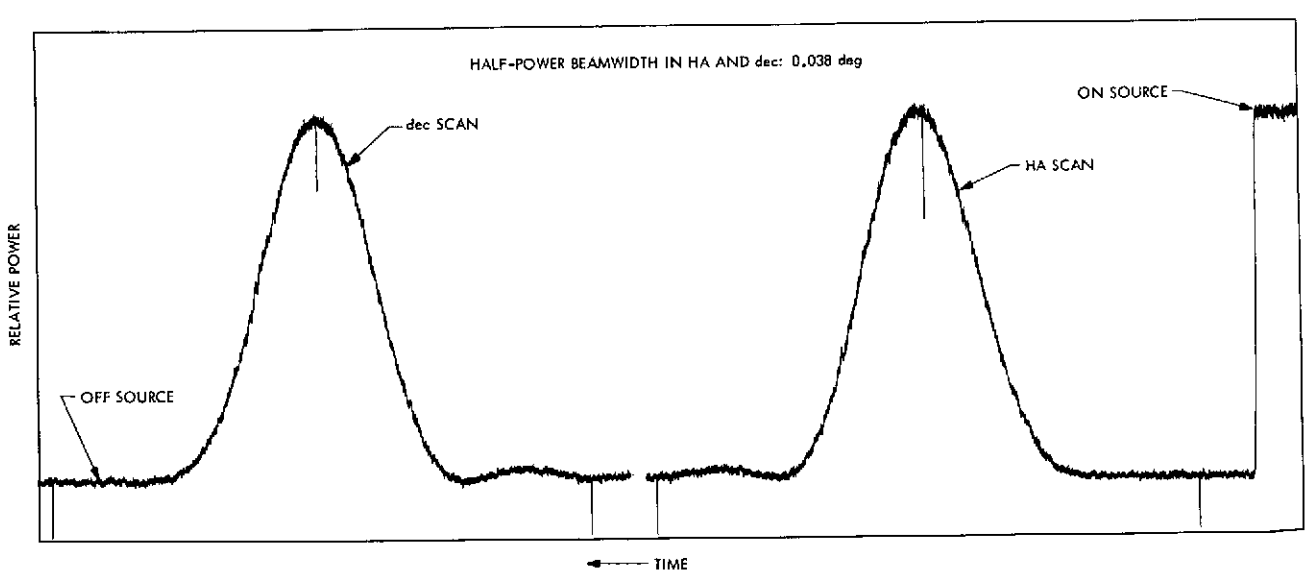

Fig. 150. Scan of 3C273 at 35-deg elevation

CHAPTER VI. UTILIZATION OF THE 64-METER-DIAMETER ANTENNA

This chapter sets forth the spacecraft missions supported, the research conducted, and other aspects of the utilization of the 64-m-diameter antenna from the start of operations to January 1, 1970. A summary of significant accomplishments since 1970 is also included.

I. INITIAL OPERATION

Radio frequency signals were first received on the 64-m-diameter antenna in March 1966. Since that time, excepting a total of about five months for major modifications and reconfigurations, the station has been in use on a full-time basis, in support of various NASA/JPL activities.

II. RULES AND RATIONALE FOR UTILIZATION

The approach to utilization of the antenna is based on its unique capability in the DSN. Because there was only the 64-m-diameter antenna and hence no backup capability available in case of a serious failure, spacecraft missions were not designed to depend absolutely for mission success on the extra capability of the 64-m antenna; rather, they were designed to execute a nominal mission without it. This constraint has led to the use of the antenna for spacecraft mission enhancement roles and for support in emergencies or other unusual situations.

This seemingly restricted use of the antenna was, however, very worthwhile. The combination of the larger aperture area of the 64-m-diameter antenna (six times larger than the 26-m-diameter antennas) and the reduced system temperatures from the later generation of experimental maser amplifiers used provided a communications capability more than ten times (a range capability in excess of three times) that available from the 26-m antenna network stations.

For illustration, consider the two-axis-stabilized solar system exploration spacecraft designs of the sophistication level of the late 1960s: spin stabilization, modestly directive (10-dB gain) antennas, and 10 watts output power. Such spacecraft exhibit a useful mission lifetime of about 6 months within communications range of the standard 26-m antennas (by virtue of being within 1/2 to 1 astronomical unit from the earth). Supported by the 64-m antenna, they can be observed with useful communications capability throughout their entire orbit around the sun (a distance of about 2 astronomical units). Thus, these spacecraft designs have their useful lifetime extended from about 1/2 year to 5 years or more – the actual operating lifetime of the spacecraft.

An analogous argument applies to the fully stabilized Mariner spacecraft designs with 10 to 20 watts of power, quasi-omnidirectional antennas for low-rate communications, and limited adjustable high-gain directive antennas for high-rate communications. For example, in the case of the quasi-omnidirectional antenna link, the added capability of the 64-m antenna allowed essentially continuous communications with the Mariner 6 and 7 spacecraft during their extended mission relativity experiment. Also, during the Mars encounter phase, the added

capability applied to the spacecraft's high-gain antenna link provided visual imaging data playback in hours rather than in days, thus allowing the exercise of "mission tactics" based on the imaging data during the critical encounter phase.

The factor-of-ten margin provided by the 64-m antenna has proved to be very useful in supporting undesigned events and emergencies in spacecraft missions, as discussed below.

The Deep Space Network must provide increased technical communications capability to support increased spacecraft mission goals; to accomplish the needed technology development, the DSN requires a spectrum of "laboratory" facilities. The 64-m antenna is used as a field laboratory facility for certain phases of the technology development; it is also used as an engineering model to resolve design problems or needed improvements of the antenna, for incorporation into the additional antennas of the 64-m antenna network. The antenna is also used for investigations into further state-of-the-art advances in antenna capability design, as it is not necessarily the last evolutionary step in antenna facilities that will be needed by NASA.

The capability of the 64-m antenna has attracted the attention of members of the scientific radio astronomy community. For certain kinds of radio astronomical observation, the antenna's low-noise, large effective aperture at high radio frequencies is exceptionally useful. Recognizing this potential, NASA concurred in allocating a small but reasonably useful amount of support by the 64-m antenna station for this activity. The scientific radio astronomy experiments supported are discussed briefly in this chapter.

To support the kinds of activities described, the allocation of the operational time of the 64-m antenna facility has been essentially as follows:

60% for spacecraft mission support.

15% for DSN technology development.

5% for radio science by the scientific community.

20% for maintenance, modification, and upgrading.

Within the allocations given, the rules developed and in use for planning or scheduling specific support by the 64-m antenna are:

(1) Only those activities that cannot be supported by the 26-m antenna network will be scheduled for the 64-m antenna.

(2) The role of the 64-m antenna in the planning of spacecraft mission support is that of enhancement to the baseline mission.

A summary of the support activities through 1969, including highlight descriptions, follows.

III. EARLY SPACECRAFT MISSION SUPPORT

A. MARINER 4

From the time of the first mission support through the end of calendar year 1969, the Mars Deep Space Station supported key activities in the Mariner, Pioneer, Surveyor, Lunar Orbiter, and Apollo programs. This support is summarized in Table 22.

On March 17, 1966, the day after the first signal was received on the 64-m antenna, daily tracking of the Mariner 4 Mars flyby spacecraft was started. Mariner 4 was nearing solar occultation; it would pass within 0.6 deg of the limb of the sun as seen from earth. The narrow beam and large aperture of the 64-m antenna provided the first opportunity for observing a coherent radio signal passing through the solar atmosphere. Measurements of S-band signal frequency spectrum and attenuation were made with unexpected results — the spectrum of the pure carrier signal was spread substantially for ray paths near the sun. Daily tracking of Mariner 4 to obtain solar occultation data was continued for 3 weeks. Later in the year, the 64-m antenna was used to track and obtain telemetry data on a regular basis to observe the aging characteristics of the Mariner 4 — this was continued until the spacecraft's demise from exhaustion of attitude control gas in December 1967, more than 3 years after its launch on November 28, 1964.

B. MARINER 5

The Mars Deep Space Station was the prime station for the support of the Mariner 5 Venus encounter on October 19, 1967. Besides providing enhanced command facilities during the critical encounter pass, the 64-m antenna was used to instrument the Venus occultation experiment to examine the Venusian atmosphere, as well as the celestial mechanics experiment requiring planetary ranging.

The value of the antenna in the analysis of spacecraft performance under abnormal conditions is illustrated by the support of the Mariner 5 mission after encounter. Following encounter, the communication distance to Mariner 5 gradually increased until communications from the unfavorably oriented low-gain antenna on the spacecraft were lost. The spacecraft continued in its heliocentric orbit and was predicted to be within telecommunications range of the antenna again by mid-July 1968. At that time, the nominal signal level was predicted to be -170 dBmW, and the spacecraft was about 1 astronomical unit distant. A search was made for the spacecraft signal, using high-sensitivity, long-integration spectral analysis techniques devised by the Deep Space Network's research and development personnel; however, no spacecraft signal was detected at that time. Efforts to blind-command the spacecraft into a more favorable communication mode also failed.

Search activity continued at regular intervals through August and September of 1968 until, finally, during the twenty-first search attempt a weak spacecraft signal was detected on October 14 and was quickly confirmed as originating from Mariner 5. However, the signal was very unstable in frequency and power level. On October 20, two-way lock with the spacecraft was obtained from the Mars Deep Space Station, but the downlink signal was still considerably unstable in power and frequency. Analysis of the signal spectrum confirmed that telemetry side bands were not present.

Observations of the spacecraft signal continued until late October, by which time there had been no change in the condition of the telemetry signals, and support of Mariner 5 was terminated. Because of the extremely low signal level, the reacquisition of Mariner 5 and the analysis of spacecraft performance would not have been possible with a 26-m antenna.

C. MARINERS 6 AND 7

Mariners 6 and 7 were launched in early 1969 to perform a twin flyby mission of the planet Mars. On July 30, as Mariner 6 was approximately 6 hours from Mars encounter, the signal from Mariner 7 was abruptly lost. When the spacecraft was reacquired, approximately 5 hours later, it had lost stabilization. After stabilization had been restored, it was determined that a battery and several critical telemetry channels had been damaged. Because of the high-bit-rate telemetry capability from the 64-m antenna, it was possible to maneuver the spacecraft in real time in such a manner that the data were obtained to analyze the spacecraft status and regain control of the spacecraft operations. This contributed significantly in saving both the far encounter and near encounter sequences of Mariner 7.

An important technological accomplishment of the Mariner 6 and 7 missions was the increased data rate for playback of science data. The rate employed was 16.2 kilobits/s, as compared with 8-1/3 and 33-1/3 on previous Mariners. Because of this increased rate, imaging data could be received in a matter of hours rather than days, as it had been previously. As a result, the pre-encounter imaging data could be used to assist in the final encounter planning for both spacecraft, and the encounter data obtained from Mariner 6 were used for optimizing the encounter sequence on Mariner 7. The approximate 10 dB extra capability of the 64-m antenna was crucial to achieving the improved link performance necessary to support the high bit rate.

D. PIONEERS 6-9

The basic design for the Pioneer 6-9 "solar weather station" spacecraft was completed before the 64-m antenna was available, and hence the mission profile was based on 26-m antenna network support. As a result of the limited telecommunication link capability with the 10-W medium-gain spacecraft antenna and the standard 26-m (85-ft) stations of the Deep Space Network, the useful mission lifetime was nominally about 6 months, depending on the particular solar orbit selected. Figure 151 gives an authentic presentation of the paths of Pioneers 6-9 in relation to a fixed earth and sun geometry. The dates, month, and year of launch and the subsequent positions of the spacecraft in relation to the earth and sun are indicated along the paths. The dashed curves drawn about the earth as center indicate the approximate threshold of the lowest bit rate (8 bits/s) for the 26-m and 64-m antenna stations – the shorter ranges for each station represent the capability of the linear polarized spacecraft antenna signals being received on a circular polarized ground antenna. After the early missions were underway, a simple linear polarizer was devised and installed on both the 26-m and 64-m antenna stations, which extended the range to the no-polarization-loss arcs (see Fig. 151). The figure shows that the use of the 64-m antenna extended the useful mission life of the Pioneers from a nominal 6 months (plus a similar period at 3- to 5-year intervals when they reappear on the 26-m antennas) to an indefinite time, depending entirely on spacecraft lifetime.

The ability to track the Pioneer spacecraft over their entire orbits around the sun allows them to be used to study the solar atmosphere. The superior conjunction of Pioneer 6 in November 1969, (see Fig. 151) provided the first opportunity of examining the solar corona with a linearly polarized monochromatic electromagnetic wave. Radio astronomers have studied the solar corona by observing the scintillation of radio stars as they pass behind the sun. However, radio stars are wide-band sources of radiation with largely random polarization. The Pioneer signals are extremely narrow band, with near-perfect linear polarization of known orientation, and can give different kinds of information about the corona that can be obtained from observing radio stars.

To observe the polarization distortions of the S-band radio waves as they passed through the solar corona and magnetic field, a precision polarimeter was installed in a Cassegrain cone on the 64-m antenna. For about 2 weeks on either side of occultation of the Pioneer 6 signals by the sun, observations were made of the "Faraday" rotation of the polarization plane.

The data obtained showed a steady increase of polarization rotation as the product of the sun's magnetic field and charged particle density, integrated along the ray path, increased as the ray path approached the sun. Large transients in the polarization rotation, which appeared to be correlated with sunspot activity (Fig. 152), also occurred. The analysis of these data has contributed to an understanding of the sun's atmosphere and magnetic field. During the same period, spectrograms and total power measurements of the radio signals were also taken. More than 450 spectrograms were taken during the experiment, and each spectrogram was processed to provide three parameters of interest: signal power, center frequency, and bandwidth. Nonhomogeneities in the corona were clearly observed, and there were correlations with the Faraday rotation data.

E. SURVEYOR

In the Surveyor lunar soft lander missions, the 64-m antenna was used to enhance the signal-to-noise ratio of strain gauge telemetry data during spacecraft touchdown. The performance of the antenna provided the extra signal level needed to allow these important data to be retrieved from the spacecraft transmissions.

During the terminal maneuver, possibilities were that each maneuver set should be followed by a roll maneuver to optimize the spacecraft orientation for scientific and/or engineering considerations. Because of the availability of the 64-m antenna, there was virtually complete flexibility in the choice of the roll attitude.

Surveyor, in turn, supported the antenna. As the Surveyor 6 signal radiated from the surface of the moon, the spacecraft was used as a far-field source for antenna pattern measurements.

F. APOLLO

The special capabilities of the 64-m antenna proved to be of value in the Apollo program. It has been used in all of the lunar flights, starting with the flight of Apollo 8 in December 1968. The thermal balance of the Apollo 8 spacecraft required the spacecraft to perform a slow roll, and this resulted in many switchings between the four omnidirectional antennas of the spacecraft. Received signal strength would characteristically drop slowly 20 to 30 dB and then jump instantly up to the former level when the antenna was switched. As the distance from earth increased, this sawtooth characteristic caused the received signal to drop below the threshold level of the high-bit-rate telemetry on a 26-m antenna, but not on the 64-m antenna. Because high-bit-rate telemetry was much more effective than the low-rate telemetry in conducting mission operations, the Mars Deep Space Station data were selected regularly for use by the Apollo Mission Control Center.

The value of the 64-m antenna to the Apollo program was shown in a different way for Apollo 11, the first lunar landing mission, in July 1969. It was realized that during the Lunar Module descent phase, the spacecraft attitude changes that were necessary to perform a landing on the moon would cause dropouts in the high-bit-rate telemetry stream into a 26-m antenna. Since such dropouts could cause the mission to be aborted, the NASA Manned Spacecraft Center decided to schedule the descent so that it would be visible from the 64-m antenna, thereby providing high-bit-rate telemetry backup by means of the spacecraft's omnidirectional antenna.

The 64-m antenna acquired the Apollo 11 Lunar Module as it was beginning its descent to the lunar surface and as it came out of lunar occultation. The station provided the life-support system telemetry coverage during this critical period. Also, in accordance with Manned Spacecraft Center requirements, high-resolution doppler data and short-time-constant signal-strength records were taken until touchdown.

The antenna also supported the television transmission showing man's first step on the moon, in collaboration with the Parkes, Australia, 64-m antenna, along with the subsequent surface operations and the return of the astronauts to the Lunar Module. The commitment of the Goldstone 64-m antenna to the mission concluded with its support of the rendezvous and docking of the Lunar Module and the Command Module. At that point, the Manned Space Flight Network released the station so that it might proceed with the Mariner 6 pre-encounter activities, with the understanding that the station would respond within 4 hours should it become necessary to support an Apollo 11 emergency.

The unique capability and emergency utility of the antenna were again demonstrated on the Apollo 12 mission in November 1969. Because of a lightning hit on the spacecraft, just after launch, Apollo Mission Control altered the flight plan in order to activate the Lunar Module at approximately 7.5 hours into the mission, instead of the previously planned time of 64 hours into the mission. This was done to confirm that none of its systems had been affected by the electrical discharge. However, the Lunar Module and the third-stage Saturn-IVB booster vehicle transmitted on the same S-band frequency and, at this point in the mission, these vehicles had not separated very widely. Thus, when the Lunar Module signal was activated, two interfering signals were received simultaneously by the 26-m antenna ground stations, and no usable data could be obtained. Apollo 12 at that time was in view of the Goldstone Complex, and the 64-m antenna, with its beamwidth of 0.14 deg, as compared with 0.33 deg for the 26-m antennas, was able to point at the Lunar Module while keeping the Saturn-IVB out of the beam. In this way, the 64-m antenna obtained usable Lunar Module telemetry, allowing an assessment of Lunar Module spacecraft condition which could not have been done otherwise.

IV. DEEP SPACE NETWORK DEVELOPMENT

A. THE USE OF PLANETARY RADAR

The objective of the Deep Space Network development effort is to investigate, develop, and demonstrate promising new technology that will be required in the DSN for support of future flight projects, or in unusual situations, for very specialized technical support of current flight projects. New technology, such as high-power transmitters, sensitive and versatile receivers, digital data processing techniques, coding for improved channel efficiency, low-noise masers, and high-efficiency feeds, are typical results of this effort.

Planetary radar has been found to be a very effective tool for managing a major part of this effort and for demonstrating this new technology. It establishes a time-critical project discipline and provides an environment representing a spacecraft mission, in which

equipment must operate reliably to exacting technical performance standards over long periods of time. Scientific results, very useful on their own merit, have been a consistent output of the activity, although the basic objective of the radar experiments has been space communications technology development. This scientific output has also been helpful for planning future planetary missions, from both scientific and engineering standpoints.

After the 64-m antenna was completed, a significant part of the development activity was shifted to using it, rather than the 26-m antenna at the Goldstone Venus Deep Space Station, a research and development facility. A principal reason for the shift was that the long-term new developments for the Deep Space Network are directly related to the 64-m antenna station configuration and its particular capability.

Deep Space Network development activity has supported work on the 64-m antenna to validate the performance potential of the antenna using X-band frequencies and to validate and refine the structural design techniques used on the antenna.

The 64-m antenna has been used as the receiver terminal of the planetary radar, with transmissions from the 26-m antenna at the Venus Deep Space Station, and also as both transmitting and receiving terminals on a time-sequenced basis. The increase in radar capability afforded by the 64-m antenna brought the planets Venus and Mars under close scrutiny, features on Mercury were hazily revealed, and the asteroid Icarus was detected. Some specific examples are given below.

B. RADAR STUDIES OF THE PLANET VENUS

Through the use of the 64-m antenna as a receiving terminal, radar studies of Venus were made, showing permanent topographic prominences on its surface. These features rotate with the planet and return to radar view year after year. Certain regions have been mapped by a technique using radar echo intensity vs radar range and doppler shift – radar can map the Venus surface, which the dense clouds keep hidden from the view of optical telescopes. A radar brightness map of a portion of Venus 800 by 4800 km (500 by 3000 miles) is shown in Fig. 153. The bright area in the lower right is the feature Alpha, previously identified by JPL in 1964.

Another result of these advanced radar studies of Venus is the precise determination of the rotation period of Venus – 243.0 ±0.1 days retrograde; the rotation is synchronously related to the orbit of the earth. Radar time-of-flight measurements to Venus have also been refined (Venus is visible to the radar throughout its entire orbit, through the use of the 64-m antenna). Such measurements form the basis for improving the value of the astronomical unit and the orbital elements of both Venus and earth and the radius of Venus. These improved fundamental parameters of the solar system are needed for accurate radio navigation of spacecraft sent close to the planets.

C. RADAR STUDIES OF THE PLANET MARS

Refined radar studies of Mars were conducted during the 1969 opposition. Mars is a difficult target for radar, reflecting less power than Venus by a factor of 100. Furthermore, the more rapid rotation spreads the returning signal over a wide bandwidth. Consequently, even with the 64-m antenna, only the areas surrounding the closest, or sub-earth point, can be studied in detail.

Simultaneous range and doppler analysis was performed on the echo signals. The measurements improved the ephemerides of Mars and earth and determined altitude variations on the planet along the sub-earth path. The altitude variation found was about 13 kilometers (8 miles) from highest to lowest, with an accuracy of 0.16 km (0.1 miles) (Fig. 154). If the earth had no oceans, and if allowance is made for the differing radii of the two planets, a similar altitude data obtained by the high-capability planetary radar are of vital importance to the future detailed investigation of Mars.

D. RADAR OBSERVATIONS OF THE ASTEROID ICARUS

Radar observations of the asteroid Icarus were made in June 1968 – the first radar contact ever made with an asteroid. The orbit of Icarus is such that it comes within about 6.5 million kilometers (4 million miles) of the earth every 19 years; the 1968 occurrence was the first opportunity for radar study.

The observation of Icarus was an exceptional exercise in weak signal detection; its radar detectability is only 10^{-3} times that of Mercury at closest approach – the signal received on the 64-m antenna was -192 dBmW (6×10^{-23} W).

From the data (Fig. 155), it was estimated that the radius of Icarus is between 0.3 and 0.6 km (0.19 and 0.37 miles) and that the rotation period is between 1.5 and 3.3 hours. Furthermore, the asteroid appeared to be paddle-shaped and, in any case, is certainly not round and uniform. This makes it plausible that Icarus was indeed created in a cataclysm, in keeping with one theory of the origin of the asteroid belt.

E. PULSAR INVESTIGATION

Shortly after the announcement of the discovery of pulsars, an investigation was started to explore their use as a source of precision timing information for the Deep Space Network stations. Using the 64-m antenna equipped with a low-frequency feed, dynamic spectrograms were made of two of the pulsating radio stars discovered in eary 1968 (CP 1919 and CP 0834). The data gathered provided instantaneous spectrum and time-frequency history of the signals over a bandwidth of 3 MHz, centered at 84 MHz. The radio frequency of each pulse decreases with time, following the dispersion relationship of electromagnetic propagation through a

medium containing free electrons. Presumably, the signals near the source contain a wide band of frequencies. Since the group velocity for waves in such a medium is less for the lower frequencies, the received signals have the form of a sliding tone, or whistle, with the higher frequencies arriving before the lower.

V. RADIO SCIENCE

A. GENERAL DISCUSSION

In 1966, representatives of the NASA Office of Space Science and Application and the Office of Tracking and Data Acquisition met with representatives of the scientific radio astronomy community to inform them of the basic capabilities of the NASA communications and tracking networks. The DSN was among those discussed. About a year later, and as a result of incipient interest by the radio astronomers, the NASA offices jointly agreed on an initial assignment of 5% of the operating time (400-450 hours a year) on the 64-m antenna for support of experiments by the scientific radio astronomy community.

Since the radio astronomy use agreement was made, experiments by radio astronomers have been regularly supported on the antenna. The experiments were initially selected by a JPL ad hoc committee, and more recently – since late 1969 – they have been selected by a formal panel of representatives from the radio science community. This Radio Astronomy Experiment Selection Panel includes members from the Massachusetts Institute of Technology, the University of California at Berkeley, the University of Maryland, Stanford University, the National Radio Astronomy Observatory, and the Jet Propulsion Laboratory; it is chaired by Professor Marshall H. Cohen of the California Institute of Technology. The charter of the panel provides that it will solicit and select radio astronomy experiments that can best be performed using facilities of the Deep Space Network.

Tables 23 and 24 illustrate types of radio science experiments that have been conducted using the 64-m antenna, including those performed before the establishment of the Radio Astronomy Experiment Selection Panel. Experiments using only the 64-m antenna are summarized in Table 23 only, while experiments using the 64-m antenna in conjunction with one or more 26-m antennas are summarized in Table 24. Table 25 summarizes the experiments that had been approved by the Panel for support by the 64-m antenna as of 1970.

B. LONG BASELINE INTERFEROMETRY

Of particular interest are experiments using very long baseline interferometry. This is one of the most exciting areas of radio astronomy, and the DSN, with the 64-m antenna and a world-wide network of compatible stations tied together with precise timing and real-time communications, is singularly well adapted to support experiments of this type. Such experiments, in addition to resolving the structure of radio sources to an extent heretofore not possible, are expected to make a major contribution to studies of irregularities in the earth's rotation vector and of continental drift, and make possible the determination of the location of points on the surface of the earth with a greatly improved accuracy; they are also likely to be needed for direct tracking of outer planets or non-ballistic spacecraft. Thus, while much of the attention of scientific radio astronomy is focused on objects outside the solar system, experiments in this field can also lead to new information about the earth and to new tracking data types for the DSN.

C. OBSERVATIONS OF PULSARS

Since their discovery in 1968, observations of pulsars – pulsating radio stars – have been of great interest to radio astronomers and astrophysicists. Although pulsars can be observed in the VHF and UHF ranges on conventional radio astronomy antennas, effective detailed observations at the higher frequencies (S-band and above) require use of an instrument of the 64-m class. The large aperture and low system temperature of the 64-m antenna have allowed observations of characteristics of single pulses of pulsars. Some of the most interesting results so far were obtained by using the precision polarimeter configuration used in the Pioneer 6 solar occultation Faraday rotation measurements to analyze the polarization characteristics within a single pulse duration.

D. JUPITER POLARIZATION EXPERIMENT

As an example of work in planetary radio astronomy using the 64-m antenna, the Jupiter polarization experiment (see Table 23) provided data for the experimenters to reach the following conclusions:

(1) Jupiter's circular polarization is less than 1% at 13 cm.

(2) The magnetosphere rotation period is longer than the presently used period by 0.35 ±0.11 seconds.

(3) The beaming of decimeter radiation has the appearance of being different when the tilt of Jupiter's rotational axis is different.

(4) A model involving the shadowing of an anomalously bright region in the magnetosphere is able to account for the asymmetric beaming curve measured in 1964 at Parkes, Australia, but it cannot simultaneously account for the symmetric beaming curve measured by JPL.

E. GENERAL RELATIVITY INTERFEROMETER EXPERIMENTATION

Another radio science study, the general relativity interferometer experiment (Table 24), illustrates the value of the 64-m antenna in that basic area of science. Findings of this experiment have helped to determine the validity of competing general relativistic theories.

F. SUMMARY

In the first section of this chapter, the use rules applied to the antenna were discussed.

Within the context of radio science use, it is interpreted that experiments must require one or more special capabilities of the 64-m antenna, not available from an existing dedicated radio astronomy facility. Also, experiments must be supported by reasonably straightforward configuration modifications to the standard 64-m antenna and station operational configuration. Any significant special hardware or software must be provided by the experimenter and must be straightforward to install and remove.

VI. SUMMARY OF MISSION SUPPORT, 1971 – 1973

During the period of January 1, 1970, through December 31, 1973, the 64-m antenna station continued to provide valuable flight project support unique to its capabilities. A highlight summary of this support is given below.

A. MARINER

The 64-m antenna provided capabilities which made the Mariner 6 and 7 extended operations achievable. The primary requirement of providing accurate tracking at a distance of 2.6 astronomical units (approximately 242 million miles) could be met only by the use of the 64-m antenna equipped with a high-power S-band transmitter.

The station played a major role in the critical Mariner 9 near-continuous cruise phase tracking and data acquisition. The orbital mission began on November 13, 1971, and there was a daily torrential flow of science data from the spacecraft. One unique capability was a 50,000 bit-per-second data link between the station and the Space Flight Operations Facility to handle high-rate science data.

By mid-March 1972, the Mariner 9 spacecraft was out of range of the 26-m antenna (except for up-link commands). The 64-m station continued its telemetry coverage of several passes per week until October 1972, when the mission was terminated.

B. PIONEER

In addition to normal tracking support of Pioneer 6 and 9, the 64-m antenna station supported such special events as radial and spiral alignment experiments, conjunctions, and the successful blind commanding of Pioneer 7 to an operational status (August 1972). The spacecraft, previous to this command, could not be located because an under-voltage condition had turned off the spacecraft's transmitter.

The 64-m antenna played a major role in the Pioneer 10 Jupiter encounter preparations, in that it was the prime medium for the initial installation (June 1973) and implementation for the Programmed Oscillator Control Assembly so necessary for encounter operations.

C. APOLLO

The unique gain characteristics of the 64-m antenna were an important feature in supporting the recovery from the in-flight failure of Apollo 13. The station also participated heavily in the Apollo 16 and 17 lunar landing missions. Data received were transmitted to the NASA Goddard Station for relay to Mission Control Center at Houston.

Communication links were provided to the Apollo Command/Service Module, the Lunar Module, the Lunar Rover, and the instrumentation stage of the Saturn 5 launch vehicle. Communication with the Lunar Rover was maintained after the astronauts left the moon, enabling unmanned television surveys to be made of the landing site.

A special radar experiment was performed with Apollo 16 in which a radio signal was reflected from the moon and received on earth, along with a direct signal from the Apollo transmitter, giving information on the properties of the lunar surface and subsurface materials.

D. RADIO SCIENCE

The 64-meter antenna has been used extensively for radio science observations by both NASA and non-NASA experimenters and radio astronomers. Regular observations were made for the purpose of examining the structure and variability of quasars and radio galaxies by several teams of scientists from Caltech, JPL, the Massachusetts Institute of Technology, the University of Maryland, and the Goddard Space Flight Center. In addition to observations made at the normal operating frequency of 13 cm, experimental equipment was used to observe at 3.5 and 2.1 cm.

The unusually high sensitivity of the 64-m antenna and the very high angular resolution (approximately 0.001 second of arc) of the very long baseline interferometry (VLBI) technique permitted resolving the quasars into structural components. A significant achievement was the extension of VLBI techniques to 2.1-cm wavelengths. An interferometer was formed by the 64-m antenna at Goldstone, the 37-m Haystack antenna of the Northeast Radio Observatory Corporation, and the 43-m antenna of the National Radio Astronomy Observatory in West Virginia. The introduction of the K-band (2-cm) equipment at these observatories resulted in attaining a baseline length of the order of 10^8 wavelengths.

The 64-m antenna was also used by JPL radio scientists to search for and detect interstellar molecules. The presence of previously detected molecules was confirmed, and formaldehyde was found in regions where it had not been detected before. Time was also devoted to observing Jupiter and Uranus. A significant development was the simultaneous observation of pulsars at 13 and 3 cm.

Table 22. Summary of spacecraft mission support by the 64-m antenna, 1966-1969

Project	Number of spacecraft passes tracked				
	1966	1967	1968	1969	Total
Mariner					272
4	58	65			
5		36	26		
6				44	
7				43	
Pioneer					1299
6	67	131	278	176	
7	2	94	283	159	
8		1	23	32	
9			1	49	
Simultaneous 6, 7				3	
Surveyor					33
1	7	1			
2	2				
3		4			
4		3			
5		6			
6		4			
7			6		
Lunar Orbiter					7
1	2				
2	2				
4		1			
5		2			
Apollo					27
8			6		
10				8	
11				6	
12				7	
Total	140	348	623	527	1638

Table 23. Early radio science experiments using only the Goldstone 64-m antenna

Experiment	Purpose	Experimenters		Date
Lunar occultation of radio sources (2295 MHz)	To determine intensity and angular size of radio sources.	A. Maxwell J. H. Taylor	Harvard University	Jul 1967 Jan 1968 Apr 1968
Pulsar measurements (2295 MHz)	To study pulse characteristics.	A. Moffet R. D. Ekers	California Institute of Technology	Apr 1967 May 1967 Mar 1969
Jupiter polarization experiment (2295 MHz)	To make circular polarization measurements of Jupiter at 13 cm.	B. Gary S. Gulkis	Jet Propulsion Laboratory	Apr 1969 May 1969

Table 24. Early radio science experiments involving the Goldstone 64-m antenna and one or more 26-m antennas

Experiment	Purpose	Experimenters	DSN 26-m antennas	Dates
Very long baseline interferometer (narrow data bandwidth, S-band)	To determine angular size of radio sources using Trans-Pacific Baseline.	J. Gubbay, A. Legg, D. Robertson — University of Adelaide, Space Research Group, WREa A. Moffet, B. Seidel — California Institute of Technology, Jet Propulsion Laboratory	Goldstone Sites Pioneer Echo Australian Sites Tidbinbilla Woomera	Sep 1967 Nov 1967 May 1968 Jun 1969
Very long baseline interferometer (NRAO wide-band terminal S-band)	To determine angular size of radio sources using Trans-Pacific Baseline.	M. Cohen, A. Moffet, D. Shaffer — California Institute of Technology B. Clark, K. Kellerman — National Radio Astronomy Observatory D. Jauncey — Cornell University S. Gulkis — Jet Propulsion Laboratory	Australian Site Tidbinbilla	Jun 1969
General relativity interferometer experiment	To measure apparent change in angular separation of two radio sources when one is occulted by the sun.	D. Muhlemann, R. Ekers, E. Fomalont — California Institute of Technology	Goldstone Site Venus	Oct 1969
Very long baseline interferometer (medium data bandwidth, S-band)	To determine angular size of radio sources.	J. Gubbay, A. Legg, D. Robertson — University of Adelaide, Space Research Group, WRE A. Moffet, B. Seidel — California Institute of Technology, Jet Propulsion Laboratory	Goldstone Site Pioneer Australian Site Tidbinbilla	Dec 1969
Solar scintillation (2295 MHz)	To determine solar wind characteristics.	R. Eckers, L. Little — California Institute of Technology	Goldstone Sites Pioneer Echo Venus	Apr 1969

[a]Weapons Research Establishment, Adelaide, Australia.

Table 25. Summary of approved experiments as of 1970

Experiment	Experimenter		Comments
Further study of radio sources using interferometer techniques; Trans-Pacific Baseline.	J. Gubbay A. Legg D. Robertson A. Moffet B. Seidel	University of Adelaide Space Research Group, WRE Space Research Group, WRE California Institute of Technology Jet Propulsion Laboratory	Continuation of previous work. See Table 24 for information.
Further study of radio sources using interferometer techniques; Trans-United States Baseline.	M. Cohen A. Moffet D. Shaffer B. Clark K. Kellermann D. Jauncey S. Gulkis	California Institute of Technology National Radio Astronomy Observatory Cornell University Jet Propulsion Laboratory	Continuation of previous work. See Table 24 for information.
Study of SCO-SR1, an X-RAY source in Scorpio.	C. Boyer	University of California, Berkeley	Scheduled observations in May and June, 1970.

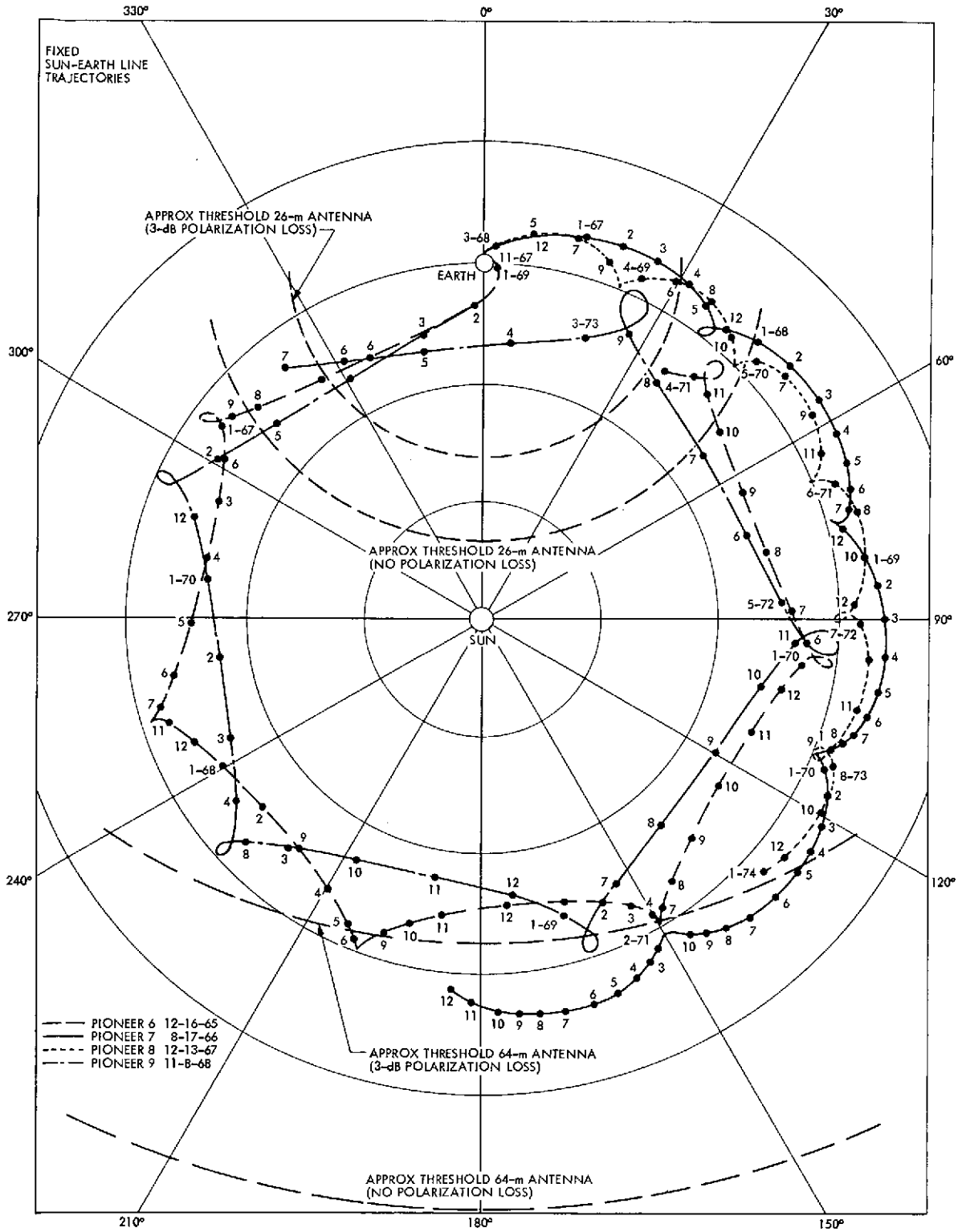

Fig. 151. Pioneer spacecraft trajectories

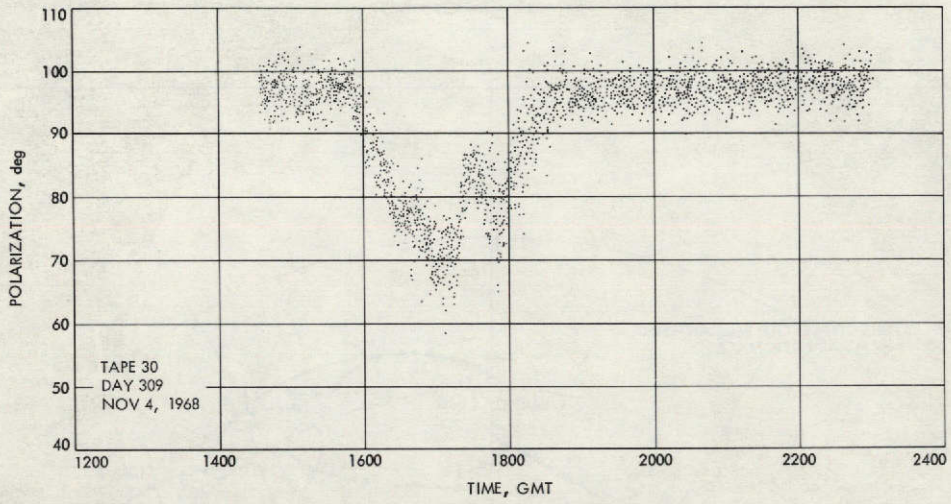

Fig. 152. Pioneer 6 Faraday rotation

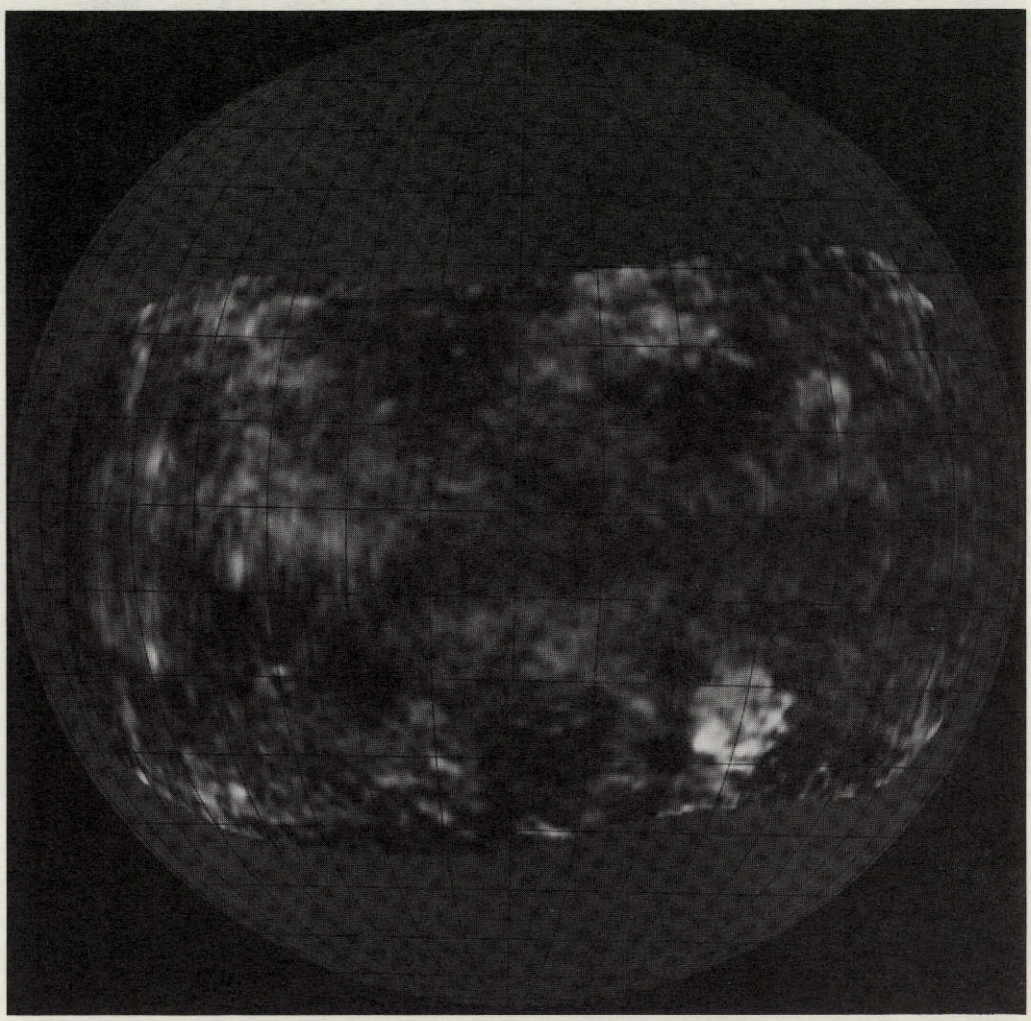

Fig. 153. Radar brightness map of Venus

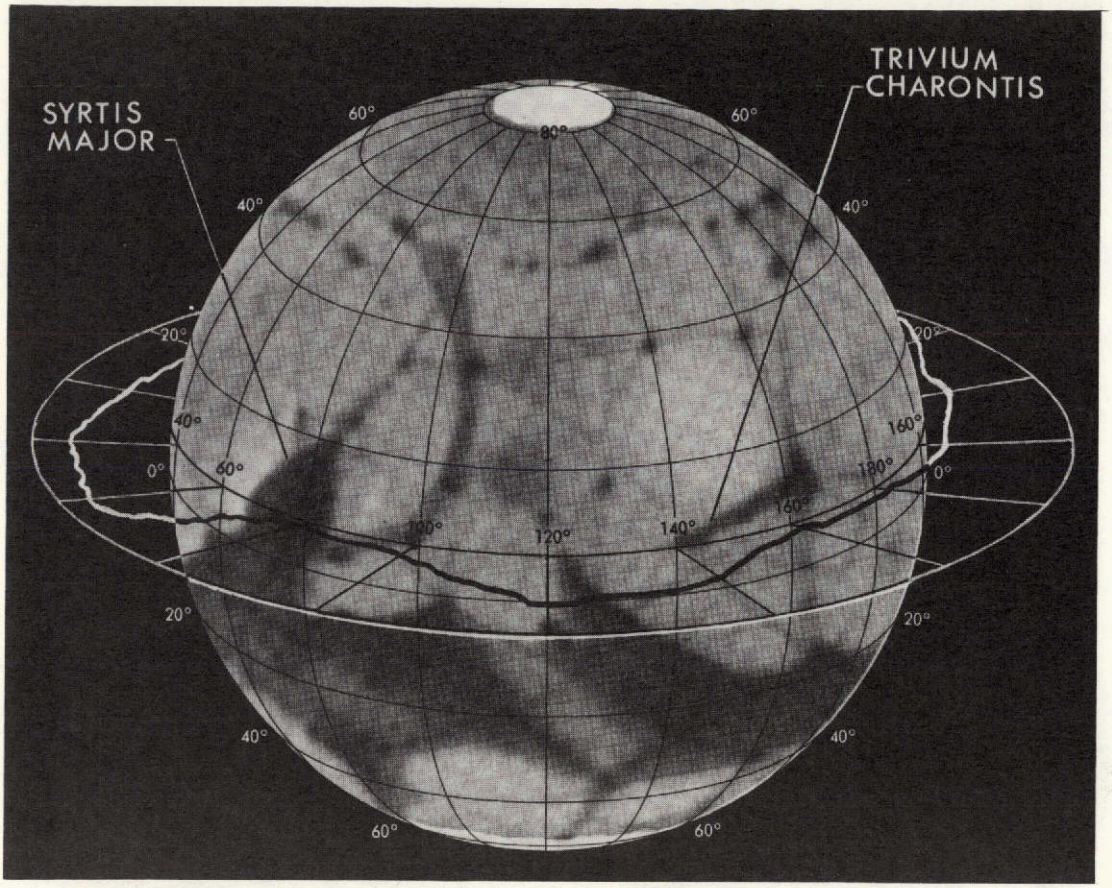

Fig. 154. Altitude variation on Mars, as shown by radar studies

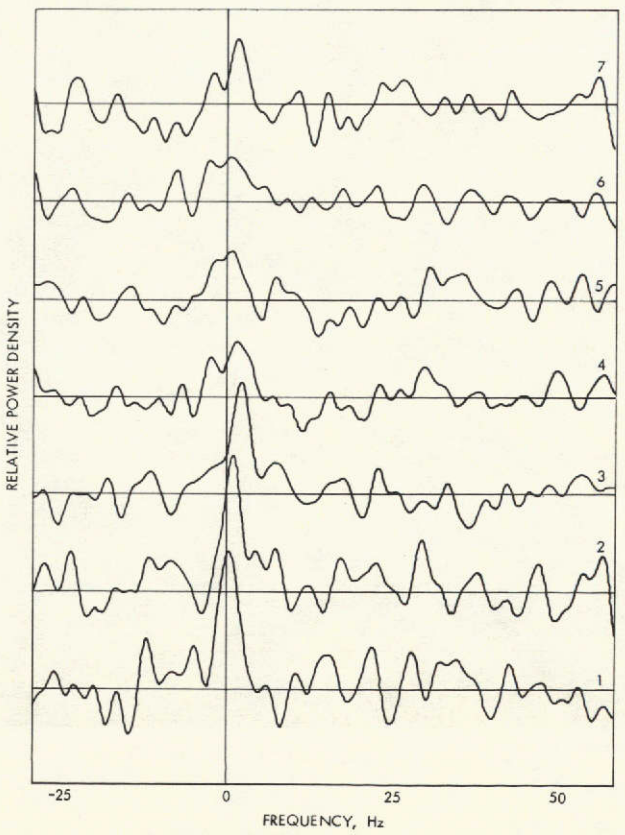

Fig. 155. Individual spectra on Icarus radar echo

CHAPTER VII. MODIFICATIONS FOR IMPROVED CAPABILITY

This chapter discusses major modifications that were made during the early years of the 64-m antenna's operation (essentially through January 1970) to improve the capability of the antenna. Modifications discussed include an innovative means for greater flexibility in utilization of RF feed cones through development and installation of a tricone multiple feed system, modification of the cable wrap-up assembly, and antenna modifications to facilitate the installation of a higher-power (400-kW) transmitter facility.

I. OTHER MODIFICATIONS

Modifications made and methods employed for greater reliability and maintainability, as determined necessary during the initial operations of the antenna, have been discussed in Chapter V.

Since the start of operations, there have also been a number of minor modifications for increased reliability and better human engineering. Such minor modifications have been made in response to changes requested by DSN Operations or as determined beneficial for antenna performance and maintainability by cognizant and sustaining engineering personnel, under a formally established Change Control Procedure. Such upgrading is a continuing process and is not discussed in specific detail in this report. Minor modifications, along with major ones, are regularly reported in established JPL forms of technical documentation.

II. TRICONE MULTIPLE CASSEGRAIN FEED SYSTEM

A. INTRODUCTION

The standard Cassegrain feed system, designed as a part of the primary antenna configuration, has been described in earlier chapters. This system was basically an outgrowth of highly successful systems that had been previously utilized on the DSN 26-m antennas.

For the 64-m antenna, the Cassegrain geometry was chosen to be a physical scale of the 26-m Cassegrain design, thereby allowing interchangeability of the feedcone structures and allowing test of the feedcones on a 26-m antenna prior to commitment for use on the 64-m antennas. The excellent performance achieved at S-band and X-band test results was discussed in Chapter V of this report.

While the standard, or unicone, Cassegrain configuration satisfied the prime tracking requirements of the 64-m antenna, a need arose to provide a more flexible and rapid method of changing RF feedcones. The unicone system not only consumed valuable operating time to change cones, it also presented risks of possible damage during the handling procedures.

It was concluded that the best overall solution to this problem was to replace the standard feedcone support structure with a new structure capable of supporting three fixed feedcones clustered about the antenna axis and pointed toward the antenna subreflector. This approach is referred to as the tricone assembly. Since each of the three feeds is displaced from the paraboloid axis, it might be supposed that a

boresight error and related gain loss would be incurred by the tricone approach. As described in the following section, both of these effects are eliminated by a movable asymmetric subreflector.

B. TRICONE GEOMETRY

The geometry of the tricone Cassegrain feed system is shown in Fig. 156; for simplicity, only one cone is shown. The line AB defines the axis of the hyperboloid with the two hyperboloid foci at the points A and B. The hyperboloid has the property of transforming a spherical wave from the feed phase center B into a spherical wave from the virtual focus at point A. Since the latter point is accurately located at the paraboloid focus, the paraboloid is illuminated by a spherical wave from its focus, and no boresight error or aperture phase error is introduced by the tricone geometry.

In the tricone system, the paraboloid aperture amplitude distribution is controlled in three ways. The first is by truncating the hyperboloid asymmetrically so that the subtended half angle at the edge as seen from the paraboloid focus A is uniformly 60 deg, the same value which was utilized in the standard unicone configuration. This asymmetric truncation was necessary to control the rearward spillover and associated noise temperature contribution of the feed system. The second method of amplitude control is by rotation of the feed about its phase center B so that the axis of radiation BE intersects the geometric center of the hyperboloid's area E. The final and implicit method of amplitude control is by the feedhorn illumination pattern. As shown in Fig. 156 by the angles η_1 and η_2, there is a slight variation of the subreflector edge angle as seen from the feedhorn; these angles compare with the standard unicone angle of 14°39.3 minutes. Because of the very small value of the change from this original value, the unicone feedhorn design has been utilized for the tricone. The three amplitude controls described herein are sufficient to insure an amplitude illumination which is negligibly different from that which was obtained with the original unicone system.

C. TRICONE CONFIGURATION AND CONE SUPPORT MODULES

Figure 157 shows the overall tricone configuration, and Fig. 158 is a photograph of the tricone system as installed on the 64-m antenna. As shown in Fig. 157, the three feedcones are mounted by Marman-type quick disconnects on a three-module support assembly which houses various ancilliary equipments. The feedcones themselves are similar to standard DSN feedcones, with the exception of cylindrical sides in the bottom section.

Module I of the feed support is designed as an open-space truss in order to provide optical line-of-sight to paraboloid surface panel targets from a theodolite mounted 381 mm (15 in.) about the antenna vertex. A heat exchanger for the tricone air-conditioning system is mounted in Module I above the optical line-of-sight envelope.

Module II of the feed support is a cylindrical section designed to house three large transmitters. A hoisting means, using the feedcone hoist, is provided to raise a 2268-kg (5000-lb) unit from the ground level into Modules II and III. Module III of the feed support has tapered sides in order to minimize the RF blockage and still provide space for mounting standard-size DSN cabinets.

Hoisting means are provided to install the following: Module I, alone; Modules II and III, separately; Modules II and III, together; and each of the three RF feedcones, individually. All means utilize the original feedcone hoist with pulleys mounted on the upper quadripod legs (Fig. 159).

D. SUBREFLECTOR ASSEMBLY

A side view of the subreflector installation is shown in Fig. 160. For purposes of explaining the mounting system, a rectangular coordinate system is established. In this coordinate system, the Z-axis is parallel to the antenna axis of symmetry; the X-axis is parallel to the cross-elevation motion direction; and the Y-axis is parallel to the elevation motion direction. A top view and elevation section of the subreflector installation are shown in Fig. 161.

Positional constraint of the subreflector assembly, longitudinal positioning, and the two degrees of lateral positioning are achieved by means of six restraint rods — each with a motorized jack and two universal joints. As shown in Fig. 160, constraint along the Z-axis is achieved by means of three restraint rods, each with two universal joints to allow X and Y motions of the main torus assembly. Three motorized ball-screw jacks, at the top of each rod, are used to provide a remotely controlled Z-motion (focusing) of ±76.2 mm (±3 in.). As shown in Fig. 161, two restraint rods and jacks are utilized in the Y-direction. These two rods prevent rotation of the assembly about the Z-axis; they also provide a Y-motion of ±101.6 mm (±4 in.) for elevation boresight control. The final constraint rod provides a motion of ±101.6 mm (± 4 in.) in the X-direction, providing azimuth boresight control.

Rotation of the subreflector about its axis of symmetry is achieved by means of a large bearing within the torus assembly. Five rotational positions are provided by an indexing pin system. Three of these positions correspond to the centers of the tops of the three feedcones; this provision was made in anticipation of a multiple-feed high-frequency feedcone.

As initially installed, all actions are remotely indicated and console-controlled at the control room. However, extra cable wires and provisions for mounting encoders for future installation of servo controls are provided.

E. SCALE MODEL TESTS AND RF PERFORMANCE

During the design of the tricone system, a series of scale model tests of the subreflector and horn assembly were made, and additional analysis was performed to verify the expected high level of performance. The analysis was

performed in two ways. One approach utilized primarily theoretical calculations, while the other made greater use of experimental data.

The analysis was begun by integrating the measured patterns of the feedhorn to determine the percentage of radiated power that was intercepted by the unicone subreflector and the tricone subreflector. The same horn patterns were then input to subreflector scattering programs. These programs computed the scattered patterns from the unicone and tricone subreflectors. The scattered patterns were then integrated to establish the aperture efficiency for the main reflector.

The method of Ruze (Ref. 8) was used to calculate the gain loss due to structural deviations of the antenna from the desired shape. These calculations, in conjunction with the preceding analysis, were used to calculate the expected antenna gain, neglecting the effect of aperture blockage by the subreflector support structure (quadripod). Since the preceding analysis is firmly based on accepted practices, the estimate of quadripod blockage was made by comparing the computed gain with the measured gain for the unicone system. The comparison gave a quadripod gain loss figure of 0.83 dB. This estimate of quadripod loss was then used throughout the remainder of the analysis. Analyzing the expected gain with the tricone gave a gain loss of 0.06 to 0.08 dB over the unicone configuration. This expected loss is virtually entirely due to the increased central blockage in the tricone configuration, rather than a difference in illumination functions.

While these analytical calculations were being performed, measurements were being made of the scattered patterns from one-seventh scale models of the unicone and tricone subreflectors. A comparison of typical computed and measured amplitude and phase patterns is shown in Fig. 162; the agreement between predicted and measured data is considered outstanding. The measured patterns were then used to again calculate antenna gain for the unicone and tricone configurations. For this calculation, the gain loss for the tricone was 0.07 to 0.09 dB over the unicone.

The gain based on the experimental pattern for the unicone subreflector was 0.1 dB less than for the theoretical pattern value. The same comparison for the tricone showed a similar difference of 0.11 dB. It is felt that the difference represents a consistent pattern measurement error on the antenna range, and the close agreement of the performance difference between the unicone and tricone is the important consideration. The most likely cause of such a consistent error would be reflections from the structure used to support the subreflector and the horn during pattern measurement. Table 26 gives the calculated 2295 MHz antenna gain for each configuration and technique.

After the successful completion of the tricone installation, verification tests of S- and X-band performance were conducted. At S-band, in order to perform a direct test of the tricone effect on performance, the same feedcone (SCU) was utilized as in prior unicone tests. Contrary to the small degradation predicted in Table 26, the tricone gain was actually found to be higher than the unicone by 0.1 dB. The measurement, utilizing the radio source technique, is calculated to have a 3σ accuracy of 0.10 dB. This discrepancy between the measured and predicted tricone efficiency has not yet been fully explained. At X-band, a larger improvement, 0.5 dB, was measured. In this case, different feedcones were utilized in the unicone and tricone tests. Because of improvements in the new X-band feedcone, insertion loss was reduced by 0.1 dB. Thus, the performance improvement of the tricone, relative to the unicone, was 0.4 dB at X-band. This improvement may be explained by a superior alignment of the tricone subreflector system and a slight improvement in the antenna surface tolerance. The improved surface tolerance is caused by the fact that the reflector panels were originally aligned for an estimated central weight which more closely resembled that of the tricone than that of the unicone.

III. MODIFICATION OF THE CABLE WRAP-UP ASSEMBLY

A. INTRODUCTION

To provide additional water flow to the rotating portion of the antenna and to improve operation and reliability, redesign and modification of the cable wrap-up were considered advisable.

Figure 163 is a cross-sectional view that shows how the water hoses and electrical cables run from the stationary antenna pedestal downward into a draped position, then upward to the movable alidade structure of the antenna. The right half of the figure shows the original system, and the left half of the figure shows the redesigned configuration. For the 64-m antenna, the required azimuth rotation range is ±270 deg.

Superimposed in the right-half view are an electrical cable, a water hose, and a support cable for the spacer rings. These three parts do not, in general, lie in a common vertical radial plane but are more or less equally spaced around the periphery. The relative radial distances shown in Fig. 163 depict the condition of zero wrap at the center of travel.

Among the features that may be seen in the right half of Fig. 163 are five inner and two outer spacer rings. The upper inner ring was supported by eight support cables attached to hooks on the alidade roof beams, the lower surfaces of which were at different elevations; hence, these uppermost cable pivot points were not in a common elevation plane. The upper outer spacer ring was supported by eight cables attached to hooks on the antenna pedestal. The lower spacer rings were connected by cables that were pivoted approximately 4 in. from the fairlead pivot axis. The two bottom spacer rings were connected by three equally spaced drive cables (not shown).

Fifty-one electrical cables were supported at their upper ends by Kellem grips, a device that gripped the cable over a distance of several

inches; the grips were, in turn, fastened to hooks. The hooks on the alidade beams were at various elevations. The cables ran from the stationary pedestal downward through the fairleads pivoted to the outside of the spacer rings, formed a loop at the bottom, ran upward through the fairleads pivoted to the inside of the spacer rings, and terminated at connectors located in the cable tray.

Nine water hoses were attached to single-swivel fittings at their upper ends. The swivel axes were horizontal and permitted the hoses to pivot about these axes. Note that these swivel axes were considerably below the upper pivot points of the support cables and electrical cables. The hoses lay on the outside of both sets of spacer rings. Each hose contained two swivel joints in the bottom loop.

As the antenna rotated about the azimuth axis, the support cables, hoses, and electrical cables moved out of their vertical planes into skew curves that spiraled around the instrument tower and around the pedestal wall. The spacer rings rotated relative to each other and all of them rose vertically. Figure 164 (left side) shows that the electrical cables running between the two lower spacer rings intersect in the plan view. They did, in fact, interfere not only with each other but also with the hoses and tow cables.

Because the support cable radius was different from those of the electrical cables and hoses, and because the distances between the support cable pivot points were different from the distances between the fairlead pivots, it was impractical to support either the electrical cables or the hoses at any of the spacer rings. For example, if the electrical cables were clamped in the fairleads of the two lower inner spacer rings when at zero wrap, then at full wrap-up each of these cable sections would be approximately 152 mm (6 in.) too long. Experience showed that the electrical cables were stretched and some of them dragged the ground floor at zero wrap. Hence, additional support of the cables was needed to prevent excessive stretching. Both electrical cables and hoses were twisted as they were moved from their planar curves at zero wrap to skew curves at a finite wrap. The hose swivels reduced but did not eliminate the twist. Most of the undesirable characteristics were eliminated by redesigning to a slightly different configuration.

B. MODIFIED WRAP-UP ASSEMBLY

The modified system is partially shown in the left half of Fig. 163. An adapter support ring is welded to the alidade roof beams so that a common elevation plane is established for mounting all cable and hose supports. The spacer rings are made of square tubing in order to obtain the necessary amount of torsional and bending stiffness. The radii of the electrical cables and hoses are the same. The radii of the support links are slightly greater than those of the cables and hoses in order to compensate for the fact that the developed length of the rigid ball-ended links is less than the developed length of the hoses and cables, which makes smooth rather than abrupt turns at the fairleads.

At the pedestal, a support ring is welded to a steel plate embedded in the concrete structure. The support link clevises, Kellem grip hooks, and the double-swivel hose fittings are all bolted to the ring so that the pivot points are at the same level. A similar arrangement is used at the alidade roof adapter ring. In Fig. 163 the double-swivel fitting is shown at the pedestal. The left-end flange of the fitting is solidly attached to a bracket which in turn is bolted to the pedestal support ring. Rigid piping connects to this flange. The vertical part of the fitting swings about the horizontal centerline, thus allowing the hoses the required freedom in that direction. The second swivel swings about the vertical axis and serves to reduce the amount of twist in the hose. The same arrangement is employed at the alidade end. The electrical cables are supported by Kellem grips that are suspended on hooks located at the same level as the horizontal pivot of the hose fitting. The ball-ended support links are pivoted at the same level.

Forty-four cables and 16 hoses run through fairleads that are pivoted on the spacer rings at the same level as that of the support link ball-end centerline. At the bottom, the cables form a loop between the bottom sets of fairleads. It is at the outer bottom fairlead where the cables undergo the most abrupt bend. Sixteen triple-swivel fittings are mounted on each bottom spacer ring. These are arranged in four equally spaced groups in order to achieve the best load distribution. The horizontal swivel allows the upward-running hose to swing as required. The upper vertical swivel reduces the amount of twist in the upper hoses. The lower vertical swivel, which always remains vertical, allows the bottom loop to remain coplanar at all times; thus, there is zero twist in the bottom loop.

The two bottom spacer rings are connected by four equally spaced drive cables (not shown in Fig. 163). These drive cables are considerably shorter than the corresponding one of the original system. The relative rotation between the two bottom spacer rings is 20 deg for the new design, whereas it is approximately 45 deg on the original system. Figure 164 (upper right) shows that none of the electrical cables and/or hoses intersect in the plan view. Analysis also proves that the drive cables and support links have ample clearance. Thus, entanglement of the bottom loops has been prevented. Since the kinematical relationships among the supports, links, hoses, and cables are approximately correct, there are several ways of obtaining additional support for the hoses and cables and, thus, reducing the stress and stretch of these parts. Each fairlead is provided with two small eyebolts fastened to its bottom. Kellem grips can be suspended from some or all of the fairleads. By inserting liners into the fairleads, the cables can be clamped into the fairleads themselves.

Certain intangible properties, such as the bending and torsional stiffnesses of the cables and hoses, make it impossible to predict exactly

the optimum kinematical design. Even though an attempt is made to measure some of these properties, there is no guarantee that they would be stable with respect to time. However, it is believed that there is sufficient design flexibility to allow the best supporting method to be determined experimentally.

Since the hoses are attached to the bottom spacer rings, there will be reactive pressure forces on the rings. These forces can be rather large when all hoses are at their maximum pressures. For the case of maximum pressure, the total load on the upper inner support links is approximately 145,000 N (32,682 lb), whereas for the zero-pressure case the corresponding total load is 104,000 N (23,445 lb). The corresponding load on the original design was 52,000 N (11,700 lb).

The hoses have been arranged so as to minimize the resultant horizontal pressure force. Balanced horizontal forces merely put the spacer rings under stress, but the resultant unbalanced force will move the whole ring horizontally. Four casters are equally spaced on the lower outer ring and will come to bear on the auxiliary steel wall (Fig. 163) whenever the ring has moved horizontally a few centimeters. Under most conditions the lower inner ring would be restrained against horizontal motion by the taut drive cables. But near zero wrap and under certain hose pressure conditions, the lower inner ring can be forced against the instrument tower. Therefore, four more casters are mounted on the inner ring so that they will contact the tower when the inner ring moves a few centimeters horizontally.

During an antenna shutdown period in February 1970, the redesigned wrap-up system was installed. Since that time, it has been performing satisfactorily. Certain aspects of the performance can be evaluated only over a long time period; for example, excessive stretch of hoses and cables. Figure 165 shows a comparison of the measured and predicted support link configuration. The upper and lower angle figures are measured and predicted values, respectively.

Photographic views of the modified cable wrap-up are shown in Fig. 166, and the structural components of the modified wrap-up are shown in Fig. 167.

IV. RECTANGULAR GIRDER BRACES

Based on predictions of improved performance for gravity loadings, new reaction bars or braces were added between the elevation bearings and the upper corner of the rectangular girder in early 1973.

The structural changes to the antenna were made by removing four existing knee braces and replacing them with two new braces. The new braces and end points are heavy structural members which weigh 100 kg/m. Because a large portion of the work was to be done without tracking interference, steel work platforms were installed on the antenna and left in place for 5 months.

During a major maintenance shutdown of the station in February-March 1973, a heavy-duty crane was used to erect the main braces, which weigh 16 metric tons each. The brace connects to the elevation bearing casting, presenting a problem in getting an acceptable mating surface on a rough casting. Welding was considered and deemed feasible but was rejected because of potential weld and casting cracking. The successful solution was to provide a special milling head fixture designed to be attached to the bearing casting and to machine a mating surface for attachment of the end pieces.

Preliminary optical and RF measurements have indicated that the predicted performance improvements were in fact realized. The present assumption is that due to the performance improvement gained at the 64-m antenna at Goldstone, this modification will probably be incorporated in the overseas 64-m-diameter antennas when funding and down time can be coordinated.

V. ANTENNA MODIFICATIONS FOR A 400-kW TRANSMITTER

A. INTRODUCTION

To facilitate the installation and operation of a higher-power transmitter for the 64-m antenna, certain modifications to the antenna and directly related site facilities have been made. Three elements of the 400-kW transmitter are considered as part of the antenna. These are the transmitter coolant system, the power supply, and the equipment pads and vaults immediately adjacent to the antenna.

The primary purpose of the high-power transmitter facilities is to supply 1 MW of power at 70,000 Vdc to the transmitter located on the 64-m antenna. The facilities also supply cooling water in large volume (0.05047 m^3/s, or 800 gal/min) to the transmitter klystron tube on the antenna. Figure 168 shows site facility additions that have been made.

B. CONSTRUCTION

Facilities constructed north of the antenna include a vault building with an area of 46.45 m^2 (500 ft^2). This building houses a transformer/rectifier which converts 400-Hz power from the motor generator to 70,000 Vdc, plus a filter choke installation. Adequate head room is provided for disassembly of the transformer/rectifier by means of a monorail hoist system. The facility is pressure ventilated with filtered air to ensure dust-free operation.

A 1-MW motor-generator set is located adjacent to the transmitter building. This unit, which has a 2610-kW (3500-hp) motor driving one generator, is mounted on a heavy concrete foundation.

The cooling system includes a 2-MW dry-type cooling tower located adjacent to the existing cooling tower on the site. Pumps are

provided to circulate the coolant to the antenna. A distillation system has been installed to furnish pure water to the closed circuit coolant system; a 4.5-m^3 (1200-gal) underground storage tank has been included.

A power distribution system has been installed. The major load is the 2610-kW (3500-hp) motor which is connected to 2400 V. In addition, a 1500-kVA, 2400/480V substation has been added to provide service to the auxiliary equipment. Power distribution is by underground ducts and manholes. Trenches are used to run piping and cabling to the auxiliary equipment. A service road is provided to the equipment areas. Required revisions to the cable wrap-up and power distribution systems on the antenna proper have been made.

C. TRANSMITTER COOLANT SYSTEM

The system is a mixed-fluid interdependent configuration. There are basically three water loops that make up the system. The first is the ground ancillary equipment cooling for the transformer rectifier and the motor generator clutch. The pure water distillation replenishing and storage is also part of the ground ancillary equipment. The second is a ground-based glycol water loop. This contains the water-to-air heat exchanger, filters, storage tanks, and the necessary pumps, piping, and hoses to maintain the proper temperature of the alidade-based pure water loop. This portion covers all the water from the ground through the cable wrap-up to the alidade roof. The third is the pure water loop, consisting of a pure water to glycol water heat exchanger and a purification, temperature control and storage facility, as well as a pump unit to provide the pure cooling water flow through the transmitter cabinet.

D. POWER SUPPLY

The power supply basically consists of five major components. The first is a 1305-kW (1750-hp), 60-Hz motor that drives a 1200-kVA, 400-Hz generator and associated peripheral equipment. The second is a transformer and rectifier assembly. The third is a filter assembly which insures consistency of the power supplied to the transmitter klystron tube. The fourth is a system of equipment and personnel safety devices, and the fifth comprises all of the other associated panels and controls required to properly monitor and control items one through four.

Table 26. Calculated antenna gains (unicone/tricone)

Elevation angle, deg	Theoretical pattern, dB		Measured pattern, dB	
	Unicone gain	Tricone gain	Unicone gain	Tricone gain
0	61.48	61.41	61.38	61.30
45	61.62	61.56	61.52	61.45
90	61.39	61.31	61.29	61.20

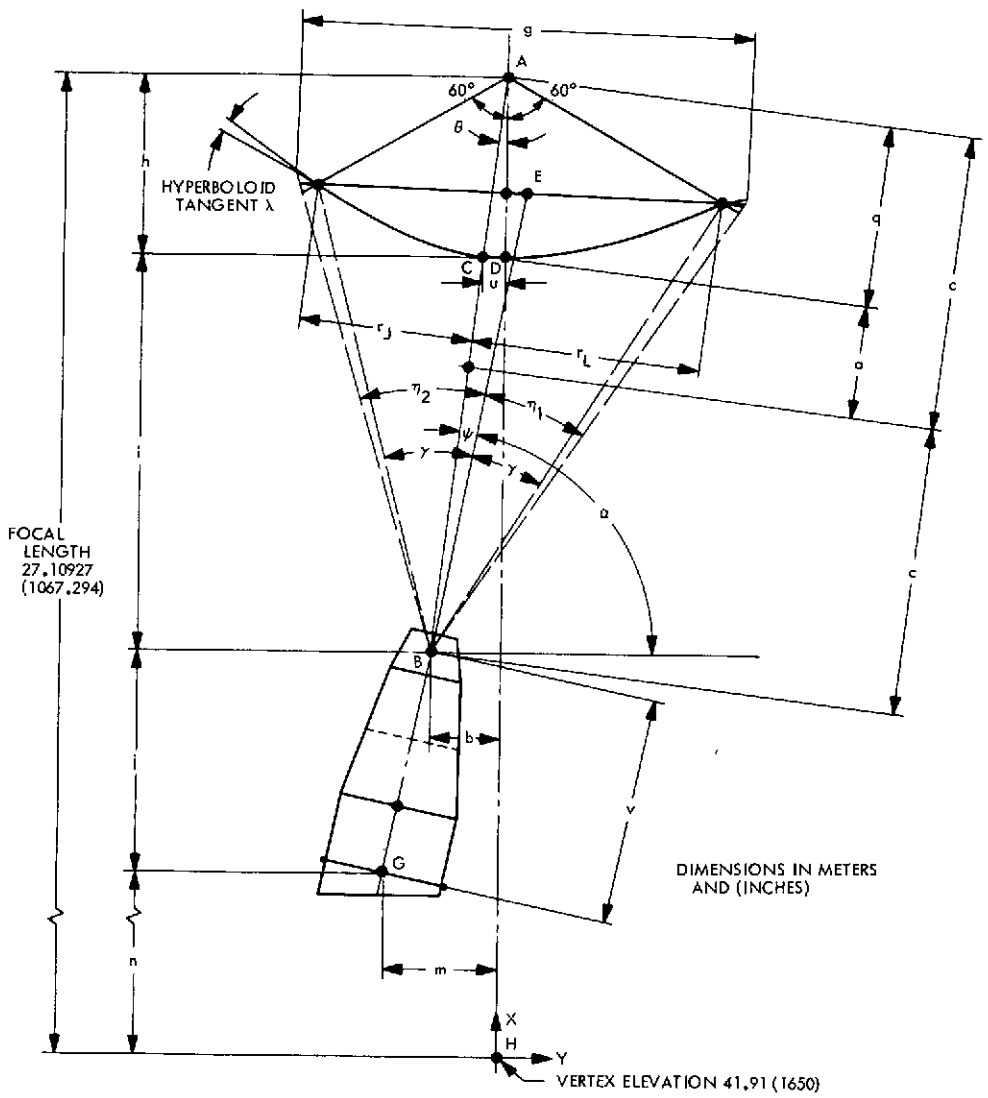

A	FOCUS OF THE PARABOLOID AND THE SECONDARY FOCUS OF THE HYPERBOLOID		
B	PRIMARY FOCUS OF THE HYPERBOLOID		
C	VERTEX OF HYPERBOLOID		
AD	ROTATION AXIS OF HYPERBOLOID		
E	GEOMETRIC CENTER OF THE HYPERBOLOID'S AREA		
G	BASE OF FEEDCONE		
H	VERTEX OF THE PARABOLOID		
a	4.521928 (178.028663)	r_L	3.211463 (126.435547)
b	1.080084 (42.523002)	u	0.183957 (7.242402)
c	6.858000 (270.000000)		
g	6.432092 (253.231949)	v	5.030000 (198.000000)
h	2.328818 (91.685756)	α	84° 15' 46"
i	11.344592 (446.637489)	γ	13° 32' 40"
j	5.004012 (197.008336)	θ	4° 31' 00"
m	1.582834 (62.316291)	η_1	14° 39' 56"
n	8.431845 (331.962419)	η_2	14° 51' 55"
q	2.336072 (91.971337)	λ	4° 44' 27"
r_J	2.605191 (102.566587)	ψ	1° 13' 14"

Fig. 156. Tricone geometry

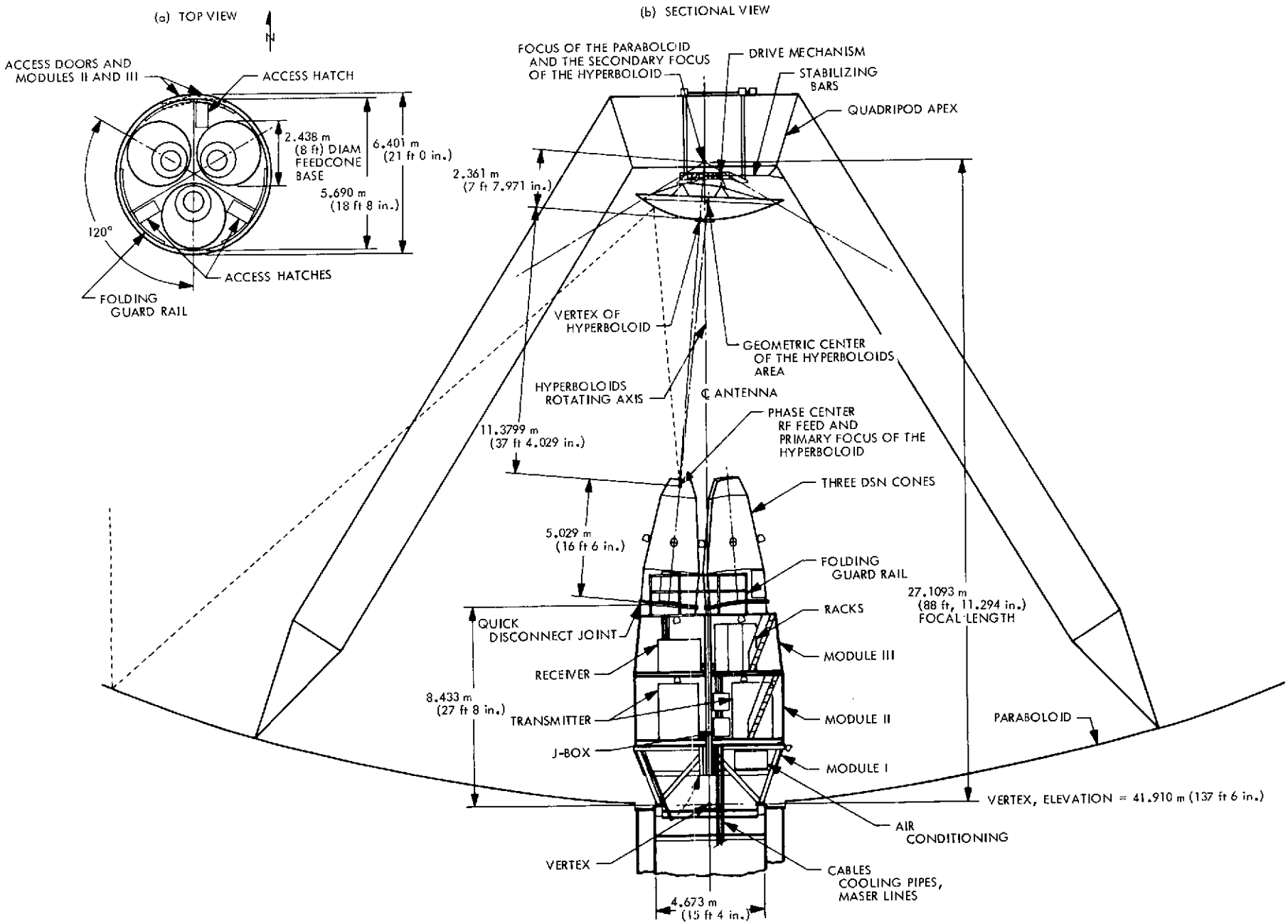

Fig. 157. Tricone configuration

Fig. 158. Tricone installed on the 64-m antenna

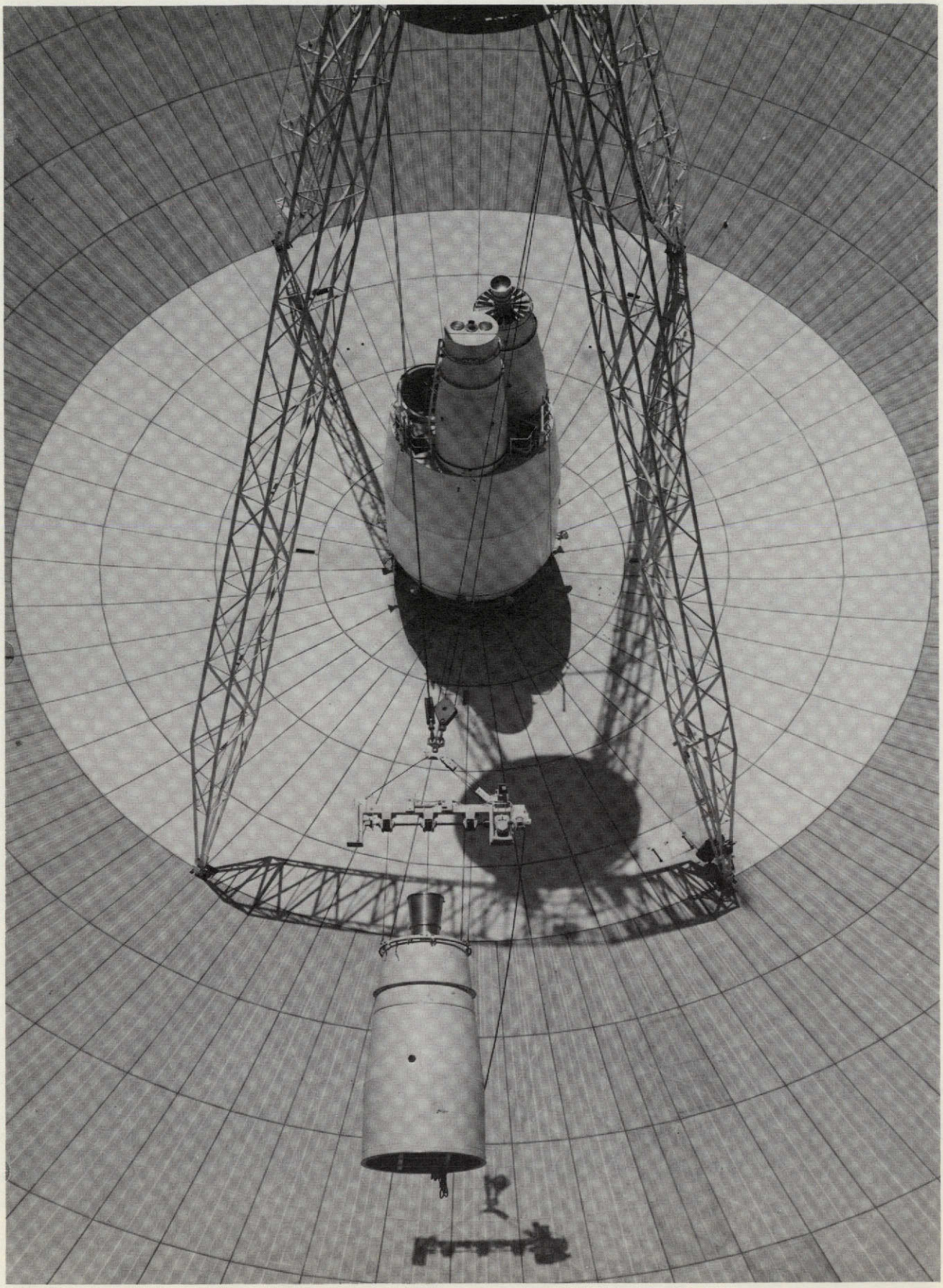

Fig. 159. Hoisting feedcone into place

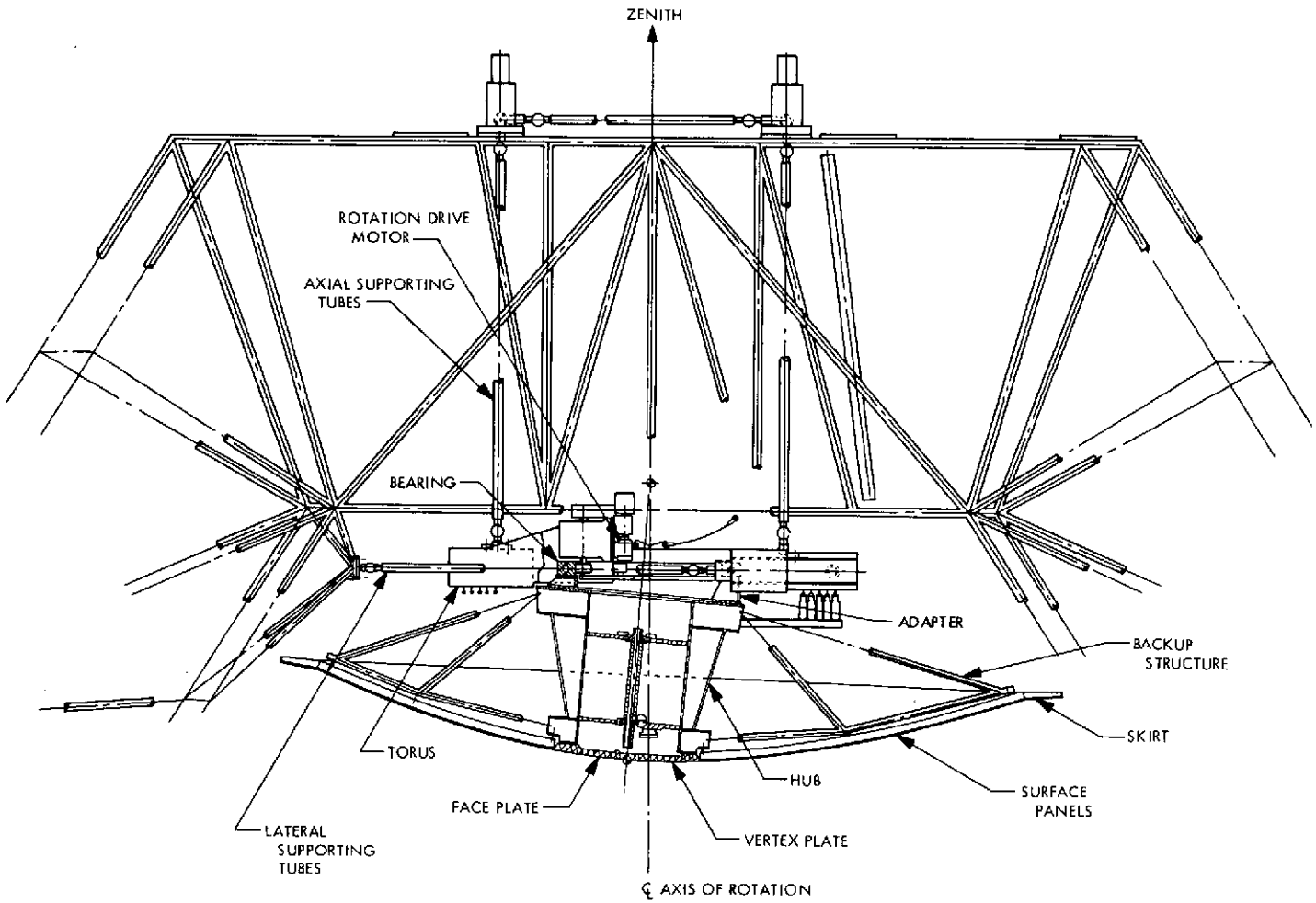

Fig. 160. Side view of subreflector structure, tricone

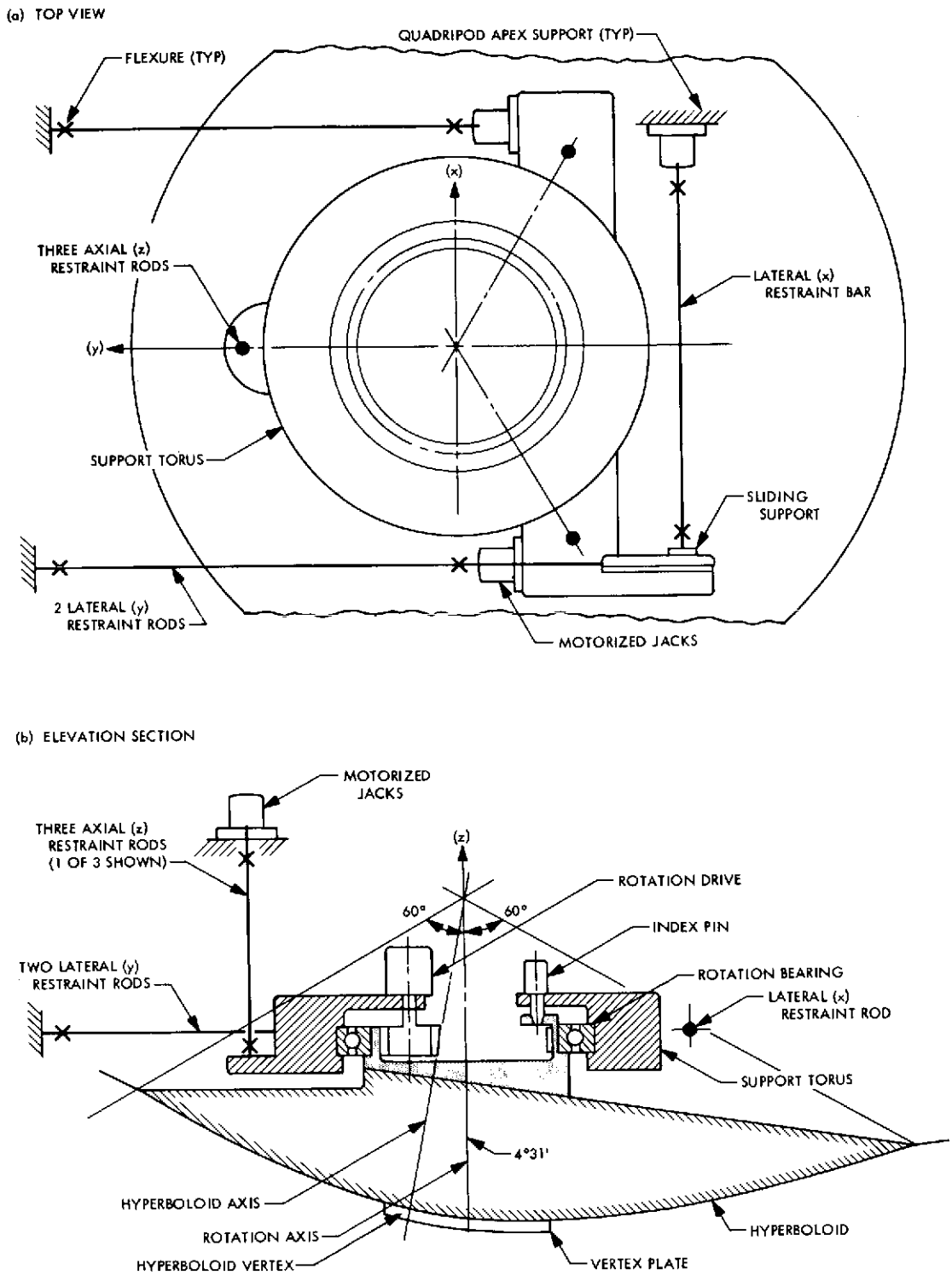

Fig. 161. Hyperboloid assembly top view and elevation section, tricone

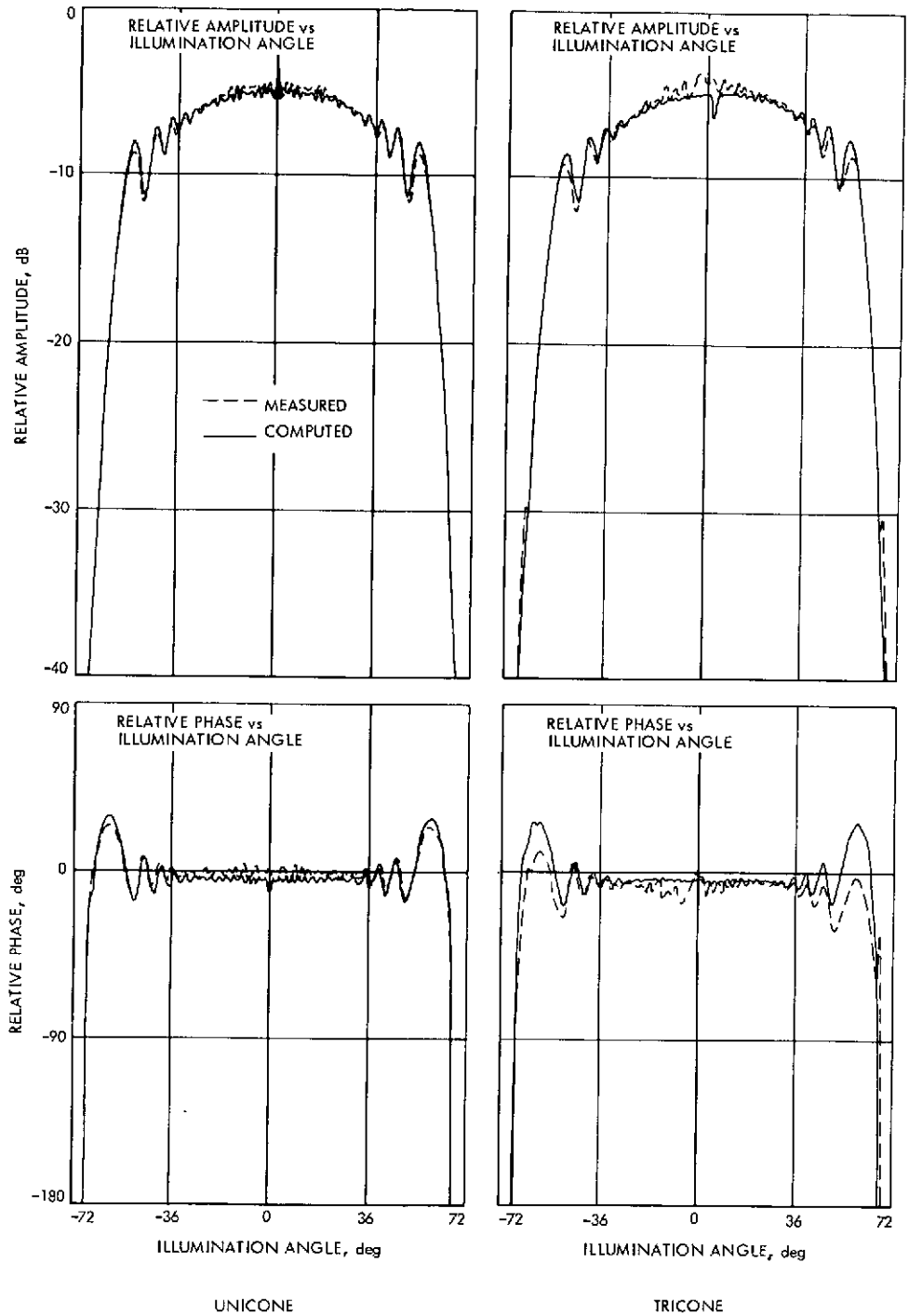

Fig. 162. Typical measured and computed antenna feed patterns, unicone vs tricone

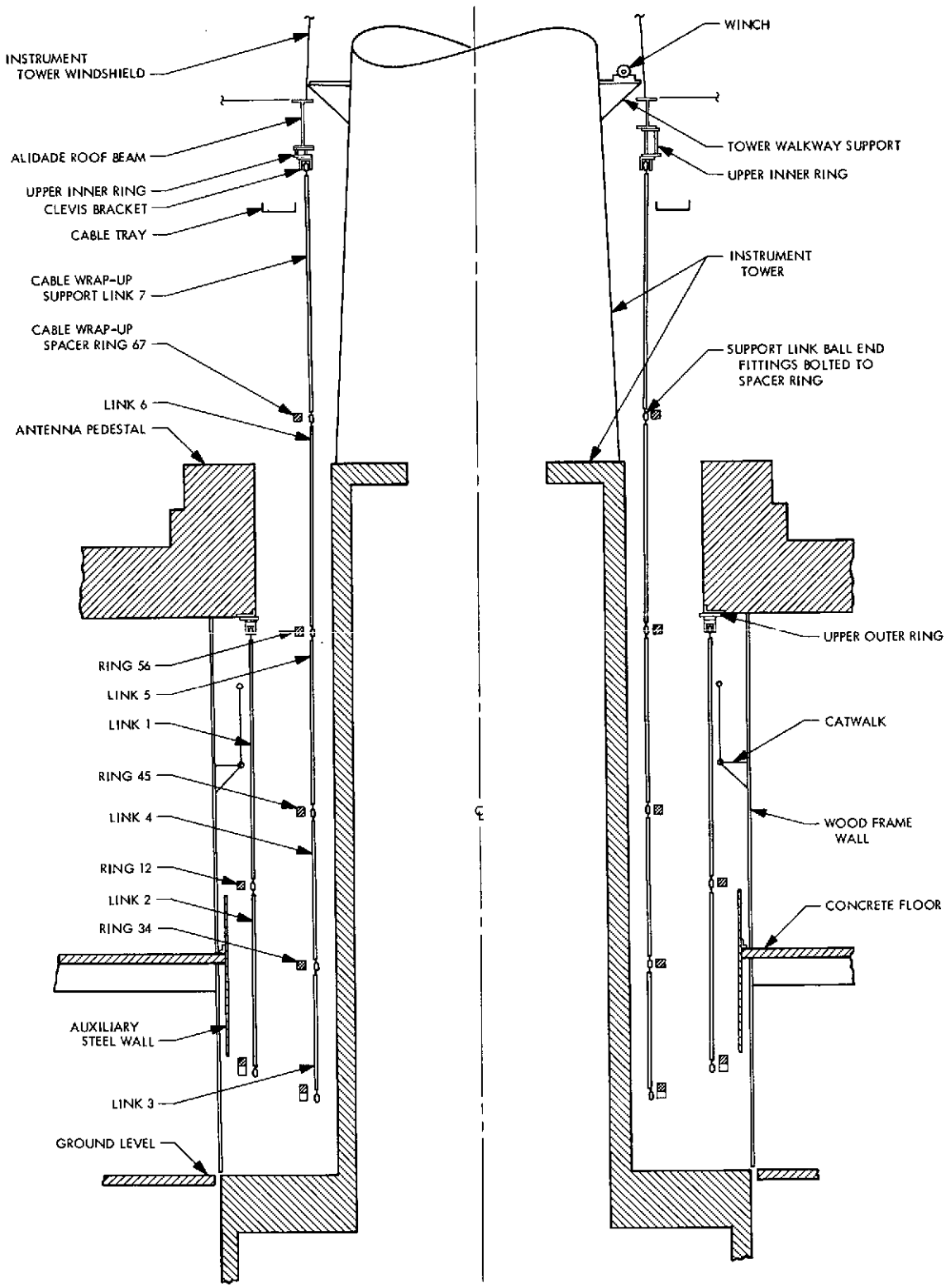

Fig. 163. Cable wrap-up configuration at zero wrap

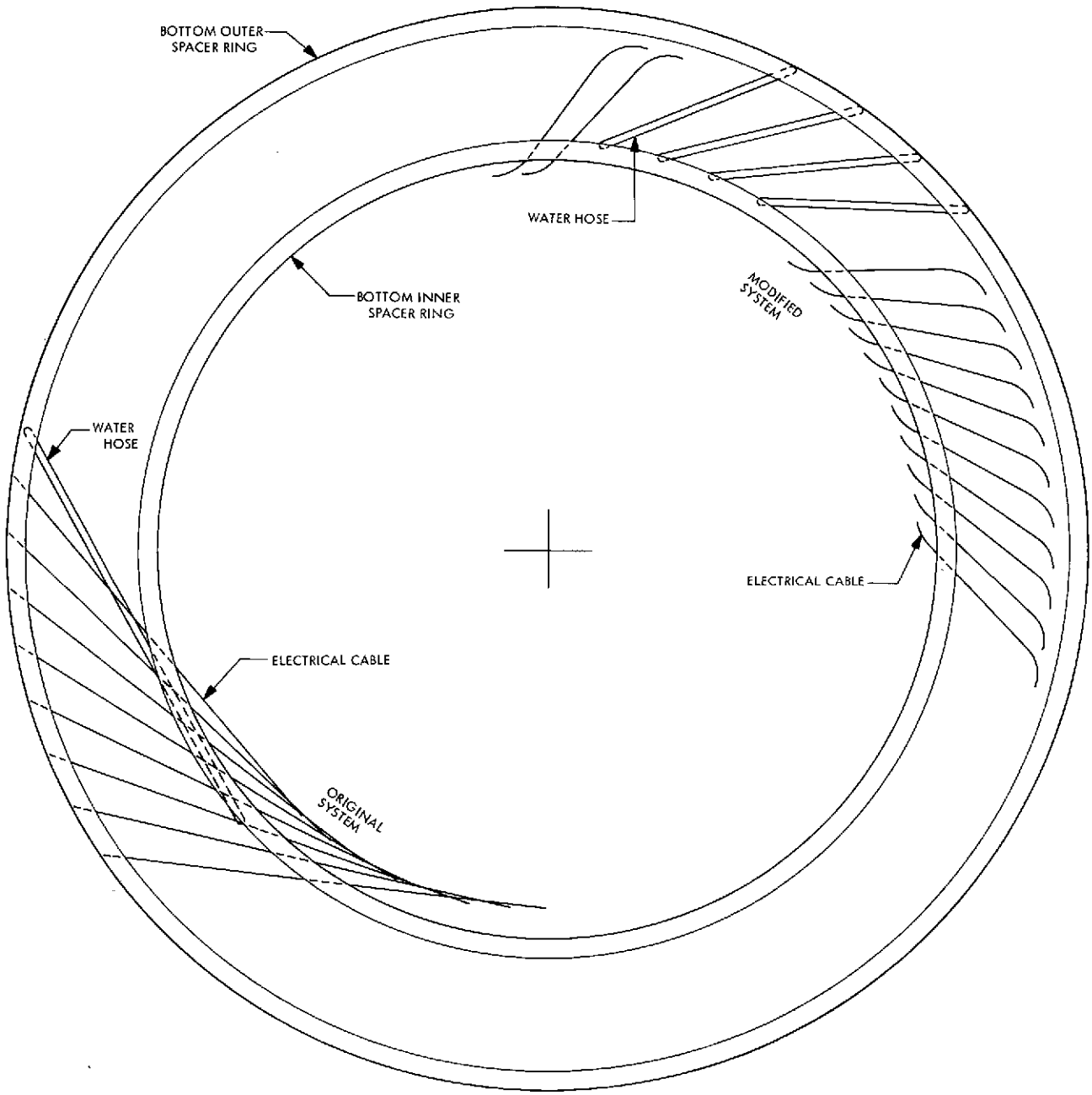

Fig. 164. Plan view of hose and cable loops at bottom of wrap-up

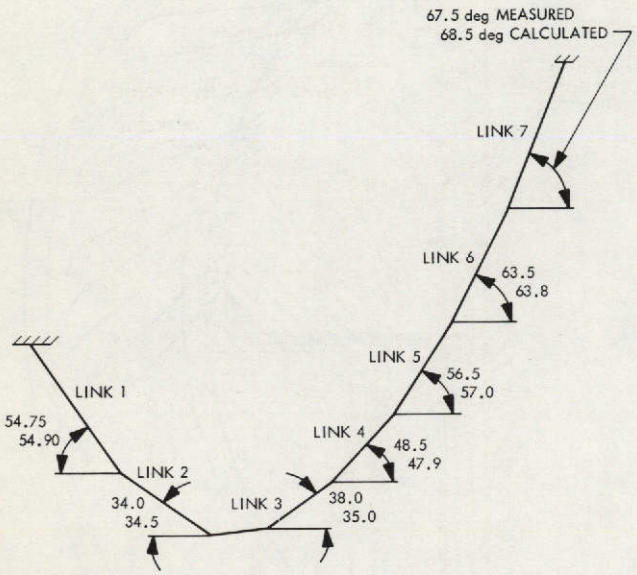

Fig. 165. Developed view of one link set showing comparison of measured and predicted configuration

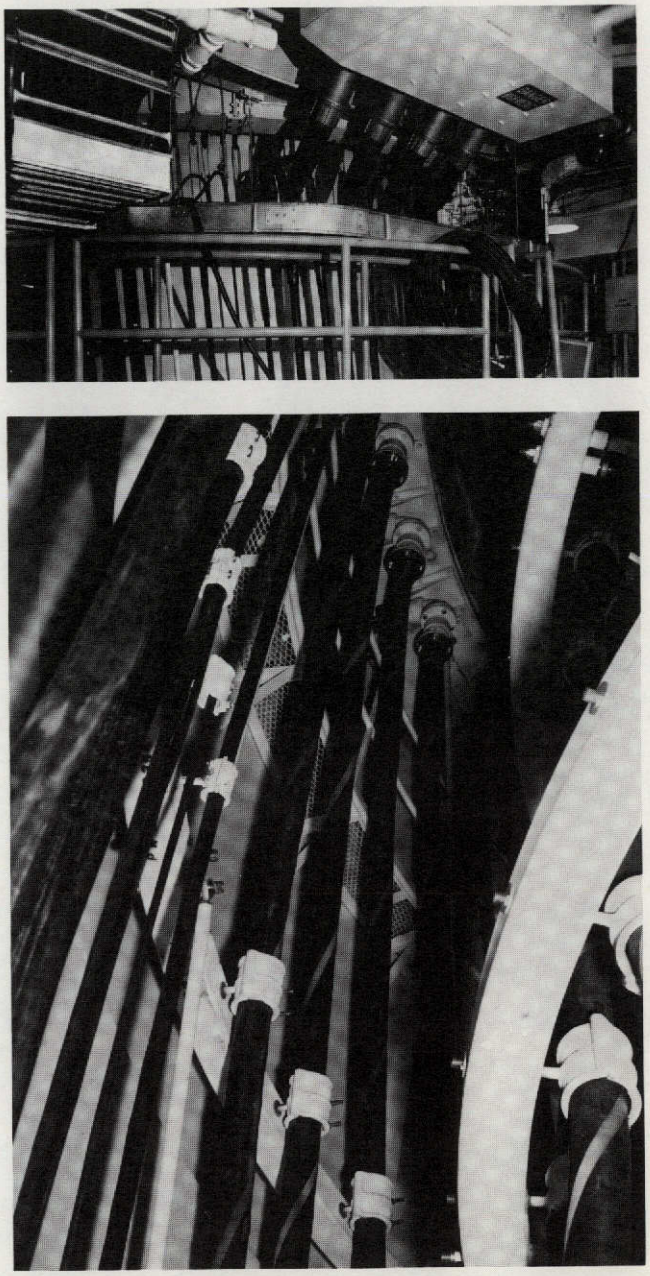

Fig. 166. Views of modified cable wrap-up; (top) upper inner end of wrap-up and (bottom) upper outer end of wrap-up

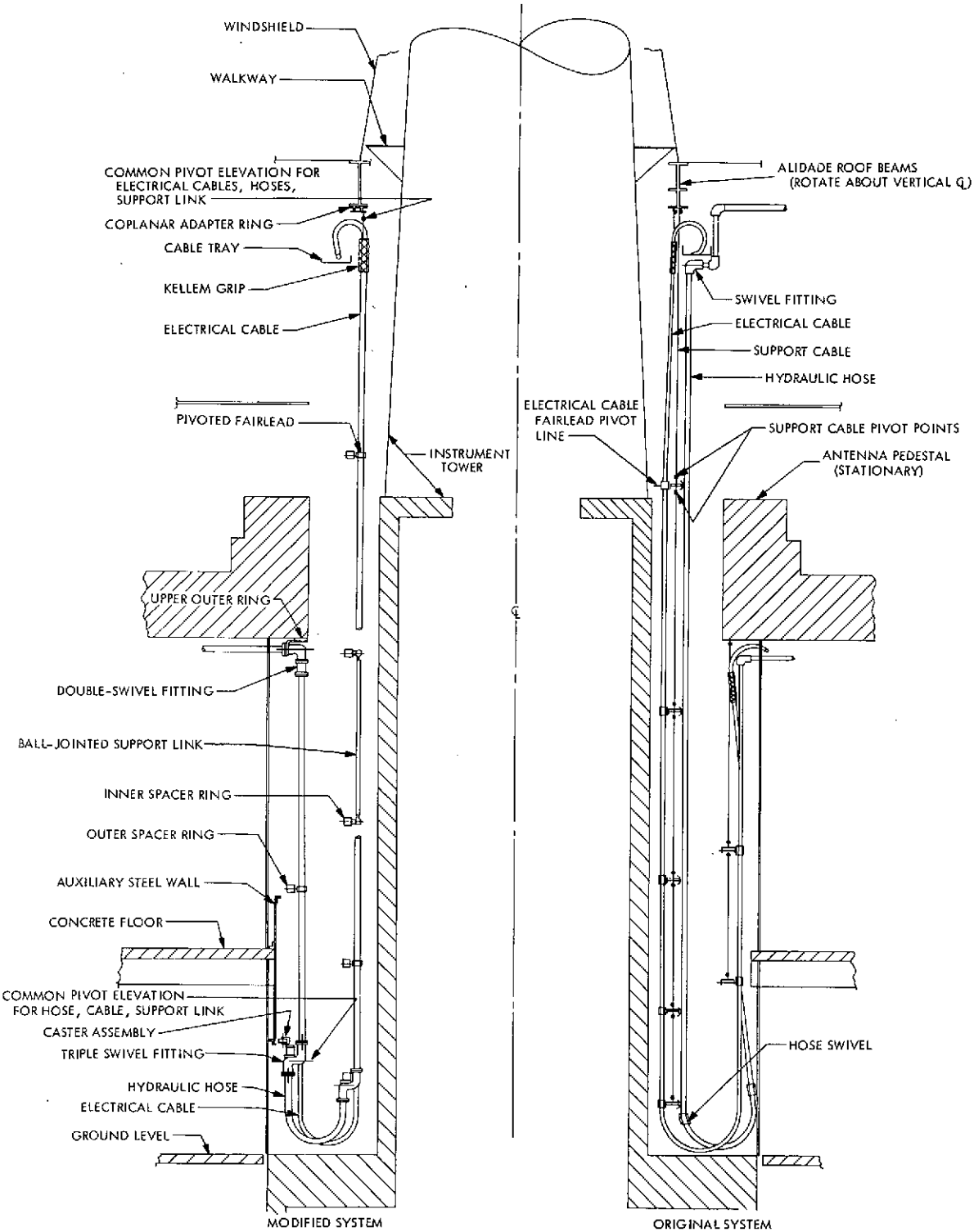

Fig. 167. Structural components of modified cable wrap-up

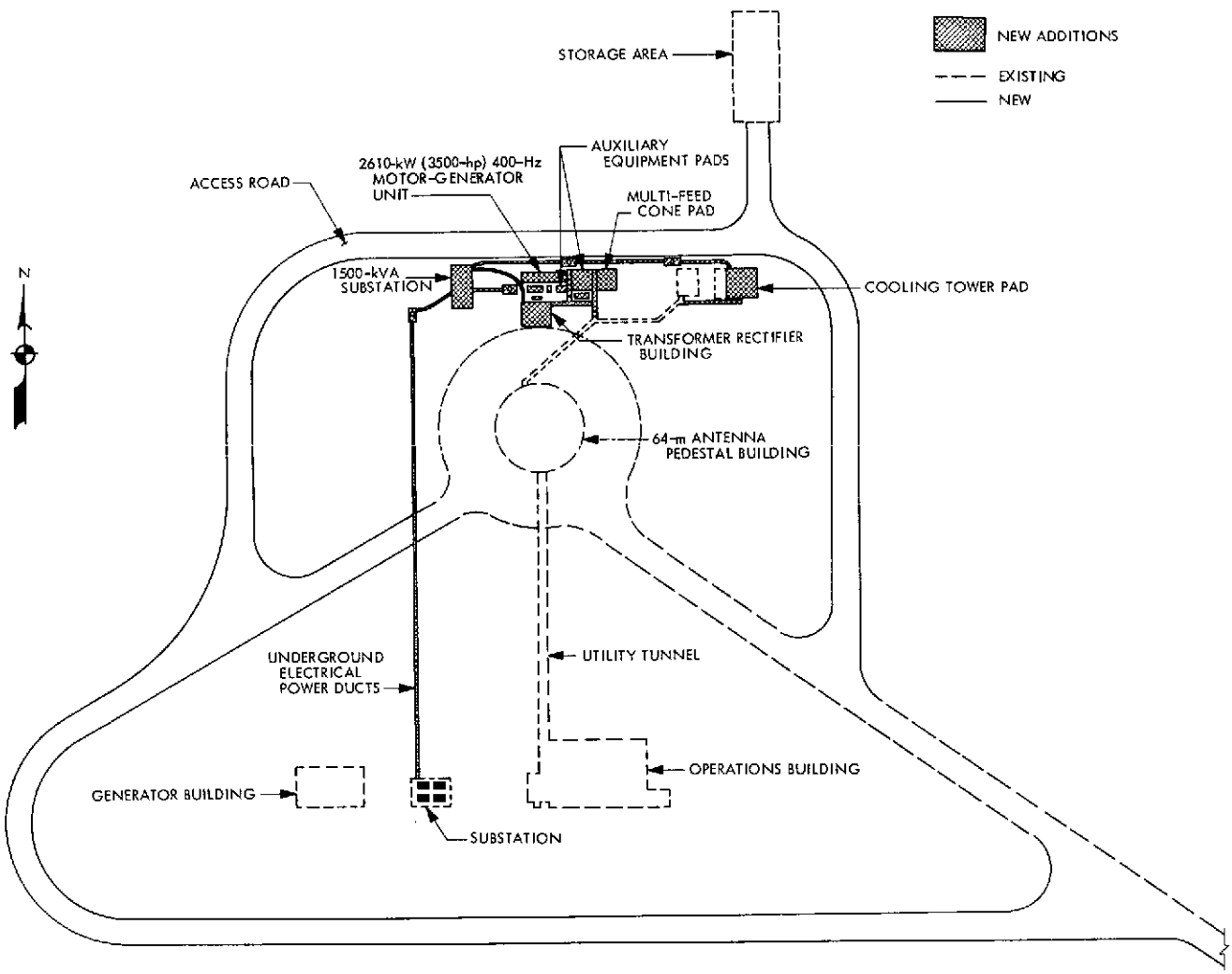

Fig. 168. Additions for high-power transmitter facilities

CHAPTER VIII. SUMMARY AND CONCLUSIONS

This chapter reviews, in summary, some of the technical and scientific achievements of the Goldstone 64-m-diameter antenna that have been discussed in this report. Included is a summary of project management information that may be of value in the accomplishment of similar type projects.

I. GENERAL SUMMARY

In actual support of spacecraft and science missions, the 64-m antenna has proved to be an instrument of value in the NASA/JPL Deep Space Network. The reliability and maintainability of the antenna, since the start of operations, have proved to be excellent. The antenna's availability and use have resulted in extension of spacecraft useful life and continuation of space missions in possible jeopardy that might not otherwise have been continued. Useful scientific data have been, and will continue to be, obtained because of the antenna's existence.

The project was undertaken at a time when national confidence in the ability to construct and successfully operate an antenna of its size and complexity was low. In the face of this, and based on the strong belief of NASA and JPL that such a facility would indeed be required, JPL and its subcontractors embarked on a project to produce an Advanced Antenna System. The result was the successful completion of a working antenna.

Completion of the antenna also extended the NASA/JPL deep space communication and tracking capabilities. The six times larger area of the 64-m antenna has provided a communications capability in excess of ten times (a range capability in excess of three times) that available from the DSN 26-m stations.

The lessons learned during the design, implementation and operation of the 64-m-diameter antenna, both at Goldstone and at the overseas locations, engender confidence that a next generation of antennas of increased size and capability will be needed and can be successfully and profitably accomplished.

II. SUMMARY OF TECHNICAL ACHIEVEMENTS

During design and construction of the antenna, increased new knowledge in many engineering areas has been obtained and reported. This knowledge will be of benefit in planning and building future aerospace and non-aerospace structures and facilities. Included are:

(1) Concrete design by computer techniques; improved methods of foundation and soil analysis; concrete deflection design; design and techniques for placement of grout to achieve critical accuracies; and controlled shrinkage of concrete by containing moisture.

(2) Computerized dynamic analysis of overall large structures; increased knowledge of gravity, thermal, seismic and wind effects on large

structures in an open environment; use of various paints to aid control of steel temperature; and control of brittle fracture by specifying nil ductility levels in structural steel.

(3) Development, analysis, and operation of very large size hydrostatic bearings; development of new techniques for analysis of fluid flow and elasticity characteristics of large bearings; and development of new, highly precise methods for aligning large machine elements (the hydrostatic bearing, at the time of design and use, was the largest known in either load-carrying capacity or physical size).

(4) Improved design, analysis, configuration, evaluation, and measurement of large antenna reflector structures and rotating supports; development and field verification of best-fit paraboloidal computer methods and accurate analysis of antenna reflector surfaces; development of gravity self-compensating Cassegrain system design for precision antenna pointing; and improved techniques for determination and analysis of wind effects.

(5) Improvement of pointing accuracy of large antennas through design and use of a precision reference instrument (master equatorial) on a stable and independently founded position.

(6) Development of a tricone multiple Cassegrain feed system providing a more flexible and rapid means of changing antenna feed cones, thus reducing time for changes in type of mission support from hours to minutes.

In support of spacecraft and science missions, the added capability of the 64-m-antenna enabled:

(1) Extension of communications distances in space and the acquisition of more data from spacecraft at shorter ranges.

(2) Location of more of the complex and sophisticated equipment on the ground, thus making possible the use of simpler and more reliable communications equipment aboard a spacecraft.

(3) Extension of the useful lifetime of spacecraft from a nominal six months to an indefinite time depending on the spacecraft lifetime within the solar system.

(4) Achievement of improved link performance necessary to support higher bit rates and increased data yield.

(5) Support of spacecraft missions during undesigned events and emergencies.

(6) Increased flexibility in the exercise of spacecraft mission tactics and control during critical phases of a spacecraft mission.

(7) Improved assessment and confirmation of in-flight spacecraft and of the spacecraft system's condition, ability to function, and aging characteristics.

(8) Increased depth of field for scientific experimentation and study of space and space objects.

(9) A field laboratory facility for further technological development of ground support methods and means.

III. SUMMARY OF SCIENTIFIC ACHIEVEMENTS

Since the start of operations of the 64-m antenna in 1966, the antenna instrument has been an important tool in the gathering of scientific knowledge and information from space. The antenna has supported key activities in the Mariner, Pioneer, Surveyor, Lunar Orbiter, and Apollo programs. Additionally, continuing support of radar observation and measurement activities has been accomplished. Achievements which were made possible through the availability of the instrument include the following examples:

(1) Increased knowledge of aging characteristics of man-made material and devices in outer space through observation of Mariner 4; analysis of Mariner 5 spacecraft performance under abnormal conditions; provision of command facilities during the Mariner 5 critical Venus encounter phase and instrumentation of the atmosphere and celestial mechanics experiment requiring planetary ranging; provision of visual imaging data playback during Mars encounter phase in hours rather than days and increased data rate for playback of science data during the Mariner 6 and 7 missions; and provision of essentially continuous communication with Mariners 6 and 7 during an extended mission relativity experiment.

(2) Increased data yield from Pioneers 6-9 due to extension of useful spacecraft lifetime from one-half year to about five years, enabling the first opportunity, using Pioneer 6, to examine the solar corona with a linearly polarized monochromatic electromagnetic wave.

(3) Increased ability to control Surveyor lunar soft landers during critical maneuver phases and receipt of important data during

spacecraft touchdown due to enhanced signal-to-noise ratio of strain gauge telemetry data.

(4) Backup support to Lunar Orbiter spacecraft missions.

(5) Support of all manned lunar flights, starting with Apollo 8; providing high-bit-rate telemetry backup via the spacecraft omnidirectional antenna; provision of the portable life-support system telemetry coverage for Apollo 11; coverage of the Apollo 11 lunar module from descent to the lunar surface to exit from moon occultation; provision of high-resolution doppler data and short-time-constant signal strength records until touchdown; support of television transmissions showing man's first step on the lunar surface, subsequent surface operations, and return to the lunar module; and enabling assessment of the Apollo 12 lunar module spacecraft condition following a lightning strike.

(6) Observation of a coherent radio signal passing through the solar atmosphere, providing important solar occultation data; provision of data contributing to the understanding of the sun's atmosphere and magnetic field; and improved information on fundamental parameters of the solar system for accurate radio navigation of spacecraft sent close to the planets.

(7) Increased knowledge of the surface of Venus, hidden from view of optical telescopes by dense clouds; precise determination of the rotation period of Venus; and refined time-of-flight measurements to Venus.

(8) Refined radar studies of Mars; measurements improving the ephemerides of Mars and Earth; and attainment of precision altitude data of vital importance to detailed investigation of Mars.

(9) Increased knowledge of Jupiter's polarization; revelation of features of Mercury; observations of characteristics of single pulses of pulsars; exploration of pulsar signals as a source of precision time information; and first radar contact and radar study of the asteroid Icarus.

(10) Support of studies of earth through experiments using very long baseline interferometry to better define (a) irregularities in the Earth's rotation vector, (b) continental drift, and (c) the accuracy of location of points on the Earth.

(11) Assistance in determining the angular size and separation of radio sources and solar wind characteristics and in determining the validity of competing general relativistic theories through general relativity interferometry experiments.

IV. SUMMARY OF PROJECT MANAGEMENT INFORMATION

In the accomplishment of this project, the validity of a number of management principles and methods was proved or learned through experience. None are entirely unique, but they can be overlooked or suppressed in the heat of project accomplishment. It is realized that each project has its own peculiar set of problems and required solutions. However, the principles in the following discussion were applicable to the 64-m antenna project and may serve as a check list for consideration, by project management teams, in accomplishment of future projects of a similar nature.

(1) The developmental project should have a basically sound and stable justification in terms of the programmatic need of the user. The overall "size of the box" should be clearly stated and remain reasonably firm but permit a degree of latitude of measurement "within the box."

(2) Feasibility should be reasonably established. The fullest possible study and use of information and developments of existing projects with related designs should be made. There should be a continual degree of extrapolation from existing designs.

(3) In a developmental project, there must be an intensive and sometimes lengthy period of design, analysis, and design review leading to establishment of the parameters and development of the project facility specifications. A reasonable rule of thumb seems to be that 50% of the scheduled project time should be utilized before the first piece of material is cut.

(4) Determination of what is wanted and what is to be accomplished is necessary. Steps should lead toward the objective without frills and excessive changes in direction. Configuration concept and subsystem elements must be iterated within early and clearly established constraints. The functional approach to the design most often results in a design that is also aesthetically pleasing.

(5) The required tools of the project must be available in terms of manpower, funds, schedule time, and experience. A proper inventory of these assets must be made before embarking on the project.

(6) Adequate planning is the important ingredient. Planning must tie together the technical approach, the schedule, the funding, and the manpower utilization into a single coordinated effort. Every possible point of difficulty must be considered, however trivial it may seem. Deep consideration, by a single element based on all inputs, must be given to the total package and the overall system design. Sufficient tradeoff study should be made to ensure maximum return for each dollar spent.

(7) A solidly dedicated and experienced hard-core project technical team must be appointed to oversee the conduct of the project from start to finish. The team must pull together toward accomplishment of the project's objectives. The project technical team should be under an uncomplicated line of supervision, preferably in a single technical line organization. Specific responsibilities should be assigned, and a reasonable amount of latitude to function within broad guidelines should be given to team members.

(8) The establishment of cost estimates at the start and for the duration of the project must never be haphazard. Quick individual judgments and hastily spoken figures should not be relied upon and let to live on to form a framework for future decisions. A number of techniques and information sources must be called upon to arrive at reasonable cost estimates within which the project can continue with only minimal revision.

(9) From the start of the project, documentation and its final depth and shape should be clearly established, specified, and costed.

(10) There must be close cooperation and working relationships between technical and administrative disciplines engaged in the project. Proper balance and the recognition that each discipline is a vital part, but that no single discipline is the only important part, are essential.

(11) The preliminary design should be reasonably firm but not excessively restrictive, so as to allow sufficient flexibility to solve some of the engineering problems as they become visible.

(12) Operations and maintenance costs must be considered from the initiation of design so as to preclude excessive costs in this area. Methods must be incorporated in the design for ease of removal and repair/replacement of major components.

(13) Key personnel who are to operate the facility upon completion should be assigned to work closely with the project as early in the event sequence as possible. Such participation is of great benefit in the development of the design, as it affects the operator, operating costs, and maintenance of the facility. The transition from engineering to operations is considerably eased by such assignment.

(14) Thorough evaluation and careful selection of the project subcontractor team are required. Effective and clear communications between the project management team and the subcontractors must be continual. Problems and potential problems must be observed, measured and alleviated promptly to preclude their growth to unsurmountable problems. To enable the required visibility, the establishment of on-site and in-plant representation, where appropriate, effective commercial communications and frequent visits to see first-hand the progress being made, are necessary.

(15) Project reporting must be regular and uncomplicated. It should be such that it provides visibility, pictorially if feasible, of the project progress. Reports must be accurate and complete, thereby maintaining a high confidence level at all levels of management to minimize the emergence of large numbers of briefcases. The project team's basic philosophy must be that close daily observation of the project progress, continuing personal liaison, and immediate attention to problems and potential problems are the most effective means of realizing project control and positive results. Complex schedule exercises and overburdening reports cannot substitute for getting in and regularly "kicking the tires."

The successful accomplishment of the 64-m-diameter antenna project can be attributed in great part to adherence to most of the management methods and principles outlined above.

REFERENCES

1. Project Description, Advanced Antenna System for the Deep Space Instrumentation Facility, Engineering Planning Document 5, Jet Propulsion Laboratory, Pasadena, California (JPL internal document). Advance copies, September 15, 1960; Revision 1, October 12, 1960; Revision 2, July 27, 1962; Revision 3, November 19, 1962; Revision 4, April 4, 1963.

2. Data System Development Plan, Advanced Antenna System for the Deep Space Instrumentation Facility, Engineering Planning Document 162, Jet Propulsion Laboratory, Pasadena, California, April 7, 1964 (JPL internal document).

3. Biot, M.A., "Bending of an Infinite Beam on an Elastic Foundation," Journal of Applied Mechanics, January 1937.

4. Hinkle, J.G., and Castelli, V., A Computer Solution for Hydrostatic Bearings With Variable Film Thickness, Final Technical Report F-B2015, The Franklin Institute Laboratories for Research and Development, Philadelphia, Pennsylvania, January 11, 1963 (JPL Reorder No. 63-615).

5. Hinkle, J.G., et al., A Computer Program for Hydrostatic Bearings Including the Effects of Nonuniform Film Thickness and Relative Velocity for Various Methods of Lubricant Supply, Final Technical Report F-B2099, The Franklin Institute Laboratories for Research and Development, Philadelphia, Pennsylvania, April 1964 (JPL Reorder No. 64-251).

6. Wada, B., Stiffness Matrix Structural Analysis, Technical Report 32-774, Jet Propulsion Laboratory, Pasadena, California, October 31, 1965.

7. STAIR (Structural Analysis Interpretive Routine), Lincoln Manual 40, Massachusetts Institute of Technology Lincoln Laboratory, Lexington, Massachusetts, March 1962.

8. Ruze, J., Physical Limitations on Antenna, Technical Report 248, Research Laboratory of Electronics, Massachusetts Institute of Technology, Cambridge, Massachusetts, October 30, 1952.

9. Katow, M.S., and Schmele, L., "Utku/Schmele Paraboloid RMS Best-Fit Program," in Computer Programs for Antenna Feed System Design and Analysis, Vol. I: Programs and Sample Cases, Technical Report 32-979, edited by A. Ludwig, Jet Propulsion Laboratory, Pasadena, California, April 15, 1967.

10. The NASTRAN Users' Manual, SP-222, edited by C.W. McCormick, National Aeronautics and Space Administration, Washington, D.C., September 1970.

11. Lang, T.E., Summary of the Functions and Capabilities of the Structural Analysis and Matrix Interpretive System Computer Program, Technical Report 32-1075, Jet Propulsion Laboratory, Pasadena, California, April 1, 1967.

12. Isber, A.M., "Obtaining Beam Pointing Accuracy With Cassegrain Antennas," Microwaves, August 1967.

13. Newell, J.S., "The Use of Symmetric and Antisymmetric Loadings," Massachusetts Institute of Technology, presented at the Structures Session, Seventh Annual Meeting, Institute of the Aerospace Sciences (now the American Institute of Aeronautics and Astronautics), January 25, 1939.

14. The Deep Space Instrumentation Facility, Space Programs Summary 37-26, Vol. III, Jet Propulsion Laboratory, Pasadena, California, March 31, 1964, pp. 73-79.

15. Bathker, D.A., Radio Frequency Performance of a 210-ft Ground Antenna: X-Band, Technical Report 32-1417, Jet Propulsion Laboratory, Pasadena, California, December 15, 1969.

APPENDIX

ENGINEERING DATA SUMMARY AND RELATED INFORMATION

64 - METER - DIAMETER ANTENNA

Table A-1. Tracking and data acquisition stations of the DSN, as of April 1974

Deep Space Communications Complex	Location	DSS	DSS serial designation	Antenna		Year of initial operation
				Diameter, m (ft)	Type of Mounting	
Goldstone	California	Pioneer	11	26(85)	Polar	1958
		Echo	12	26(85)	Polar	1962
		(Venus)a	13	26(85)	Az-el	1962
		Mars	14	64(210)	Az-el	1966
Tidbinbilla	Australia	Weemala (formerly Tidbinbilla)	42	26(85)	Polar	1965
		Ballima (formerly Booroomba)	43	64(210)	Az-el	1973
–	Australia	Honeysuckle Creek	44	26(85)	X-Y	1973
–	South Africa	Hartebeesthoek	51	26(85)	Polar	1961
Madrid	Spain	Robledo	61	26(85)	Polar	1965
		Cebreros	62	26(85)	Polar	1967
		Robledo	63	64(210)	Az-el	1973

[a]A maintenance facility. Besides the 26-m (85-ft) diam az-el mounted antenna, DSS 13 has a 9-m (30-ft) diam az-el mounted antenna that is used for interstation time correlation using lunar reflection techniques, for testing the design of new equipment and for support of ground-based radio science.

Table A-2. Engineering summary of the Goldstone 64-m-diameter antenna

Parameter or Component	Value or Material		
Primary reflector			
Diameter	64 m (210 ft)		
Focal length	27.109 m (88.941 ft)		
f/d	0.4235		
Reflecting surface area	3454 m^2 (37,183 ft^2) (approx 0.85 acre)		
Depth of paraboloid	9.45 m (31 ft)		
Precision I	13.4 m/s (30 mph), velocity 0.5 deg/s; acceleration 0.2 deg/s^2		
Precision II	20.1 m/s (45 mph), velocity 0.2 deg/s; acceleration 0.1 deg/s^2		
Limit (drive to stow)	22.4 m/s (50 mph), velocity 0.1 deg/s; acceleration 0.05 deg/s^2		
Survival (any position)	31.3 m/s (70 mph)		
Survival (stowed)	53.6 m/s (120 mph)		
Axis torques			
31.3 m/s (70 mph)			
Az	18,000,000 N-m (13,300,000 lb-ft)		
El	20,000,000 N-m (15,300,000 lb-ft)		
53.6 m/s (120 mph)			
Az	2,700,000 N-m (2,000,000 lb-ft)		
El	24,400,000 N-m (18,000,000 lb-ft)		
Maximum acceleration or deceleration	2.5 deg/s^2		
Stow locks	Elevation only		
Travel			
El	+5 to +91 deg		
Az	±270 deg		
Locked rotor frequency, Hz			
	Specified	Calculated	Measured
Az	1.5	1.58	1.55
El	1.5	1.65	1.80
Maximum overall height from ground	73.15 m (240 ft)		

Parameter or Component	Value or Material
Weights	
Overall	
On el bearings	1,090,000 kg (2,400,000 lb)
On az bearings (inc. bearings)	2,300,000 kg (5,100,000 lb)
On soil	6,860,000 kg (15,125,000 lb)
Component	
Hyperboloid	1860 kg (4,100 lb)
Misc. equipment weight (field handling)	2080 kg (4,600 lb)
Feedcone (unicone)	15,900 kg (35,000 lb)
Feedcone equipment	6800 kg (15,000 lb)
Quadripod	17,700 kg (39,000 lb)
Primary reflector surface	26,300 kg (58,000 lb)
Reflector structure	320,000 kg (705,400 lb)
Counterweight	81,600 kg (180,000 lb)
Alidade and buildings	997,900 kg (2,200,000 lb)
Azimuth bearings	181,400 kg (400,000 lb)
Pedestal and foundation	4,535,900 kg (10,000,000 lb)
Instrument tower — steel (inc. wind shield)	43,500 kg (96,000 lb)
Instrument tower — concrete	522,100 kg (1,151,000 lb)
Miscellaneous	
Diameter of elevation wheel	25.3 m (83 ft)
Inertia of rotating mass about elevation axis	135×10^6 kg-m^2 (100×10^6 slug ft^2)
Inertia of rotating mass about azimuth axis	

Table A-2. Engineering summary of the Goldstone 64-m-diameter antenna (contd)

Parameter or Component	Value or Material
Feedcone	
Height	12.19 m (40 ft)
Base diameter	4.57 m (15 ft)
Top diameter	3.05 m (10 ft) modified to accept 26-m (85-ft) antenna cone
Quadripod	
Height	27.13 m (89 ft)
Base diameter	34.14 m (112 ft)
RF shadow	7.65% (inc. subreflector)
Lowest quadripod frequency	1.3 Hz (about symmetric axis)
Alidade	
Height	23.47 m (77 ft)
Base diameter	23.37 m (76 ft, 8 in.)
Floor space	279 m^2 (3,000 ft^2)
Pedestal	
Height	13.72 m (45 ft) (3.35 m (11 ft) are below grade)
Outside diameter	25.30 m (83 ft)
Wall thickness	1.07 m (3.5 ft)
Floor space	650 m^2 (7,000 ft^2)
Concrete characteristics	
Slump	38.1 mm to 63.5 mm (1.5 in. to 2.5 in.)
Mix	Dry, coarse aggregate mix Add mixture — Plastiment Low water-cement ratio Seven-sack mix
Ultimate strength	34,470,000 to 41,370,000 N/m^2 (5,000 to 6,000 psi)
Modulus of elasticity in compression E_c	42,747,490,000 N/m^2 (6,200,000 psi)
Total concrete	1990 m^3 (2,600 yds^3)
Instrument tower	
Overall height	42.37 m (139 ft)
Height of concrete section	20.73 m (68 ft) (10.67 m (35 ft) are below grade)

Parameter or Component	Value or Material	
Instrument tower (contd)		
Height of steel section	21.64 m (71 ft)	
Base diameter	7.01 m (23 ft)	
Top diameter	2.74 m (9 ft)	
Total concrete	222 m^3 (290 yd^3)	
Elevation bearings		
Number and type	Four spherical roller bearings	
Shaft diameter	609.6 mm (24 in.)	
Distance between bearing pairs	17.07 m (56 ft)	
Load requirements		
Dead load + 22.4 m/s (50 mph) wind	3,069,000 N (690 kips)	
Dead load + 31.3 m/s (70 mph) wind	3,336,000 N (750 kips)	
Dead load + 53.6 m/s (120 mph) wind	3,647,000 N (820 kips) radial 667,000 N (150 kips) axial	
Azimuth hydrostatic bearing		
Loads	Total	Maximum on any pad
Dead load	22,685,900 N (5100 kips)	8,260,300 N (1857 kips)
Wind load	5,938,400 N (1335 kips)	2,780,100 N (625 kips)
Seismic load	3,905,500 N (878 kips)	3,380,600 N (760 kips)
Runner		
Mean diameter	23.37 m (76 ft, 8 in.)	
Wide bearing surface	1.12 m (44 in.)	
Thickness	0.127 m (5 in.)	
No. of segments	11 (for complete circle)	
Material	ASTM A-36	

Table A-2. Engineering summary of the Goldstone 64-m-diameter antenna (contd)

Parameter or Component	Value or Material
Azimuth hydrostatic bearing (contd)	
Pads	
No. required	3
Width	1.016 m (40 in.)
Length	1.524 m (60 in.)
Thickness	0.508 m (20 in.)
Pressure recesses per pad	6
Total area of recesses	4645 cm^2 (720 $in.^2$)
Steel forging	ASTM A151 C1040
Tolerances	
Foundation creep deflection	0.076 mm (0.003 in.)
Flatness pad and runner	0.038 mm (0.0015 in.) each
Pointing error contribution	20 arc second
Maximum out-of-flatness	
Over entire runner circle	(Pointing accuracy) 1.70 mm (0.067 in.)
Over any pad area	(Bearing operation) 0.076 mm (0.003 in.)
Hydraulic requirements	
Liftoff	
Pressure	17,237,000 N/m^2 (2500 psi) minimum
Operational	
Pressure	6,205,000 N/m^2 (900 psi)
Flow	0.000505 m^3/s (8 gal/min)
Oil film height	0.127 to 0.254 mm (0.005 to 0.010 in.)
Oil	0.000217 m^2/s (1000 SUS)
Oil operating temperature	26.6 to 32.2°C (80 to 90°F)

Parameter or Component	Value or Material	
Hydraulic requirements (contd)		
Supercharge to 103,000 N/m^2 (15 psi) at high-pressure pump inlet		
Reservoir capacity	20.8 m^3 (5500 gal)	
Horsepower required		
	Available	Normal operation
Supercharge	29.8 kW (40 hp)	14.9 kW (20 hp)
High pressure	134.2 kW (180 hp)	134.2 kW (180 hp)
Total	164.0 kW (220 hp)	149.1 kW (200 hp)
Redundancy		
Go	Failure of flow to two diametrically opposite recesses in a pad.	
No-go	Failure of flow to any other pattern of two or more recesses in a pad.	
Azimuth radial bearing		
Diameter	9.14 m (30 ft)	
No. of trucks	3 at 120 deg	
Wheels	Two, 914 mm (36 in.) in diameter with 292 mm (11.5 in.) face per truck	
Runner		
Material	ASTM A36 steel	
Thickness	127 mm (5 in.)	
Wear strip		
Material	U.S. Steel Corp. T1 steel	
Thickness	38.1 mm (1.5 in.)	
Preload	1,470,000 N (330,000 lb) for each of the three azimuth axis trucks to maintain azimuth axis concentricity	
Stiffness	272×10^7 N/m (18.7×10^7 lb/ft)	
Tolerances		
Perpendicularity	0.127 mm (0.005 in.) in 317.5 mm (12.5 in.)	

Table A-2. Engineering summary of the Goldstone 64-m-diameter antenna (contd)

Parameter or Component	Value or Material
Azimuth radial bearing (contd)	
Tolerances (contd)	
Total indicator reading	0.254 mm (0.010 in.)
Operating temperature	9.99 to 32.2°C (50 to 90°F)
Reducers	
Arrangement	Tangential load link with backup rollers
No. required per axis	4
Ratio	610:1 for az; 515:1 for el
Pinions	457.2 mm (18 in.) pitch diameter, 254 mm (10 in.) face width
Maximum loading	94,900 N-m (70,000 lb-ft)
Stiffness	
Specified	2.98×10^7 N-m/radian (2.2×10^7 lb-ft/radian)
Tested	3.39×10^7 N-m/radian 2.5×10^7 lb-ft/radian)
Bull gear pinion ratio	45:1 for az; 56.1 for el
Drive motors per reducer	Two; one drive, one countertorque
Maximum rev/min of antenna	1/12
Bull gears	
Material	AISI 4140 Steel, 245-285 BHN
Face width	247.7 mm (9.75 in.) az and el
Pitch diameter	25.30 m (83 ft) for el and 21.34 m (70 ft) for az
Pressure angle	25 deg az and el
Circular pitch	88.9 mm (3.5 in.) az and el
Brakes	
Type	Disk, hydraulic release, spring set
Maximum dynamic torque	162 N-m (120 lb-ft)
Minimum static torque	217 N-m (160 lb-ft)

Parameter or Component	Value or Material
Servo	
Type	Hydraulic servo with pump and flow control servo valves
Input power rating	223.7 kW (300 hp) per axis
Counter-torqued system operational	Up to a 15.6-m/s (35-mph) wind
Overall axis ratio	28,800
Maximum rev/min of servo motors	2400
Bandwidth adjustable	From 0.01 Hz to 0.2 Hz
Axis tracking error	0.002 deg (measured)
Angle readouts	
Primary	Shaft encoders on master equatorial axis hour angle and declination coordinates
Secondary	Multi-turn encoders geared 36:1 to antenna axis az and el
Axis alignments, arc seconds	Calculated / Measured
Az axis to gravity	20
El over az (orthogonality)	20 / 10
Reflector axis to el axis	28 / 2
Pitch diameter	25.30 m (83 ft) for el; 21.34 m (70 ft) for az
Pressure angle	25 deg az and el
Circular pitch	88.9 mm (3-1/2 in.) az and el
Brakes	
Type	Disk, hydraulic release, spring set
Maximum dynamic torque	162.7 N-m (120 ft-lb)
Minimum static torque	216.9 N-m (160 ft-lb)
Servo	
Type	Hydraulic servo with pump and flow control servo valves

Table A-2. Engineering summary of the Goldstone 64-m-diameter antenna (contd)

Parameter or Component	Value or Material		
Servo (contd)			
Input power rating	223.7 kW (300 hp) per axis		
Counter-torqued system operational	Up to a 15.6-m/s (35-mph) wind		
Overall axis ratio	28,800		
Maximum rev/min of servo motors	2400		
Bandwidth adjustable	From 0.01 to 0.2 Hz		
Axis tracking error	0.002 deg (measured)		
Angle readouts			
Primary	Shaft encoders on master equatorial axis hour angle and declination coordinates		
Secondary	Multi-turn encoders geared 36:1 to antenna axis az and el		
Axis alignments, arc seconds			
	Calculated	Measured	
Az axis to gravity	20		
El over az (orthog-onality)	20	10	
Reflector axis to el axis	28	2	

Parameter or Component	Value or Material
Generator building	
Floor space area	214 m^2 (2300 ft^2)
Capacity	Contains four Caterpillar diesel generators and associated switch gear rated at 500 kW each, or 2000 kW total, 2400 volts AC
Air conditioning	
Codes	American Society of Heating, Ventilating, Refrigeration, and Air Conditioning
Evaporative coolers	9.44 m^3/s (20,000 ft^3/min)
Water chillers	Two 37.3-kW (50 hp), each
Cooler	Direct expansion
Compressor	Reciprocating for operation with R-12 refrigerant
Cooling tower	Double cell type—closed circuit
Volume of water used	45.4 m^3 (12,000 gal) daily under maximum operating conditions
Heating	Strip heaters in ducts
Humidity control	In control and computer areas
Cable wrap	
Number and size of cables	60 cables, 44.45 mm (1.75 in.) in diameter
Rotation limit	±270 deg
Electrical cables carry a maximum of 140 conductors of various gauges	

Table A-3. RF Cassegrain system surface distortions (unicone), 1σ rms

Antenna Component	Distortion, mm (in.)[a]					
	Zenith Look			Horizon Look[b]		
	Calculated	Field Measured	RF Measured	Calculated	Field Measured	RF Measured
Primary reflector structure[c]						
Gravity load – best fit	1.91(0.075)	1.60(0.063)		1.02(0.040)	0.86(0.034)	
Gravity load – focal point lateral Y-offset	1.27(0.050)	1.27(0.050)		0.48(0.019)	0.51(0.020)	
Primary surface panels						
Manufacturing error[d]		0.89(0.035)			0.89(0.035)	
Position setting error[d]		0.48(0.019)			0.48(0.019)	
Subreflector						
Manufacturing and setting error[d]		0.69(0.027)			0.69(0.027)	
Total error (Subreflector focused axially – wind and thermal loads not included)	2.59(0.102)	2.39(0.094)	2.34(0.092)	1.65(0.065)	1.57(0.062)	1.70(0.067)

[a]Panels set at 45-deg elevation.

[b]Horizon field position at 6 deg elevation.

[c]Computer model – quadrant symmetric pin-jointed truss.

[d]Field-measured values used for computing the total error.

Table A-4. Environmental loading distortions – calculated Precision I operation at horizon look

Source	Distortion, 1σ rms	
	mm	in.
5.55°C (10°F) temperature difference + 13.4 m/s (30 mph) wind at 135 deg yaw plus horizon look gravity minus reflector structure distortion.	1.88	0.074 in.
Same as above for focal point offset. Equivalent distortion.	1.07	0.042 in.
Surfaces manufacturing and setting distortion.	1.22	0.048 in.
Total Distortion (subreflector focused axially only for gravity distortions.	2.49	0.098 in.

Table A-5. Mars Deep Space Station power load tabulation as of January 1, 1974

Element	Power, kW
PEDESTAL	
O-bus power	
400-Hz M-G sets for 20-kW transmitter	80
Transmitter	
T-bus power	
500-kW transmitter	1,200
Substation US-1U 500-kVA MCC-1 and MCC-3	50
Summary pedestal loads	
O-bus power	80
T-bus power	1,250
ALIDADE	
T-bus power	
Substation US-2 1,250-kVA MCC-2 and MCC-2A Distribution panels and lighting panels Klystron pumps and heaters	400
T-bus power, 2.4 kV	
Two 149-kW (200-hp) servo pumps	100
Summary alidade loads	
O-bus power	
T-bus power	500
OPERATION SUPPORT BUILDING	
O-bus power	100
T-bus power	325
POWER PLANT[a]	
T-bus power	150
Mars station site load	
O-bus power	1,205
T-bus power	1,200
TOTAL O AND T POWER	2,205

[a]Power plant load: diversity factor of O-bus = 80% (960 kW).

NASA — JPL — Comi., L.A., Calif.